UNIVERSITY OF CALIFORNIA SAN DIEGO

A new model for telomere length homeostasis

A dissertation submitted in partial satisfaction of the requirements for the degree
Doctor of Philosophy

in

Biology

by

Cynthia M. Reyes

Committee in charge:

Professor Vicki Lundblad, Chair
Professor Arshad Desai
Professor Jan Karlseder
Professor Lorraine Pillus
Professor Steven Wasserman

2018

The Dissertation of Cynthia M. Reyes is approved, and is acceptable in quality and form for publication on microfilm and electronically:

Chair

University of California San Diego

2018

DEDICATION

I dedicate this dissertation to Professor Costello Brown, who played an integral role in setting me on this path many years ago. Dr. Brown stands out from a large number of professors that I have encountered in my 8+ years of higher education, as the most influential, engaging, and supportive teacher. He took a real interest in me and saw something that I did not know was there. He was my first mentor, and I cannot thank him enough for that.

TABLE OF CONTENTS

LIST OF FIGURES

LIST OF TABLES

ACKNOWLEDGEMENTS

I would first like to thank my advisor Vicki Lundblad for all the time and effort she dedicated to helping me become a better scientist. Her guidance throughout my graduate career was invaluable to the growth and confidence in my skills.

I would also like to thank my committee members Arshad Desai, Jan Karlseder, Lorraine Pillus, and Steve Wasserman, for all of their helpful insights throughout the years.

I am extremely grateful to the members of the Lundblad lab, past and present. I would especially like to thank Margherita Paschini for all the years we spent side by side in lab and her continuing support and friendship. The work presented in this dissertation, would not have been possible without the amazing collaboration we had (detailed in Chapter 3) and her willingness to teach me all she knew about yeast genetics. I would also like to thank John Lubin for the numerous scientific conversations and disputes we have had regularly in our many years together in lab.

Chapter Three is currently being prepared for submission for publication of the material. Paschini, Margherita; Reyes, Cynthia M.; Mandell, Edward K.; Lewis, Karen A.; Glustrom, Leslie W.; Sharpee, Tanya O.; Wuttke, Deborah S.; Lundblad, Victoria. The dissertation author along with Margherita Paschini, are the primary investigators and co-first authors of this material.

Appendix A is currently under review at *PNAS*. Glustrom, Leslie W.; Lyon, Kenneth R.; Paschini, Margherita; Reyes, Cynthia M., Toro, Tasha B.; Lundblad,

Victoria; Wuttke, Deborah S. The dissertation author was a collaborator and a contributing author of this material.

VITA

EDUCATION:

University of California San Diego La Jolla, CA
Ph.D. in Biology. 2018.

California State University, Los Angeles
M.S in Biology, 2011.

California State University, Los Angeles
B.S in Biology, 2008

ABSTRACT OF THE DISSERTATION

A new model for telomere length homeostasis

by

Cynthia M. Reyes

Doctor of Philosophy in Biology

University of California San Diego 2018

Professor Vicki Lundblad, Chair

The ends of linear chromosomes are composed of distinctive structures that maintain chromosome stability and cellular viability. Both sequence and structure of

telomeres are important to their function. They are composed of TG-rich, repetitive, non-coding sequences and present unique challenges for genomes. A balance of both shortening and lengthening pathways maintains telomere length homeostasis. Telomere length dysregulation has been linked to human aging, cancer, and disease (telomeropathies), so studying the details of how this regulation occurs is vital to our understanding of telomere biology and human health.

Telomeres have been proposed to serve two distinct functions; end protection and end replication. As end protection factors, they help distinguish the natural ends of linear chromosomes from double stranded breaks of DNA that need to be repaired by DNA repair mechanisms and prevent end-to-end fusions. Telomeric DNA is lost at every round of replication due to incomplete replication. This loss is compensated by *de novo* synthesis of telomeric repeats by the enzyme telomerase. A lot has been learned about the factors implicated in both these functions and how they contribute to telomere length regulation.

In the budding yeast, *Saccharomyces cerevisiae*, a trimeric complex composed of Cdc13-Stn1-Ten was initially proposed to be the main players in telomere "capping" and serving an end-protection function. More recently, this complex has been shown to have homology to the RPA complex and function in the efficient replication of duplex telomeric DNA, and so was aptly named t-RPA. This discovery led to multiple questions about the role of replication at telomeres and how that contributes to telomere length regulation.

This dissertation describes my efforts in identifying a new model for telomere length regulation, which revolves around the significant effects of efficient replication to telomere length homeostasis. Errors that lead to replication fork collapse within the genome can have detrimental and even lethal results for the cell. At chromosome ends, that are recognizably difficult to replicate regions of the genome, replication fork collapse has been exploited by the cell to regulate telomere length. By following the events that occur immediately after a replication fork collapse, I found that collapsed forks at telomeres are recognizes by telomerase with high efficiency and subject to extensive elongation. Moreover, this process is under genetic control. Strikingly, when I studied the effects of known telomere length regulators, I found that they were modulating telomere length through their effects on replication fork collapse. This illustrated the previously unappreciated role of replication, and supported a new model for telomere length homeostasis that is driven by replication fork collapse and the subsequent response by telomerase.

CHAPTER ONE:

Introduction

Telomeres, the structures at the end of linear chromosomes, are essential for genomic stability and the proliferative capacity of cells. Telomeric DNA is composed of duplex TG-rich, non-coding, repetitive sequences, that terminate with a G-rich single strand of DNA. The sequence and structure of telomeres assure the recruitment of a number of factors that form a complex of proteins, and together, result in the protection of the ends of chromosomes from a number of deleterious, genome destabilizing activities. While telomeres are conserved in virtually all eukaryotic chromosomes, telomere length varies among species, anywhere from hundreds of bps (~350 in *S. cerevisiae*, Shampay et al. 1984) to multiple kbs (2-14kbs in humans, de Lange et al. 1990). A balance of both shortening and lengthening pathways maintains telomere length homeostasis. Since the discovery of telomeres, various mechanisms have been implicated in a dynamic relationship between proteins and telomeric DNA that leads to this homeostasis.

The end replication problem

During cell division, telomeres continuously lose sequence due to incomplete replication. Genome duplication requires both leading and lagging strand synthesis of DNA. The leading strand polymerase synthesizes DNA from 5' to 3', all the way to the end of the chromosome (Ohki et al. 2001). The problem arises from lagging strand synthesis. Lagging strand replication involves discontinuous replication that is initiated from RNA primers that are extended by a polymerase, to form Okazaki fragments (Sakabe & Okazaki, 1966). These primers are later degraded and gaps filled by DNA polymerase. The Okazaki fragments are joined by the DNA ligase Lig 1. But

to fill in the sequence left by the degraded primer would require upstream DNA, which is not present at the site of the final RNA. This leaves un-replicated DNA at the terminal chromosome at every round of replication (the end-replication problem, Olovnikov 1973, Watson 1972). This is an obstacle for the genomic replication of all linear chromosomes. Left unchecked, this continuous loss of DNA after each cell division, leads to gradual attrition of telomeres until cells are no longer able to maintain genomic stability or viability, a process known as senescence (Lendvay et al. 1996).

This loss of sequence can be counterbalanced by addition of new telomeric repeats to the 3' G-rich strand by the enzyme telomerase. While initially identified in *Tetrahymena* (Grieder & Blackburn 1985), telomerase is conserved among most eukaryotes. This ribonucleoprotein complex contains both essential proteins and an RNA component. The catalytic core of telomerase is composed of a reverse transcriptase (TERT in humans and Est2 in *S. cerevisiae*) and an RNA template (TERC in humans and TLC1 in *S. cerevisiae*). In yeast, telomerase is composed of three proteins; Est1, Est2 and Est3, and an RNA component, TLC1. All subunits are necessary for telomere synthesis and short telomeres result when any of them are defective (Lendvay et. al 1996). The RNA component of telomerase serves as template for *de novo* telomere synthesis. While all telomeric DNA consists of short, tandem, TG-rich sequences, the sequence composition varies by species. In humans and other mammals, telomerase adds invariant TTAGGG repeats, while in *Tetrahymena* the repeats are TTGGG. Yeast telomeric repeats, unlike ciliates and

humans, are made up degenerate telomeric repeats of $G_{1\text{-}3}T$ (Shampay et al. 1984), a unique feature that made certain assays in this thesis possible (discussed in detail in Chapter 3).

In single cell eukaryotes, like *S. cerevisiae*, telomeres are maintained by constitutively active telomerase. In humans (and other multicellular eukaryotes) there is variable telomerase activity among different cell types. Germ line cells, stem cells, and immune cells express telomerase, while somatic cells have little to no telomerase activity (Kim et al. 1994). In somatic cells that lack telomerase expression, telomeres shorten after every cell division and subsequently undergo replicative senescence. The limit for the number of cell divisions a normal human cell population can undergo in culture is called the Hayflick Limit (Hayflick & Moorehead 1961). This limit is correlated to telomere length. Cells that start off with longer telomeres can undergo more cell divisions than those that started off with shorter telomeres. Despite the low levels of telomerase expression in most somatic cells, numerous studies have shown that mutations that result in impaired telomerase activity can have disastrous consequences and contribute to age-related pathophysiologies (Armanios & Blackburn 2012).

The end protection problem and telomere binding proteins

In addition to incomplete replication, the ends of linear chromosomes face another problem because of their unique location in the genome. Due to their structure as ends of DNA, telomeres have a likeness to the structure of double stranded breaks (DSBs). Cells must be able to distinguish between the two. Repair of DSBs is

necessary for the viability of the cell, while applying those same repair mechanisms to telomeres can lead to the opposite, genomic instability.

Double stranded breaks can arise due to a number of events. Both endogenous and environmental factors can contribute, making it a frequent event. Regardless of their source, DSBs are toxic to the cell. To combat this damage, the cell has developed mechanisms to mend broken DNA. DSBs can trigger a DNA damage response (DDR) through two distinct signaling pathways, ATM (ataxia telangiectasia mutated) kinase pathway and ATR (ataxia telangiectasia and Rad3 related) kinase pathway. Once detected, there are two primary mechanisms to repair the break, homologous recombination (HR) and non-homologous end joining (NHEJ) (Jasin & Rothstein 2013). If telomeres are mistakenly recognized as double stranded breaks, either of these repair mechanisms can mean havoc for the cell. Homologous recombination with another telomere leads to telomeres of atypical lengths. NHEJ at telomeres leads to end-to-end fusions creating dicentric telomeres. Both scenarios cause major genomic instability, so it is crucial that telomeres avoid detection by these repair mechanisms.

How cells distinguish natural chromosome ends from DSBs has been a topic of much study. In mammals, the shelterin complex has been identified as playing the essential role in telomere protection (de Lange 2005). This telomere-specific complex resides at the end of chromosome and is made up of six proteins (TRF1, TRF2, POT1, RAP1, TIN2, and TPP1). In the absence of a functional shelterin complex, the canonical DNA damage response is triggered and telomeres are susceptible to

destructive repair by HR or NHEJ. The shelterin complex is held together at the telomere through a number activities including; double stranded DNA binding activity, protein-protein interactions, and SS-DNA binding activity. In the many years since its initial discovery, the shelterin complex and all its individual components have been extensively studied. It has been shown that POT1 is responsible for repression of ATR, while TRF2 represses ATM (Lazzerini & de Lange 2007) thereby facilitating telomeric escape from DDR. Additionally, shelterin is thought to solve the end protection problem by affecting the physical structure of telomeric DNA. In humans, and other mammals, shelterin is responsible for forming physical barriers at the end of telomeres, called t-loops. T-loops are formed when the single stranded 3' telomeric DNA loops back into the double stranded region of the same chromosome, to form a duplex lariat structure (de Lange 2009).

Most shelterin components have homologs in other eukaryotes, with the exception of *S. cerevisiae*. In budding yeast only one of the six shelterin components has been found, Rap1 (Li et al. 2001). In *S. cerevisiae*, a trimeric complex made up of essential proteins Cdc13, Stn1, Ten1, is proposed to take on the role as the end-protection complex, like the shelterin complex in humans. This complex binds to telomeric single stranded DNA with high affinity through the DNA binding domain of its main component, Cdc13 (Hughes et al. 2000). As a complex with Stn1-Ten1, it is thought to "cap" the ends of telomeres inhibiting their resection and detection by DDR. These capping functions were originally proposed to occur after replication of telomeric DNA. However, this complex shares structural and biochemical similarities

with RPA (Gao et al. 2007) resulting in the moniker t-RPA. RPA is the major single-stranded DNA binding protein in eukaryotic cells and has multiple roles, including one in DNA replication. Therefore, t-RPA's role in telomere homeostasis could be due to its contribution to telomere replication rather than telomere capping (discussed in detail in Chapter 3).

Telomere length regulation

Telomere length homeostasis is a balancing act between factors that contribute to telomere lengthening and those that contribute to shortening them. This balance can be shifted in either direction by a number of elements, and mechanisms. In most organisms, telomerase is the main mechanism for telomere elongation. In telomerase-proficient cells telomere length is a tightly regulated process. The average telomere length in a population will not vary, irrespective of the number of times it is propagated. In the unicellular organism, *S. cerevisiae,* in which telomerase is constitutively active, the average telomere length is ~350bp (Shampay et al. 1994). This is a result of a not fully understood balance. Both critically short and significantly long telomeres are detrimental to the cell, so understanding this tightly controlled process is crucial.

The protein counting model:

The major pathway of telomere elongation involves telomeric sequence addition by the enzyme telomerase. The prevailing model for the regulation of telomere length involves limited telomerase access to the ends of chromosomes. The Shore lab proposed the "protein counting model" to explain how telomerase

preferentially elongates the shortest telomeres in budding yeast, and this model has dominated the field for 15 to 20 years. This model describes a sensing mechanism able to regulate different modes of telomerase elongation in short versus average to long telomeres. Specifically, the model states that a trimeric complex made up of Rap1, Rif1, and Rif2 works in a negative feedback loop to maintain telomere length (Marcand et al. 1997), specifically by inhibiting telomerase access to telomeres. Duplex telomeric DNA is bound by multiple Rap1 proteins (only shelterin component found in yeast) and its two associated factors, Rif1 and Rif2. The deletion or impairment of components of this complex results in the over elongation of telomeres to varying degrees: *rif1*-Δ 0.5-1kb, and *rif2*-Δ 0.35-0.5kb (Hardy et al. 1992; Wotton & Shore 1997, respectively). Therefore, it was suggested that the bound complexes act to inhibit telomere elongation by telomerase. Long telomeres bound with multiple complexes inhibit telomerase, and short telomeres with less bound complex are unable to inhibit telomerase, and are subsequently elongated.

The protein model involves many other proteins in its suggested regulation mechanisms. Cdc13, the major component of the t-RPA complex, is responsible for telomerase recruitment (Nugent et al. 1996). This activity was proposed to be dependent on phosphorylation of the recruitment domain of Cdc13 by the kinase Tel1 (homolog of mammalian ATM). Tel1 interacts with Xrs2, a member of the MRX complex (Mre11-Rad50-Xrs2), to localize to DNA ends. Rif2 protein is thought to compete with Tel1 for binding of the C-terminal domain of Xrs2 (Hirano et al. 2009),

so that an abundance of Rif2 will inhibit Tel1 recruitment and subsequent Cdc13 phosphorylation and telomerase action.

The strength of this model is questioned by a number of conflicting data. In 2013, the Lundblad lab showed that combining a *rif2*-Δ mutation and *tlc1*-Δ (the RNA component of telomerase) had an additive effect on replicative senescence (Ballew & Lundblad 2013). This is contrary to what would be expected if these two were functioning in the same pathway. A set of experiments that tested the effect of eliminating every potential Tel1 target for phosphorylation on Cdc13, showed almost normal telomere length (Gao et al. 2010). Again, conflicting the proposed mechanism of protein counting model. Additionally, a high-resolution analysis of a specific telomere (Chr. 1L) from a multiple isolates of *rif2*-Δ, showed a very different pattern of telomere length than what was originally reported. While the expected overly elongated telomeres were observed, an unexpected population of short, and ultra short telomeres was also present (discussed in detail in Chapter 3).

Telomere shortening pathways:

The other side of telomere length homeostasis is telomere shortening. Most somatic cells have little to no telomerase activity. Telomerase acts at only 7% of telomeres during each cell cycle (Teixeira et al. 2004), so mechanisms independent of telomerase, and specifically shortening mechanisms, are equally important to genome stability and cell viability. The significance of telomerase-independent mechanisms is evident in the broad range of age-dependent characteristics exhibited by members of a family with an identical inherited mutation in the catalytic domain of telomerase

(Alder et al. 2011). Multiple lines of data argue that there are more than one shortening pathways acting at telomeres and that telomere shortening significantly contributes to telomere length heterogeneity. An established mechanism for telomere loss is that which occurs as a consequence of semi-conservative replication (discussed in the end replication problem). In addition, mature telomeres must undergo modification to generate the 3' single strand overhang. This is not a result of telomerase elongation of the 3' end (Dionne & Wellinger 1996), and therefore it is proposed that resection of the 5' end is carried out by a 5'-3' nuclease. The work described in this thesis will show that a very complex network of genes controls the regulation of replicative senescence (an outcome telomere shortening) in the absence of telomerase (Chapter 2) and define another mechanism for telomere shortening that was previously underappreciated, which is directly related to the replication of duplex telomeric DNA (Chapter 3).

Telomere Replication

Telomeres are made up of mostly double stranded telomeric DNA, terminating with a single stranded G-rich 3' end. As discussed earlier, the maintenance of telomere length is crucial to cell viability. At each round of replication telomeric DNA is lost as a consequence of semi-conservative replication. While telomerase is responsible for telomere elongation (by addition to the 3' strand) most of telomere replication (double stranded telomeric DNA) is carried out by the conventional replication machinery. The intrinsic complexity of telomeric DNA challenges the progression of the replication machinery causing replication stress, fork regression, and fork collapse

(Fouche et al. 2006, Sfeir et al. 2009). Therefore, efficient replication of telomeric DNA at every cell cycle must be maintained. Due to the unique sequence composition and location of telomeres, the cell must have robust mechanisms to ensure efficient telomere replication or have a mechanism that counterbalances this increased vulnerability at telomeres.

Telomeric DNA is made up repetitive TG rich repeats (hexameric repeats in humans) and has been shown to causes replication stress at the natural occurring end of the chromosome, when placed interstitially, and when cloned into a plasmid (Ohki & Ishikawa 2004; Bosco & de Lange 2012; Edwards et al. 2014; Paschini & Reyes et al. in review). This suggests that the stress on replisome can be attributed, at least partly, to the telomeric DNA itself. Difficult to replicate repetitive DNA is not exclusive to telomeres; indeed fragile sites exist throughout the genome. But unlike genomic fragile site, a converging replication fork cannot rescue a stalled replication fork at the end of the chromosome. In humans and mice, replication initiates in the subtelomeric region, and seldom in the actual telomere (Sfeir et al. 2009; Drosopoulos et al. 2012; Drosopoulos et al. 2015). In yeast there is no evidence for ARS in the telomeric region, they are located in the subtelomeric regions (in X or Y' elements, Chan et al. 1983) and are responsible for facilitating replication to the end of the chromosome.

In addition to sequence composition of telomeres, the architecture of telomeres is also thought to be a challenge to telomere replication. It is proposed that the conformation of telomeric chromatin (t-loops, d-loops, and G-quartets) stall fork

progression. Proteins with helicase activity have been implicated in the resolution of these secondary structures, and are therefore essential for efficient telomere replication. In *S. cerevisiae*, the 5' to 3' helicase Rmr3 was shown to play a role in replication fork progression through both subtelomeric and telomeric DNA (Ivessa et al. 2002). In humans, RecQ helicases WRN and BLM, are both necessary for efficient telomere replication (Crabbe et al. 2004; Barefield & Karlseder 2012). Defects in BLM and WRN are both associated with premature ageing disease, highlighting the importance of telomere replication mechanisms to human health.

In yeast, the trimeric complex made up of Cdc13, Stn1, and Tel1 was originally proposed to function as an end-binding factor whose role is to protect telomere ends from degradation. In 2007, while studying the structural and biochemical similarities between this complex and RPA, the Lundblad lab proposed that this complex was a telomere dedicated paralog of RPA, and termed it the t-RPA (Gao et al 2007). This was the start of a new model for telomere length homeostasis, where the t-RPA complex serves to ensure efficient replication through telomeric DNA (Paschini 2015, Paschini & Reyes et al. in review). This mounting data suggests that efficient telomere replication contributes significantly to telomere length homeostasis, and therefore genomic stability.

Telomere length analysis

Telomere homeostasis is a major contributor to the health and genomic integrity of the cell, and is maintained by a balance of shortening and lengthening mechanisms. Telomere length that is either too long or too short have both been shown

to have significant effects on human health (reviewed by Bernardes & Blasco 2013). For these reasons it important to have reliable methods to measure telomere length. Current methods vary in resolution, and in their advantages and drawbacks. So much of what we know about telomere biology and telomere phenotypes has been established on the backs of earlier assays. A lot of the discoveries detailed in this thesis come from the modification of established assays and the development of new ones.

Telomere restriction fragment (TRF) analysis:

One of the first, and most exploited methods to measure telomere length is through terminal restriction fragment (TRF) analysis. This protocol uses a modified southern blot technique, and involves exposing genomic DNA to extensive restriction digest (Allshire et al. 1989; Harley et al. 1990). Telomeres are unlike the rest of the genome in that their DNA is made up of repetitive TG sequences. Through the use of a specific enzyme, or a cocktail of restriction enzymes, that lack recognition sites for telomeric DNA (and some subtelomeric), telomeres can be isolated from the rest of the genome. The freshly digested DNA fragments are resolved by size through agarose gel electrophoresis. Telomere fragments are visualized using either radioactive probes, or chemiluminescent probes. The results resemble a broad band, or smear, that corresponds to the heterogeneous range of telomere lengths within a cell population. This method can be used with any eukaryotic cells as long as restriction enzymes can be found to isolate telomeres. The integrity of the extracted DNA must be maintained. Degradation of DNA can lead to misleading results, skewing the data towards short

fragments. Because the telomeric signal is a result of binding between telomeric DNA and probe, longer fragments undoubtedly bind more probes. This creates a condition for size bias, wherein smaller fragments and smaller populations of telomeres emit significantly less probe and therefore less signal. The results obtained with this method also give no insight into individual telomere length, just bulk telomere length. A detail, that is not without significance. A number of studies have proposed that even a small number (sometimes just one) of critically short telomeres are associated with cellular senescence (Abdallah et al. 2009; Henmann et al. 2001). Much of what has been established about telomere length has been a result of TRF analysis. It remains a dependable assay for reproducibly measuring telomere length, and has been the gold standard in the field. Modifications to improve its sensitivity have been developed, like in-gel hybridization and the applications of programs that analyze band intensities (Gohring et al. 2014).

PCR based methods for telomere length analysis:

Unlike the previous method, PCR based telomere length analysis requires very small amounts of DNA (nanograms vs. micrograms needed for TRF). Over 15 years ago, the Lingner lab developed a terminal transferase-mediated PCR method that could amplify a genetically marked *S. cerevisiae* telomere (Förstemann et al. 2000). The first part of this process involves tailing telomeres with C-tails (dCTP in the presence of terminal deoxynucleotidyl transferase). Later, using a G-oligo that binds the C-tail, and an oligo that binds the subtelomeric region of an individual telomere, allows the amplification of a specific telomere out of a population of many. The

amplified telomeres are resolved by size through agarose gel electrophoresis. Individual amplified telomeric molecules are subsequently sequenced. This method has the advantage of yielding not only telomere length data, but data with single nucleotide level resolution for an individual telomere. In the initial experiments, the specific telomere amplified was genetically marked with an inserted *ADE2* gene upstream of chromosome V. Since then, this protocol has been successfully used to additionally amplify chromosome 1L and 6R (Teixeira et al. 2004; Chang et al. 2007; Claussin & Chang 2016, Paschini & Reyes et al. in review). In recent years, the Lundblad lab has made substantial modifications to this protocol to generate an extensive amount of high-resolution data on a number of different genetic backgrounds. This type of analysis has enabled us to make paradigm shifting discoveries.

In 2003 Baird et al. described another PCR based assay for the amplification of individual chromosome ends in human cells. A "telorette" linker, made up of TTAGGG homology and an additional 20 bases of non-homologous sequence, is annealed to the 5' end using the G–rich overhang as a template. After the telorette is ligated to the 5'end, the PCR reaction is accomplished using an oligo with homology for the upstream region of a specific chromosome end and an oligo with homology to the telorette (teltail). This method, like the last, is limited to a small number of chromosome ends, due to the lack of suitable subtelomeric sequences for oligo design. This assay has been successfully used to amplify human chromosome ends Xp, Yp, 12q and later 2p, 11q, and 17p (Baird et al. 2003; Britt-Compton et al. 2006,

respectively). The PCR products are resolved by agarose gel electrophoresis and then visualized through Southern hybridization with a telomere specific probe. This method has improved sensitivity over TRF analysis, and has been used to assess if individual telomeres adhere to the telomere length pattern observed by TRF analysis of the population of telomeres.

PCR based methods to measure telomere length are not limited to the two mentioned above. A number of quantitative PCR methods have also been developed: quantitative PCR, monochrome multiplex quantitative PCR, and absolute telomere length PCR. Quantitative PCR telomere length measurement involves using oligos that anneal to the C-strand and the G-strand of telomeres (Cawthon 2002; Cawthon 2009; O'Callaghan & French 2010, respectively). The quantification of telomere length involves comparing the amplification product of telomeres (T) to that of a single copy gene (S). Again this gives a value for total telomere length of the population, and does not specify individual telomere length.

Fluorescent labeling of telomeres:

Lastly, there are quantitative methods that use fluorescence labeled telomere specific probes to measure telomere length; quantitative fluorescence *in situ* hybridization (Q-FISH). This method uses labeled peptide nucleic acid oligonucleotides $(CCCTAA)_3$ to hybridize to $(TTAGGG)_n$ targets (telomeres), that can then be visualized using fluorescent microscopy (Lansdrop et al. 1996; Poon et al. 1997; Zijlmans et al. 1997). Using this method you can detect telomeric repeats for specific chromosome ends (p or q arm) in a samples made up of <30 cells. Q-FISH is

capable of detecting telomeric repeats below 0.1kb, and therefore can quantify critically short telomeres. This type of assay has been useful in detecting individual telomere length, fusions, and differences in telomere between two distinct populations (cancerous vs. non-cancerous). Modifications have been made to this assay to allow for high throughput analysis of telomere length (Canela et al. 2007). Similar to Q-FISH, flow cytometry fluorescence *in situ* hybridization (Flow-FISH) combines the use of PNAs with flow cytometry (Rufer et al. 1998). This method allows for the analysis of thousands of cells in a short period of time. However, unlike Q-FISH, the telomere length read out is an average telomere length.

REFERENCES

Abdallah P, Luciano P, Runge K, Lisby M, Geli V, Gilson E & Teixiera T (2009) A two-step model for senescence triggered by a single critically short telomere. *Nat Cell Biol* 8, 988-993.

Alder JK, Cogan JD, Brown AF, Aderson CJ, Lawson WE, Landsdorp PM, Phillips JA III, Loyd JE, Chen JJ & Armanios M (2011) Ancestral mutation in telomerase causes defects in repeat addition processivity and manifests as familial pulmonary fibrosis. *PLOS Genet.* 7, e1001352.

Allshire RC, Dempster M & Hastie ND (1989) Human telomeres contain at least three types of G-rich repeats distributed non-randomly. *Nucleic Acids Res.* 17, 4611-4627.

Armanios M & Blackburn EH (2012) The telomere syndromes. *Nat Rev. Genet.* 13, 693-704.

Baird DM, Rowson J, Wyngord-Thomas D & Kipling D (2003) Extensive allelic variation and ultrashort telomeres in senescent human cells. *Nat Genetics* 33, 203-207.

Ballew B & Lundblad V (2013) Multiple genetic pathways regulate replicative senescence in telomerase-defective yeast. *Aging Cell*. 12, 719-727.

Barefield C & Karlseder J (2012) The BLM helicase contributes to telomere maintenance through processing of late-replicating intermediate structures. *Nucleic Acid Res*. 40, 7358-7367.

Bernardes de Jesus B & Blasco MA (2013) Telomerase at the intersection of cancer and aging. *Trends Gen* 9, 513-1520.

Britt-Compton B, Rowson J, Locke M, Mackenzie I, Kipling D & Baird D (2006) Structural stability and chromosome-specific telomere length is governed by cis-acting determinants in humans. *Hum Mol Genetics* 15, 725-733.

Bosco N & de Lange T (2012) A TRF1-controlled common fragile site containing interstitial telomeric sequences. *Chromosoma* 121, 465-474.

Canela A, Vera E, Klatt P & Blasco MA (2007) High-throughput telomere length quantification by FISH and its application to human population studies. *PNAS* 104, 5300-5305.

Cawthon RM (2002) Telomere measurement by quantitative PCR. *Nucleic Acid Res.* 30, e47.

Cawthon RM (2009) Telomere length measurement by novel monochrome multiplex quantitative PCR method. *Nucleic Acid Res.* 37, e21.

Chan CS & Tye BK (1983) Organization of DNA sequences and replication origins at yeast telomeres. *Cell* 33, 563-573.

Chang M, Arneric M & Lingner J (2007) Telomerase repeat addition processivity is increased at critically short telomeres in a Tel1-dependent manner in *Saccharomyces cerevisiae*. *Genes & Development* 21, 2485-2494.

Claussin C & Chang M (2016) Multiple Rad52-mediated homology-directed repair mechanisms are required to prevent telomere attrition-induced senescence in *Saccharomyces cerevisiae*. *PLOS Genetics* 12, e1006176.

Crabbe L, Verdun RE, Haggblom CI & Karlseder J (2004) Defective telomere lagging strand synthesis in cells lacking WRN helicase activity. *Science* 306, 1951-1953.

de Lange T (2009) How telomeres solve the end-protection problem. *Science* 326, 948-952.

Dionne I & Wellinger RJ (1996) Cell cycle-regulated generation of single-stranded G-rich DNA in the absence of telomerase. *PNAS* 93, 13902-13907.

Drosopoulos WC, Kosiyatrakul ST, Yan Z, Calderano SG & Schildkraut CL (2002) Human telomeres replicate using chromosome-specific, rather than universal, replication programs. *J. Biol. Chem.* 197, 253-266.

Drosopoulos WC, Kosiyatrakul ST, & Schildkraut CL (2015) BLM helicase facilitates telomere replication during leading strand synthesis of telomeres. *J. Biol. Chem.* 210, 191-208.

Edwards DN, Machwe A, Wang Z & Orren DK (2014) Intramolecular telomeric G-quadruplexes dramatically inhibit DNA synthesis by replicative and traslesion polymerases, revealing their potential to lead to genetic change. *PLoS One* 9, e80664.

Förstemann K, Höss M & Lingner J (2000) Telomerase-dependent repeat divergence at the 3' ends of yeast telomeres. *Nucleic Acids Res.* 28, 2690-2694.

Fouché N, Özgür S, Roy D & Griffith JD (2006) Replication fork regression in repetitive DNAs. *Nucleic Acid Res.* 34, 6044-6050.

Gao H, Cervantes RB, Mandell EK, Otero JH & Lundblad VL (2007) RPA-like proteins mediate yeast telomere function. *Nature* 14, 208-214.

Gohring J, Fulcher N, Jacak J & Riha K (2014) TeloTool: a new tool for telomere length measurement from terminal restriction fragment analysis with improved probe intensity correction. *Nucleic Acid Res* 42, e21.

Greider CW & Blackburn EH (1985) Identification of a specific telomere terminal transferase activity in Tetrahymena extracts. *Cell* 43, 405-413.

Hande MP, Samper E, Lansdrop P & Blasco M (1999) Telomere length dynamics and chromosomal instability in cells derived from telomerase null mice. *JCB*. 144, 589-601.

Hardy CFJ, Sussel L & Shore D (1992) A RAP1-interacting protein involved in transcriptional silencing and telomere length regulation. *Genes and Dev.* 6, 801-813.

Harley CB, Futcher AB & Greider CW (1990) Telomeres shorten during ageing of human fibroblast. *Nature* 345, 458-460.

Hayflick L & Moorhead PS (1961) The serial cultivation of human diploid cell strains. *Exp. Cell Res.* 25, 585-621.

Hemann M, Strong M, Hao L & Grieder C (2001) The shortest telomere, not the average telomere length, is critical for cell viability and chromosome stability. *Cell* 107, 67-77.

Hirano Y, Fukunaga K & Sugimoto K (2009) Rif1 and Rif2 inhibit localization of Tel1 to DNA ends. *Cell* 33, 312-322.

Hughes TR, Weilbaecher RG, Walterscheid M, & Lundblad VL (2000) Identification of the single-stranded telomeric DNA binding domain of the Saccharomyces cerevisiae Cdc13 protein. *PNAS* 97, 6457-6462.

Ivessa AS, Zhou JQ, Schulx VP, Monson EK & Zakian VA (2002) Saccharomyces Rmr3p, a 5' to 3' DNA helicase that promotes replication fork progression through telomeric and subtelomeric DNA. *Genes and Dev.* 16, 1383-1396.

Jasin M & Rothstein R (2013) Repair of strand breaks by homologous recombination. *Cold Spring Harbor Perspect. Biol.* 5, a012740.

Kim NW, Piatyszek MA, Prowse KR, Harley CB, West MD, Ho PL, Covillo GM, Wright WE, Weinrich SL & Shay JW (1994) Specific association of human telomerase activity with immortal cells and cancer. *Science* 266, 2011-2015.

Lansdrop PM, Verwoerd NP, van de Rijke FM, Dragowska V, Little MT, Dirks RW, Raap AK & Tanke HJ (1996) Heterogeneity in telomere length of human chromosomes. *Human Molecular Genetics*. 5, 685-691.

Lazzerini D & de Lange T (2007) Protection of telomeres through independent control of ATM and ATR by TRF2 and POT1. *Nature* 448, 1068-1071.

Lendvay TS, Morris DK, Sah J, Balasubramanian B & Lundblad V (1996) Senescence mutants of Saccharomyces cerevisiae with a defect in telomere replication identify three additional EST genes. *Genetics* 144, 1399-1412.

Li B, Oestreich S & de Lange T (2000) Identification of human Rap1: implications for telomere evolution. *Cell* 101, 471-483.

de Lange T (2005) Shelterin: the protein complex that shapes and safeguards human telomeres. *Genes and Dev.* 19, 2100-2110.

Marcand S, Gilson E & Shore D (1997) A protein-counting mechanism for telomere length regulation in yeast. *Science* 275, 986-990.

McEachern MJ & Blackburn EH (1994) A conserved sequence motif within the exceptionally diverse telomeric sequences of budding yeast. *PNAS* 91, 3453-3457.

Nugent CI, Hughes TR, Lue NF & Lundblad V (1996) Cdc13p: a single-strand telomeric DNA-binding protein with a dual role in yeast telomere maintenance. *Science* 274, 249-252.

O'Callaghan NJ & French M (2011) A quantitative PCR method for measuring absolute telomere length. *Biol Proceed Online*. 13:3.

Ohki R, Ishikawa F (2004) Telomere-bound TRF1 and TRF2 stall the replication fork at telomeric repeats. *Nucleic Acid Research* 32, 1627-1637.

Ohki R, Tsurioto T & Ishikawa F (2001) In vitro reconstitution of the end replication problem. *Mol Cell Biol.* 17, 5753-5766.

Olovnikov AM (1973) A theory of marginotomy. The incomplete copying of template margin in enzymic synthesis of polynucleotides and biological significance of the phenomenom. *J. Theor. Biol.* 41, 181-190.

Poon SS, Martens UM, Ward RK & Lansdrop PM (1999) Telomere length measurements using digital fluorescence microscopy. *Cytometry* 36, 267-278.

Rufer N, Dragowska W, Thornbury G, Roosnek E & Lansdrop PM (1998) Telomere length dynamics in human lymphocyte subpopulations measured by flow cytometry. *Nat Biotechnol.* 16, 743-747.

Sakabe K & Okazaki R (1966) A unique propertiy of the replicating region of chromosomal DNA. *Biochim Biophys. Acta.* 129, 651-654.

Sfeir A, Kosiyatrakul ST, Hockemeyer D, MacRae SL, Karlseder J, Schildkraut CL & de Lange T (2009) Mammalian telomeres resemble fragile sites and require TRF1 for efficient replication. *Cell* 138, 90-103.

Shampay J, Szostak JW & Blackburn EH (1984) DNA sequences of telomeres maintained in yeast. *Nature* 310, 154-157.

Teixeira MT, Arneric M, Sperisen P & Ligner J (2004) Telomere length homeostasis is achieved via a switch between telomerase- extendible and –nonextendible states. *Cell* 117, 323-335.

Watson JD (1972) Origin of concatemic T7 DNA. *Nature New Biol.* 239, 197-201.

Wotton D & Shore D (1997) A novel Rap1-interacting factor, Rif2p, cooperates with Rif1p to regulate telomere length in *Saccharomyces cerevisiae*. *Genes and Dev.* 11, 748-760.

Zijlmans JM, Martens UM, Poon SS, Raap AK, Tanke HJ, Ward RK, & Landsdrop (1997) Telomeres in the mouse have large inter-chromosomal variations in the number of T2AG3 repeats. *PNAS*. 14, 7423-7428.

CHAPTER TWO:

Multiple pathways contribute to replicative senescence in the absence of telomerase

Replicative senescence is a consequence of the gradual decline in telomere length that occurs when the enzyme telomerase is inactive. Most human tissue has little to no telomerase activity, and therefore is susceptible to this process. Accelerated replicative senescence has been implicated in cellular aging and a number of human diseases. It has also been shown that this process is under the control of multiple pathways and genetic factors. In this chapter a genetic approach was taken to investigate the regulatory pathways that underlie replicative senescence in the absence of telomerase, using the budding yeast *S. cerevisiae*. This work was initiated by previous graduate students Hao Gao and Bari Ballew. They contributed to establishing a new assay to monitor replicative senescence in the Lundblad lab that revealed that the replicative capacity of telomerase-defective yeast is under the control of multiple pathways (Gao et al. 2007; Ballew & Lundblad 2013). Specifically, the MRX (Mre11-Rad50-Xrs2) complex and its negative (Rif2) and positive (Tel1) regulators comprise a single pathway that promotes replicative senescence, in a way that recapitulates how these proteins act in the resection of DNA ends. In contrast, the Rad51 recombinase acts in a separate opposing pathway to MRX in replicative senescence, unlike its role downstream of MRX at double stranded break repair.

In this chapter, I expand this network by showing that the 9-1-1 complex affects replicative senescence by acting upstream of Rad51, and that Rad52 plays a comparable/redundant role to Rad51. Additionally, my preliminary work suggests that Upf1 contributes to another independent pathway that acts as a positive regulator of replicative senescence.

INTRODUCTION

Most cells cannot divide indefinitely. This limitation on replicative lifespan was first described over 50 years ago by Hayflick & Moorhead (1961) who demonstrated that human fibroblast gradually, but inevitably lose the ability to proliferate in culture. This loss of replicative capacity is linked to the loss of telomeric repeats, earning telomeres the designation as the cell's "mitotic clock". During cell division, telomeres continuously shorten, due to incomplete duplex DNA replication (the end-replication problem; Watson 1972) and eventually telomere length falls below a threshold. Cells will then irreversibly exit from the cell cycle, and lose their proliferative capability, a process called replicative senescence. This is a fundamental feature of somatic cells, with the exception of tumor and stem cells. The loss of sequence can be counterbalanced by addition of new telomeric repeats by the enzyme telomerase (Grieder & Blackburn 1985). In most cells there is little to no telomerase activity (Kim et al. 1994) and telomeres will progressively shorten. This eventual block to cell division is particularly important in tissues that require continual replenishment during human lifespan. The contribution of short telomeres to a wide variety of age-dependent pathophysiologies has led to the concept that a number of late-in-life clinically distinct diseases have a common mechanism that has been termed "syndromes of telomere shortening" or "telomeropathies (Armanios 2009; Armanios & Blackburn 2012). These clinical studies have also shown that patients who inherit mutations in telomerase or other telomere-associated proteins (such as subunits of the shelterin complex) are pre-disposed to these syndromes of telomere shortening.

However, it is clear that factors other than telomerase or shelterin can also influence the proliferative ability of human cells undergoing telomere shortening. Prior studies published by Ballew & Lundblad (2013) showed that multiple genetic pathways regulate replicative senescence in telomerase-deficient yeast.

This chapter continues this prior study of the proliferative capacity of cells that lack telomerase (by elimination of the RNA sub-unit) and genes that modulated this property. Multiple studies involving telomerase-deficient cells have focused on the ability of a proportion of the population to escape senescence, through recombination. This alternative pathway for telomere maintenance occurs at the later stages of senescence when cellular viability has significantly decreased (Lundblad & Blackburn 1993). This chapter is focused instead on the early stages of replicative senescence, when cells have just lost telomerase activity. In yeast, senescence is commonly measured by observing how individual cells form colonies at various generations (Lundblad & Szostak 1989; Rizki & Lundblad 2001). Initially, there is no distinguishable difference between the colony forming ability of newly generated telomerase-deficient yeast and a telomerase-proficient yeast strain. However, the decline in viability becomes detectable by approximately 50 generation, as evidenced by an increase in the number of individual cells that no longer give rise to full-sized colonies. By 75-100 generations, the majority of cells are unable to undergo sufficient cell divisions to form a colony.

While every telomerase deficient strain senesces, there is significant isolate-to-isolate variation in the senescence progression even among isogenic isolates. This can

be attributed to the variability of telomere loss of multiple chromosomes during each cell division. This is a major obstacle when trying to accurately and reproducibly monitors senescence, as the variability is substantial enough to mask results. To deal with this, prior work in the Lundblad lab established a semi-quantitative assay for senescence (Rizki & Lundblad 2001, Gao et al. 2010) that was shown to reproducibly monitor senescence in both individual genetic backgrounds as well as the epistatic relationships present. The semi-quantitative assay used for all the analysis in this chapter was described in previous publications (Rizki & Lundblad 2001; Gao et al. 2010; Ballew & Lundblad 2013) and is described in detail in Figure 2.2. The key features of the protocol are the inclusion of a very large number of samples for each genotype, genotype-blind scoring, and statistical analysis of the difference between *tlc1*-Δ vs. *tlc1*-Δ *geneX*-Δ. This comparison is restricted to isolates derived from the same parental diploid, an important yet overlooked flaw of previous assays (discussed further, below). All these improvement in how replicative senescence is quantified allows the identification of both inhibiting and promoting pathways on replicative senescence.

Through the use of this assay, two separate, and opposing, pathways have been identified that regulate senescence (Ballew & Lundblad 2013; Figure 2.1). One group of genes (MRX, *TEL1* and *RIF2*) acts in one pathway to regulate senescence, whereas a second pathway works through Rad51 and opposes the effects of MRX-Tel1-Rif2. My focus was to extend these initial results by identifying other factors that affect the progression of senescence, and determining whether they would fall into previously

identified pathways, or additional independent pathway(s). This epistasis map relies on senescence data, an indirect measurement of telomere length. The results of this type of analysis could then be used to drive future experiments using new assays developed in the lab that use a direct measurement of telomere length (discussed in Chapter 3 and 4). The end goal is to connect what I discover about the genetic networks that impact replicative senescence with specific molecular mechanisms that effect telomere length homeostasis.

RESULTS

The 9-1-1 complex contributes to replicative senescence

There have been many parallels drawn between DSBs and telomeres. To study these parallels, a number of DNA damage response genes were included in the list of candidates that contribute to replicative senescence in the absence of telomerase. The heterotrimeric 9-1-1 complex (Rad9-Rad1-Hus1 in fission yeast and humans and Ddc1-Rad17-Mec3 in budding yeast) is involved in early response to DNA damage (Volkmer et al. 2000; Majka & Burgers 2003). This complex forms a clamp that is structurally similar to that of replication clamp PCNA. I tested two 9-1-1 complex components for their effects on replicative senescence. Following dissection of a *tlc1*-Δ/*TLC1* strain bearing an additional mutation of interest (*mec3*-Δ or *rad17*-Δ), multiple isolates of each genotype were propagated as single colonies for ~25, ~50, and ~75 generations. Growth characteristic for each isolate was assessed on a scale of 1 (maximal senescence) to 5 (equivalent to wild-type), always genotype blind. The

results were plotted as either a histogram summarizing the growth scores of the complete dataset for each genotype (as shown in Figure 2.3 A for *tlc1*-Δ vs *tlc1*-Δ *mec3*-Δ) or as a graph of relative senescence where the average growth score for *tlc1*-Δ *geneX*-Δ was compared with the average growth score for *tlc1*-Δ (Figure 2.3 B). In both cases, a defect in a component of the 9-1-1 complex, in the absence of a functional telomerase, resulted in an attenuation of replicative senescence (relative to *tlc1*-Δ). The comparison of 43 *tlc1*-Δ and 43 *tlc1*-Δ *mec3*-Δ isolates showed that a loss of *MEC3* attenuated senescence, with a statistically significant difference at ~75 generations (p <0.001). Similarly, the comparison of 22 *tlc1*-Δ and 32 *tlc1*-Δ *rad17*-Δ isolates showed that loss of *RAD17* attenuated senescence (statistical significance at both ~50 and ~75 generations, p <0.001). Additionally the effects on senescence were tested in the absence of *RAD24*, the 9-1-1 clamp loader (Figure 2.3 B, blue) and again an attenuated senescence was observed (p <0.05 at ~75g). This argues that the 9-1-1 complex is performing a function at telomeres that contributes to the decline in replicative capacity in telomerase-deficient cells, so that when it is absent senescence is significantly attenuated.

The 9-1-1 complex functions in a pathway separate from the MRX-Tel1-Rif2 pathway

To study the epistatic relationship between the 9-1-1 complex and those genes implicated in the current epistasis map, growth characteristics were compared between isolates defective for a component of the 9-1-1 complex and a components of the MRX-Tel1-Rif2 epistasis arm. A defect in the MRX complex results in reduced

resection at both DSBs and telomeres (Bonetti et al. 2010). Previous results showed that the deletion of either *MEC3* (9-1-1 complex) or *RAD50* (MRX complex) conferred an attenuated senescence in a telomerase defective background. Surprisingly, when the growth characteristics of 16 *tlc1*-Δ *rad50*-Δ*,* 16 *tlc1*-Δ *mec3*-Δ and 19 *tlc1*-Δ *mec3*-Δ *rad50*-Δ isolates were compared to *18 tlc1*-Δ isolates*,* the significant alleviation of senescence seen in the doubles was attenuated in the *tlc1*-Δ *mec3*-Δ *rad50*-Δ. While there was still a pattern of alleviated senescence in the triple, it was not to the same degree as in the doubles. The alleviated senescence was significant at 75 generation for both doubles (p <0.01) and not significant for the triple (p = 0.07, Figure 2.4 A).

In response to this result, I turned my attention the upstream inhibitor of MRX. Earlier work showed that Rif2 and the MRX complex function in the same pathway in a telomerase defective background, with Rif2 acting as an inhibitor of MRX (Figure 2.2 A). To probe the role of the 9-1-1 complex in relation to Rif2, 22 *tlc1*-Δ *mec3*-Δ*, 23 tlc1*-Δ *rif2*-Δ*,* and 31 *tlc*-Δ *mec3*-Δ *rif2*-Δ isolates were monitored for their effects on growth characteristics, compared to 30 *tlc1*-Δ isolates (Figure 2.5 B). Previously, an accelerated senescence was observed when *RIF2* was absent, whereas the absence of *MEC3* resulted in attenuated senescence, in a telomerase-defective background. In this case I combined mutations that give opposite effects. The result was an intermediate senescence phenotype. Notably, the *tlc*-Δ *mec3*-Δ *rif2*-Δ isolates still show a significant effect on relative senescence at 75 generations when compared to *tlc1*-Δ (p = 0.03), but not nearly as significant as the accelerated senescence seen in

tlc1-Δ *rif2*-Δ at 75 generations (p = 0.000001), or the significant attenuation in senescence seen in *tlc1*-Δ *mec3*-Δ (p = 0.0004). These results suggest that Mec3 and Rif2 are in distinct and opposing pathways.

Left untested was the relationship between the 9-1-1 complex and Tel1. Tel1 is a well recognized telomere effector protein, with effects in both telomerase-proficient and telomerase-defective background. Previous studies in our lab showed that its role as a positive effector on the MRX complex in DSB repair is recapitulated in replicative senescence. A defect in Tel1 has also been shown to delay the senescence of a telomerase-defective strain by multiple labs (Ritchie et al 1999; Gao et al. 2010; Chang & Rothstein 2011). To test for possible combined effects with the 9-1-1 complex, again two components of the 9-1-1 complex (Rad17 or Mec3) were mutated in combination with Tel1, in a telomerase-defective background. Initially, an experiment comparing the growth characteristics of 34 *tlc1*-Δ *mec3*-Δ, 20 *tlc1*-Δ *tel1*-Δ, 30 *tlc1*-Δ *mec3*-Δ *tel1*-Δ isolates, to 26 *tlc1*-Δ isolates gave conflicting results. The expected alleviated senescence of the *tlc1*-Δ *mec3*-Δ was lost, but the alleviated senescence of *tlc1*-Δ *tel1*-Δ remained (Figure 2.5 A). This phenomenon was also observed in a comparable experiment with another member of the 9-1-1 complex, Rad17. 35 *tlc1*-Δ, 24 *tlc1*-Δ *rad17*-Δ, 20 *tlc1*-Δ *mec3*-Δ, and 16 *tlc1*-Δ *mec3*-Δ rad17-Δ were monitored (Figure 2.5 B). In both cases, the differences in relative senescence of *tlc1*-Δ *mec3 or tlc1*-Δ *rad17*-Δ double mutant isolates were insignificant at every generation (25-75g). This inconsistency may be due to the starting length of telomeres in the parental diploid strains. Former studies have shown that the deletion of a copy

of *TEL1* has an effect on telomere length even in the presence of a wild type copy (Abdallah et al. 2009), a condition termed haploinsufficiency. Experiments show the senescence of a *tlc1*-Δ derived from a *tlc1*-Δ/TLC *tel1*-Δ/TEL1 strain had an accelerated senescence phenotype when compared to the senescence phenotype of a *tlc1*-Δ derived from a *tlc-1Δ/TLC1* strain. This is not Tel1-specific, as similar effects can be seen in the absence of Rif1. A *RIF1* deletion confers an elongation of telomeres, and *tlc1*-Δ isolates derived from *tlc-1Δ/TLC rif1*-Δ*/RIF1* senesce slower than those derived from a diploid strain with two copies of *RIF1*. The sizeable disparity in relative senescence of *tlc1*-Δ *mec3*-Δ or *tlc1*-Δ *rad17*-Δ strains, derived from a parental diploid containing *tel1*-Δ/TEL1 and one with two copies of *TEL1* is illustrated in Figure 2.5. One possibility is that the 9-1-1 complex might be restricted to events that act early in senescence, so that in a strain that has already undergone a degree of telomere shortening, the alleviation of replicative senescence is lost.

Alternatively, the attenuation of senescence in *tlc1*-Δ *tel1*-Δ isolates was reproducible. When compared to the triple mutant (either *tlc1*-Δ *mec3*-Δ *tel1*-Δ *or tlc1*-Δ *rad17*-Δ *tel1*-Δ) the alleviated senescence of *tlc1*-Δ *tel1*-Δ was significantly decreased, at 50 generations ($p < 0.05$) for *tlc1*-Δ *mec3*-Δ *tel1*-Δ and at both 50 and 75 generations for *tlc1*-Δ *rad17*-Δ *tel1*-Δ ($p < 0.01$). Despite the discrepancies in the pattern of senescence of *tlc1*-Δ *rad17*-Δ and *tlc1*-Δ *mec3*-Δ, these results, along with those attained with Rad50 and Rif2, point to the 9-1-1 complex acting in a distinct, and possibly opposite, pathway to the MRX-Rif2-Tel1 pathway.

The 9-1-1 complex works upstream of Rad51, as an inhibitor, to regulate replicative senescence

To determine the relationship between the 9-1-1 complex and the other major arm of our epistasis map (Rad51), growth characteristics were compared between a isolates defective for a component of the 9-1-1 complex and Rad51, in the absence of telomerase. Earlier published data showed that the absence of Rad51 in a *tlc1*-Δ background significantly accelerated senescence (Ballew & Lundblad 2013). The combination of a defect in the 9-1-1 complex (*mec3*-Δ) and Rad51, resulted in a pattern of accelerated senescence, that was indistinguishable from that seen in *tlc1*-Δ *rad51*-Δ (Figure 2.6 A). The previously observed attenuation of senescence in *tlc1*-Δ *mec3*-Δ was ablated in *tlc1*-Δ *mec3*-Δ *rad51*-Δ. This argues that the 9-1-1 complex and Rad51 are in a common pathway. Specifically, the 9-1-1 complex is acting upstream of Rad 51 as an inhibitor of an inhibitor, to regulate replicative senescence (Figure 2.6 B).

Rad51 and Rad52 play redundant roles in replicative senescence

In *S. cerevisiae*, mutations in the Rad52 epistasis group (*RAD50*, *RAD51*, *RAD52*, *RAD54*, *RAD55*, *RAD57*, *RAD59*, *MRE11*, and *XRS2*) result in severe defects in DSB repair (reviewed by Symington 2002). The epistatic relationships that a subset of these genes (*RAD50*, *RAD51*, *XRS2*) have in DSB repair, was not recapitulated in replicative senescence. In DSB processing, Rad51 is known to act downstream of MRX mediated resection by binding newly exposed ss-DNA and subsequently initiating homologous recombination (Costanzo et al. 2011). In replicative senescence,

Rad50 and Rad51 act in separate and opposing pathways (Ballew & Lundblad 2013). In DSB processing Rad52 is responsible for recruiting Rad51 to RPA coated ss-DNA (Sung 1997). Previous work showed that the loss of *RAD52* conferred a pronounced acceleration in senescence. To test the epistatic relationship between *RAD51* and *RAD52* in replicative senescence, the growth characteristics of 32 *tlc1*-Δ *rad51*-Δ, 27 *tlc1*-Δ *rad52*-Δ, and 29 *tlc1*-Δ *rad51*-Δ *rad52*-Δ isolates, were compared to 21 *tlc1*-Δ isolates. The pattern of accelerated senescence was indistinguishable among all three genotypes (Figure 2.7 A), suggesting that Rad51 and Rad52 are functioning in the same pathway in replicative senescence.

When I tested for an epistatic relationship between Rad52 and the 9-1-1 complex, as I had done with Rad51, the results were indistinguishable from those observed for *tlc1*-Δ *rad51*-Δ *mec3*-Δ isolates. The alleviated senescence of a *tlc1*-Δ *mec3*-Δ strain was replaced by an accelerated senescence in *tlc1*-Δ *rad52*-Δ *mec3*-Δ isolates (Figure 2.7 B). The result of loss of *RAD52* was identical to the results seen with loss of *RAD51*, putting these two proteins in the same group of inhibitors of replicative senescence, downstream of the 9-1-1 complex. It is important to note that this comparison was done with a limited number of isolates, well below what we would consider a robust dataset, so this final conclusion is tentative.

Rif1 has additive effect with Rad51 in regulating replicative senescence

Both Rif1 and Rif2 proteins have significant effects on telomere length in telomerase-proficient cells. The loss of either leads to an over elongation phenotype on telomere length. These two proteins are implicated in the prevailing model for

telomere length regulation, the "protein counting model" (Marcand et al. 1997). This model argues that duplex telomeric DNA bound by Rap1-Rif1-Rif2 complex, acts to control telomere length regulation by limiting telomerase access to telomeres. The Lundblad lab has pursued several lines of investigation suggesting that the prevailing model is incorrect. We previously published results where the progression of senescence in *tlc1*-Δ *rif2*-Δ isolates was significantly accelerated when compared to *tlc1*-Δ. This result conflicts with the assumptions of the current models under which predict little effect in senescence. In our current epistasis map, Rif2 acts to inhibit the actions of MRX in replicative senescence. Previous experiments involving the loss of *RIF1* (Rap1-interacting factor 1) in a telomerase-defective background, showed no significant effects on replicative senescence. In multiple experiments, totaling the analysis of 125 isolates, there was no significant effect on senescence when comparing *tlc1*-Δ *rif1*-Δ to *tlc1*-Δ (Ballew & Lundblad 2013). These effects on senescence were only detectable in combination with defects in *rif2*-Δ, and effects were specific to the early stages of senescence. This result placed Rif1 in a distinct pathway from MRX/Rif2. To determine if Rif1 lies in the same pathway as Rad51, 24 *tlc1*-Δ *rad51*-Δ, 22 *tlc1*-Δ *rif1*-Δ, and 28 *tlc1*-Δ *rif1*-Δ *rad51*-Δ isolates were compared to 20 *tlc1*-Δ isolates. Loss of *RIF1* in combination with the loss of *RAD51* produced a significant effect on the relative senescence in *tlc1*-Δ *rif1*-Δ *rad51*-Δ isolates at both 25 and 50 generations, when compared to *tlc1*-Δ isolates (p <0.001, Figure 2.8). This was also true when comparing relative senescence between *tlc1*-Δ *rif1*-Δ isolates to *tlc1*-Δ *rif1*-Δ *rad51*-Δ, (p <0.05 at 25 generations and p <0.01 at 50 generations) and when

comparing *tlc1*-Δ *rad51*-Δ isolates to *tlc1*-Δ *rif1*-Δ *rad51*-Δ (p <0.05). Similar to the effects observed in *tlc1*-Δ *rif1*-Δ *rif2*-Δ, again this effect was absent at later generations. This temporal-additive effect suggests that Rif1 is contributing to replicative senescence in a pathway that is distinct from Rad51.

Rad9 has no effect on replicative senescence

Next on the list of DNA damage response genes was *RAD9*. Rad9 is a checkpoint protein whose role at DSBs and de-protected telomeres is to inhibit Rad50-dependant resection (Lydall & Weiner 1995; Lazzaro et al. 2008). Surprisingly, unlike the previously tested DNA damage response genes, which either accelerated or attenuated senescence progression, *tlc1*-Δ *rad9*-Δ isolates showed no significant difference is senescence progression when compared to *tlc1*-Δ (Figure 2.9). Because Rad9 is known to influence the effects of MRX (Mre11-Rad50-Xrs2) by inhibiting Rad50-dependant resection (Bonetti et al. 2015) we would expect an accelerated senescence, as the absence of *Rad9* would mean the loss of that inhibition and therefore a progressive shortening of telomeres in the absence of telomerase. The lack of phenotype suggests that the parallels between DSBs and telomeric ends are not as straight-forward as predicted.

MME genes *MSH2* and *PMS1* have opposite effects on replicative senescence

Another type of DNA damage response is DNA mismatch repair (MMR). Mismatch repair involves recognizing and repairing or error that arise during replication or recombination. As we previously observed significant effects on replicative senescence with other DNA repair genes, it was important that we test the

effects of these MMR mediating proteins on replicative senescence. In *S. cerevisiae* MMR requires Msh2, Pms1, and Mlh1 proteins (Kolodner & Marsischky 1999). The Msh2 heterodimers are responsible for recruiting Pms1 endonuclease enabling MMR. Comparing 35 *tlc1*-Δ *pms1*-Δ to 35 *tlc1*-Δ isolates gave a significant attenuation of senescence at 75 generations (p <0.01, Figure 2.10 A). This indicates that the Pms1 protein, in its wild-type state, is acting as a positive regulator of senescence in the absence of telomerase. Surprisingly, experiments with Msh2 gave opposite results. Comparing 28 *tlc1*-Δ *msh2*-Δ to 24 *tlc1*-Δ showed and accelerated senescence in the absence of *MSH2* (p <0.05, Figure 2.10 B). These two proteins are in the same pathway in MMR, with defects in MMR being indistinguishable in *pms1*-Δ and *msh2*-Δ (Alani 1999). In replicative senescence, Pms1 is acting as positive regulator, while Msh2 as an inhibitor (Figure 2.10 C).

Upf1 acts as a positive regulator of replicative senescence in a manner that is distinct from the Rad51 pathway

My initial experiments focused on genes involved in DNA replication and repair, and genes that could fall into either of the previously identified pathways. To probe for separate pathways I chose to test genes that are known to effect telomeres but would not involve either MRX or *RAD51*. To this end, I first tested the effects of *UPF1* (up-frameshift) on replicative senescence. *UPF1* is best known for its role in non-sense mediated mRNA decay (NMD). In *Saccharomyces cerevisiae*, the *UPF1*, *UPF2* and *UPF3* genes are required for NMD (Lelivelt & Culbetson 1999; Cui et al. 1995). Prior studies show extremely short telomeres in a *upf1*-Δ in the presence of

telomerase (>150bp shorter than average wild type length, Askree et al. 2004), and an attenuation of senescence when introduced into a telomerase-deficient strain background (Enomoto et al. 2004).

First I verified that the loss of *UPF1* in a telomerase null background leads to alleviated senescence. Expectedly, *tlc1*-Δ *upf1*-Δ isolates had attenuated senescence when compared to *tlc1*-Δ. This was the case for multiple experiments totaling 61 *tlc1*-Δ *upf1*-Δ vs. 72 *tlc1*-Δ (Figure 2.11). Of all the genes, and gene combinations, tested to date *tlc1*-Δ *upf1*-Δ isolates had the most significant attenuation on replicative senescence. Unlike most of the genotypes tested, which could only be propagated until 75 generations due to inviability, *tlc1*-Δ *upf1*-Δ isolates had a prolonged significant effect on replicative senescence that was observed from 50-125 generations (both experiments had a p <0.000000001 at 75 generations). To probe for an epistatic relationship between Upf1 and Rad51, a strain that was null for both *UPF1* and *RAD51* was tested. The pattern of alleviated senescence seen in 23 *tlc-1*Δ *upf1*-Δ isolates was replaced by an accelerated senescence in 29 *tlc1*-Δ *upf1*-Δ *rad51*-Δ isolates, but not as severe as that of 28 isolates of *tlc-1*Δ *rad51*-Δ (Figure 2.12 A). This places *UPF1* in a pathway distinct from that of *RAD51,* where it acts as a promoter of replicative senescence (Figure 2.12 C).

The other major pathway on our current epistasis map is the MRX complex and its two upstream regulators Rif2 and Tel1. The loss of *UPF1* has such a significant attenuation of senescence, that it would be difficult to analyze the combination of that with loss of *RAD50*, which also alleviates senescence. So to

further test for an epistatic relationship with the MRX pathway, I turned to *RIF2*. A mutation in *RIF2* in the absence of telomerase results in accelerated replicative senescence. Comparing 21 *tlc1*-Δ *upf1*-Δ isolates, 20 *tlc1*-Δ *rif2*-Δ isolates, and 14 *tlc1*-Δ *upf1*-Δ *rif2*-Δ isolates, to 17 *tlc1*-Δ isolates, produced conflicting results (Figure 2.12 B). The huge alleviation on replicative senescence previously seen in *tlc1*-Δ *upf1*-Δ isolates derived from a *tlc1*-Δ/TLC1 *upf1*-Δ/UPF1 diploid was muted in isolates derived from a *tlc1*-Δ/TLC1 *upf1*-Δ/UPF1 *rif2*-Δ/RIF2 diploid. Again, the change in relative senescence could be attributed to telomere length changes in the parental diploid. As seen in previous experiments, the senescence rate of a *tlc1*-Δ derived from a parental diploid heterozygous for a deletion of *RIF2*, will senesce faster than one derived from a diploid with two copies of *RIF2*. The *tlc1*-Δ *rif2*-Δ isolates still showed the predicted accelerated senescence seen in previous experiments that was significant at both 25 and 50 generations ($p < 0.05$). The triple mutant is not statistically different in relative senescence than either double mutant. Unfortunately, this experiment was not replicated so I cannot give a definitive conclusion on the genetic relationship between of *UPF1* and *RIF2*. But it is clear that *UPF1* is acting as a positive regulator of replicative senescence in a pathway that is distinct from the Rad51 pathway.

Genes that confer growth defects complicate the semi-quantitative assay for replicative senescence: *MMS1* and *MMS22*

Early on it became clear that genes involved in the replication of DNA would be a high priority to probe for the multiple genetic relationships involved in the regulation of replicative senescence. In parallel to these studies, the importance of

efficient replication of telomeres and its effects on telomere length maintenance took center stage in the lab. Accordingly, I decided to test Mms1 and Mms22, two proteins known to be involved in replisome stabilization (Duro 2008) for their effects on replicative senescence. When combining defects in replication with a defective telomerase, I would expect to see an enhancement in the progression of replicative senescence. Attempting to study this relationship led me to identify a limitation of our assay. The quantitative assay for replicative senescence relies on comparing growth characteristic in two or more populations of telomerase defective backgrounds for consecutive generations. Here the loss of *MMS22* or *MMS1* leads to an immediate and significant loss of viability (Figure 2.13). Because the expected results of combining *mms1*-Δ or *mms22*-Δ with *tlc1*-Δ, is an acceleration in senescence progression, the decreased viability conveyed by the single mutations excluded these genes from being put through the current assay. Testing a null mutation that already has a growth defect, unrelated to senescence, adds a layer of complexity that would make this a suboptimal strain to test effects on replicative senescence.

DISCUSSION

Telomere length is a result of factors that contribute to lengthening and shortening of telomeres, as telomeres that are either too short or too long are both detrimental to the cell. The enzyme telomerase contributes to the main pathway of telomere elongation, and in its absence telomeres shorten and inevitably cells senesce. It has become increasing clear that when telomerase is deficient there is complex

system of telomere length regulation that occurs. Because telomerase in down regulated in most tissues in humans, it is important to understand what genetic factors regulate telomere length when telomerase is absent. In this chapter multiple genes involved in various pathways were tested for their effects on replicative senescence through the use of a semi-quantitative assay. This assay was previously established in the lab and shown to be a powerful tool for the identification of pathways that positively or negatively affect replicative senescence. By testing additional genes in additional pathways, in this assay, I successfully added multiple genes to this initial network and therefore expanded our current understanding of the complex regulation of replicative senescence in the absence of telomerase (Figure 2.14).

My starting point stemmed from prior findings by Bari Ballew-Braunstein that showed that multiple genetic pathways are involved in the regulation of replicative senescence in telomerase-defective yeast (Ballew & Lundblad 2013).. The two major pathways identified in the study were Rad51 and MRX-Tel1-Rif2 (Figure 2.2). My first major finding was an addition to the Rad51 pathway, where I found the 9-1-1 complex acts upstream of Rad51 as an inhibitor of an inhibitor of replicative senescence (Figure 2.6). Earlier, the accelerated senescence seen in *tlc1*-Δ *rad51*-Δ isolates was attributed to the role Rad51 plays in DNA replication where ss-DNA coated with Rad51 is protected from MRX degradation at stalled forks (reviewed by Costanzo 2011). The results reported in this chapter show that in the absence of the 9-1-1 complex (or its clamp loader Rad24), replicative senescence is alleviated, and that effect is ablated if Rad51 or Rad52 is not present. The 9-1-1 complex is known to

promote extensive Exo1-dependant resection, an activity that is conserved from yeast to humans (Lydall & Weinert 1995; Tsang et al. 2014; Ngo et al. 2014). This activity might contribute to a role in DNA replication at telomeres. The alleviated senescence observed in the absence of *MEC3*, *RAD17* or *RAD24* (Figure 2.3) could be due to a decrease in replication stress/fork collapse (a topic that will be discussed in detail in chapters 3 and 4). While not tested directly (yet), a study using a Cdc13-defective yeast showed that in the absence of the 9-1-1 complex (*mec3*-Δ) the accumulation of ss-DNA distal to telomeres (Ngo et al. 2014) was significantly decreased. Our results suggest that this effect is dependent on Rad51 and Rad52 (Figure 2.6 and 2.7, respectively). An unanticipated observation from my analysis was that the loss of *RAD9* function had no effect on replicative senescence (Figure 2.9). This conflicts with findings that showed that loss of Rad9 increased ss-DNA accumulation distal to telomeres, an activity that was dependent on 9-1-1.

A second major finding was the effect that Upf1 had on replicative senescence. By combining the loss of *UPF1* with multiple factors implicated in either of the two major arms of my previously established epistasis map I showed that Upf1 acts independently as a promoter of replicative senescence (Figure 2.12). While the delayed senescence in *tlc1*-Δ *upf1*-Δ had previously been shown (Enomoto et al. 2004), that delay was reported to occur 10-25 population doublings later (compared to *tlc1*-Δ). Here I showed that senescence was delayed substantially longer than that, and that that effect was independent of both Rad51 and (tentatively) Rif2.

For Rif1 I was able to show that it acts independently of Rad51 (Figure 2.8), and Bari had already shown that Rif1 and Rif2 play distinct roles. This adds yet another independent arm to our network of genes implicated in replicative senescence. In both cases, the loss of *RIF1* led to accelerated senescence in *tlc1*-Δ *rif1*-Δ *rad51*-Δ and *tlc1*-Δ *rif1*-Δ *rif2*-Δ isolates, which argues that in its wild type state it is acting as a positive regulator of replicative senescence. Further analysis is needed to distinguish if it, like Rif2, is acting through the MRX complex. In addition to the extensive analysis that led to the addition of arms in my epistasis map, and the expansion of the Rad51 pathway, I also accumulated an abundance of preliminary data for other genes that contribute to replicative senescence. For the Pms1 and Msh2, I observed opposite effects on senescence (Figure 2.10) where the loss of *PMS1* led to alleviation in replicative senescence in a telomerase defective background, and loss of *MSH2* led to accelerated senescence. Again, further analysis is needed to gauge whether MMR genes are working through pre-established pathways affecting senescence or if they make up new ones.

This chapter focused on expanding our knowledge of genes that contribute to telomere length homeostasis, by examining the genes that mediate replicative senescence. The assay proved to be an effective tool for uncovering novel roles for genes that function in DSB repair, DNA replication stabilization, NMD, and telomere length regulation. These findings not only established a role for these genes, but they revealed genetic relationships between previously identified mechanisms that contribute to telomere biology, that have long remained absent in high-

throughput/genome-wide analysis. The caveat of this type of assay is that it relies on the assessment of growth characteristics as an output for senescence. This limits the analysis to genes that do not cause a growth defect when absent in the presence of telomerase (like *MMS1* and *MMS22*, Figure 2.13). Additionally, using replicative senescence as a readout for telomere shortening is an indirect way to measure telomere length. Changes that affect the response to telomere shortening would also effect replicative senescence and not necessarily reflect telomere length. But building this extensive network of genes and genetic relationships that regulate replicative senescence together was extremely important, and contributed to guiding future experiments. The work presented in this chapter was the start to a much bigger project that involved new assays for the direct measurement of telomeres as well as an emphasis on one specific mechanism that regulates telomere homeostasis.

FIGURES

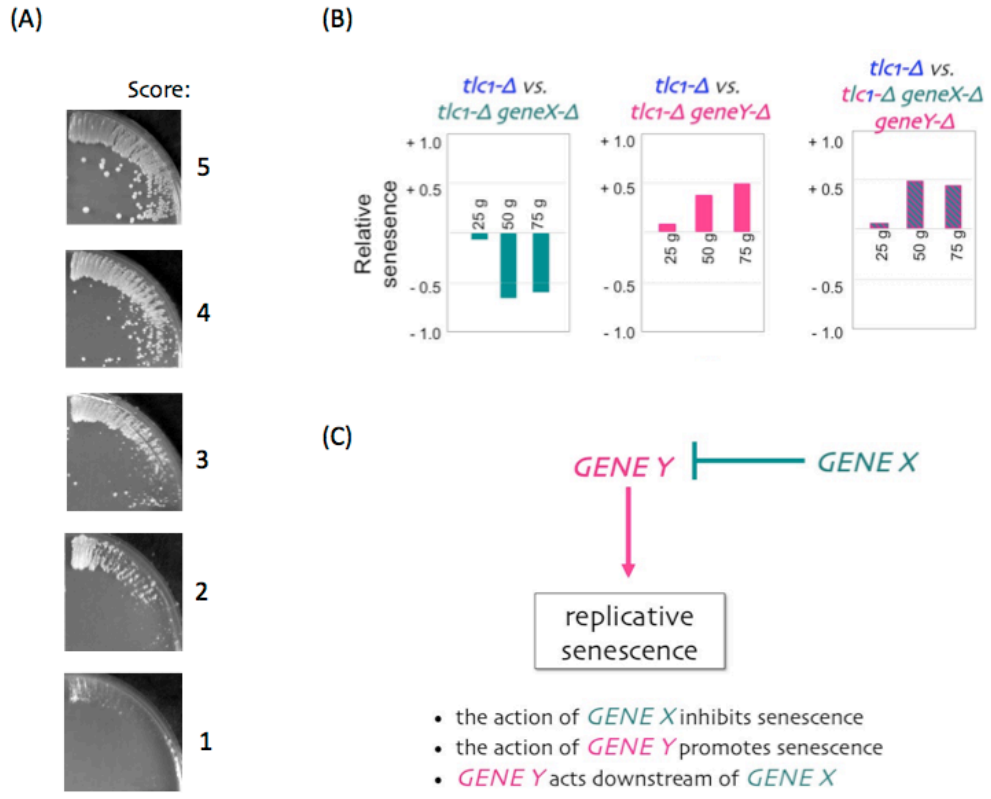

Figure 2.1: Schematic of the semi-quantitative assay for replicative senescence. Multiple isolates are generated after the dissection of a diploid *tlc1*-Δ/TLC1 *geneX*-Δ/*GENE X* and propagated for consecutive generations. Using the legend in (A) they are designated growth scores. Scores are tabulated and graphed for relative senescence comparing average growth scores for *tlc1*-Δ *geneX*-Δ isolates to *tlc1*-Δ isolates, where accelerated senescence is negative and attenuated senescence is on the positive Y axis (B). Analysis of a high number of isolates for each genotype allows for statistical significance to be calculated for the differences between different genotypes. Roles for the genes in their wild type state can be extrapolated from effects on replicative senescence in their absence (C).

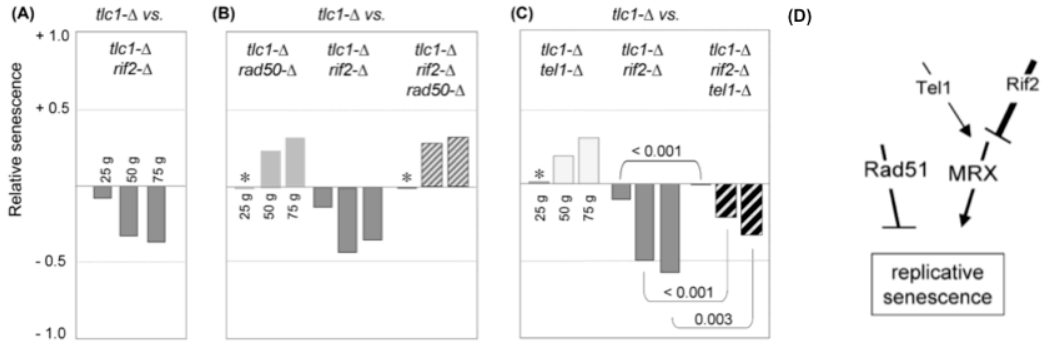

Figure 2.2: Genes involved in replicative senescence. These results were published in Ballew & Lundblad 2013 and were the initiating events for the experiments in this chapter. (A-C) Examples of the results that led to model illustrated in (D). Loss of *RIF2* in a telomerase defective background leads to accelerated senescence (A) that is ablated when combined with a loss of *RAD50* (B) or subdued when combined with a loss of *TEL1* (C). The effects of these three genes on replicative senescence are summarized in the epistasis map in (D). Additionally, loss of *RAD51* was shown to accelerate senescence in a telomerase defective background (Ballew & Lundblad 2013) and is shown on the map as inhibitor of replicative senescence.

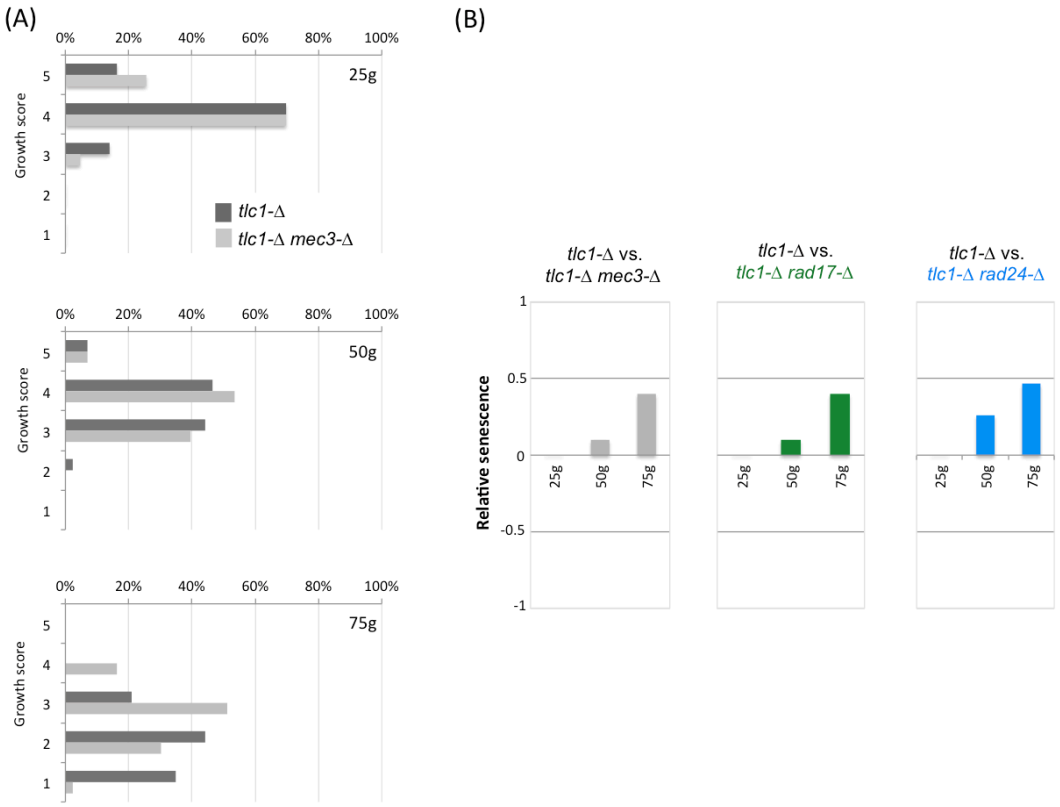

Figure 2.3: Loss of the 9-1-1 complex leads to accelerated senescence in a telomerase defective background. The growth scores for multiple *tlc1*-Δ *mec3*-Δ and *tlc1*-Δ isolates is summarized in histograms for 25, 50, and 75 generations (A). (B) The data in (A) was graphed in a histogram of relative senescence, where the senescence of *tlc1*-Δ *mec3*-Δ isolates showed an attenuation of senescence, relative to *tlc1*-Δ isolates. Additionally, loss of *RAD17* (a member of the 9-1-1 complex) and *RAD24* (the clamp loader for the 9-1-1 complex) in a telomerase defective background also alleviated senescence.

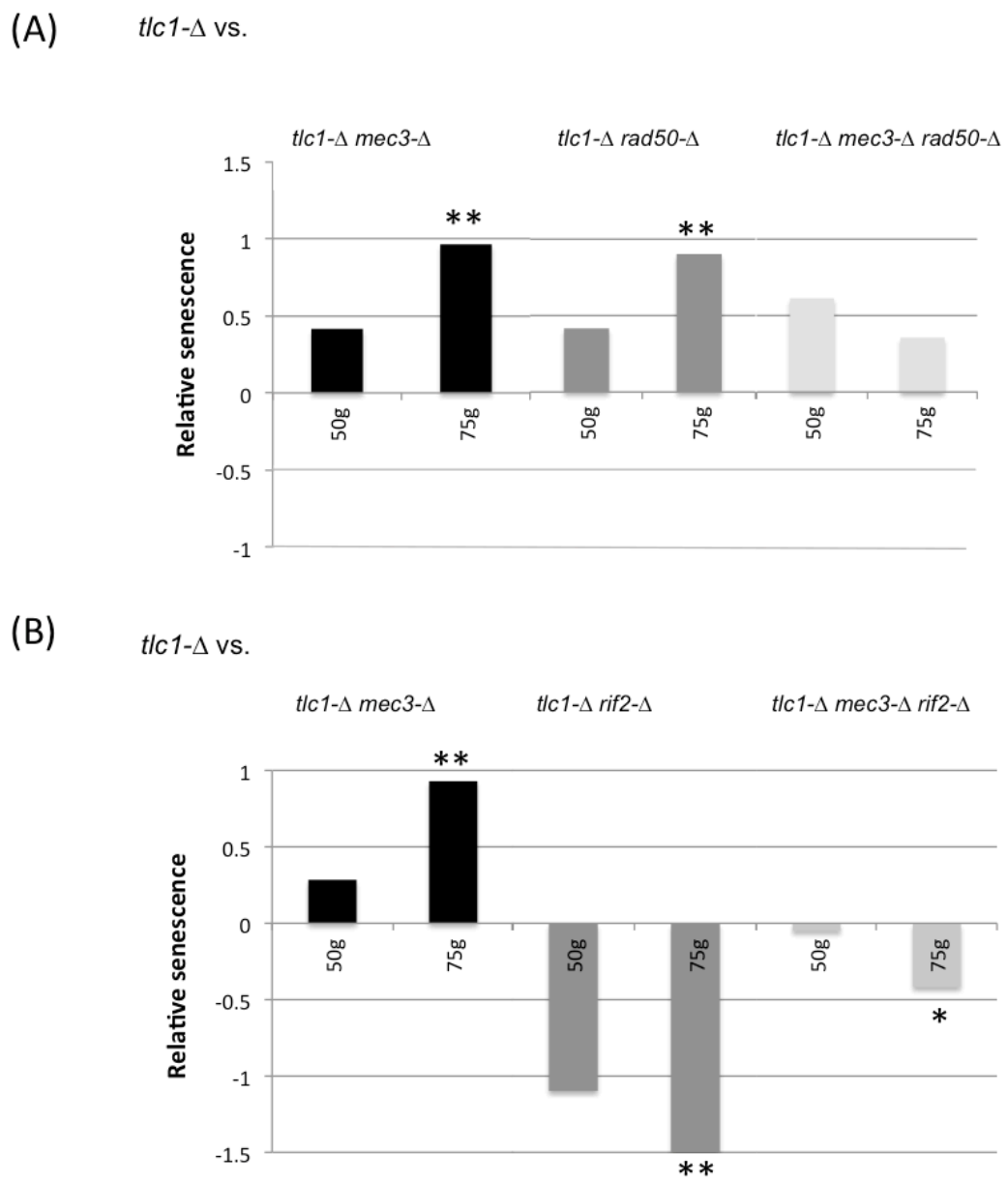

Figure 2.4: The 9-1-1 complex acts in a pathway distinct from the MRX-Rif2 pathway. (A) Relative senescence scores for *tlc1*-Δ *mec3*-Δ, *tlc1*-Δ *rad50*-Δ, and *tlc1*-Δ *mec3*-Δ *rad50*-Δ, with each compared to *tlc1*-Δ, showed that the attenuated senescence in both *tlc1*-Δ *mec3*-Δ and *tlc1*-Δ *rad50*-Δ is subdued in the triple mutant. (B) Relative senescence scores for *tlc1*-Δ *mec3*-Δ, *tlc1*-Δ *rif2*-Δ, and *tlc1*-Δ *mec3*-Δ *rif2*-Δ, with each compared to *tlc1*Δ, showed an intermediate phenotype in the triple. Both histograms summarize the data for 50 and 75 generations. * designates $p < 0.05$ and ** designates $p < 0.01$.

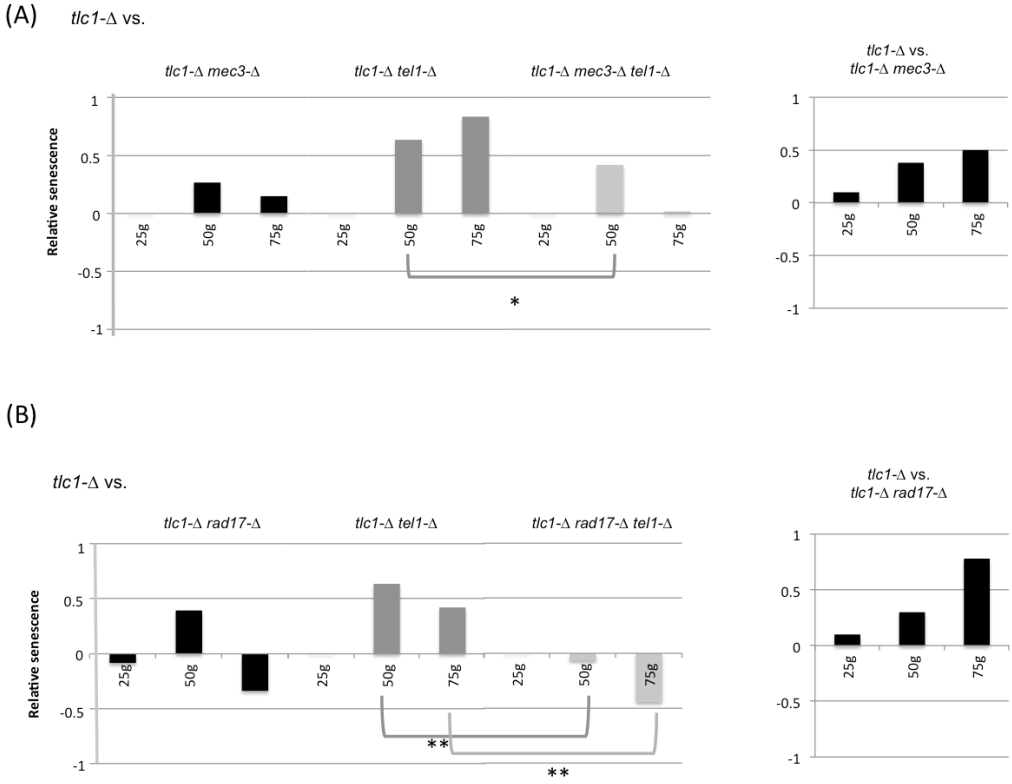

Figure 2.5: Loss of *TEL1* confers haploinsufficiency. (A) Relative senescence scores for *tlc1*-Δ *mec3*-Δ, *tlc1*-Δ *tel1*-Δ, and *tlc1*-Δ *mec3*-Δ *tel1*-Δ, with each compared to *tlc1*-Δ, showed that the attenuated senescence of *tlc1*-Δ *mec3*-Δ isolates was greatly decreased in isolates derived from *tlc1*-Δ/TLC1 *mec3*-Δ/MEC3 *tel1*-Δ/TEL1 (left) than those derived from *tlc1*-Δ /TLC1 *mec3*-Δ/MEC3 (A, right side). (B) Similar phenomenon seen when graphing relative senescence scores for isolates derived from *tlc1*-Δ/TLC1 *rad17*-Δ/RAD17 *tel1*-Δ/TEL1. For both sets of experiments (in A and B), the *tlc1*-Δ *tel1*-Δ isolates retained their alleviation of senescence, which was either decreased in combination with *mec3*-Δ (A) or *rad17*-Δ (B). * designates $p < 0.05$ and ** designates $p < 0.01$.

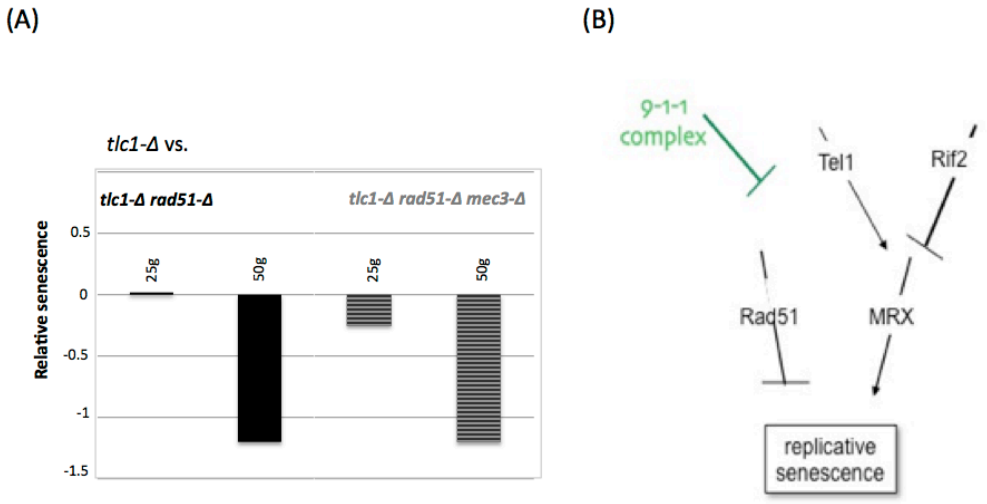

Figure 2.6: The 9-1-1 complex acts upstream of Rad51. (A) Relative senescence scores for *tlc1*-Δ *rad51*-Δ and *tlc1*-Δ *rad51*-Δ *mec3*-Δ with each compared to *tlc1*-Δ showed an accelerated senescence that is indistinguishable between both mutants. (B) Schematic illustration of the impact of the 9-1-1 complex on the current epistasis map for replicative senescence; see text for discussion.

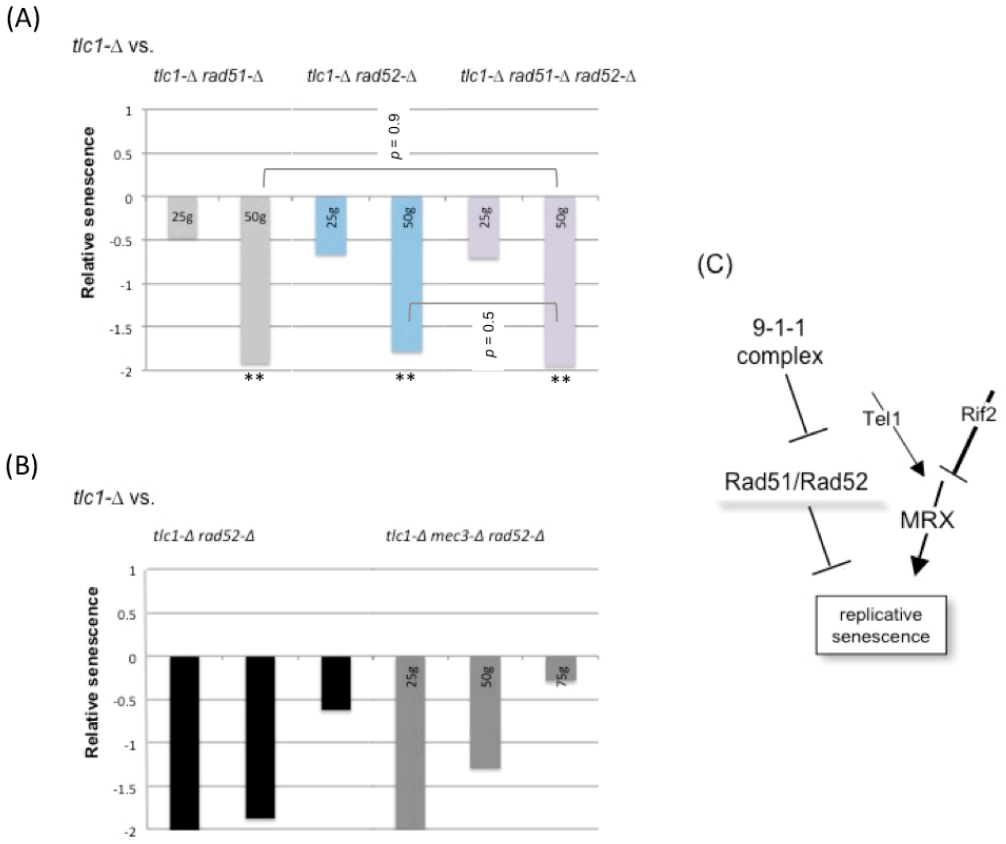

Figure 2.7: Rad51 and Rad52 have redundant functions in replicative senescence. (A) Relative senescence scores for *tlc1*-Δ *rad51*-Δ, *tlc1*-Δ *rad52*-Δ, and *tlc1*-Δ *rad51*-Δ *rad52*-Δ, with each compared to *tlc1*-Δ showed that the pattern of accelerated senescence was identical across all three genotypes, all of which had a statistically significant difference in replicative senescence of $p < 0.00000001$ when compared to *tlc1*-Δ isolates at 50 generations. However, there is no statistically significant difference in accelerated senescence when comparing either double to one another or to the triple. (B) Relative senescence scores for *tlc1*-Δ *rad52*-Δ and *tlc1*-Δ *mec3*-Δ *rad52*-Δ, with each compared to *tlc1*-Δ showed a pattern of accelerated senescence indistinguishable between either mutant. (C) Schematic illustration of the impact of the Rad52 on the current epistasis map for replicative senescence; see text for discussion. * designates $p < 0.05$ and ** designates $p < 0.01$.

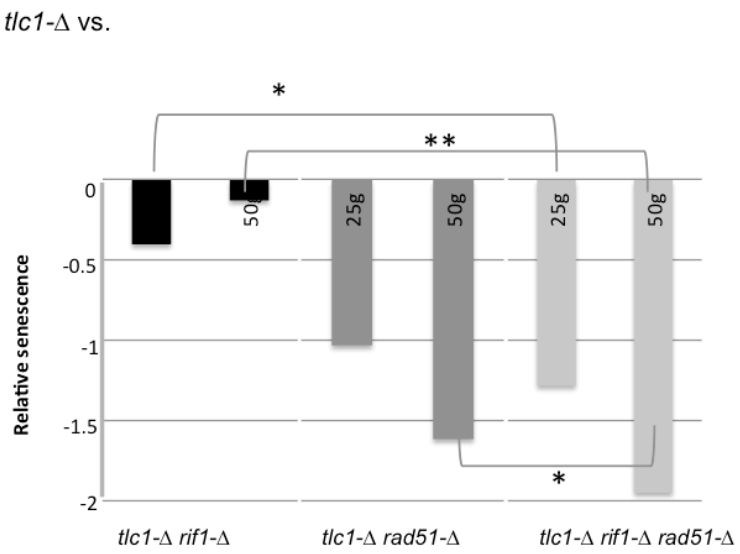

Figure 2.8: Rif1 contributes to replicative senescence in a pathway that is distinct from Rad51 pathway. (A) Relative senescence scores for *tlc1*-Δ *rif1*-Δ, *tlc1*-Δ *rad51*-Δ, and *tlc1*-Δ *rif1*-Δ *rad51*-Δ, with each compared to *tlc1*-Δ, showed that the pattern of relative senescence between either double and the triple is significantly different at 50 generations for *tlc1*-Δ *rad51*-Δ and at both 25 and 50 generations for *tlc1*-Δ *rif1*-Δ. * designates $p < 0.05$ and ** designates $p < 0.01$.

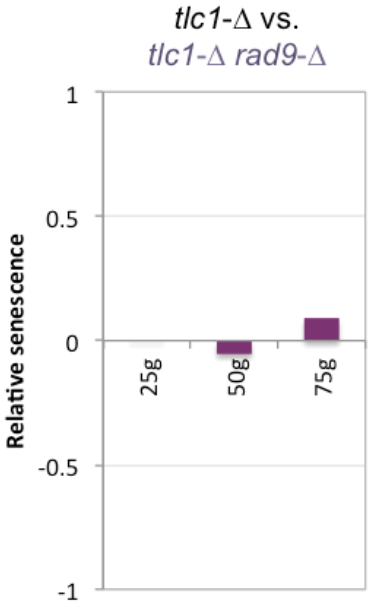

Figure 2.9: Rad9 has no significant effect on replicative senescence. Relative senescence scores for *tlc1*-Δ *rad9*-Δ compared to *tlc1*-Δ showed no difference in senescence, with P values of 0.09, 0.81, and 0.46 for generations 25-75, respectively.

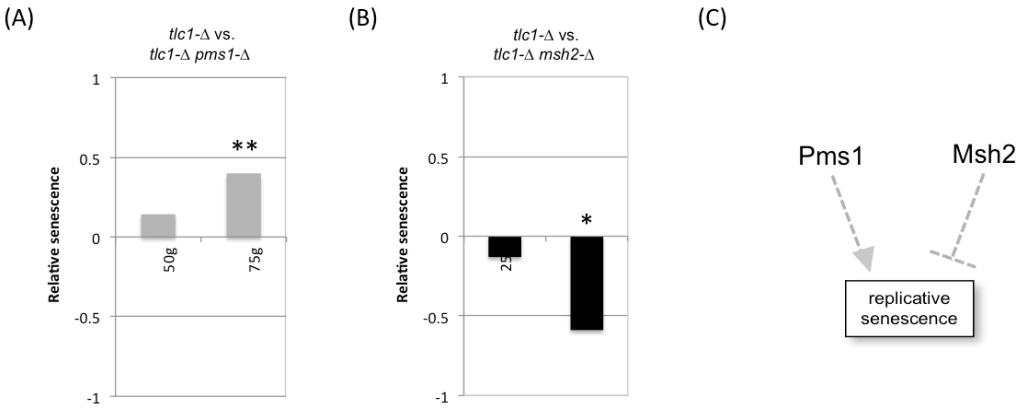

Figure 2.10: Pms1 and Msh2 contribute to regulation of replicative senescence in opposite roles. (A) Relative senescence scores for *tlc1*-Δ *pms1*-Δ compared to *tlc1*-Δ showed an attenuation of the progress of replicative senescence that was statistically different from that of *tlc1*-Δ. (B) Relative senescence scores for *tlc1*-Δ *msh2*-Δ compared to *tlc1*-Δ showed acceleration in the progress of replicative senescence, that was statistically different from that of *tlc1*-Δ. (C) Schematic illustration of the impact of the Pms1 and Msh2 on the current epistasis map for replicative senescence; see text for discussion. * designates $p < 0.05$ and ** designates $p < 0.01$.

(A) (B)

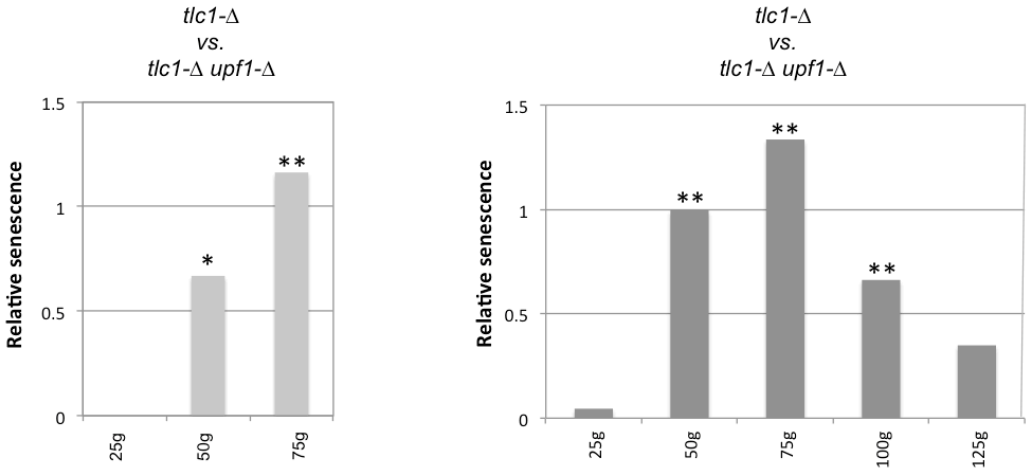

Figure 2.11: Loss of *UPF1* confers a huge and prolonged attenuation of replicative senescence. (A) Relative senescence scores for *tlc1*-Δ *upf1*-Δ compared to *tlc1*-Δ showed an attenuation in the progress of replicative senescence, that was statistically different from that of *tlc1*-Δ at both 50 and 75 generations. (B) The experiment in (A) was repeated, but this time until isolates could no longer be propagated. The effect on replicative senescence was observed up to 125 generations, a phenomenon not seen for any other gene mutants that relieved senescence. * designates $p < 0.05$ and ** designates $p < 0.01$.

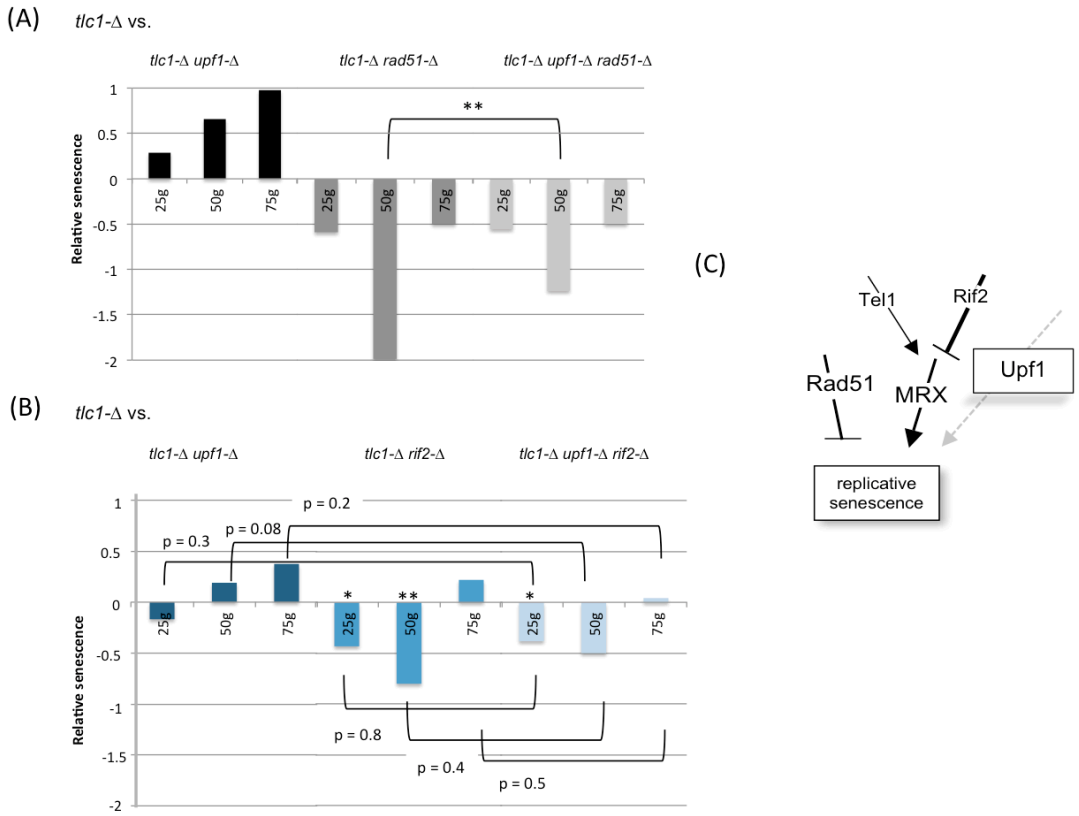

Figure 2.12: Upf1 acts in a pathway separate from both Rad51 and (tentatively) MRX/Rif2. (A) Relative senescence scores for *tlc1*-Δ *upf1*-Δ, *tlc1*-Δ *rad51*-Δ, and *tlc1*-Δ *upf1*-Δ *rad51*-Δ, compared to *tlc1*-Δ, showed an intermediate pattern of senescence in the triple mutant strain. (B) Relative senescence scores for *tlc1*-Δ *upf1*-Δ, *tlc1*-Δ *rif2*-Δ, and *tlc1*-Δ *upf1*-Δ *rif2*-Δ, compared to *tlc1*-Δ failed to show significant differences between both doubles, and the triple. Both *tlc1*-Δ *rif2*-Δ and *tlc1*-Δ *upf1*-Δ *rif2*-Δ had a significant difference in senescence at 25 generations, that was displayed as a pattern of accelerated senescence. (C) Schematic illustration of possible placement of Upf1 in the current epistasis map for replicative senescence; see text for discussion. * designates $p < 0.05$ and ** designates $p < 0.01$.

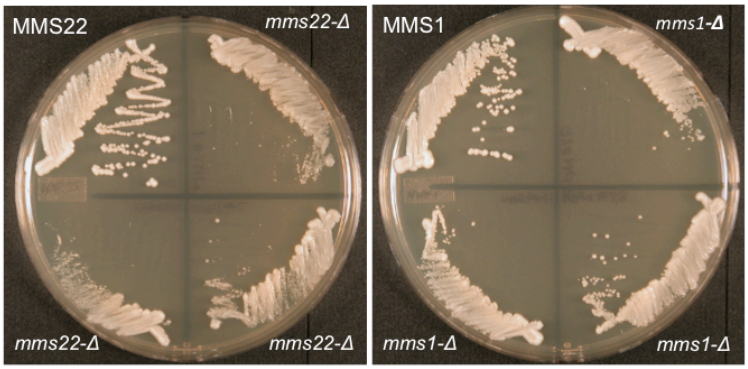

Figure 2.13: Significant growth defects conferred upon loss of *MMS22* or *MMS1*. Multiple isolates of either *mms22*-Δ or *mms1*-Δ isolates that were streaked out next to their wild type counter part (upper left quadrant on each plate) showed a significant disparity in viability.

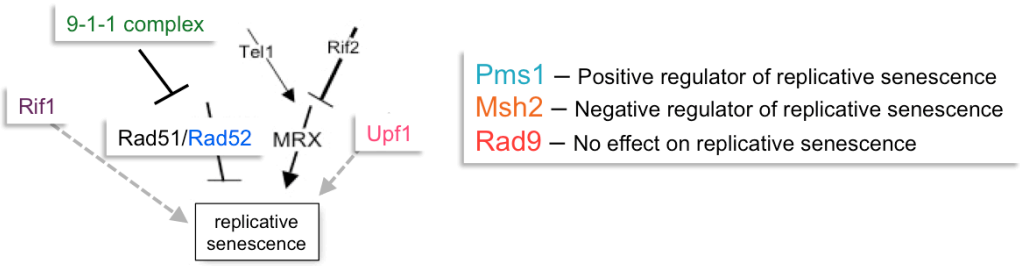

Figure 2.14: Multiple pathways contribute to replicative senescence. Schematic for the additional genes identified in this chapter (in color) and their relation to the previously established epistasis map of genes involved in replicative senescence (left). Additional genes that were tested and showed either a positive, negative, or no effect on replicative senescence, but were not tested for their relationships with the pre-established pathways are listed on the right.

Table 2.1: List of strains used in this study.

YVL	Genenotype
3584	*MAT**a**/α tlc1-Δ::HIS3/TLC1*
3568	*MAT**a**/α tlc1-Δ::HIS3/TLC1 rif2-Δ::kanMX6/RIF2*
3706	*MAT**a**/α tlc1-Δ::HIS3/TLC1 rad50-Δ::natMX4/RAD50*
3015	*MAT**a**/α tlc1-Δ::HIS3/TLC1 tel1-Δ::kanMX6/TEL1*
3785	*MAT**a**/αtlc1-Δ::HIS3/TLC1 rif1-Δ::natMX4/RIF1 tel1-Δ::kanMX6/TEL1*
3995	*MAT**a**/α tlc1-Δ::HIS3/TLC1 mec3-Δ::kanMX6/MEC3*
3999	*MAT**a**/α tlc1-Δ::HIS3/TLC1 mec3-Δ::kanMX6/MEC3 rad51-Δ::natMX4/RAD51*
4000	*MAT**a**/α tlc1-Δ::HIS3/TLC1 mec3-Δ::kanMX6/MEC3 rad52-Δ::natMX4/RAD52*
3996	*MAT**a**/α tlc1-Δ::HIS3/TLC1 rad9-Δ::kanMX6/RAD9*
3997	*MAT**a**/α tlc1-Δ::HIS3/TLC1 rad17-Δ::kanMX6/RAD17*
3998	*MAT**a**/α tlc1-Δ::HIS3/TLC1 rad24-Δ::kanMX6/RAD24*
4001	*MAT**a**/α tlc1-Δ::HIS3/TLC1 rad51-Δ::natMX4/RAD51 rif1-Δ::kanMX6/RIF1*
5573	*MAT**a**/α tlc1-Δ::HIS3/TLC1 upf1-Δ::natMX4/UPF1*
5631	*MAT**a**/α tlc1-Δ::HIS3/TLC1 upf1-Δ::natMX4/UPF1 rif2-Δ::kanMX6/RIF2*
5632	*MAT**a**/α tlc1-Δ::HIS3/TLC1 upf1-Δ::natMX4/UPF1 rad51-Δ::kanMX6/RAD51*
5633	*MAT**a**/α tlc1-Δ::HIS3/TLC1 pms1-Δ::kanMX6/PMS1*
5634	*MAT**a**/α tlc1-Δ::HIS3/TLC1 msh2-Δ::kanMX6/MSH2*
5635	*MAT**a**/α tlc1-Δ::HIS3/TLC1 mec3-Δ::kanMX6/MEC3 rif2-Δ::natMX4/RIF2*
5636	*MAT**a**/α tlc1-Δ::HIS3/TLC1 mec3-Δ::kanMX6/MEC3 rad50-Δ::natMX4/RAD50*
5637	*MAT**a**/α tlc1-Δ::HIS3/TLC1 rad51-Δ::natMX4/RAD51 rad52-Δ::natMX4/RAD51*
additional genotypes: ura3-52/ura3-52 lys2-801/lys2-801 trp-Δ1/trp1-Δ1 his3-Δ200/his3-Δ200 leu2-Δ1/leu2-Δ1	

MATERIALS AND METHODS

Yeast strains

All yeast strains in table 2.1 were derived from the parental heterozygous telomerase null strain YVL3584 (*tlc1*-Δ*::HIS3/TLC1*) and therefore are isogenic. Additional gene knockouts are complete deletions of the open reading frames and were made through PCR-generated gene disruption fragments using either KanMX4 or NatMX4 cassettes as templates, and using lithium acetate transformation method (Schiestl and Gietz, 1989). Strains were verified by both molecular and genetic methods. PCR amplification of the region encompassing the gene knockout was done on mutant haploids, to verify both size difference between GENE X and *gene X*-Δ, and digestion pattern. Known phenotypes of gene knockouts were also verified. All strains used in this study are isogenic to YVL2967, which is derived from S288C and is the parent to all strains currently constructed in the Lundblad lab.

Semi-quantitative assay for replicative senescence

Diploid strains (*tlc1*-Δ/*TLC geneX*-Δ/*GENE X*) were sporulated in liquid sporulation medium for 3-5 days. For each experiment 20-50 tetrads were dissected, and allowed to grow for 3 days before *tlc1*-Δ isolates were streaked out at 30˚ for 3-5 successive generations, all on complete media plates. Following three days of growth, plates were photographed. Once all images were collected, strains were scored according to the legend in figure 2.1, where a score of 5 is the healthy and comparable to wild type growth, and 1 is severe senescence. Scoring was done genotype-blind. For each experiment 15-40 isolates for each genotype was analyzed. Growth scores were

graphed as relative senescence by comparing the average score of *tlc1*-Δ *geneX*-Δ to *tlc1*-Δ, or by plotting them on a histogram where a positive value signifies attenuated senescence and a negative value, accelerated senescence. The growth scores for different genotypes (populations) were compared using a two-tailed student's t-test to determine if they were significantly different.

REFERENCES

Alani E, Reenan RA, & Kolodner RD (1999) Interaction Between Mismatch Repair and Genetic Recombination in *Saccharomyces cerevisiae. Genetics* 137, 19-9.

Askeree SH, Yehuda T, Smolikov S, Gurevich R, Hawk J, Coker C, Krauskopf A, Kupiec M, & McEachern MJ (2004) A genome-wide screen for *Saccharomyces cerevisiae* deletion mutants that affect telomere length. *PNAS* 101, 8658-8663.

Bonetti D, Clerici M, Manfrini N, Lucchini G & Longhese MP (2010) The MRX complex plays multiple functions in resection of Yku- and Rif2- protected DNA ends. *PLoS ONE* 5, e14142.

Chang HY, Lawless C, Addinall SG, Oexle S, Taschuk M, Wipat A, Wilkinson DJ, & Lydall D (2011) Genome-wide analysis to identify pathways affecting telomere-initiated senescence in budding yeast. *G3 Genes Genomes Genetics* 1, 197-208.

Chang M, Rothstein R (2011) Rif1/2 and Tel1 function in separate pathways during replicative senescence. *Cell Cycle* 10, 3798-3799.

Cui Y, Hagan KW, Zhang S, & Peltz SW (1995). Identification and characterization of genes that are required for the accelerated degradation of mRNAs containing a premature translational termination codon. *Genes & Development*. 9, 423-436.

Costanzo V (2011) Brac2, Rad51, and Mre11: performing balancing acts on replication forks. *DNA Repair* 10, 1060-1065.

Duro E, Vaisica JA, Brown GW & Rouse J (2008) Budding yeast Mms22 and Mms1 regulate homologous recombination induced by replisome blockage. *DNA Repair (Amst.)* 7, 811-818.

Enomoto S, Glowczewski L, Lew-Smith J & Berman JG (2004) Telomere cap components influence the rate of senescence in telomerase-deficient yeast cells. *Mol. Cell. Biol.* 24, 837-845.

Gatbonton T, Imbesi M, Nelson M, Akey JM, Rudefer DM, Kruglyak L, Simon JA & Bedalov A (2006). Telomere length as a quantitative trait: Genome-wide survey and genetic mapping of telomere length-control genes in yeast. *PLOS* 2, 304-315.

Gao H, Toro TB, Paschini M, Braunstein-Ballew B, Cerevantes RB & Lundbland V (2010) Telomerase recruitment in *Saccharomyces cerevisiae* is not dependent on Tel1-mediated phosphorylation of Cdc13. *Genetics* 186, 1147-1159.

Greider CW & Blackburn EH (1985) Identification of a specific telomere terminal transferase activity in Tetrahymena extracts. *Cell* 43, 405-413.

Kim NW, Piatyszek MA, Prowse KR, Harley CB, West MD, Ho PL, Coviello GM, Wright WE, Weinrich SL & Shaw JW (1994). Specific association of human telomerase activity with immortal cells and cancer. *Science* 266, 2011-2015.

Kolodner RD & Marsischky GT (1999) Eukaryotic DNA mismatch repair. *Curr. Opin. Genet.* 25, 229-253.

Lazzaro F, Sapountzi V, Granata M, Pellicioli A, Vaze M, Haber JE, Plevani P, Lydall D & Muzi-Falconi M (2008) Histone methyltransferase Dot1 and Rad9 inhibit single-stranded DNA accumulation at DSBs and uncapped telomeres. *EMBO J* 27, 1502-1512.

Lelivelt MJ & Culbertson MR (1999) Yeast Upf Proteins required for RNA surveillance affect global expression of the yeast transcriptome. *Molecular and Cellular Biology* 19, 6710-6719.

Lendvay TS, Morris DK, Sah J, Balasubramanian B, Lundblad V (1996). Senescence mutants of Saccharomyces cerevisiae with a defect in telomere replication identify three additional EST genes. *Genetics* 144, 1399-1412.

Lundblad V & Blackburn EH (1993) An alternative pathway for yeast telomere maintenance rescues est1- senescence. *Cell* 23, 347-360.

Lundblad V & Szostak JW (1989) A mutant with a defect in telomere elongation leads to senescence in yeast. *Cell* 57, 633-643.

Lydall D & Weinert T (1995) Yeast checkpoint genes in DNA damage processing: implications for repair and arrest. *Science* 270, 1488-1491.

Ngo GH, Balakrshnan L, Durbarry M, Campbell JL & Lydall D (2014) The 9-1-1 checkpoint clamp stimulates DNA resection by Dna2-Sgs and Exo1. *Nucleic Acids Research* 42, 10516-10528.

Ritchie KB, Mallory JC & Petes TD (1999) Interactions of *TLC1* (which encodes the RNA subunit of telomerase), *TEL1*, and *MEC1* in regulating telomere length in the yeast *Saccharomyces cerevisiae*. *Mol. Cell. Biol.* 19, 6065-6075.

Rizki A & Lundblad V (2001) Defects in mismatch repair promote telomerase-independent proliferation. *Nature* 411, 713-716.

Sung P (1997) Function of yeast Rad52 protein as a mediator between replication protein A and the Rad51 recombinase. *J Biol Chem* 272, 28194-28197.

Symington LS (2002) Role of Rad52 epistasis group genes in homologous recombination and double-stranded break repair. *Microbiol Mol Biol Rev* 66, 630-670.

Tsang E, Miyabe I, Iraqui I, Zheng J, Lambert SA & Carr AM (2014) The extent of error-prone replication restart by homologous recombination is controlled by Exo1 and checkpoint proteins. *J Cell Sci.*127, 2983-2994.

Ungar L, Yosef N, Sela Y, Sharan R, Ruppin E, & Kupiec M (2009) A genome-wide screen for essential yeast genes that affect telomere length maintenance. *Nucleic Acid Research* 37, 3840-3849.

CHAPTER THREE:

Replication fork collapse drives telomere length homeostasis in wild type cells

During DNA replication, errors that lead to fork collapse can be a pathological event for the genome. Here, we show that at chromosome ends, replication fork collapse has been co-opted to regulate telomere length in budding yeast. By monitoring the molecular footprint of telomerase activity immediately following fork collapse, we show that collapsed forks that arise during replication of duplex telomeric DNA are recognized by telomerase with high efficiency and subject to extensive elongation. This shows that the preferred substrate for telomerase in wild type cells is a collapsed replication fork, rather than the G-rich overhang that characterizes fully replicated termini. Furthermore, an elevated frequency of fork collapse at yeast telomeres simultaneously increases the sub-populations of both shorter-than-average and longer- than average telomeres, with a consequent impact on average telomere length. We propose that a balance between replication fork collapse and the subsequent response by telomerase dictates telomere length homeostasis.

INTRODUCTION

Telomeres – the physical ends of linear chromosomes – present unique challenges for genomes. In cells that rely on continuous proliferation, telomeres must overcome the DNA end replication problem, which stems from the inability of the semi-conservative DNA replication machinery to fully replicate the ends of linear molecules. In addition, chromosome termini must be shielded from DNA damage signaling pathways and subsequent inappropriate DNA repair, a process that is referred to as chromosome end protection. These two threats to chromosome integrity

are addressed by telomere-dedicated factors that associate with either duplex telomeric DNA or the single-stranded extension present at chromosome ends, aided by sequence-specific recognition of the G-rich telomeric repeats that characterize chromosome termini in most species (reviewed in Palm & de Lange 2008; Pfeiffer & Lingner 2013; Wu et al. 2017).

In virtually all eukaryotes, the end-replication problem is solved by the enzyme telomerase through the templated addition of telomeric repeats to chromosome ends (Greider & Blackburn 1985), thereby counter-balancing the consequences of incomplete semi-conservative DNA replication and ensuring a steady-state telomere length. The prevailing model for telomere length maintenance postulates that telomeres interconvert between telomerase-extendible and telomerase-non-extendible states, through a feedback mechanism that senses the length of the duplex telomeric tract of individual telomeres (Marcand et al. 1997; Smogorzewska et al. 2000; Teixeira et al. 2004). According to this model, this promotes preferential elongation of shorter-than-average telomeres by telomerase, due to the increased probability that shorter telomeres will persist in an "extendible" state. Although this length-sensing process is thought to rely on negative regulatory proteins bound to duplex telomeric DNA (Bianchi & Shore 2009), both the mechanism by which this information is relayed to telomerase and the nature of the extendible state itself have remained elusive (Greider 2016). Telomerase access is also positively regulated, through a separate set of proteins that recruit the enzyme complex to chromosome termini. In budding yeast, this recruitment activity is promoted by a direct interaction between

telomerase and the telomere-bound Cdc13 protein (Nugent et al. 1996; Bianchi et al. 2004; Tucey & Lundblad 2013), whereas several subunits of the end protection complex promote this process in mammalian cells (Nandakumar et al. 2012; Zhong et al. 2012; Frank et al. 2015). It is also widely assumed that yeast telomerase only acts after DNA replication is complete, since passage of the replication fork through duplex telomeric DNA is required to form the terminal single-stranded G-rich overhang (Dionne & Wellinger 1998; Marcand et al. 2000), which is thought to be the primary substrate for telomerase. However, it is still not understood how these disparate positive and negative regulatory interactions coalesce into a coordinated view of telomere length regulation.

In parallel, efforts have been directed at elucidating the chromosome end protection problem. Initial insights came from analysis of a heterodimeric protein complex bound tenaciously to single-stranded DNA (ssDNA) present at chromosome termini in a ciliated protozoan (Gottschling & Cech 1984; Gottschling & Zakian 1986; Horvath et al. 1998). This led to the identification of a widely conserved ssDNA binding activity, called Pot1/Tpp1, in fission yeast, human cells and numerous other species (Bauman & Cech 2001; Xin et al. 2007; Hockemeyer et al. 2007; Miyoshi et al. 2008). In most species, end protection also employs additional factors that are anchored by duplex telomere DNA binding proteins, such as Taz1 in fission yeast (Cooper et al. 1997; Ferreira & Cooper 2001) or TRF1 and TRF2 in human cells (van Steensel et al. 1998; Celli & de Lange 2005); in mammalian cells, these telomere-associated factors form a six-subunit complex that is referred to as shelterin (de Lange

2005; Palm & de Lange 2008). Functional analysis has also expanded the end protection concept (for example, Ferreira & Cooper 2004) beyond the original proposal that chromosome ends are simply protected from a breakage-fusion-bridge cycle (McClintock 1941). Indeed, in human cells, the shelterin complex performs a series of discrete functions that target individual components of the DNA damage sensing machinery as well as DNA repair factors (Sfeir & de Lange 2012).

A striking feature of these two aspects of telomere biology is the high degree of evolutionary conservation, with both telomerase subunits and end protection proteins conserved from single-celled organisms to humans. A puzzling evolutionary outlier, however, has been a yeast heterotrimeric complex composed of three essential proteins (Cdc13, Stn1 and Ten1; Lustig 2001) that associate with single-stranded telomeric DNA through a high affinity DNA binding domain in Cdc13 (Milton-Fry et al. 2002). According to a long-standing model, this complex performs an end protection role in budding yeast by shielding telomeres from recognition as DSBs and subsequent unregulated resection by an unknown nuclease (Garvik et al. 1995; Lydall & Weinert 1995; Booth et al. 2001). However, identification of the proposed resecting nuclease has remained elusive (Maringele & Lydall 2002; Zubko et al. 2004), and subsequent studies questioned whether the increased levels of ssDNA in these mutant strains was in fact end-specific, as this DNA lesion was not sensitive to in vitro pre-treatment with end-specific exonucleases (Petreaca et al. 2007; Xu et al. 2009). Furthermore, this heterotrimeric yeast complex does not resemble end protection proteins in other species; instead, Cdc13, Stn1 and Ten1 form a telomere-dedicated

version of the canonical RPA complex (Gao et al. 2007; Gelinas et al. 2009; Sun et al. 2009; Paschini et al. 2010), which we have named t-RPA.

The starting point for this current study, therefore, was to re-assess the role of the t-RPA complex at yeast telomeres. To do so, we turned our attention to an alternative suggestion put forward at the same time as the end protection model (Garvik et al. 1995), which was that Cdc13 facilitated lagging strand DNA synthesis of telomere-proximal regions in budding yeast. To distinguish between these two models, we developed an assay, called the RepFC assay (for Replication Fork Collapse), to monitor spontaneous replication fork collapse at an interstitial telomeric tract. Using this assay, we show that the primary function of the t-RPA complex at yeast telomeres is to promote progression of the replisome through telomeric duplex DNA. This re-interpretation is supported by numerous studies in fission yeast, Xenopus, plants and mammalian cells showing that an analogous RPA-like complex (CST, for CTC1-STN1-TEN1) facilitates lagging strand synthesis during DNA replication (Goulian et al. 1990; Casteel et al. 2009; Nakaoka et al. 2012; Gu et al. 2012; Stewart et al. 2012; Chen et al. 2013; Derboven et al. 2014; Takikawa et al. 2017; Matmati et al. 2018).

The vulnerability of telomeres to duplex DNA replication is not solely dictated by the activity of the t-RPA/CST complex, however. It has been clear for more than a decade that duplex telomere binding proteins (Taz1 in fission yeast and TRF1 in mammalian cells) are crucial for protecting telomeres from replication stalling and subsequent telomere breakage (Miller et al. 2006; Sfeir et al. 2009; Martinez et al.

2009). Furthermore, numerous studies have revealed that defects in factors that are not telomere-specific can confer pronounced replication defects at telomeres (for example, Ding et al. 2004; Crabbe et al. 2004; Saharia et al. 2008; Vannier et al. 2013). Collectively, this argues that there is a considerable investment in preventing the dysfunction that arises in response to aberrant levels of replication stress at telomeres.

In this study, we propose an alternative view of the role of the consequences of replication stress at telomeres. Specifically, we propose that replication fork collapse, followed by extensive elongation by telomerase of newly generated collapsed forks, is a major determinant of telomere length homeostasis in wild type budding yeast. Using an expanded version of the RepFC assay described above, we show that the primary mechanism for repair of collapsed forks that arise during replication of duplex telomeric DNA is the enzyme telomerase. By monitoring the molecular footprint of telomerase activity in the same cell division in which fork collapse occurs, we provide the first direct evidence that a regressed replication fork produced during duplex DNA replication – long speculated to be a substrate for telomerase – is recognized with high efficiency and extensively elongated by telomerase. Thus, telomerase has two temporally and structurally distinct substrates in wild type cells, with the robust activity of telomerase at collapsed forks providing a striking contrast to the more limited activity that telomerase exhibits at fully replicated chromosome ends. We also show that in contrast to assumptions that drive current models, telomere length homeostasis in budding yeast is determined not only by average telomere length but also by the extent to which the length of individual telomeres deviate, both shorter and

longer, from the mean (which we call the t-DAM phenotype, for deviation away from the mean). Furthermore, when the frequency of fork collapse at telomeres is elevated, we show that the proportion of both shorter-than-average and longer-than average telomeres increases, in parallel with an impact on average telomere length.

Based on these observations, we propose that the preferred substrate for telomerase is a collapsed replication fork, rather than a fully replicated shorter-than-average telomere. In this new model, the two previously proposed categories of telomere ends (telomerase-extendible vs. telomerase-non-extendible) are instead collapsed replication forks vs. fully replicated termini, with preferential action by telomerase dictated by a choice between substrates, rather than the length of the duplex $G_{1\text{-}3}T$ tract. We conclude that replication fork collapse, and the subsequent response by telomerase, is a key regulatory mechanism at wild type telomeres, with a balance between these two activities determining the extent of telomere length variation and hence telomere length homeostasis.

RESULTS

Wild type telomeres exhibit extensive length variation

In telomerase-proficient (i.e. wild type) yeast, the average length of the G-rich telomeric tract is remarkably stable. Even when a culture of budding yeast is propagated for an extensive period of time, the average length does not drift either up or down, both for unique telomeres as well as the sub-set of telomeres that have a common sub-telomeric element referred to as Y' (for example, Paschini et al. 2012).

Despite this overall length stability, examination of chromosome termini at single nucleotide level resolution reveals that individual chromosome ends exhibit substantial length variation. In the experiment shown in Figure 3.1, one chromosome end (Chr I-L) was PCR-amplified from three sibling single colonies of wild type yeast (with four independent PCR reactions from each colony; Figure 3.1 A). Individual PCR molecules were cloned and multiple isolates from each PCR reaction were sequenced and aligned (Figure 3S.1). This analysis employed several modifications of a previously published protocol (Förstemann et al. 2000; Chang et al. 2007), including elimination of a size selection step (gel purification of PCR-amplified chromosome ends) to ensure that very long and very short sub-populations were not excluded and a substantial increase in the number of independent isolates analyzed for each genotype to provide a more reproducible assessment of the range of telomere lengths (see Materials and Methods for more details). Based on the analysis of 241 independent isolates of Chr I-L (Figures 3.1 B and 3S.1), the average length of the $G_{1\text{-}3}T$ telomeric tract was 316 bp, which was comparable to the average length derived previously from lower resolution techniques. However, among these 241 isolates, the length of individual chromosome termini spanned 600 bp, from 60 to 671 bp, and >20% of the clones diverged from the mean (either shorter or longer) by more than 100 bp. These observations were not restricted to this particular chromosome end, as a similar analysis of Chr VI-R from the same three sibling yeast colonies also displayed substantial length variation (from 33 to 730 nucleotides; data not shown). Furthermore, an independent repeat yielded a virtually identical Chr I-L telomere

length profile (Figure 3.1 C), demonstrating that this extensive telomere length variation was not a protocol artifact and instead reflected an inherent property of a wild type yeast strain. This suggests that telomere homeostasis in wild type yeast cells is composed of two properties that are each under genetic control: (i) mean telomere length and (ii) the extent to which individual telomeres in a population deviate from the mean.

Spontaneous replication fork collapse at an interstitial telomeric tract

A striking feature of the data in Figure 3.1 was the presence of a persistent population of very short (< 100 bp) and potentially genome-destabilizing telomeres, which were reproducibly detected at a frequency of ~3 to 4% at multiple chromosome termini in wild type budding yeast (Figure 3.1 C; data not shown; Chang et al. 2007). Two potential mechanisms could be responsible for this sub-population: these very short termini could be the result of extensive erosion from the chromosomal terminus, or they could arise, as previously suggested (Miller et al. 2006; Chang et al. 2007; Dehé et al. 2012), as the result of fork collapse during replication of duplex telomeric DNA. To distinguish between these two possibilities, we developed an assay to measure spontaneous fork collapse at an interstitial tract of $G_{1\text{-}3}T$ telomeric DNA, which exploits the fact that yeast telomeric repeats, which are difficult-to-replicate sequences, can induce replication stress (Makovets et al. 2004; Aksenova et al. 2013). A key feature of our experimental design is that fork collapse events that occur during replication of the interstitial telomeric DNA can be recovered and analyzed at single-nucleotide resolution.

The starting point for this assay was the introduction of ~400 bp of $G_{1\text{-}3}T$ telomeric DNA at a site on Chr IX, immediately adjacent to a high efficiency origin of replication (ARS922; McGuffee et al. 2013). This location was 27 kb from the natural terminus (Figure 3.2 A), thereby separating terminus-specific activities from events occurring during duplex DNA replication. Furthermore, because all of the downstream genes were non-essential, loss of the 27 kb distal segment of Chr IX was not lethal. To monitor loss of this segment, the *URA3* gene was placed immediately distal to the $G_{1\text{-}3}T$ telomeric tract, so that presumed replication fork collapse events could be recovered by plating on 5-FOA-containing media (Figure 3.2 B), which selects for Ura^- colonies (Boeke et al. 1987). The frequency of $5\text{-}FOA^R$ colonies in this strain was 10-3 / viable cells which was 1,000-fold higher than in an isogenic strain lacking the interstitial $G_{1\text{-}3}T$ repeat tract (Figure 3S.2 A), demonstrating that the interstitial duplex telomeric DNA conferred a genome-destabilizing effect on this region of Chr IX.

To determine whether 5-FOA-resistance was due to loss of the distal segment versus other types of genomic rearrangements, 50 independent $5\text{-}FOA^R$ colonies were examined for changes in the structure of Chr IX. As shown by Southern blot analysis (Figures 3.2 C, 3S.2 B and data not shown), all 50 Ura^- isolates exhibited the molecular features consistent with formation of a new telomere at the location of the previously internal $G_{1\text{-}3}T$ repeat tract. For each Ura^- colony, the chromosome-internal 3.9 kb restriction fragment was replaced by a ~2.3 kb band that displayed the size heterogeneity characteristic of a terminal (i.e. telomeric) restriction fragment. Subsequent PCR amplification and sequence analysis demonstrated that these newly

formed termini arose as the result of a presumed fork collapse within the interstitial $G_{1-3}T$ repeat tract, followed by *de novo* elongation by telomerase. This was revealed by aligning multiple sequenced telomeres recovered from the progeny of each individual 5-FOA^R colony, compared to the sequence of the interstitial telomeric tract (Figures 3.2 D and 3S.2 C). Due to the slightly degenerate nature of yeast telomere sequences (Shampay et al. 1984; Förstemann et al. 2001), alignments could precisely identify the site at which telomerase synthesis initiated, as the position at which the telomeric DNA sequence diverged from that of the interstitial $G_{1-3}T$ repeat tract (as indicated in the example shown in Figure 3.2 D). Examination of sequenced telomeres recovered from the progeny of 12 independent 5-FOA^R colonies showed that the point of telomerase-mediated sequence divergence in these 12 colonies was distributed throughout the internal telomeric tract (Figure 3.2 E), with no obvious sequence preference (Figures 3.2 D, 3S.2 C and data not shown). Notably, replication fork collapse occurred even within the first 100 bp of the interstitial tract in five of these isolates, consistent with the premise that a similar mechanism that occurs during replication of natural chromosome ends could give rise to the subset of telomeres that were $\leq$ 100 bp, as observed in Figure 3.1. We did not recover any 5-FOA^R isolates in which these events occurred at sites outside the interstitial $G_{1-3}T$ tract, arguing that fork collapse and subsequent loss of the distal 27 kb of Chr IX was a specific response to the difficulty in replicating duplex telomeric DNA.

To test whether the sequence addition observed in the above analysis was in fact telomerase-mediated, we examined Chr IX telomeres in 5-FOA^R colonies

recovered from a strain lacking telomerase (due to a deletion of the *TLC1* gene encoding the telomerase RNA; Singer & Gottschling 1994). As expected, the newly generated telomeric restriction fragment was ~150 – 250 bp shorter in 5-FOA-resistant *tlc1*-Δ cells, consistent with the lack of telomerase-mediated elongation (Figure 3S.2 B). The molecular structure of these newly exposed termini was also examined by sequencing cloned telomeres recovered from the progeny of individual 5-FOA^R *tlc1*-Δ colonies. A total of 47 independent 5-FOA^R single colonies from the tlc1-Δ strain were PCR-amplified, and 6 to 8 cloned telomeres from each *tlc1*-Δ colony were sequenced. If the newly exposed collapsed fork was acted upon by non-telomerase-mediated sequence addition mechanisms, this predicts that the sequence of telomeres from these *tlc1*-Δ colonies should diverge from the sequence of the interstitial tract. This experiment instead showed that replication fork collapse was not accompanied by sequence addition to the newly exposed $G_{1\text{-}3}T$ tract, for every one of the 47 *tlc1*-Δ 5-FOA^R single colonies. Figure 3.2 F shows the data from one *tlc1*-Δ colony following fork collapse; all 8 sequenced telomeres from this colony are identical to that of the interstitial telomeric tract. Similarly, the majority of sequenced telomeres from the other 46 *tlc1*-Δ colonies could be perfectly aligned with the sequence of the interstitial tract (Figure 3S.2 D and data not shown); progeny with divergent sequence patterns were observed only infrequently and as a minority sub-population (specified by white arrows in Figure 3S.2 D), indicating that they arose during subsequent growth of the colony. We conclude that in the absence of telomerase, collapsed replication forks generated during replication of duplex telomeric DNA were not substrates for either

break-induced replication or recombination; by inference, neither pathway was active in the presence of telomerase. Thus, in wild type cells, when a fork collapse occurs during replication of duplex telomeric DNA, it is repaired by the enzyme telomerase.

Although these results show that the primary pathway for elongation of *de novo* Chr IX termini is telomerase-mediated, the frequency of replication fork collapse events was unaffected in mutant cells that lacked telomerase, as the incidence of 5-FOA^R colonies was indistinguishable in *TLC1* vs. *tlc1*-Δ strains (Figure 3.2 B). This is a critical observation, because it shows that recovery of cells that had undergone fork collapse was not dependent on subsequent elongation of the newly exposed terminus. Therefore, the frequency of 5-FOA^R colonies in this assay was solely dependent on mechanism(s) that influenced the frequency of fork collapse. Furthermore, when fork collapse occurred within this internal $G_{1\text{-}3}T$ telomeric tract in the absence of telomerase, the rate at which cells lost viability (i.e. senescence) was unaffected, as shown in Figure 3S.2 E. Immediately following replication fork collapse at the internal Chr IX site, *tlc1*-Δ isolates exhibited a gradual decline in viability that was indistinguishable from the behavior of isogenic *tlc1*-Δ isolates that were propagated in parallel but did not undergo fork collapse (Figure 3S.2 E). This argues that these newly exposed termini were not perceived as unrepaired DNA damage, but instead exhibited the same characteristics as natural eroding chromosome ends.

If loss of the distal tract is occurring in response to fork collapse, known perturbations that increase replication stress should increase the frequency of such events. To test this, the strain containing the interstitial telomeric tract was modified

by the introduction of the *ADE2* gene on the 27 kb distal segment of Chr IX (Figure 3.2 G), with a corresponding deletion of the *ADE2* endogenous locus. As the result of this modification, if a replication fork collapse occurs during the first cell division, the resulting colony will be 50% Ade+ and 50% Ade$^-$ (Figure 3.2 H), due to loss of the *ADE2*-marked distal segment. These half-sectored colonies can be readily identified, due to the accumulation of red pigment in the Ade$^-$ half of the colony (Roman 1956). Ade$^-$ half-sectored colonies occurred in one in ~1100 colonies, at a frequency of 0.09%, which was comparable to the frequency observed by monitoring 5-FOA-resistance. Molecular analysis confirmed that Ade$^-$ half sectors arose due to *de novo* telomerase-mediated elongation following loss of the distal tract, exactly as observed for 5-FOA^R colonies (discussed further, below). This sectoring strain therefore provides a direct read-out of the effects of replication stress, by exposing the first cell division to conditions that destabilize the replication fork, including even conditions that are not compatible with long-term viability.

This modified assay allowed us to test whether loss of the distal segment was a direct consequence of fork collapse, rather than spontaneous double strand breaks (DSBs), by subjecting this sectoring strain to conditions that specifically increase replication fork collapse. In a wild type strain, exposure to even high levels of HU results in reversible replication fork stalling; cells arrest but then resume cell cycle progression once HU is depleted. In contrast, in the S-phase-checkpoint-deficient *rad53*-21 strain, stalled replication forks that arise in response to HU cannot be reversed (Desany et al. 1998; Lopez et al. 2001). We therefore compared the

frequency of Ade⁻ sectors in wild type vs. *rad53*-21 strains in the presence of HU. In a wild type strain, the frequency of Ade⁻ sectors was unaffected in the presence of HU as high as 40 mM and only showed a 2-fold increase when HU levels were raised to 80 mM (data not shown). In contrast, in a *rad53*-21 strain, replication fork collapse at the interstitial telomeric tract was elevated 3-fold when cells were grown in the presence of just 1 mM HU; in the absence of HU, the *rad53*-21 defect had no effect (Figure 3.2 I). This *rad53*-21 dependency provides direct evidence that loss of the distal tract occurs in response to replication fork collapse, rather than spontaneous DSB formation. This assay was also responsive to defects in the replisome itself. When cells from a strain expressing a temperature sensitive mutation in DNA pol α (*pol1*-1; Gutiérrez & Wang 2003) were incubated on plates that had been pre-warmed to 23°, 30° or 31°, there was a marked temperature-dependent increase in the frequency of Ade⁻ sectors in the resulting *pol1*-1 colonies, with a 5-fold increase at the semi-permissive temperature of 31° (Figure 3.2 J). A similar increase in Ade⁻ sectors was observed in response to a temperature-sensitive defect in the *PRI2* subunit of the Pol α-primase complex (data not shown). We note that the instability of this interstitial yeast telomeric repeat tract in response to defects in Pol α-primase is reminiscent of the aphidicolin-induced fragility observed at human duplex telomeric repeats (Sfeir et al. 2009).

Collectively, the molecular data (Figure 3.2 C–F), as well as the genetic response to replication stress (Figure 3.2 I–J), establish that this assay – which we call the RepFC assay (for Replication Fork Collapse assay) – specifically monitors the

frequency of replication fork collapse when the replisome traverses an interstitial telomeric tract. Notably, this assay measures fork collapse that occurs as a spontaneous response to a difficult-to-replicate region of the genome, without experimental induction or selection for events, in contrast to other assays for genetic instability (for example, Chen & Kolodner 1999; Lambert et al. 2005). Furthermore, recovery of cells that have undergone fork collapse does not rely on elongation of the newly exposed telomeric tract, by either telomerase or telomerase-independent elongation mechanisms. Thus, the interstitial telomeric tract serves two purposes: it presents a challenge to the replication machinery but it also allows fork collapse events to be "captured" as viable sectors in a colony, because the newly exposed telomeric tract behaves as a functional chromosome end. This therefore provides a mechanism for assaying the effects of both telomere-specific and genome-wide DNA replication factors on the ability to replicate duplex telomeric DNA, separate from the effect that these factors might have on telomere end structure and/or end protection.

Finally, the above observations were not specific to the location of the telomeric tract on Chr IX, as comparable results were observed in a second strain with ~400 bp of $G_{1\text{-}3}T$ telomeric DNA inserted 38 kb from the natural terminus of Chr XV, immediately adjacent to ARS1529.5. 5-FOA^R clones from this modified Chr XV strain were recovered at a frequency comparable to that observed with the Chr IX interstitial telomeric construct (Figure 3S.2 A), and 100% of 47 independent Ura$^-$ clones from this second strain exhibited the molecular characteristics consistent with *de novo* telomere formation, rather than other types of genomic rearrangements (data

not shown). Similarly, the frequency of replication fork collapse in this second strain was not dependent on telomerase (Figure 3S.2 A). This argues that the behavior of the telomeric tract inserted in either Chr IX or Chr XV reflects a destabilizing effect of interstitial telomeric DNA that is independent of the specific genomic location.

A regressed replication fork is a substrate for telomerase

The above results show that following replication fork collapse, the product(s) can be elongated by telomerase. There are two distinct mechanisms by which a fork collapse could generate a substrate for telomerase. A collapsed fork could lead to a double-strand break (DSB), producing two DNA ends (Figure 3.3 A). Alternatively, the collapsed fork could regress to form a so-called "chicken foot" structure (Higgins et al. 1976; Sogo et al. 2002; Fouché et al. 2006), whereby the newly synthesized strands re-anneal to produce a single DNA end (Figure 3.3 B). A key difference between these two outcomes is that the first scenario results in two termini that can each be independently elongated by telomerase, whereas the second outcome yields only a single substrate for telomerase. The RepFC assay provides a means of differentiating between these two models, by analyzing the pattern of newly added telomeric sequences following fork collapse. Since fork collapse events that occur during a single cell division can be identified as Ade$^-$ half-sectors, sequence analysis can reveal whether there is a pattern of telomerase-mediated addition in these half-sectors that is consistent with elongation of two termini (as predicted by the DSB model) vs. a single point of addition (as predicted by the chicken foot model). If the former occurs, two "founder" chromosomes with non-identical patterns of telomerase

addition will be inherited by the Ade$^-$ progeny, as indicated by (i) and (ii) in Figure 3.3 A, creating a 50:50 pattern of inheritance when multiple sibling telomere sequences are aligned. If the latter occurs, the progeny of the Ade$^-$ sector will descend from a single founder chromosome that was elongated by telomerase during the first cell division (Figure 3.3 B); as a result, all of the progeny will share a common sequence divergence (this latter outcome is in fact what is shown in the example in Figure 3.2 D).

To rigorously test this, Ade$^-$ half-sectors from a wild type strain were PCR amplified, and 20 to 25 cloned individual telomeres were sequenced from each PCR reaction. For five Ade$^-$ half-sectors, this identified a single point of sequence divergence, at positions ranging from 24 to 146 nucleotides in the interstitial telomeric tract, with a pattern of inheritance indicative of a single founder chromosome. Figure 3.3 C shows the results for one of these five sectors, where a sequence divergence at nucleotide 57 was inherited by 24 of 25 sequenced Ade$^-$ telomeres; comparable results were observed when progeny from the other four Ade$^-$ sectors were similarly analyzed (Figure 3S.3 A). We conclude that during the cell division that gave rise to each of these 5 Ade$^-$ half sectors, a single terminus was generated that was elongated by telomerase in this first cell division. As noted above, this result was also supported by the experiment shown in Figures 3.2 D and 3S.2 C, which mapped the site of *de novo* telomere formation for 12 5-FOA^R isolates.

This provides direct evidence that a regressed fork is recognized by telomerase, which demonstrates that in vivo there are two temporally and structurally

distinct substrates for telomerase: (i) a fully replicated chromosome end that arises *after* the completion of DNA replication, and (ii) a DNA replication intermediate that is generated *during* replication of duplex telomeric DNA. This experiment also revealed that telomerase-mediated elongation of the newly collapsed fork during the first cell division was quite extensive. In the example shown in Figure 3.3 C, at least 168 bp was synthesized by telomerase during this first cell division, which was subsequently inherited by the majority of the progeny that comprised this half sector (indicated by the horizontal bracket in Figure 3.3 C); this pattern of inheritance argues that this extensive elongation could only occur during the first cell division. A similar analysis, applied to four other sectors (Figure 3S.3 A), showed that an average of 120 bp of $G_{1\text{-}3}T$ telomeric DNA was added to the newly collapsed fork by telomerase (summarized in Figure 3.3 D). We postulate that this extensive elongation reflects a property of telomerase that is specific to elongation of newly collapsed replication forks.

We also sought evidence that telomerase was capable of elongating collapsed replication forks at natural telomeres by tracking the sequence added by a telomerase that synthesized a slightly altered telomeric repeat. In this experiment, a telomerase RNA construct with an altered template was transiently expressed in an otherwise wild type strain just prior to colony formation. Subsequent PCR amplification and sequence analysis of Chr I-L telomeres from individual single colonies identified telomeres with mutant telomeric repeats introduced close to the sub-telomeric boundary. One example is shown in Figure 3.3 E, with a pattern of sequence divergence starting only 64

nucleotides from the boundary between telomeric and sub-telomeric DNA (indicated by a yellow arrow). Figure 3S.3 B shows two additional examples, with mutant repeats introduced 31 and 52 nt from the sub-telomeric boundary. This is consistent with the premise that when a fork collapse occurs during DNA replication of bona fide chromosome ends, this creates a substrate for telomerase.

However, in our analysis of the pattern of sequence addition in Ade$^-$ half sectors in the above experiment, not every half sector showed evidence of telomerase-mediated elongation during the first cell division. Although a single site for *de novo* telomere formation was detected in 5 Ade$^-$ half sectors, a single point of sequence divergence could not be identified for an additional 6 Ade$^-$ half sectors from this experiment. Instead, multiple points of sequence divergence were apparent among sequenced telomeres from progeny from each of these 6 Ade$^-$ half sectors (Figure 3.4 A and 3S.4), indicating that telomerase failed to elongate the collapsed fork during this first cell division, and did not act until subsequent cell divisions. This category of Ade$^-$ half sectors exhibited a second notable feature, as telomeres recovered these sector often retained extensive homology with the interstitial tract. In the Ade$^-$ half sector shown in Figure 3.4 A, sequenced telomeres from this half sector retained > 350 bp of telomeric DNA inherited from the interstitial tract, showing that fork collapse did not occur until the replisome had progressed through almost the entire 390 bp interstitial tract. Thus, if a fork collapse occurred at a more distal site in the interstitial tract, it was less likely to be elongated by telomerase (summarized in Figure 3.4 B). This bias also fulfills a key prediction of a model for a model for telomere length

regulation recently proposed by Carol Greider (Greider 2016), in which telomerase travels with the replication fork; this point is re-visited in the Discussion.

Collectively, the experiments in Figures 3.3 and 3.4 show that when a fork collapse occurs during replication of duplex telomeric DNA in wild type cells, this creates a substrate for telomerase that is recognized with very high efficiency, as roughly 50% of the replication fork collapse events (recovered by two different protocols, by selecting for 5-FOA resistance or screening for Ade^{-} half sectors) were elongated by telomerase (Figure 3.4 B). Furthermore, our data demonstrate that the newly synthesized $G_{1\text{-}3}T$ repeats added to collapsed forks is extensive (Figure 3.3 D), arguing that telomerase-mediated elongation of this substrate has the potential to make a substantial contribution to telomere length.

The t-RPA complex promotes progression of the replisome through telomeric duplex DNA

The above analysis demonstrated that a regressed fork was a robust substrate for telomerase. In parallel, we sought to identify telomere-associated factors that regulated the frequency of fork collapse during replication of duplex telomeric DNA. We were particularly interested in the role of the t-RPA complex in this process (Gao et al. 2007), as a test of a long-standing model for the role of this complex at yeast telomeres. The prevailing model posits that the t-RPA complex associates with telomeres in budding yeast by binding to the 3' terminal G-rich ssDNA overhang at chromosome termini, where it functions as a telomeric "cap" that blocks unregulated resection, with reduced cell viability if resection is unchecked (Lydall & Weinert,

1995; Booth et al. 2001). However, *in vitro* binding data did not dictate an obligatory role for this complex at a terminal 3' ssDNA extension, as the Cdc13 subunit of the t-RPA complex bound equally well to internal tracts of G-rich telomeric DNA that are bracketed by duplex DNA (Nugent et al. 1996; Figure 3S.5 A). This suggested that *in vivo*, the t-RPA complex could associate with single-stranded $G_{1\text{-}3}T$ DNA that became exposed when the replication fork moved through duplex telomeric DNA. Consistent with this expectation, Cdc13 physically associated with the internal telomeric tract on Chr IX, as measured by chromatin immunoprecipitation (Figure 3.5 A).

This association of Cdc13 with the interstitial tract prompted us to examine the effects of reduced t-RPA activity in the RepFC assay. We initially examined the effect of a temperature-sensitive mutation in *CDC13*, by monitoring the frequency of Ade^{-} sectors in *cdc13*-ts cells at 23°, 30° and 31°. This revealed a substantial 10-fold increase in the frequency of replication fork collapse at 31° (Figure 3.5 B). This was not simply due to destabilization of the t-RPA complex in response to a thermolabile mutation, as structure-driven mutations in two surfaces of the t-RPA complex also had substantial effects on replication fork collapse. The first of these mutations (*cdc13*-F539A, in the high affinity DNA-binding domain of Cdc13; Anderson et al. 2003) reduced DNA binding *in vitro* (Glustrom et al. 2018) as well as association of Cdc13 with telomeric chromatin (Figure 3S.5 E). A second separation-of-function allele was located on the surface of a wHLH domain in the Stn1 subunit (*stn1*-W466E), which we previously showed performed an as-yet-unspecified function at telomeres (Gelinas et al. 2009). As shown in Figure 3.5 C, both of these mutations altered the frequency

of replication fork collapse in the RepFC assay, with increases of 10- to 20-fold for the *cdc13*-F539A and *stn1*-W466E strains, respectively. This is the opposite of what would be expected from the capping model, which predicts a decreased recovery of viable Ade^{-} cells, due to an inability to protect these newly exposed termini from the lethal consequences of unregulated resection. Instead, the results in Figures 3.5 B and 3.5 C demonstrate that the t-RPA complex is required for efficient progression of the replisome through an interstitial telomeric tract, with this activity mediated by the wHLH domain of Stn1.

The increased replication fork collapse frequency in these two t-RPA mutant strains was accompanied by a pronounced growth defect, with colonies composed of a high number of inviable cells (Figure 3.5 D and see below). This suggested that there might be a threshold for the number of replication fork collapse events that an individual cell could tolerate and still retain viability. To investigate this, the behavior of the *stn1*-W466E mutant strain was examined using a single-cell-division variation of the sectoring assay (Figure 3.5 E). Individual *stn1*-W466E or *STN1* cells at the start of S phase (identified as small budded cells from a mid-log phase culture) were micro-manipulated to fixed positions on a rich media plate. Following completion of the cell cycle and cytokinesis, mother and daughter progeny were moved to adjacent positions, and plates were incubated at 30° to allow colony formation. Viable colonies were subsequently genotyped for the presence/absence of the distal segment of Chr IX, to determine whether a replication fork collapse had occurred during the cell division prior to separating these two cells. A total of 1055 and 1996 *stn1*-W466E and *STN1*

cells, respectively, were assessed by this protocol. This revealed a replication fork collapse rate (2.0%) in the *stn1*-W466E strain (Figure 3.5 F) that was comparable to the frequency observed in the sectoring assay (Figure 3.5 C); in contrast, only one event was observed in the wild type strain (for a frequency of 0.05%). This micro-manipulation assay also revealed two characteristics that could not be quantified in the sectoring assay. In the wild type strain, newly divided mother and daughter cells each formed a full-sized colony in 99% of the 1996 cell divisions. In contrast, only 42% of the *stn1*-W466E cell divisions gave rise to two visible colonies, with the remaining cell divisions producing either one (31%) or no (26%) colonies (Figure 3.5 G). This high degree of inviability was accompanied by a striking impact on cell cycle progression times in the *stn1* mutant strain. Only 35% of the *stn1*-W466E cells completed cell division in ~1 hour (compared to 99% for wild type), with 45% taking 2 to 3 hours to progress through cell division and 25% exhibiting cell cycle delays of 4 hours or longer (Figure 3.5 H). Strikingly, all three of these characteristics were partially suppressed by defect in Exo1 which is recruited to stalled replication forks where it counters fork regression and replication fork breakdown (Cotta-Ramusino et al. 2005; Segurado & Diffley 2008). In the *stn1*-W466E *exo1*-Δ strain, the frequency of replication fork collapse was reduced 4-fold to 0.5% (Figure 3.5 F). Similarly, cell viability and normal cell cycle progression were partially suppressed (Figures 3.5 G–H), arguing that all three phenotypes stem from a single molecular defect that confers an elevated rate of fork collapse.

We suggest that the extended cell division times and high degree of inviability displayed by a subset of *stn1*-W466E cells correspond to those cells that have undergone replication fork collapse events at multiple chromosome ends. Assuming a normal distribution of fork collapse events in a population of *stn1*-W466E cells, some cell divisions will occur without any chromosome ends undergoing a fork collapse, some will have a fork collapse at a single telomere, and some cell divisions will be accompanied by replication fork collapse events at multiple telomeres. This distribution mirrors the range of cell division times for *stn1*-W466E cells, from times that are similar to wild type (1 hour), longer than wild type (~2 – 3 hours), or extensively prolonged (≥ 4 hours). We postulate that there is threshold for the number of replication fork collapse events at telomeres that can be handled during a single cell division; if this threshold is exceeded, this leads to extended cell division times and/or inviability, an issue that is re-visited in the Discussion.

The t-DAM phenotype: an increase in replication fork collapse drives telomere length variation

The increased frequency of fork collapse in the RepFC assay predicts that strains bearing mutations in the t-RPA complex will exhibit an increased frequency of short telomeres at natural chromosome ends. To test this, the high resolution assay described in Figure 3.1 was used to assess telomere length in the *cdc13*-F539A strain. Chr I-L termini were PCR-amplified from multiple *cdc13*-F539A single colonies, and 318 independent cloned PCR products were sequenced. The resulting telomere length profile for the *cdc13*-F539A strain, when compared to wild type, revealed a marked

increase in the category of very short telomeres, with a 4-fold increase in the number of termini shorter than 100 bp (boxed in red, in Figure 3.6 A and 3.6 B). In fact, 15 termini (~5%) in the *cdc13*-F539A strain were ≤ 25 bp, including three chromosome ends that terminated in the sub-telomeric tract, with no detectable telomeric DNA (Figure 3.6 C). This sub-population of ultra-short telomeres was recovered from 7 of the 8 *cdc13*-F539A colonies used to construct this profile, ruling out that this was due to a single aberrant mutant colony. Combined with the behavior of this mutant strain in the RepFC assay, this argues that this expanded sub-population of critically short telomeres is a direct result of replication fork collapse, in response to reduced t-RPA function.

Unexpectedly, this analysis also showed that in addition to the increase in the fraction of very short telomeres, there was also a notable increase in the proportion of elongated telomeres in the *cdc13*-F539A strain, as illustrated by a superimposition of the wild type telomere length profile on the *cdc13*-F539A profile (Figure 3.6 B). We propose that this phenotype – an increase in the sub-populations of both shorter-than-average and longer-than-average telomeres – is the direct result of an elevated frequency of replication fork collapse, as incomplete duplex telomeric DNA replication due to fork collapse will produces short telomeres as well as substrates that are subject to extensive elongation by telomerase. This results in a unique telomere length phenotype in response to fork collapse – an increase in the number of telomeres that deviate from the mean length – which we have named the t-DAM (deviation away from the mean) phenotype. This also predicts that the *cdc13*-F539A telomere length

profile should respond to mutations that influence replication fork breakdown, such as *exo1*-Δ (Cotta-Ramusino et al. 2005; Segurado & Diffley 2008). Consistent with this prediction, the increased frequency of fork collapse, the t-DAM phenotype and the severe growth defect of the *cdc13*-F539A strain were all partially suppressed by an *exo1*-Δ mutation, including in a decrease in both shorter-than-average and longer-than-average sub-populations of telomeres (Figures 3.6 C–E, data not shown).

The above argues that defects in the wHLH domain of Stn1, which also had increased frequency of fork collapse in the RepFC assay, should similarly confer a t-DAM phenotype. To test this, we turned to an alternative approach to evaluate telomere length variation in this mutant strain, since the sub-population of exceptionally long *stn1*-W466E telomeres precluded unbiased PCR amplification. Instead, the length of a restriction fragment of one specific telomere was assessed from 15 independent isolates of the *stn1*-W466E strain (Figure 3.6 H–I). This revealed a range of telomere lengths spanning ~8 kb, with individual $G_{1\text{-}3}T$ telomeric tracts as short as < 100 bp or as long as ~8 kb. In contrast, multiple isolates of this same restriction site fragment from a wild type strain exhibited very little size variation (Figures 3.2 C, 3S.2 B, 3S.7 A and 3S.7 B). Thus, the *stn1*-W466E strain exhibited a very strong t-DAM phenotype, with an extraordinary increase in the extent of telomere length variation when compared to wild type. In fact, the *stn1*-W466E t-DAM phenotype- and in particular, the greatly expanded population of elongated telomeres- was far more pronounced than that conferred by the *cdc13*-F539A mutation, which suggest is due to a key mechanistic difference between these two t-RPA mutations. In

the *cdc13*-F539A strain, association of the t-RPA^{F539A} complex with telomeres was substantially reduced (Figure 3S.5 E), due to the reduced ability of Cdc13-F539A to bind DNA (Glustrom et al. 2018). As a consequence, every telomere-specific activity performed by the t-RPA^{F539A} complex should be diminished in the *cdc13*-F539A mutant strain, including the ability to recruit telomerase. In contrast, the *stn1*-W466E separation-of-function mutation conferred a specific defect in the wHLH domain of the t-RPA^{W466E} complex (Gelinas et al. 2009), without impacting other t-RPA activities (such as telomerase recruitment). Thus, although both mutant strains sustained a comparable level of replication fork collapse (Figure 3.5), we argue that the t-DAM phenotype in the *cdc13*-F539A strain was partially attenuated as a result of reduced recruitment of telomerase to the increased number of collapsed forks but also by the ability of telomerase to respond to these collapsed forks, a point that is re-visited in the discussion.

Extensive sequence loss due to replication fork collapse occurs at native chromosome ends

The RepFC assay predicts that replication fork collapse frequencies at bona fide telomeres should be rare, occurring at each chromosome end every ~1100 cell divisions. If this prediction is accurate, replication fork collapse should not significantly contribute to telomere function in wild type yeast cells. However, several observations suggested that the frequency of spontaneous fork collapse at native telomeres is substantially higher than at the interstitial tract. The first stemmed from an analysis of the single-nucleotide-resolution telomere length analyses performed on

~ 350 single colonies during the course of this study. If a fork collapse occurs during the first cell division that gives rise to a colony, sequenced progeny will show a 50:50 split in the pattern of their sequenced telomeres, corresponding to the location at which the collapse occurred. Figure 3S.7 A shows an example of such an event: a sequence divergence was detected at nucleotide 251 for ~50% of the 19 cloned Chr VI-R sequences from a wild type single colony, indicative of a fork collapse during the first cell division. Additional examples are shown in Figures 3S.2 C and 3S.3 A. If a fork collapse only occurred once in every ~1100 cell divisions, the likelihood of identifying colonies with 50:50 pattern of sequence divergence should be extremely low. However, we identified 5 colonies with a sequence divergence that arose during the first cell division among ~350 single colonies. This argues that replication fork collapse occurs at a substantially higher frequency at the ends of native chromosomes than at interstitial telomeric DNA. We speculate that this increase may be due to a deceased ability of fork stabilization systems to prevent fork collapse and/or re-load replisomes onto stalled or collapsed forks during the very last stages of replicating the genome.

A second set of observations stemmed from further analysis of the wild type and *cdc13*-F539A telomere length profiles shown in Figure 3.6. Because these profiles were constructed from a large number of cloned telomeres from each colony, it was possible to determine the minimum length of $G_{1\text{-}3}T$ sequence in the founder Chr I-L telomere (present in the single cell that founded each colony) from alignments of sibling telomeres (see Figure 3S.1 and Materials and Methods for more details). This

information was subsequently used to determine the extent of founder Chr I-L $G_{1\text{-}3}T$ DNA (indicated in blue in Figure 3.6) that was retained by each of the 241 cloned telomeres, by re-aligning the telomere length profiles based on the length of inherited founder DNA (Figures 3.6 F and G). For the wild type profile, which was composed from three colonies, the three founder chromosomes contained 433, 383 or 340 bp of telomeric DNA (indicated by arrows in Figure 3.6 F; see Figure 3S.1 for more details). This re-aligned wild type profile also showed that many individual telomeres had lost a substantial amount of founder telomeric DNA, as ~1 in 20 telomeres had inherited less than 75 bp of telomeric DNA from the founder Chr I-L chromosomes. This represents a loss of as much as 350 bp of founder DNA during the growth to form these three colonies. This is not readily explained by terminus-specific erosion, as previously discussed by Lingner and colleagues (Chang et al. 2007), who calculated that the probability of a telomere declining in length from 300 bp to 125 bp due to terminus-specific processes was 2.6×10^{-7}; this led them to suggest that replication fork collapse was instead responsible for the extensive loss of founder sequence DNA. If so, this predicts that loss of founder sequence DNA should be even greater in the *cdc13*-F539A strain, due to the increased frequency of fork collapse (Figure 3.5). Strikingly, the sub-population of telomeres that retained less than 75 bp of founder sequences increased from 5.4% in the wild type strain to 23.6% in the *cdc13*-F539A strain ($p = 0.001$), even though many founder chromosomes were longer ($\geq$ 400 bp) in the *cdc13*-F539A strain than in the wild type strain (Figure 3.6 F and G). We conclude that the pronounced loss of founder sequences that occurs in wild type yeast, during

the limited growth necessary to form a single colony, is largely due to replication fork collapse.

DISCUSSION

The prevailing model to explain telomere length homeostasis postulates that in telomerase-expressing cells, telomeres are tightly maintained around a mean length. This is thought to be achieved by preferentially directing telomerase to shorter-than-average telomeres while limiting telomerase activity at longer-than-average telomeres, with the length of each telomere determining its accessibility to telomerase (Marcand et al. 1997; Smogorzewska et al. 2000; Teixeira et al. 2004; Pfeiffer & Lingner, 2013). Mechanistically, this is accomplished by "counting" the number of proteins bound to the duplex portion of each telomere (the "protein counting" model, reviewed by Bianchi & Shore, 2009), which dictates whether a telomere is in a telomerase-extendible or telomerase-non-extendible state. In this model, restricting telomerase to under-elongated chromosome ends serves a dual purpose, by tightly maintaining average telomere length and also ensuring that telomerase-plus cells do not accumulate a population of "critically short" telomeres that are recognized as DSBs. Inherent in this model is that this regulation occurs after duplex telomeric DNA replication has been completed.

We propose instead that the major contribution to telomere length occurs at collapsed replication forks that arise during duplex DNA replication (Figure 3.7), rather than at fully replicated telomeres. Fork collapse is generally viewed as a

pathological process that requires a considerable cellular investment to prevent, but we suggest that at chromosome ends, replication fork collapse has been co-opted to drive telomere homeostasis. Central to this proposal are newly defined activities for two key complexes: a role for telomerase in elongating regressed replication forks (Figure 3.3 and 3.4) and a re- assignment of the role of the yeast t-RPA complex from end protection to facilitating duplex DNA replication (Figure 3.5). We also show that telomere homeostasis is dictated not just by average length but is also dependent on the extent of telomere length variation (Figure 3.1), with both properties controlled by replication fork collapse (Figures 3.6 and 3S.6). Below, we amplify these key observations, followed by our proposed model.

Telomerase elongates two temporally and structurally distinct substrates *in vivo*

The current model assumes that the substrate recognized by telomerase is a fully replicated chromosome, produced after semi-conservative DNA replication is complete. However, an increasing number of studies have speculated that a second substrate for telomerase is generated during DNA replication in response to aberrantly high levels of replication fork stalling (for example, Dehé et al. 2012). Left unresolved by prior work has been the molecular structure of the DNA replication intermediate that is recognized by telomerase following fork collapse, and whether such an intermediate will contribute to telomere homeostasis in a wild type setting. Here, we provide the first direct evidence that regression of a stalled fork generates a substrate for telomerase, by analyzing the molecular footprint of telomerase activity immediately following fork collapse (Figure 3.3).

The demonstration that there are two temporally and structurally distinct substrates for telomerase in wild type cells invokes the possibility of distinct regulatory pathways (and possibly even different modes of substrate recognition by the telomerase active site), which is supported by the substantially different behavior of telomerase at these two substrates. We show that a collapsed fork is subject to extensive elongation (Figure 3.3), whereas fully replicated telomeres undergo much more restricted synthesis (Teixeira et al. 2004). Furthermore, our data show that collapsed replication forks are a preferred substrate for telomerase, as ~50% of these termini are elongated by telomerase (Figure 3.4 B), in contrast to the ~7% frequency observed at chromosome ends that are presumably fully replicated (Teixeira et al. 2004). This also suggests a re-examination of prior work that did not differentiate between these two substrates. For instance, studies that were thought to be observing events at fully replicated chromosome ends, such as preferential association of telomerase protein subunits and telomerase length regulators with short telomeres (Bianchi & Shore, 2007; Hector et al. 2007; Sabourin et al. 2007; McGee et al. 2010), may have instead monitored events at substrates that arose as the result of replication fork collapse during duplex telomeric DNA replication.

Telomerase preferentially elongates collapsed forks, rather than short telomeres

The prior inability to experimentally differentiate between these two categories of telomerase substrates also has implications for the long-standing premise that telomerase preferentially elongates short telomeres. This premise initiated with a pivotal study that measured the extent and frequency of telomerase-mediated

elongation of individual chromosome termini during a single cell cycle (Teixeira et al. 2004). This revealed a remarkable length preference: very few telomeres that retained ≥ 300 bp of $G_{1\text{-}3}T$ sequences were substrates for telomerase, whereas ~ 50% of telomeres that were ≤ 100 bp were elongated. This sub-population of very short telomeres also underwent extensive elongation by telomerase (which the authors postulated was due to a "loss of normal telomerase control"), in contrast to the much more limited synthesis at telomeres that were closer to physiological lengths.

The above study led Lingner and colleagues to propose that telomeres switch between telomerase- extendible and telomerase-non-extendible states, with the "switch" determined by the length of the duplex telomeric tract (Teixeira et al. 2004). However, this model rested on the assumption that telomerase only elongates fully replicated telomeres. We propose that these two "states" are instead two different substrates for telomerase: one generated by fork collapse (which was the sub-category in Lingner's study that was subject to substantial telomerase-mediated lengthening) and a second substrate produced after DNA replication is complete. Thus, this posits that the preferential bias previously observed by Lingner's group was not dictated by the length of the duplex $G_{1\text{-}3}T$ tract, but instead by a choice between substrates. This also provides a mechanistic answer to the long-standing question of how telomerase preferentially acts at one particular sub-category of chromosome ends: it is simply due to substrate preference.

A role for telomerase at replication forks also argues that the structure of the collapsed fork may contribute a previously unrecognized role in regulating telomerase

activity. For example, the role of the Mre11-Rad50-Xrs2 (MRX) complex in yeast telomere length regulation has long been assumed to be due to an end-processing activity at fully replicated termini (Larrivée et al. 2004; Martina et al. 2012); however, increasing evidence for a function for this complex at stalled replication forks suggests that MRX may instead regulate telomere length homeostasis by protecting fork integrity (Costanzo, 2011; Bentsen et al. 2013; Kolinjvadi et al. 2017). In support of this idea, our unpublished data have shown that the frequency of elongation of newly collapsed forks by telomerase is reduced in mutant yeast strains defective for proteins that protect regressed forks from degradation (manuscript in preparation). This also argues for an alternative interpretation of the recent observation that there is a pathological interaction between replication forks and telomerase in RTEL1 -/- mammalian cells (Margalef et al. 2017). We suggest instead that collapsed forks generated in the absence of the RTEL1 helicase may be structurally incompatible as a telomerase substrate, which results in an unproductive interaction between telomerase and collapsed forks in RTEL1-depleted cells. Such a model would also explain the impaired elongation of the shortest sub-population of chromosome ends in RTEL1 -/- cells (Ding et al. 2004), due to a presumed inability of telomerase to recognize and elongate these atypical collapsed forks.

The essential function of the t-RPA complex is to promote duplex telomeric DNA replication

This study also re-assessed the current model for the role of the t-RPA complex at yeast telomeres, which initiated with a pivotal observation that Cdc13-

depleted cells accumulated single-stranded regions in telomere and telomere-proximal regions of the genome (Garvik et al. 1995). To explain these DNA lesions, Hartwell and colleagues put forth two alternative models: Cdc13 protected chromosome termini from unregulated resection by an unknown nuclease and recognition as DSBs (the "capping" or end protection model), or Cdc13 instead facilitated lagging strand DNA synthesis of telomere-proximal regions. Although the end protection model has largely dominated for the past 20 years, an increasing body of evidence in other species has established that this conserved RPA-like complex promotes duplex DNA replication (Goulian et al. 1990; Gu et al. 2012; Chen et al. 2013; Derboven et al. 2014; Takikawa et al. 2017; Nakaoka et al. 2012).

The RepFC assay provides a means of distinguishing between the two hypotheses proposed by Garvik et al. 1995, as these two models make opposing predictions about the effect of mutations in the t-RPA complex on the frequency of Ade^- sectors. The end protection model predicts that the frequency of fork collapse during duplex DNA replication should not be altered by a t-RPA deficiency; however, once a collapse has occurred, the reduced viability due to a predicted inability to protect these newly exposed termini should decrease the recovery of Ade^- half sectors. In contrast, if the t-RPA complex facilitates DNA replication, this predicts that frequency of fork collapse will increase in response to a t-RPA defect, resulting in an increase in Ade^- half sectors, which is exactly what we observed in response to mutations in t-RPA (Figure 3.5). We conclude that the essential function of the t-RPA

complex is to promote faithful replication of duplex telomeric DNA, rather than to protect termini from resection.

A new model for telomere length homeostasis

We propose that replication fork collapse, and subsequent extensive elongation by telomerase, is the major determinant of telomere length regulation. Mechanistically, we propose that this is achieved by association of both t-RPA and telomerase with the replication fork (Figure 3.7; Greider, 2016), with the t- RPA complex facilitating progression of the replisome through duplex telomeric DNA. Nevertheless, even in wild type cells, semi-conservative replication of telomeres is not always successful, resulting in fork collapse. Our data show that most of these termini are elongated by telomerase (Figure 3.7 A), with an average extension length of 120 bp in a single cell division. However, if telomerase is not recruited to these collapsed forks, these replication errors can result in abruptly shortened telomeres (Figure 3.7 B); since fork collapse can occur at any position in the ~320 bp duplex telomeric tract, a collapsed fork that is not re-elongated by telomerase could lose ~160 bp on average. Therefore, these two counter- balancing activities at collapsed forks have the potential to confer large increases or decreases in the length of individual telomeres. In contrast, the extent of elongation by telomerase at fully replicated telomeres is more modest, with more than 90% of fully replicated telomeres that fail to be elongated by telomerase in each cell division (Figure 3.7 C; Teixeira et al. 2004). Telomere shortening at fully replicated telomeres also occurs, in order to re-create the G-rich overhang on leading strand termini (boxed in red in Figure 3.7; Lingner et al. 1995),

but this has also been estimated to be fairly limited in scope (Singer & Gottschling, 1994). Thus, the potential for substantial changes in length during each cell division at fully replicated telomeres is much less and therefore makes a more minor contribution to telomere length maintenance.

As noted above, this model invokes the idea that telomerase travels with the replication fork, mediated by its previously established association with the t-RPA complex (Tucey & Lundblad, 2013; Jiang et al. 2015). This was first suggested by Carol Greider (Greider, 2016), who proposed that telomerase could be delivered to the ends of chromosomes through its association with the replication fork. Although Greider's proposal was based on the assumption that telomerase only had a single substrate (a fully replicated telomere end), her model can be readily extended to collapsed forks. In fact, her idea provides a simple mechanism to explain why such a high percentage of fork collapse events in the interstitial telomeric tract are elongated by telomerase, as association with the replication fork would ensure immediate proximity of telomerase to its substrate. In support of this premise, we show that if a fork collapse occurred immediately adjacent to the telomeric/sub-telomeric boundary, it was much more likely to be elongated by telomerase (i.e. in the same cell cycle) than more distal fork collapse events (Figure 3.4 B). This argues that there is a gradient of telomerase association with the replication fork that decreases as the fork proceeds towards the terminus, which is a key prediction of Greider's model.

This model also raises the question of whether previously identified telomere length regulators perform their regulatory role by mediating the frequency of fork

collapse and/or subsequent telomerase activity at collapsed forks, rather than events at fully replicated termini. If so, strains defective for this category of telomere length regulators should exhibit a t-DAM phenotype. In fact, we have identified a t-DAM phenotype in a yeast strain defective for the Rif2 protein (Figure 3S.7), with a notable increase in the sub- population of short telomeres and a pronounced loss of founder sequence DNA. This phenotype is not readily explained by the protein counting model and instead suggests that Rif2 contributes to the mechanism for telomere homeostasis proposed in Figure 3.7. We are currently re-evaluating telomere length in a wide spectrum of mutant strains to determine whether additional telomere length regulators may have an altered t-DAM phenotype when defective.

Is there a threshold for telomere dysfunction due to collapsed forks?

We end this discussion by speculating about the molecular basis for "telomere dysfunction", which has widely been assumed to arise in response to telomeres that are too short to support chromosome end protection. However, wild type yeast cells clearly tolerate a persistent sub-population of so-called "critically short" telomeres, which contradicts the long-standing notion that very short telomeres are both infrequent and transient in telomerase-plus cells. Extrapolating from the Chr I-L and VI-R data (Figures 3.1 C and 3S.1; data not shown) to all 32 yeast telomeres argues that the majority of wild type cells contain one or more chromosome termini with ≤ 100 bp of $G_{1\text{-}3}T$ telomeric DNA. Nevertheless, wild type yeast does not appear to exhibit a response, such as a transient cell cycle arrest, to these presumably critically short termini (Figure 3.4 H). Similarly, in the checkpoint-proficient human male

germline, high- resolution telomere length analysis at the single molecule level has identified a sub-population of severely shortened telomeres at a frequency of 3.5% (Baird et al. 2006).

Nevertheless, there obviously is a limit to the extent of telomere dysfunction that cells can tolerate. This threshold has been widely assumed to be solely determined by length, when the proportion of short telomeres exceeds a certain limit. We propose that the number of collapsed (and/or stalled) replication forks may constitute a separate threshold for telomere dysfunction. This proposal stems in part from our single cell analysis of the *stn1*-W466E strain, which suggested that the range of cell progression times and/or viability was dictated by the number of telomere-associated replication fork collapses occurring in each cell division (Figures 3.5 G–H). In the small sub-population of *stn1*-W466E mutant cells with cell division times that were indistinguishable from *STN1* cells, this "wild-type" growth behavior would be due to very few (or no) telomere-associated fork collapse events in these *stn1*-W466E cells. We suggest that in those mutant cell divisions that experienced a higher frequency of fork collapse events, this resulted in an increasing delay in cell cycle progression, until the number of fork collapse events exceeded a certain threshold, leading to a permanent growth arrest.

More direct support for the idea of a telomere dysfunction threshold due to replication stress comes from an assessment in human cells of the extent of association of DDR-specific proteins with telomeres, referred to as telomere dysfunction-induced foci (TIFs; Takai et al. 2003). Quantitation of the association of DDR proteins in a

recent study (in this case, phosphorylated H2AX) concluded that a threshold of five dysfunctional telomeres was sufficient to confer a growth arrest (Kaul et al. 2012). However, this DDR signal did not correlate with either telomere length or an increase in telomere fusions, which led Reddel and colleagues to conclude that the DDR signal "did not result from lack of telomeric DNA". Thus, this study apparently monitored a threshold for DNA replication stress, instead of (or in addition to) the extent of telomere uncapping. By extrapolation, the transient recruitment of DDR proteins to sub-populations of telomeres in both budding yeast and mammalian cells may reflect association with stalled and/or collapsed replication forks, rather than a response to (fully replicated) critically short telomeres (as also suggested by Rog & Cooper, 2008).

IMPLICATIONS

We suggest that the model proposed in Figure 3.7 is likely to be widely applicable, as a causative relationship between replication fork stress and telomere length has been extensively observed in other well-studied systems such as fission yeast and human cells. For example, depletion of Taz1 (in fission yeast) or TRF1 (in mammalian cells) leads to extensive telomere elongation (Cooper et al. 1997; van Steensel & de Lange, 1997) in parallel with a profound defect in replication fork progression through duplex telomeric DNA (Miller et al. 2006; Sfeir et al. 2009; Martinez et al. 2009), resulting in high levels of recruitment of telomerase to these sites of defective DNA replication (Dehé et al. 2012). Similarly, inhibition of DNA

Pol α, either through genetic manipulation or treatment with aphidicolin, confers telomere elongation in yeast and human cells (Carson & Hartwell, 1985; Sfeir et al. 2009) as well as increased frequency of replication fork collapse in yeast (Figure 3.2 J) or telomere fragility in human cells (Sfeir et al. 2009); we suggest that the telomere length change in response to impaired lagging strand synthesis in both species is due to telomerase elongation of an increased number of collapsed forks, as proposed in Figure 3.7. These selected examples, among many, argue that replication fork collapse during duplex telomeric DNA replication, and the subsequent response by telomerase, is widely-conserved mechanism that contributes to telomere homeostasis across the eukaryotic spectrum.

FIGURES

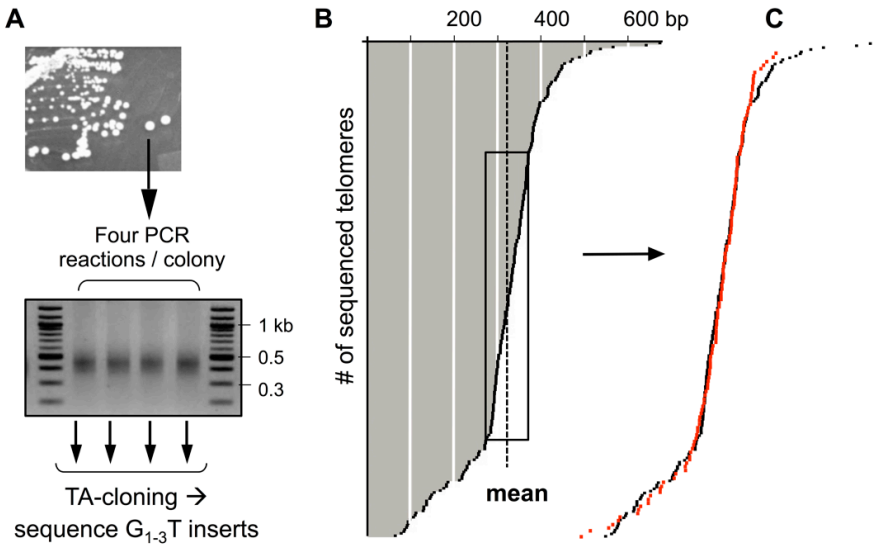

Figure 3.1: Wild type yeast telomeres exhibit extensive length variation. (A) Schematic illustration of the protocol for generating a telomere length profile at single nucleotide resolution. From a yeast culture was grown for ~25 generations from a single cell, the Chr I-L telomere was amplified by four independent PCR reactions, as shown. $G_{1\text{-}3}T$ inserts in multiple independent plasmids were cloned from each PCR reaction without gel purification, and the resulting sequence information was used to construct the profile shown in part (B). (B) Telomere length analysis of a wild type yeast strain assessed at single-nucleotide resolution, as illustrated by an alignment of the length of the $G_{1\text{-}3}T$ telomeric tracts from 241 individual sequenced isolates recovered by PCR amplification of Chr I-L from three wild type yeast single colonies, as described in (A); see Materials and Methods for protocol details. The sub-set of telomeres that are within 50 bp of the mean (either shorter or longer) are boxed. Primary sequence data are in Figure 3S.1. (C) Superimposition of two independently generated profiles of wild type Chr I-L telomere length from a wild type strain, from (B), in black, and from an independent assessment, in red (from 135 sequenced isolates of Chr I-L recovered from 8 wild type yeast colonies); based on a Kolmorogov Smirnov test, these two profiles are not statistically different from each other ($p = 0.65$).

Figure 3.2: The RepFC assay: spontaneous replication fork collapse at an interstitial telomeric tract. (A) Structure of the left end of Chr IX in a strain containing an interstitial telomeric tract, composed of 302 bp of sub-telomeric DNA and 390 bp of $G_{1\text{-}3}T$ telomeric repeats from the Chr I-L telomere, inserted 6.7 kb distal to ARS922 and 27 kb upstream of the Chr IX chromosome terminus. (B) Serial dilutions of cultures of *TLC1* and *tlc1*-Δ strains (generated by dissection of *TLC1*/*tlc1*-Δ diploid strain containing the telomeric tract on Chr IX) were plated on 5-FOA-containing media to assess the spontaneous frequency of Ura$^-$ cells in each culture. (C) Southern blot analysis of Xmn1-digested genomic DNA from four 5-FOA^R isolates (out of 50 tested) from a *TLC1* strain shows the appearance of a "fuzzy" 2.3 kb band, due to the formation of a new telomere at the interstitial telomeric tract; in 5-FOA^R isolates from *tlc1*-Δ cells, this newly formed telomere was ~150 – 250 bp shorter (Figure 3S.2 B). Restriction sites and position of the probe are indicated in (A). (D) Alignment of the sequence of de novo telomeres recovered by PCR amplification of a 5-FOA^R colony from a *TLC1* strain, compared to the sequence of the interstitial tract (top line of alignment); this comparison identifies the site of replication fork collapse that occurred in the 5-FOA^R colony, based on sequence divergence due to telomerase-mediated elongation. PCR amplification employed a primer, indicated in (A), that recognized a unique sequence present on the proximal side of the interstitial tract and a second primer that recognized the poly(C)n tract that was added onto chromosome ends prior to the amplification step. Sequence data for progeny cloned from six additional 5-FOA^R colonies are shown in Figure 3S.2 C. The color code for the sequence data is GATC. (E) Schematic illustrating the location of 12 replication fork collapse events from a *TLC1* strain, analyzed as in (D) and Figure 3S.2 C. (F) The same analysis as in (D), showing a sequence alignment of 8 progeny from a 5-FOA^R colony isolated from a *tlc1*-Δ strain. Sequence data for progeny from 16 additional 5-FOA^R colonies are shown in Figure 3S.2 D. (G and H) The strain shown in Figure 3.2 A, bearing an interstitial telomeric tract on Chr IX, was modified by inserting the *ADE2* gene 14.4 kb from the natural telomere. When cells from this strain are plated on rich media with limiting amounts of adenine, a replication fork collapse during the first cell division gives rise to a colony composed of Ade+ (white) and Ade$^-$ (red) half-sectors, as depicted in (H). Fork collapse events in subsequent cell divisions that give rise to 1/4 sectors, 1/8 sectors, etc. also occur, but are not indicated in this schematic. The selectable marker downstream of the telomeric tract was also changed from *URA3* to *HIS3* in this strain, for minor technical reasons. (I) The frequency of Ade$^-$ half-sectors in a rad53-21 strain is increased by the presence of 1 mM HU; a total of 7,084 and 12,905 colonies were examined in the absence or presence of HU, respectively. (J) The percentage of sectored colonies in *POL1* vs. *pol1*-1 strains at 23°, 30° or 31° C, with ~2,000 to 2,500 colonies examined for each genotype at each temperature; because the effects of the *pol1*-1 mutation (which is a "leaky" Ts allele) did not become pronounced until the second cell division at semi-permissive temperatures, the frequency of Ade$^-$ 1/4 sectors was evaluated in this experiment. We confirmed that the increase in Ade$^-$ quarter sectors was due to loss of the distal tract (rather than due to the mutator effect of the *pol1*-1 allele; Gutiérrez & Wang 2003), by showing that a second genetic marker immediately distal to the telomeric tract (*HIS3*) was also lost in 100% of 38 Ade$^-$ sectors tested.

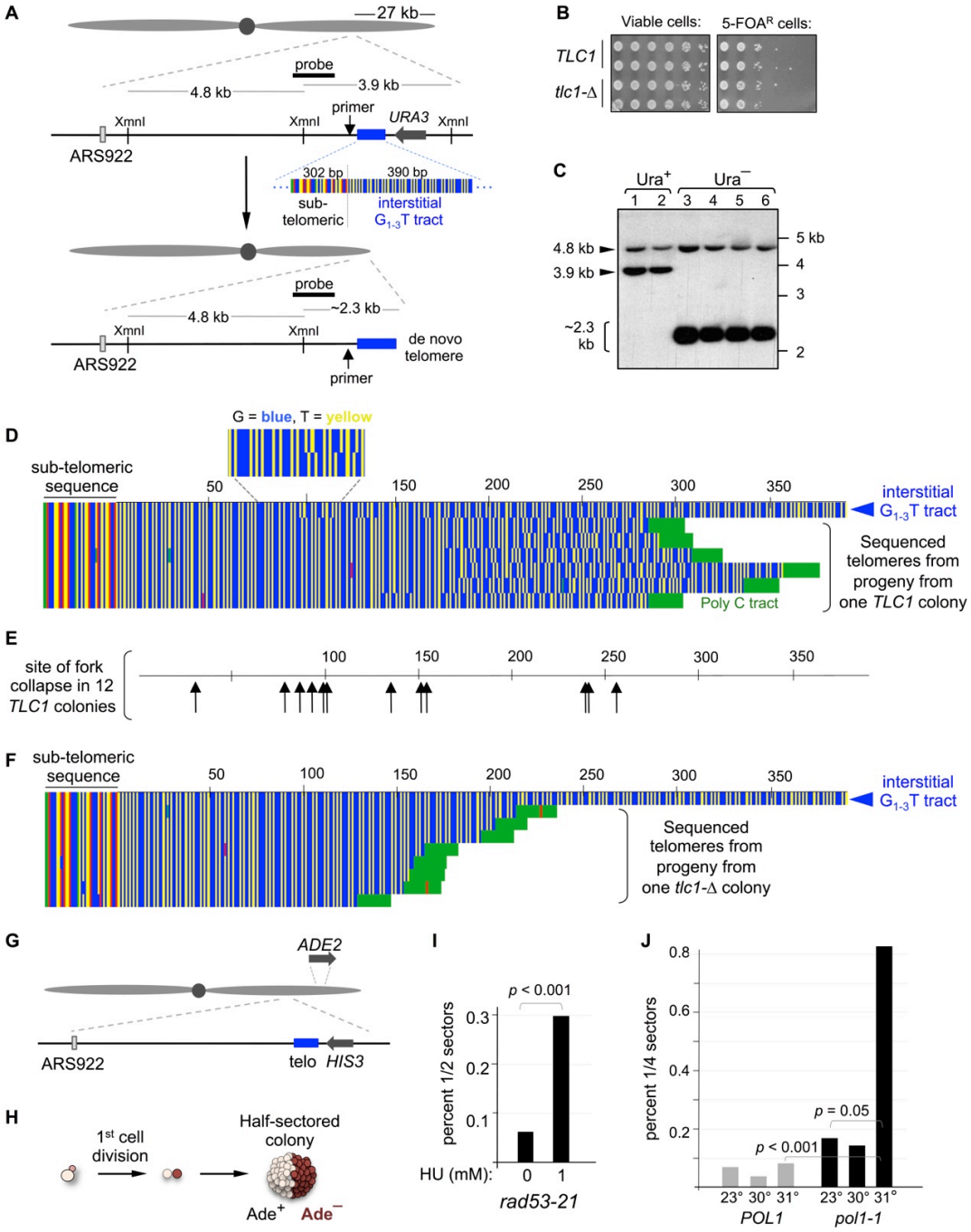
A
—27 kb—
probe
4.8 kb
3.9 kb
primer
URA3
XmnI
XmnI
XmnI
ARS922
302 bp
390 bp
sub-telomeric
interstitial G1-3T tract
probe
4.8 kb
~2.3 kb
XmnI
XmnI
de novo telomere
ARS922
primer
B
Viable cells:
5-FOAR cells:
TLC1
tlc1-Δ
C
Ura+
Ura−
1 2 3 4 5 6
4.8 kb
3.9 kb
~2.3 kb
5 kb
4
3
2
D
G = blue, T = yellow
sub-telomeric sequence
50 150 200 250 300 350
interstitial G1-3T tract
Sequenced telomeres from progeny from one TLC1 colony
Poly C tract
E
site of fork collapse in 12 TLC1 colonies
100 150 200 250 300 350
F
sub-telomeric sequence
50 100 150 200 250 300 350
interstitial G1-3T tract
Sequenced telomeres from progeny from one tlc1-Δ colony
G
ADE2
ARS922
telo HIS3
H
1st cell division
Half-sectored colony
Ade+
Ade−
I
p < 0.001
percent 1/2 sectors
0.3
0.2
0.1
HU (mM): 0 1
rad53-21
J
0.8
0.6
0.4
0.2
percent 1/4 sectors
p = 0.05
p < 0.001
23° 30° 31° 23° 30° 31°
POL1
pol1-1

Figure 3.3: Telomerase elongates regressed replication forks. Two possible outcomes (A and B) for a stalled replication fork. (A) A double strand break that occurs within the vicinity of the stalled fork would generate two termini, which could each be independently elongated by telomerase, indicated as (i) and (ii). This model assumes that this event occurs in the second cell division during colony formation, in order to give rise to an Ade⁻ half-sectored colony in the RepFC assay (if it occurred in the first cell division, both progeny cells would be Ade⁻). (B) Regression of a stalled replication fork results in a so-called "chicken foot" structure, with a 3' G-rich single-stranded substrate that can be elongated by telomerase; our unpublished data has shown that resolution of the proposed Holliday junction relies on redundant structure-specific nucleases. In both (A) and (B), telomerase elongation is indicated by a dotted line; for clarity, subsequent synthesis of the corresponding C-strand is omitted. (C) An alignment of 25 telomeric sequences, recovered by PCR amplification from a single Ade⁻ half- sector from the RepFC assay, reveals a single point of sequence divergence, located 57 nucleotides from the junction of the $G_{1\text{-}3}T$ telomeric tract with sub-telomeric DNA, when compared to the sequence of the interstitial telomeric tract. The horizontal bracket (in yellow) demarcates newly synthesized $G_{1\text{-}3}T$ DNA that is common to >60% of the progeny and was therefore synthesized by telomerase during the first cell division that gave rise to the Ade⁻ half sector. The Ade+ half of this colony was amplified and sequenced, to confirm that the interstitial tract was intact prior to the cell division that gave rise to the Ade⁻ half sector (data not shown). Figure S3A shows four other Ade⁻ half sectors with a common point of sequence divergence among the majority of sequenced progeny. The yellow arrow indicates a telomere with a sequence divergence only 24 nucleotides from the sub-telomeric junction, which we suggest was the result of an additional fork collapse event that arose in a later cell division during growth of this Ade⁻ half sector. (D) A schematic map of the extent of telomerase-mediated elongation in the founder cell division that gave rise to 5 Ade⁻ half-sectored colonies, based on a common sequence that was inherited by >60% of the progeny for each half sector, shown in (C) above or Figure S3A. The point of sequence divergence for these five Ade⁻ half sectors is also indicated. (E) A mutant telomerase RNA (with the wild type template 3'-CACACC**CA**CACCAC-5' changed to 3'- CACACC**uc**CACCAC-5'; Förstemann et al. 2003) under control of the GAL promoter was transiently expressed in liquid culture containing galactose for four hours, followed by plating for single colonies on rich media containing glucose (which shuts down the GAL promoter). Chr I-L was PCR-amplified from single colonies and cloned isolates were sequenced; shown are four sequenced telomeres from one single colony. Figure 3S.3 B shows two additional examples.

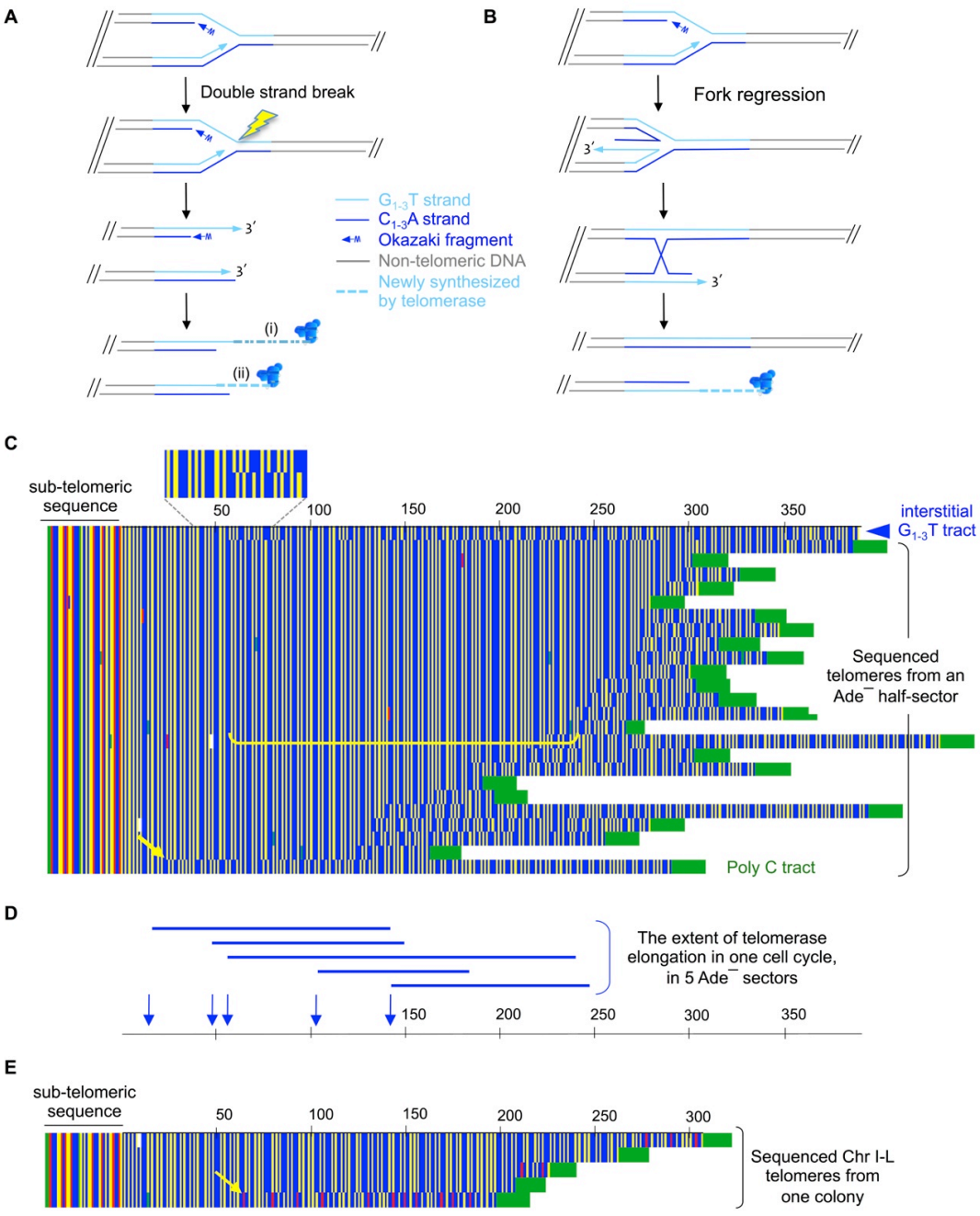
A
Double strand break
3′
3′
(i)
(ii)
G1-3T strand
C1-3A strand
Okazaki fragment
Non-telomeric DNA
Newly synthesized by telomerase
B
Fork regression
3′
3′
C
sub-telomeric sequence
50
100
150
200
250
300
350
interstitial G1-3T tract
Sequenced telomeres from an Ade− half-sector
Poly C tract
D
The extent of telomerase elongation in one cell cycle, in 5 Ade− sectors
150
200
250
300
350
E
sub-telomeric sequence
50
100
150
200
250
300
Sequenced Chr I-L telomeres from one colony

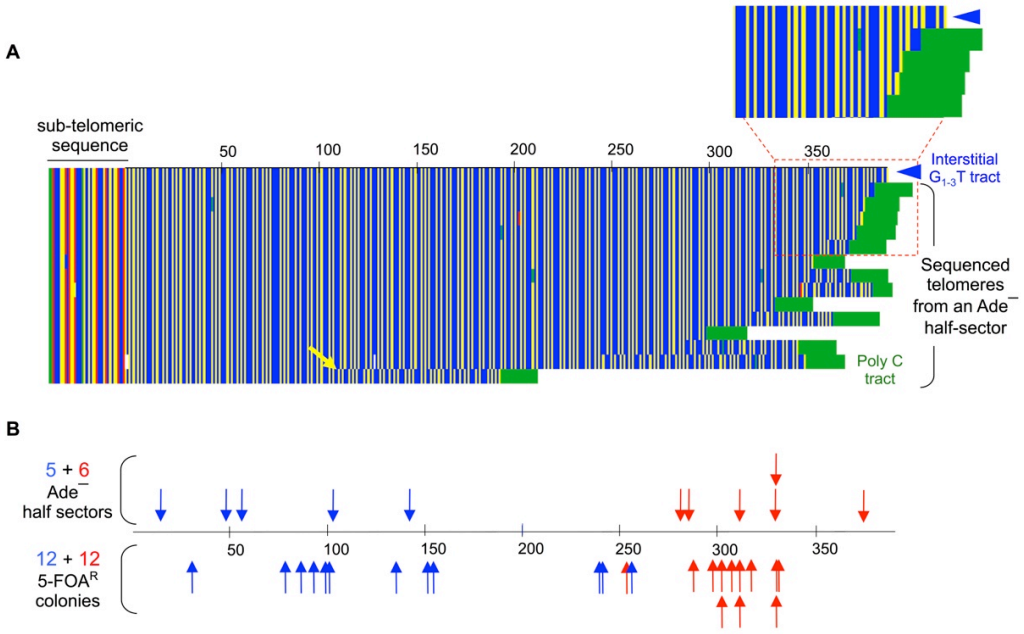

Figure 3.4: The pattern of telomerase elongation at distal replication fork collapse events. (A) Alignment of 13 telomeric sequences recovered from progeny from a single Ade$^-$ half sector, in which there is not a single point of sequence divergence when compared to the sequence of the interstitial telomeric tract, indicating that telomerase did not elongate the collapsed fork during the first cell division that gave rise to this Ade$^-$ half sector. The boxed portion of the alignment highlights a subset of progeny that exhibited extensive homology with the interstitial $G_{1-3}T$ sequence, revealing that fork collapse occurred only ~15 nucleotides from the distal end of the interstitial telomeric tract. Figure S4 shows five additional examples of this category of Ade$^-$ half sectors. The yellow arrow points out a telomere with a sequence divergence within ~100 bp of the sub-telomeric junction, which presumably arose as the result of a fork collapse event that occurred during subsequent growth of the half sector. (B) A summary of replication fork events in wild type cells, recovered from 5-FOA^R colonies (below the line; Figures 3.2 C, 3S.2 and data not shown) or Ade$^-$ half sectors (above the line; Figures 3C, 4A, S3 and S4). Blue arrows indicate the position of telomerase-mediated elongation of the newly generated fork collapse in the "founder" cell division that gave rise to each analyzed colony. Red arrows indicate the approximate position of fork collapse (determined based on the extent of homology with the interstitial tract shared by at least three progeny telomeres), for those colonies in which the collapsed fork was not accompanied telomerase elongation in the first cell division that founded each colony.

Figure 3.5: The t-RPA complex promotes replication of duplex telomeric DNA. (A) Cdc13 association with the interstitial telomeric tract introduced on Chr IX or the natural Chr VI-R telomere, as measured by ChIP; values are calculated from duplicate isolates (and three technical replicates) for each strain, normalized to a non-telomeric locus. The reduced association at the internal tract, relative to the natural Chr VI-R terminus, is presumably because the interstitial G-rich strand is replicated in the opposite orientation in 30% of cell divisions, based on the efficiency of the immediately adjacent ARS922 (McGuffee et al. 2013); in these cell divisions, there would be no appreciable exposed single-stranded G-rich DNA to provide a substrate for Cdc13 binding, resulting in a reduction in the association of Cdc13 with the interstitial tract, relative to the association with the native Chr VI-R telomere (B) The frequency of replication fork collapse in wild type and *cdc13*-ts strains at 23°, 30° or 31° C, as assessed by the frequency of Ade$^-$ half-sectored colonies in the RepFC assay, with ~2,100 to 2,500 colonies examined at each temperature for the wild type strain, and 2,900 to 3,500 colonies at each temperature for the *cdc13*-ts strain. The *cdc13*-ts mutation was isolated and characterized in a prior study (Paschini et al. 2012). (C) The frequency of replication fork collapse for two separation-of-function mutations in the t-RPA complex, as measured by the RepFC assay, with 8,223, 2,836 and 5,891 colonies assessed for the wild type, *cdc13*-F539A and *stn1*-W466E strains, respectively. For the *stn1*-W466E strain, 133 Ade$^-$ sectors were tested for loss of the genetic marker immediately downstream of the telomeric tract (*HIS3* in Figure 3.3 G); 100% were His$^-$, confirming that the increase in Ade$^-$ sectors was due to loss of the entire 27 kb distal tract. (D) Growth of *stn1*-W466E and *cdc13*-F539A haploid strains on rich media at 30°, following dissection of the appropriate heterozygous diploids; colony size for both mutant strains continued to increase with additional incubation. (E) Schematic representation of the experiment shown in (F) – (H); individual cells in early G1-phase (i.e. with small buds) from a mid-log culture were placed in fixed positions on rich media, allowed to complete the cell cycle, and the newly divided cells were physically separated and moved to adjacent positions. Cells were physically separated only after they had progressed into the next cell cycle (i.e. displaying visible buds corresponding to the second cell division), to minimize inviability due to the micromanipulation step. Following incubation at 30° for 48 hours (for *STN1*) or 72 to 96 hours (for *stn1*- W466E and *stn1*-W466E *exo1*-Δ), progeny were evaluated for the ability to form visible colonies and the loss of the distal tract on Chr IX; a total of 1996, 1055 and 1673 cells from isogenic *STN1*, *stn1*-W466E and *stn1*-W466E *exo1*-Δ strains, respectively, were examined by this protocol. The primary data and statistics for (F) – (H) are shown in Figure 3S.6. (F) The frequency of replication fork collapse that occurred during the cell division prior to cell separation, for the indicated genotypes, for cell divisions that produced two visible progeny colonies. (G) The proportion of newly divided cells that either gave rise to only one or zero visible colonies, for the indicated genotypes. (H) The proportion of newly budded cells that took 2, 3 or ≥ 4 hours to complete the cell cycle, for the indicated genotypes.

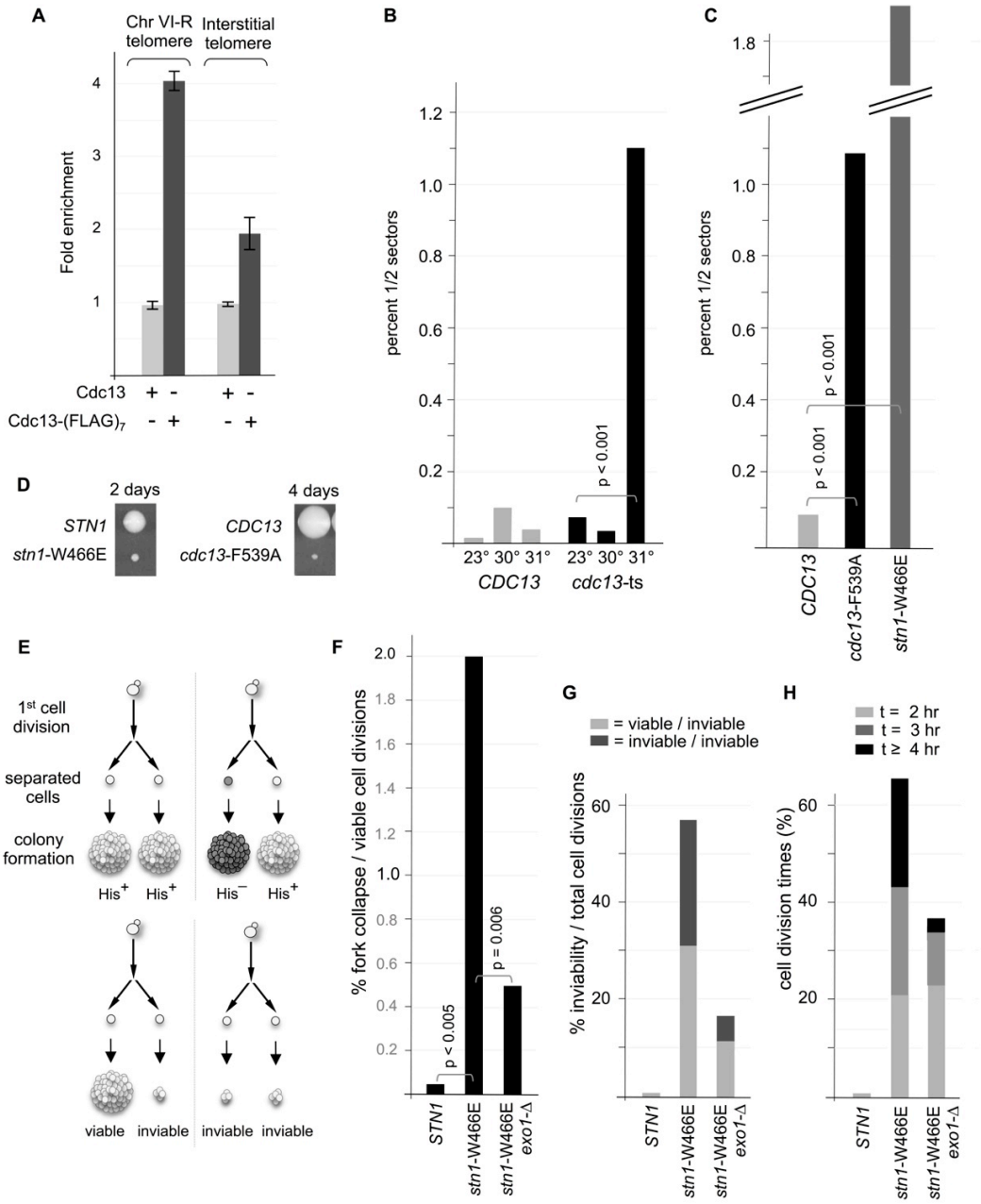
A
Chr VI-R telomere
Interstitial telomere
Fold enrichment
Cdc13
Cdc13-(FLAG)7
B
percent 1/2 sectors
p < 0.001
23° 30° 31°
CDC13
cdc13-ts
C
percent 1/2 sectors
p < 0.001
p < 0.001
CDC13
cdc13-F539A
stn1-W466E
D
2 days
4 days
STN1
stn1-W466E
CDC13
cdc13-F539A
E
1st cell division
separated cells
colony formation
His+ His+
His− His+
viable inviable
inviable inviable
F
% fork collapse / viable cell divisions
p < 0.005
p = 0.006
STN1
stn1-W466E
stn1-W466E exo1-Δ
G
= viable / inviable
= inviable / inviable
% inviability / total cell divisions
H
t = 2 hr
t = 3 hr
t ≥ 4 hr
cell division times (%)

Figure 3.6: The t-DAM phenotype: increased replication fork collapse alters telomere homeostasis. (A) and (B) Telomere length profiles for wild type (A) and *cdc13*-F539A (B) strains. Blue corresponds to sequences inherited from the founder Chr I-L telomeres, and green to sequences that are unique to each cloned telomere and hence were synthesized by telomerase; see text, Figure 3S.1 and Materials and Methods for more discussion. The wild type profile is identical to that shown in Figure 3.1 B; the *cdc13*-F539A profile was constructed from 318 independent cloned PCR products from eight *cdc13*-F539A single colonies. The proportion of telomeres that are ≤ 100 bp in both profiles are boxed in red. The telomere length profile from the wild type strain (in black) is superimposed on the *cdc13*-F539A profile; the statistical difference between these two profiles is $p = 3 \times 10^{-6}$, as determined by a Kolmorogov Smirnov test. (C) The phenotype of the *cdc13*-F539A *exo1*-Δ strain in the RepFC assay, based on the frequency of Ade^- half sectors in 8,223 wild type colonies vs. 14,957 *cdc13*-F539A *exo1*-Δ colonies; the result for *cdc13*-F539A from Figure 3.5 C is included for comparison. (D) The growth phenotype of haploid strains with the indicated genotypes, following dissection of a *cdc13*-F539A/*CDC13 exo1*-Δ/*EXO1* diploid strain and growth on rich media at 30° for three days; after an additional 48 hours of growth, the haploid *cdc13*-F539A mutant strain produced a visible colony. (E) A comparison of the telomere length profiles from *cdc13*-F539A and *cdc13*-F539A *exo1*-Δ strains, for telomeres less than 100 bp. The *cdc13*-F539A *exo1*-Δ profile was constructed from 193 sequenced Chr I-L progeny from four single colonies (data not shown). (F) and (G) The same telomere length profiles as in (A) and (B), re-aligned based on the length of founder sequence inherited by each progeny. The three or eight founder chromosomes for the wild type or *cdc13*-F539A profiles, respectively, are indicated. The founder length profile for the wild type strain (in aqua) is superimposed on the *cdc13*-F539A profile in (G). (H) Southern blot analysis of the length of the telomeric tract on Chr IX (following loss of the distal segment and de novo telomere formation at the interstitial tract, as illustrated in Figure 3.2 A) from 5-FOA^R single colonies of *STN1* and *stn1*-W466E strains, which shows substantial length variation in the *stn1*-W466E mutant for this chromosome terminus even in this low resolution assay. (I) The length of individual Chr IX telomeres (following loss of the distal segment) in the *stn1*-W466E strain were "captured" by mating single cells from the four 5-FOA^R *stn1*-W466E cultures in part (H) with single cells from a wild type strain that contained a normal Chr IX terminus; genomic DNA was prepared from individual zygote colonies immediately following mating, and the lengths of the Chr IX telomere contributed by the *stn1*-W466E haploid were examined by Southern blot analysis as in part (H). To illustrate the range of telomere lengths contributed by the *stn1*-W466E strain, the original Southern blot was cropped and reformatted (indicated by lines) to emphasize the extent of the length variation among individual isolates.

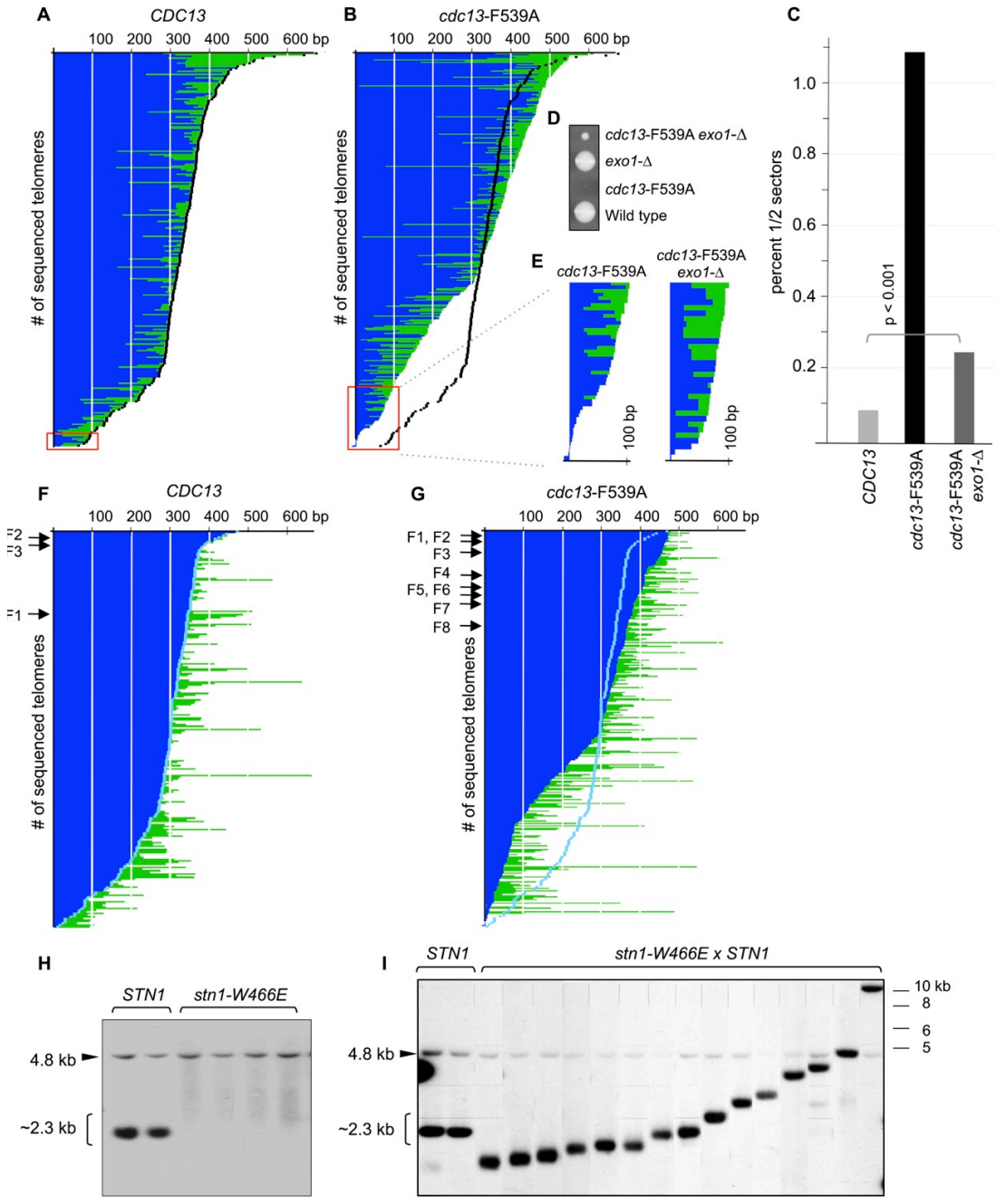
A
CDC13
100 200 300 400 500 600 bp
# of sequenced telomeres
B
cdc13-F539A
100 200 300 400 500 600 bp
# of sequenced telomeres
D
cdc13-F539A exo1-Δ
exo1-Δ
cdc13-F539A
Wild type
E
cdc13-F539A
cdc13-F539A exo1-Δ
100 bp
100 bp
C
percent 1/2 sectors
1.0
0.8
0.6
0.4
0.2
p < 0.001
CDC13
cdc13-F539A
cdc13-F539A exo1-Δ
F
CDC13
100 200 300 400 500 600 bp
F2
F3
F1
# of sequenced telomeres
G
cdc13-F539A
100 200 300 400 500 600 bp
F1, F2
F3
F4
F5, F6
F7
F8
# of sequenced telomeres
H
STN1
stn1-W466E
4.8 kb
~2.3 kb
I
STN1
stn1-W466E x STN1
4.8 kb
~2.3 kb
10 kb
8
6
5

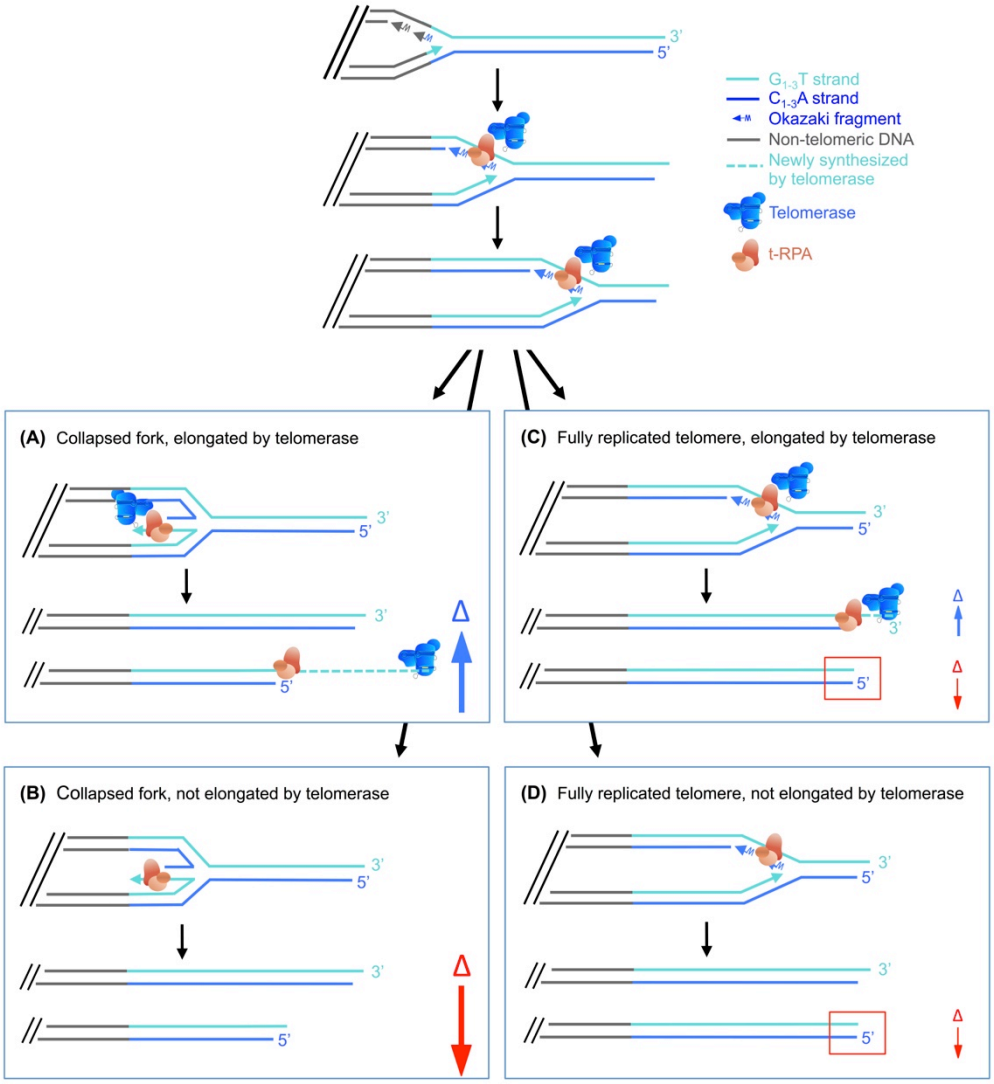

Figure 3.7: A new model for telomere length homeostasis in budding yeast. We propose that once the replication fork enters duplex telomeric DNA, the t-RPA complex becomes associated with the fork, through recognition of single-stranded G-rich DNA exposed on the lagging strand by the high affinity DNA binding domain of Cdc13 (Anderson et al. 2003). Association of telomerase with the fork (Greider, 2016), mediated by the t-RPA complex, would increase the probability that if a fork collapse occurs, the resulting substrate for telomerase would be efficiently recognized and extensively elongated, as illustrated in (A). If telomerase has dissociated from the fork (potentially due to a weak association between telomerase and the recruitment domain of Cdc13; Tucey & Lundblad, 2013) as depicted in (B), the resulting telomere could be substantial shortened in just one cell division. In contrast, the extent of elongation by telomerase at fully replicated telomeres, which has been estimated to be ~15 bp in a single cell division (Marcand et al. 1999), is much more modest (C). Furthermore, >90% of fully replicated telomeres fail to be elongated by telomerase (Teixeira et al. 2004), either because telomerase has dissociated from the replication fork (D), as proposed by Greider (2016) or because recruitment to the fully replicated terminus (not shown) is not efficient. Telomere shortening at fully replicated telomeres can also occur (boxed in red), due to the requirement to re-create the G-rich overhang on the leading strand terminus (Lingner et al. 1995).

SUPPLEMENTAL FIGURES

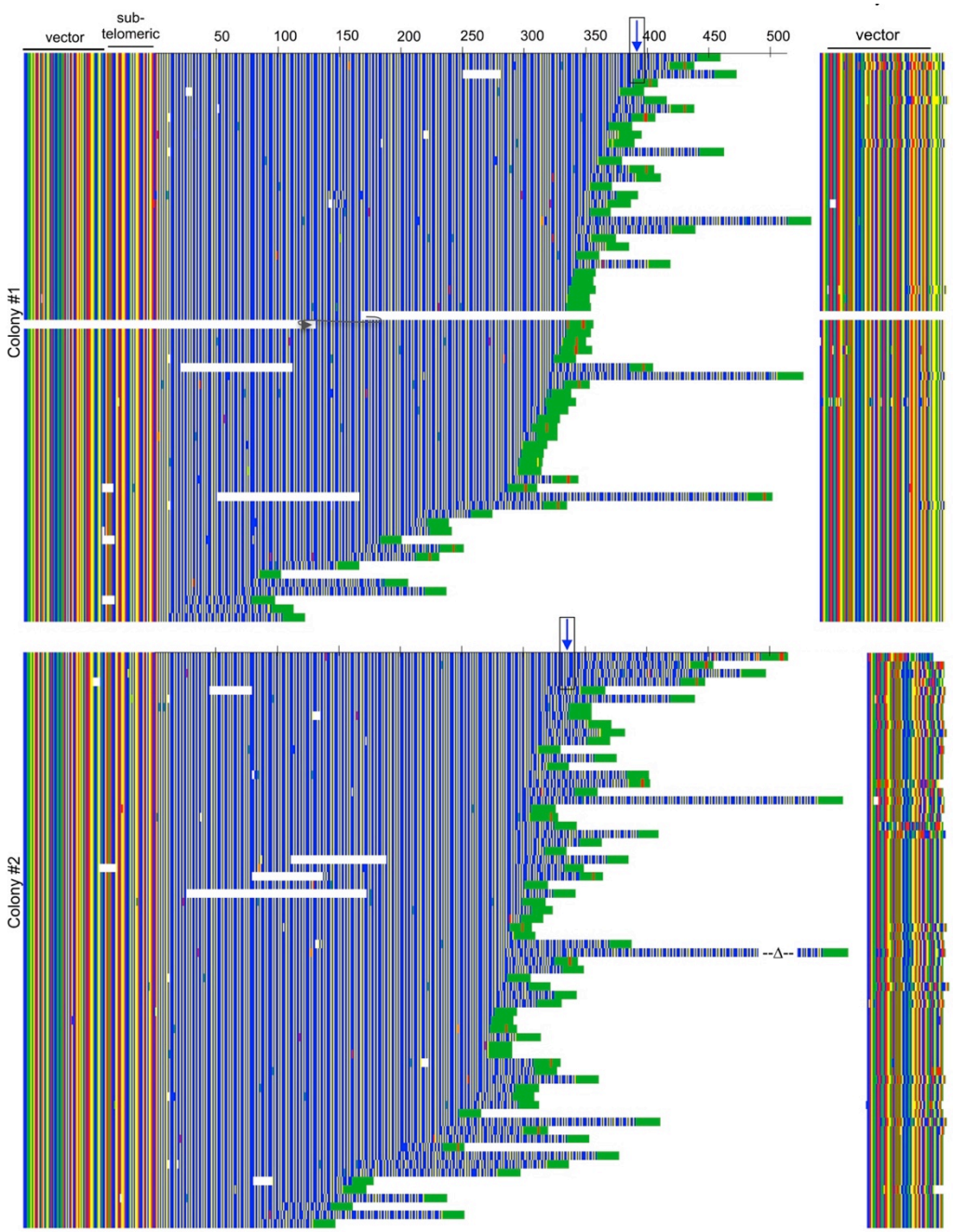

Figure 3S.1: Sequence analysis of 241 independent isolates of Chr I-L, Related to Figure 3.1 Primary sequence data of cloned telomeres from three wild type single colonies, aligned based on the extent of shared telomeric sequences. The boxed blue arrows mark the boundary of $G_{1\text{-}3}T$ DNA present in the founder Chr I-L telomere for each colony, defined as an identical stretch of sequence present in three of the longest cloned telomeres. Only clones that retained flanking vector sequences, as well as the poly C tract, were included (see Materials and Methods for more discussion); color code for sequence details GATC.

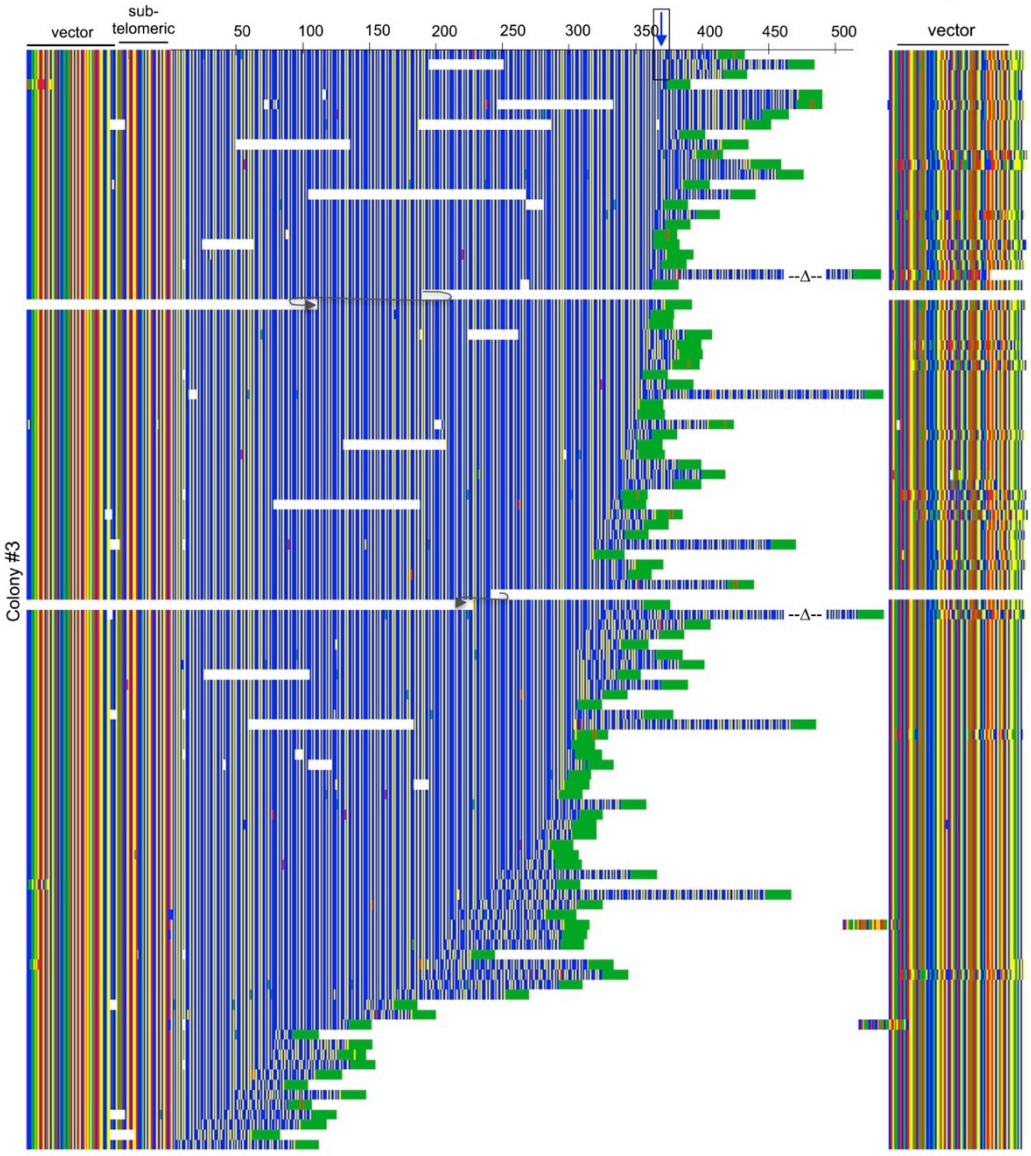

Figure 3S.1: Sequence analysis of 241 independent isolates of Chr I-L, Related to Figure 3.1 Continued.

Figure 3S.2: Additional analysis of replication fork collapse at an interstitial tract, Related to Figure 3.2. (A) Frequency of *TLC1* vs. *tlc1*-Δ strains that have lost the distal tract containing an interstitial $G_{1\text{-}3}T$ tract on Chr IX (left hand panel) or Chr XV (right hand panel), compared to isogenic strains bearing a mock version (i.e. a comparable chromosomal insertion except for the $G_{1\text{-}3}T$ telomeric tract). (B) Southern blot analysis of 5-FOA-resistant isolates from *TLC1* and *tlc1*-Δ strains containing the interstitial telomeric tract on Chr IX, demonstrating that newly formed telomeres at the interstitial $G_{1\text{-}3}T$ tract are shorter in the absence of telomerase. Vertical lines (marked with an asterisk) indicate where additional (duplicate) isolates were cropped out of the image. (C) Alignments of sequenced telomeres from six 5-FOA-resistant colonies from a *TLC1* strain (analyzed as in Figure 3.2 D), compared to the interstitial tract (top line of each alignment, blue arrowhead); the position of replication fork collapse is indicated by a black arrowhead for each alignment. For this experiment, PCR-amplified reactions were gel-extracted prior to cloning and sequence analysis, which intentionally skewed the analysis towards longer clones and also explains why shorter telomeres are under-represented. Red arrows indicate clones that have lost the poly C tract (in green) plus adjacent vector sequences; since a portion of the $G_{1\text{-}3}T$ telomeric tract was presumably lost as well, this category of sequences were excluded from the alignments in Figure 3S.1.Yellow arrows indicate sequenced telomeres that display a sequence divergence within ~75 bp of the junction between telomeric and sub-telomeric DNA, which we propose arose due to an additional replication fork collapse that occurred during subsequent growth of the colony. In the first alignment, the large red arrow marks the location of an apparent fork collapse that occurred at nucleotide 147during the second cell division that gave rise to this colony. (D) Alignments of sequenced telomeres from sixteen 5-FOA-resistant colonies from a *tlc1*-Δ strain compared to the interstitial tract (top line of each alignment, blue arrowhead), analyzed as in part (C) above; the white arrows indicate telomeres with a sequence divergence, presumably due to recombination during the growth of the *tlc1*-Δ colony. The 34 bp deletion in the second *tlc1*-Δ alignment arose in yeast, rather during subsequent PCR amplification or propagation through E. coli, as shown by independent PCR amplification and analysis from genomic DNA prepared from this yeast isolate.(E) Senescence progression of *tlc1*-Δ strains following replication fork collapse at the interstitial telomeric tract on Chr IX, compared to isogenic *tlc1*-Δ strains that contained an identical construct on Chr IX except for the presence of the interstitial $G_{1\text{-}3}T$ tract. Freshly generated *tlc1*-Δ strains were streaked in succession on rich media for each strain, and streak-outs were photographed after 48 hours growth at 30° for each time point.

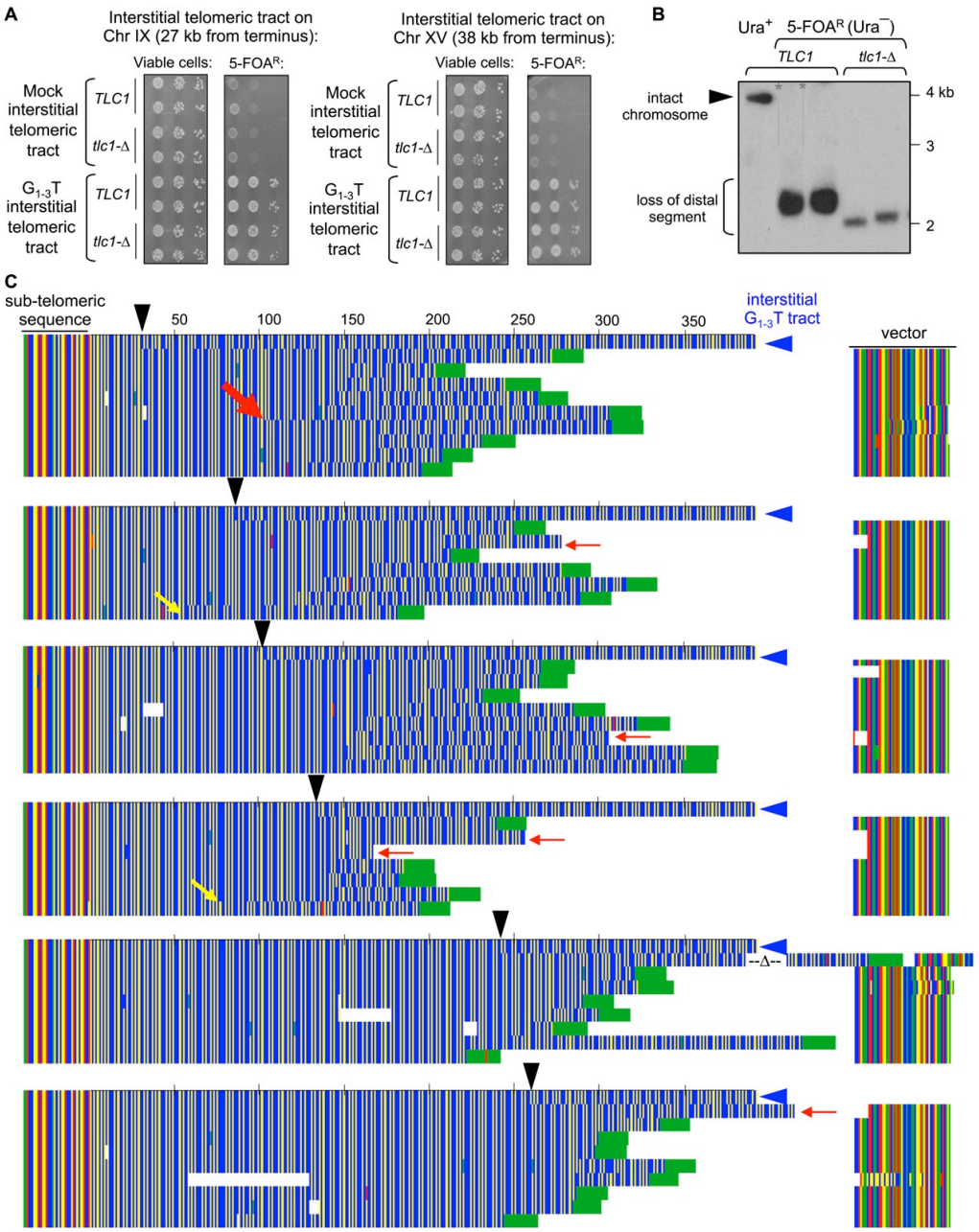
A
Interstitial telomeric tract on Chr IX (27 kb from terminus):
Viable cells:
5-FOA^R:
Mock interstitial telomeric tract
TLC1
tlc1-Δ
G1-3T interstitial telomeric tract
Interstitial telomeric tract on Chr XV (38 kb from terminus):
B
Ura+ 5-FOA^R (Ura−)
TLC1
tlc1-Δ
intact chromosome
loss of distal segment
4 kb
3
2
C
sub-telomeric sequence
50
100
150
200
250
300
350
interstitial G1-3T tract
vector
--Δ--

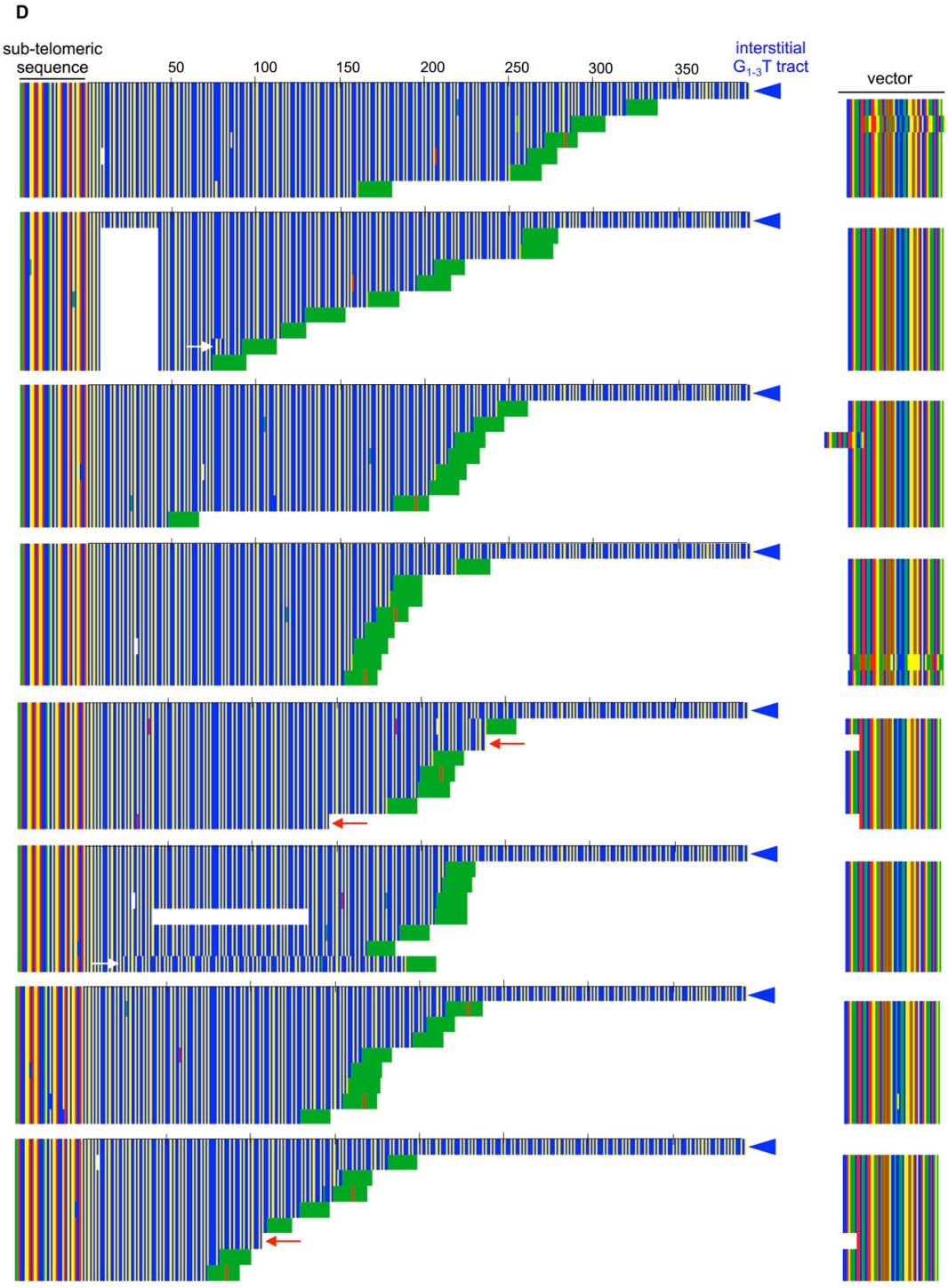

Figure 3S.2: Additional analysis of replication fork collapse at an interstitial tract, Related to Figure 3.2 Continued.

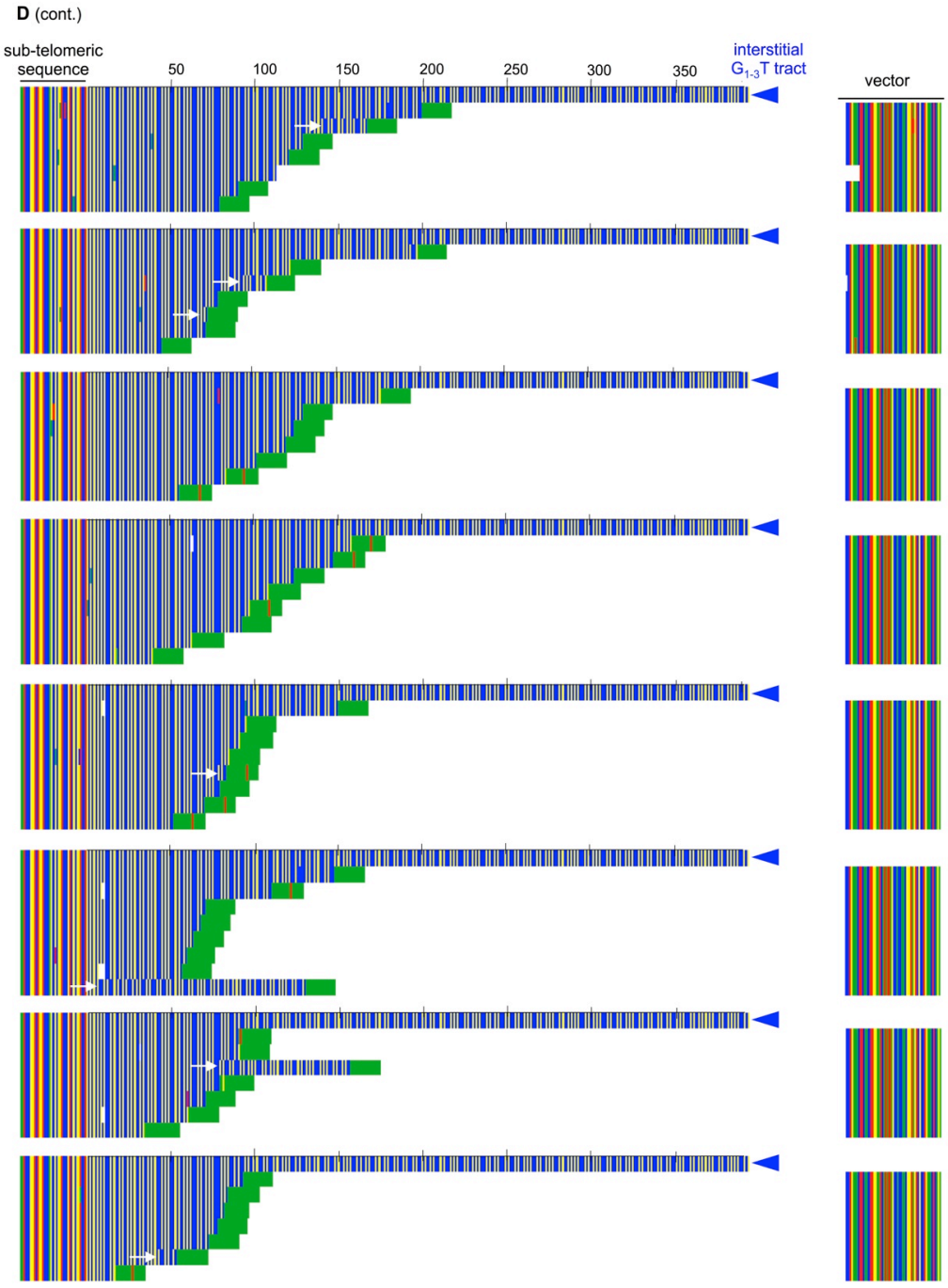

Figure 3S.2: Additional analysis of replication fork collapse at an interstitial tract, Related to Figure 3.2 Continued.

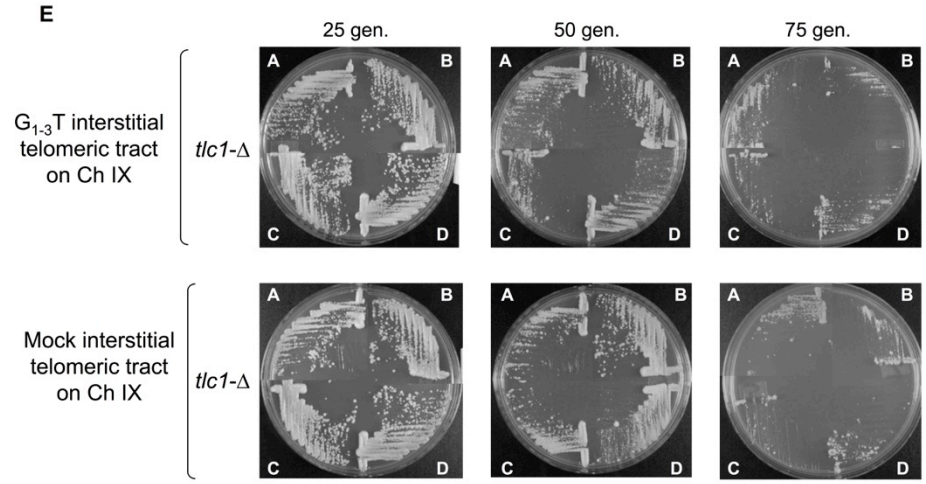

Figure 3S.2: Additional analysis of replication fork collapse at an interstitial tract, Related to Figure 3.2 Continued.

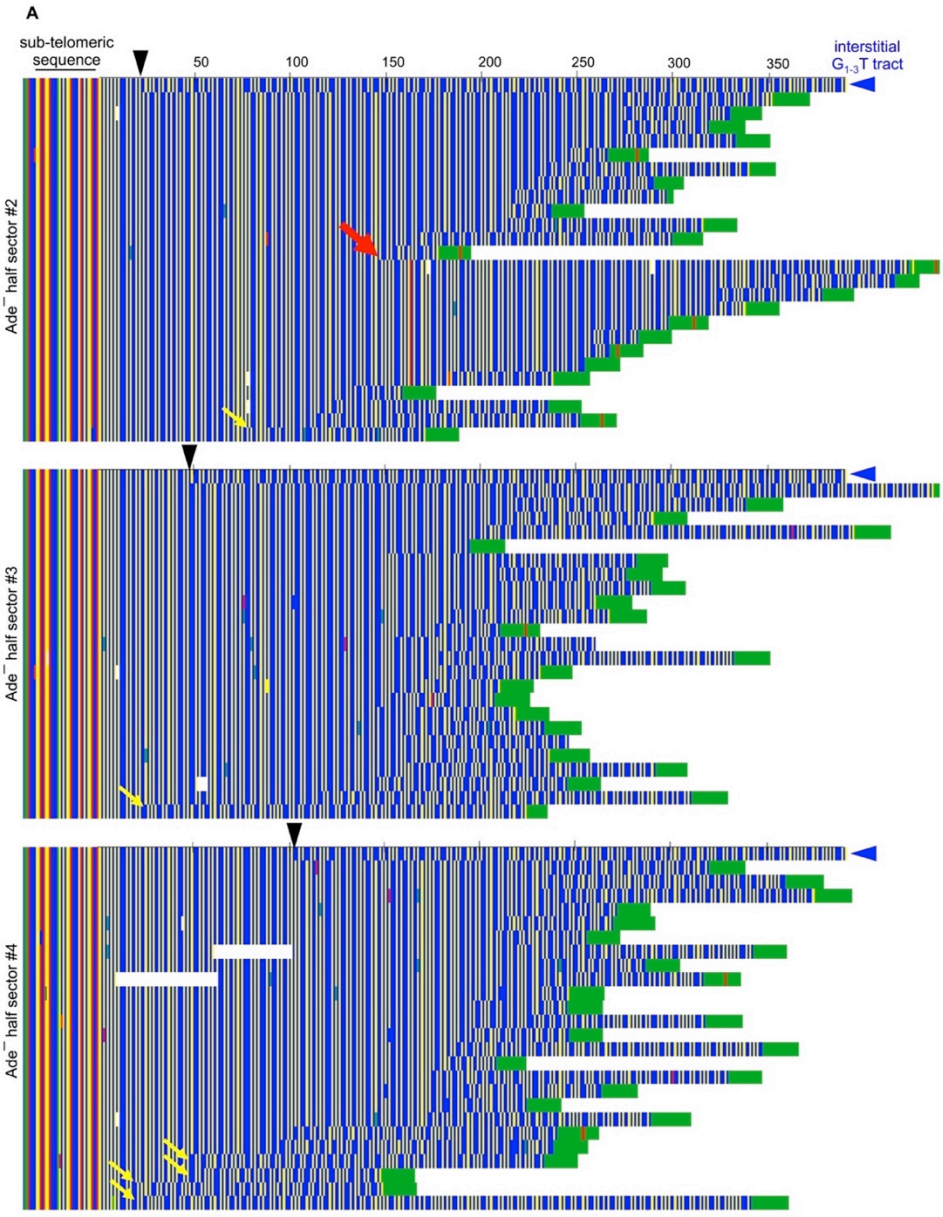

Figure 3S.3: Additional analysis of telomerase elongation at collapsed replication forks, Related to Figure 3.3. (A) Alignment of telomeric sequences recovered from four additional Ade⁻ half-sectors, in addition tot he example shown in Figure 3.3 C, compared to the sequence of the interstitial telomeric tract (top line of each alignment, blue arrowhead); the position of replication fork collapse is marked by a black arrowhead for each alignment. Yellow arrows indicate the subset of clones that display a sequence divergence within ~75 bp of the junction between telomeric and sub-telomeric DNA. In Ade⁻ half-sector #2, the red arrow indicates the location of an apparent fork collapse that occurred during the first cell division of this half-sector (which would be the second cell division of the colony). (B) The sequence of Chr I-L telomeres cloned from two colonies, in addition to the example in Figure 3.3 E, following transient expression of a telomerase RNA with a mutant template, that resulted in mutant telomeric repeats introduced close to sub-telomeric boundary (indicated by yellow arrows).

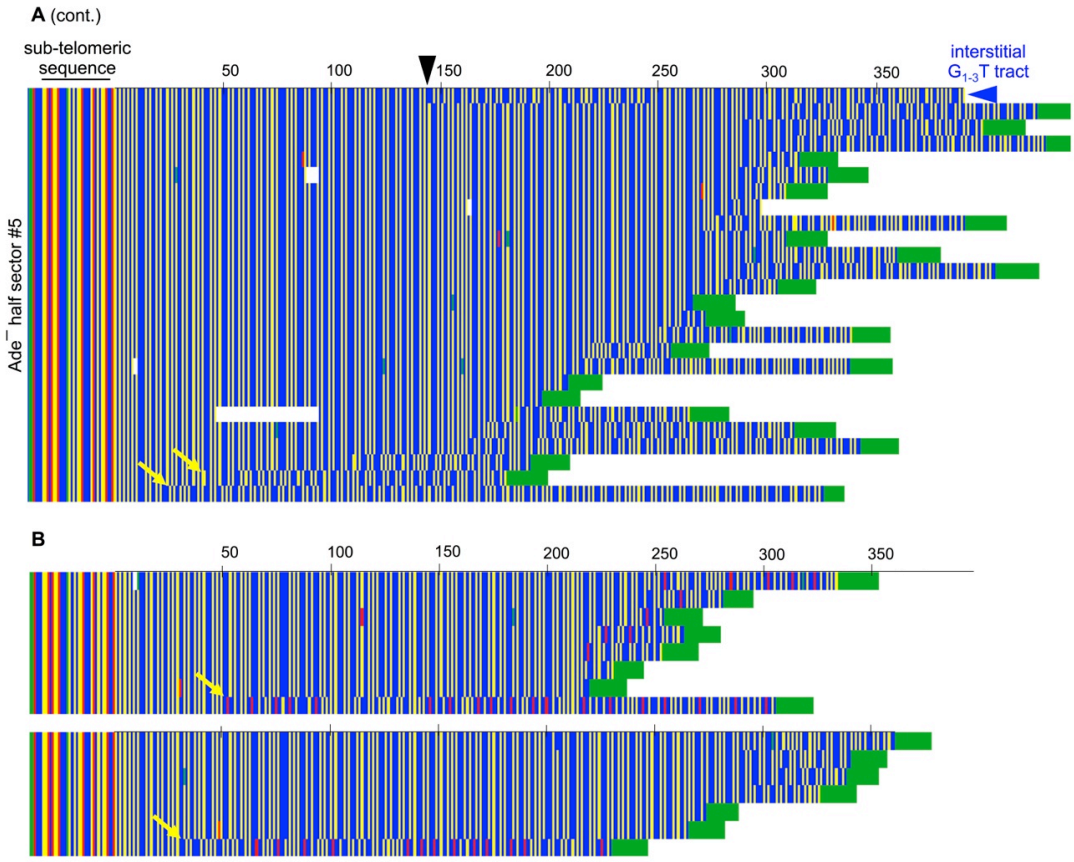

Figure 3S.3: Additional analysis of telomerase elongation at collapsed replication forks, Related to Figure 3.3 Continued.

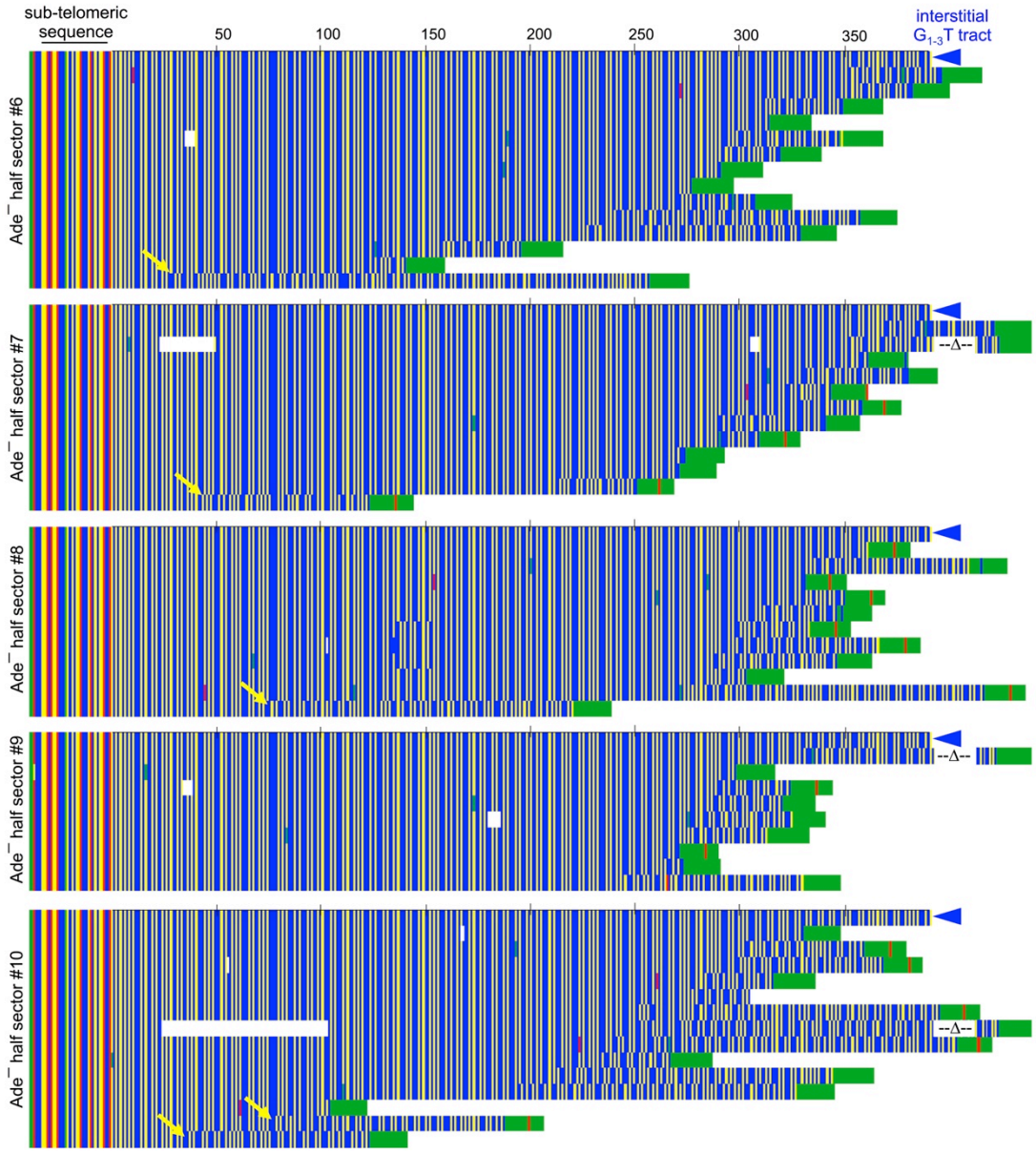

Figure 3S.4: Additional analysis of distal replication fork collapse events, Related to Figure 3.4. Alignment of telomeric sequences recovered from five Ade⁻ half-sectors that do not display an apparent telomerase-elongation event during the first cell division, similar to the example shown in Figure 3.4. Yellow arrows indicate clones with a sequence divergence within ~75 bp of the junction between telomeric and sub-telomeric DNA, that arose during subsequent growth of the half-sector.

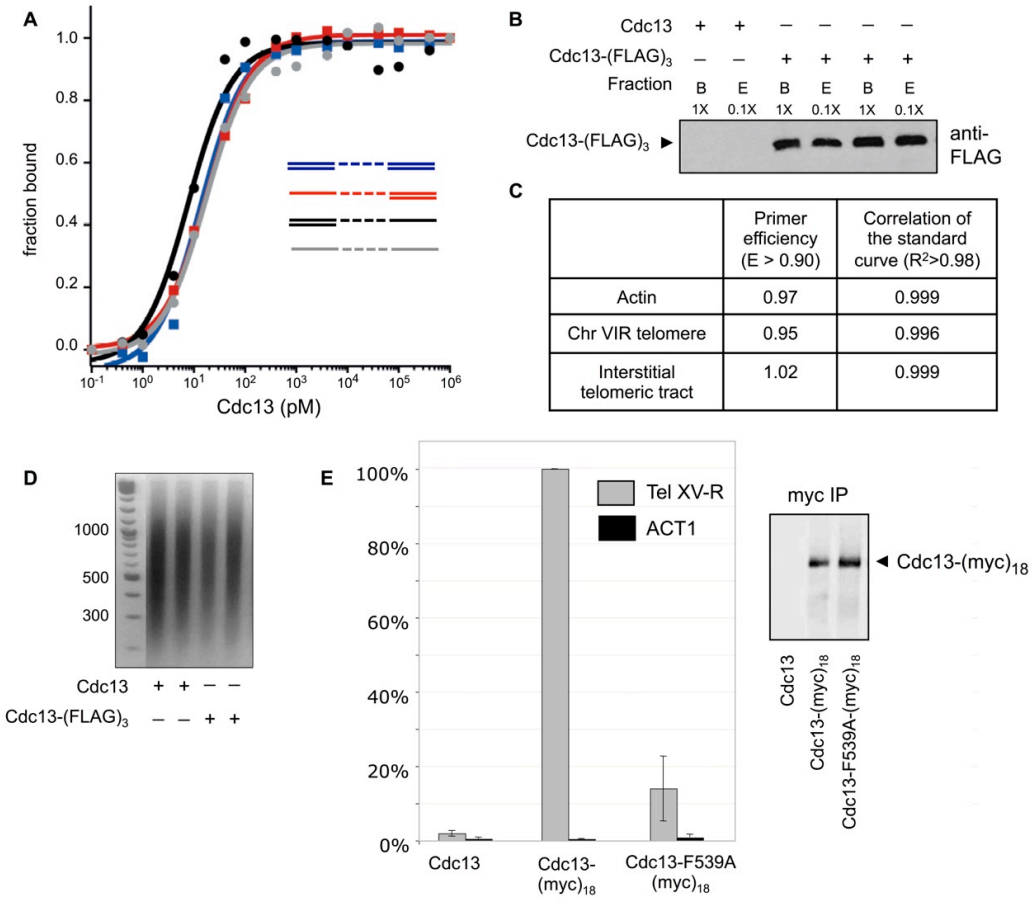

Figure 3S.5: Additional analysis of Cdc13 binding to telomeric DNA or chromatin, Related to Figure 3.5. (A) Binding of Cdc13 protein to telomeric single-stranded DNA (dashed lines) flanked by single-stranded and/or double-stranded non-telomeric sequence (solid lines). The fraction bound was normalized to a range of 0 to 1, and plotted as a function of Cdc13 concentration; solid curves show the fitted binding isotherm for each ligand. (B) Anti-FLAG western monitoring elution of the Cdc13-$(FLAG)_3$ protein after anti-FLAG immunoprecipitation; E = 10% of protein eluted from beads (used in the ChIP experiment in Figure 3.5 A) and B = 100% of protein that remained bound to beads after elution. (C) Linear standard curves (not shown) yielded R^2 values that were ≥ 0.99 for all samples, with amplification efficiency that was ≥ 99%, for the ChIP experiment in Figure 3.5 A. (D) Samples used in the ChIP experiment in Figure 3.6 A, resolved on a 2% agarose gel after removal of cross links, demonstrating that chromatin shearing was efficient and comparable among samples. (E) Binding of full length Cdc13-$(myc)_{18}$ or Cdc13-F539A-$(myc)_{18}$ proteins to sheared chromatin from clarified whole cell extracts; qPCR was used to detect Chr VIR telomere or ACT1 DNA following anti-myc IP. Data were assembled from three independent repeats, with three technical replicates of input and IP samples for each experiment. IP efficiency for the Cdc13-F539A$(myc)_{18}$ mutant protein was normalized to wild type Cdc13-$(myc)_{18}$; the anti-myc western shows a representative IP.

A

	Total	His^+ / His^-	
STN1	1977	1 (0.05%)	p < 0.005
stn1-W466E	443	9 (2.0%)	p < 0.005
stn1-W466E *exo1*-Δ	1383	7 (0.5%)	

B

		Viability of divided cells					
	Total	Viable / Viable		Viable / Inviable		Inviable / Inviable	
STN1	**1996**	1977 (99%)	p < 0.001	14 (0.7%)	p < 0.001	5 (0.3%)	p < 0.001
stn1-W466E	**1055**	443 (42%)	p < 0.001	327 (31%)	p < 0.001	276 (26%)	p < 0.001
stn1-W466E *exo1*-Δ	**1673**	1383 (83%)		208 (12%)		77 (5%)	

C

		Cell division times							
	Total	1 hr		2 hr		3 hr		> 4 hr	
STN1	**1996**	1959 (98%)	p < 0.001	33 (2%)	p < 0.001	4 (0.2%)	p < 0.001	0 (<0.05%)	p < 0.001
stn1-W466E	**1055**	367 (35%)	p < 0.001	226 (21%)	p = 0.4	228 (22%)	p < 0.001	234 (22%)	p < 0.001
stn1-W466E *exo1*-Δ	**1673**	1043 (62%)		383 (23%)		191 (11%)		56 (3%)	

Figure 3S.6: Primary data and statistics, Related to Figure 3.5. (A) Primary data and statistics, for the proportion of divided cells that underwent a replication fork collapse, among those cell divisions that produced two visible progeny colonies, for the indicated genotypes, as shown in Figure 3.5 F. (B) Primary data and statistics, for the proportion of divided cells that either gave rise to two, one or zero visible colonies, for the indicated genotypes, as shown in Figure 3.5 G. (C) Primary data and statistics, for the proportion of newly budded cells that took 2, 3 or ≥ 4 hours to complete the cell cycle, for the indicated genotypes, as shown in Figure 3.5 H.

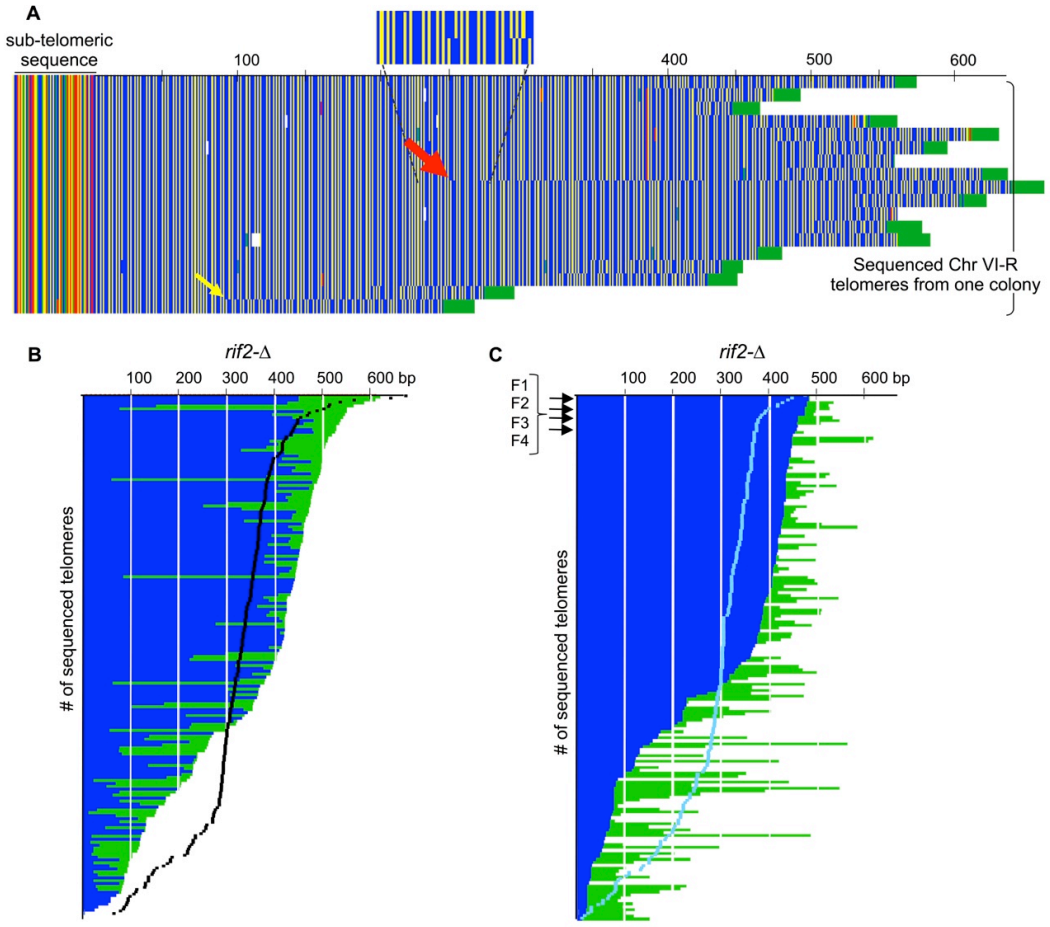

Figure 3S.7: Additional analysis of the t-DAM phenotype, Related to Figure 3.6. (A) Alignment of 18 sequenced Chr VI-R telomeres recovered from a single wild type colony reveals a sequence divergence at nucleotide 251, which we propose arose due to a fork collapse during the first cell division. The yellow arrow points to a telomere from this yeast colony that displays a sequence divergence within ~100 bp of the sub-telomeric junction, presumably due to an additional fork collapse that occurred during subsequent growth of the colony. (B) The t-DAM phenotype of a *rif2*-Δ strain, illustrated by a telomere length profile composed of 176 Chr I-L telomeres from four *rif2*-Δ single colonies; the average *rif2*-Δ telomere length is 340 bp (compared to 316 bp for wild type). The wild type telomere length profile (from Figure 3.1) is superimposed in black; the statistical difference between these two profiles is $p = 0.0006$ (based on a Kolmorogov Smirnov test). (C) The same telomere length profile as in part (C), re-aligned based on the length of founder sequence (in blue) inherited by each *rif2*-Δ progeny. The founder length profile for the wild type strain (in aqua, from Figure 3.6 F) is superimposed.

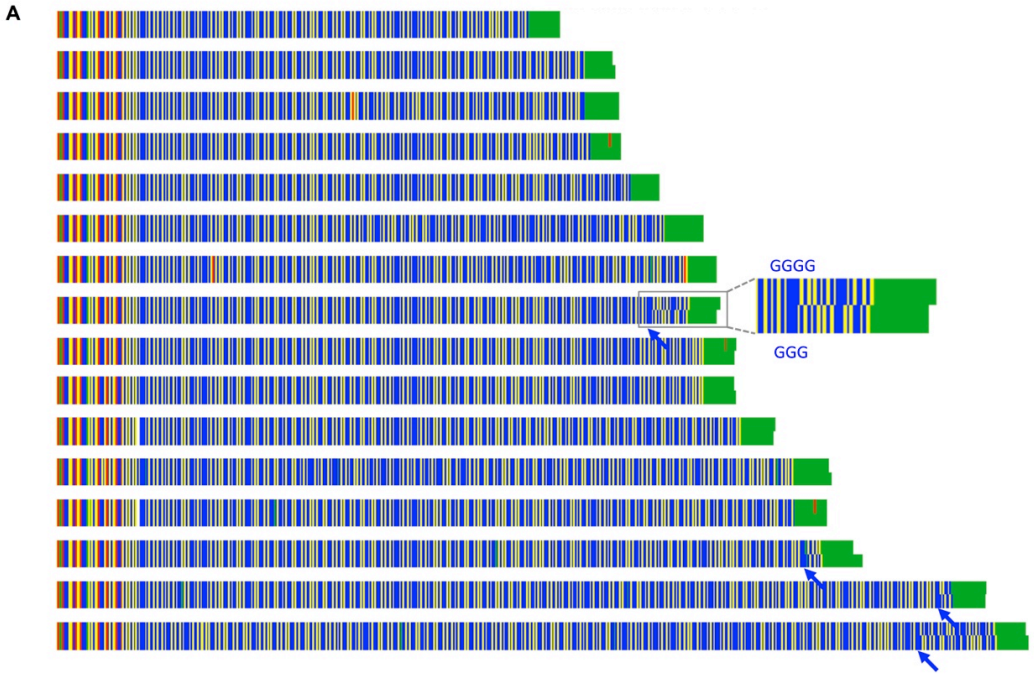

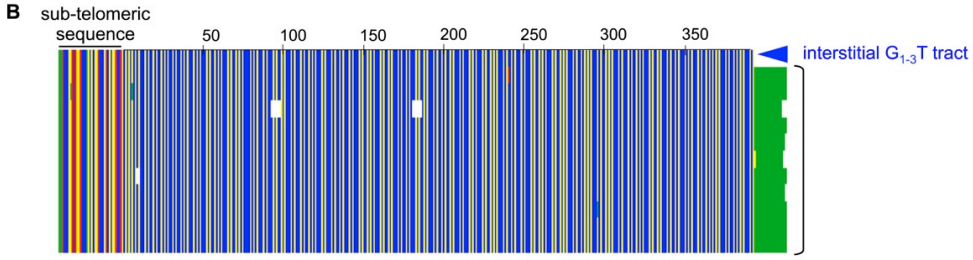

C

	% of mis-matches	% of deletions			
		1 bp	2 bp	4-10 bp	Big slippages
sub-telomeric DNA	0.2 %	0.02 %	< 0.002 %	0.005 %	< 0.002 %
telomeric DNA	0.3 %	0.02 %	0.03 %	0.02 %	0.01 %

Figure 3S.8: Assessing the fidelity of single-nucleotide analysis of telomeres, Related to Materials and Methods. (A) Duplicate sequence analysis of 16 clones showed that the sequencing error rate was 0.07%; sequence errors (GGG mis-read as GGGG) are indicated by arrows. See Materials and Methods for more discussion. (B) and (C) Analysis of the fidelity of amplification and cloning of the interstitial tract in YVL4836; a representative experiment in (B) shows the $G_{1\text{-}3}T$ telomeric sequence from 11 sibling clones from one amplification. The table in (C) summarizes the error rate for the 240 bp sub-telomeric tract vs. the 390 bp telomeric tract, from 170 sequenced clones from 24 independent amplifications of the interstitial telomeric tract.

Table 3S.1: List of yeast strains used in this study.

Strain	Genotype
YVL2967	*MAT***a** *ura3*-52 *lys2*-801 *trp1*-Δ1 *hist3*-Δ200 *leu2*-Δ1
YVL5193**	*MAT***a**/*MAT*α *stn1*-W466E/*STN1*
YVL5383**	*MAT***a**/*MAT*α *cdc13-F539A*/*CDC13*
YVL4097**	*MAT***a**/*MAT*α *cdc13-F539A*/*CDC13 exo1*-Δ:: KAN^R/*EXO1*
YVL4640*	*MAT***a** Chr IX(415,379)::*TRP1*-Tel01L-*URA3*
YVL4679*	*MAT***a** Chr XV(1,055,929)::*TRP1*-Tel01L-*URA3*
YVL4778**	*MAT***a**/*MAT*α Chr IX(415,379)::*TRP1*-Tel01L-*URA3 TLC1/tlc1*-Δ::*HIS3*
YVL4618*	*MAT***a** Chr IX(415,379)::*TRP1*-Tel01L-*HIS3*
YVL4631*	*MAT***a** Chr IX(415,379)::*TRP1*-Tel01L-*HIS3 stn1*-W466E
YVL4867*	*MAT***a** Chr IX(415,379)::*TRP1*-Tel01L-*HIS3 stn1*-W466E *exo1*-Δ
YVL4836*	*MAT***a** Chr IX(415,379)::*TRP1*-Tel01L-*HIS3* Chr IX(425434)::*ADE2 ade2*-Δ::*LEU2*
YVL4855*	*MAT***a** Chr IX(415,379)::*TRP1*-Tel01L-*HIS3* Chr IX(425434)::*ADE2 ade2*-Δ::*LEU2 pol1*-1
YVL5319*	*MAT***a** Chr IX(41,5379)::*TRP1*-Tel01L-*HIS3* Chr IX(425434)::*ADE2 ade2*-Δ::*LEU2 rad53*-21
YVL4922*	*MAT***a** Chr IX(41,5379)::*TRP1*-Tel01L-*HIS3* Chr IX(425434)::*ADE2 ade2*-Δ::*LEU2 cdc13*-ts (F684S)
YVL5292**	*MAT***a**/*MAT*α Chr IX(41,5379)::*TRP1*-Tel01L-*HIS3* / Chr IX(41,5379)::*TRP1*-Tel01L Chr IX(425434)::*ADE2* / Chr IX(425434)::*ADE2 ade2*-Δ::*LEU2/ade2*-Δ::*LEU2 cdc13*-F539A / *CDC13*
YVL5310**	*MAT***a**/*MAT*α Chr IX(41,5379)::*TRP1*-Tel01L-*HIS3* / Chr IX(41,5379)::*TRP1*-Tel01L Chr IX(425434)::*ADE2* / Chr IX(425434)::*ADE2 ade2*-Δ::*LEU2/ade2*-Δ::*LEU2 cdc13*-F539A / *CDC13 exo1*-Δ:: KAN^R/*EXO1*
YVL5240**	*MAT***a**/*MAT*α Chr IX(41,5379)::*TRP1*-Tel01L-*HIS3* / Chr IX(41,5379)::*TRP1*-Tel01L Chr IX(425434)::*ADE2* / Chr IX(425434)::*ADE2 ade2*-Δ::*LEU2/ade2*-Δ::*LEU2 stn1*-W466E / *STN1*
YVL5285**	*MAT***a**/*MAT*α Chr IX(41,5379)::*TRP1*-Tel01L-*HIS3* / Chr IX(41,5379)::*TRP1*-Tel01L Chr IX(425434)::*ADE2* / Chr IX(425434)::*ADE2 ade2*-Δ::*LEU2/ade2*-Δ::*LEU2 stn1*-W466E / *STN1 exo1*-Δ:: KAN^R/*EXO1*

* *ura3*-52 *lys2*-801 *trp1*-Δ1 *his3*-Δ200 *leu2*-Δ1

** *ura3*-52/*ura3*-52 *lys2*-801/*lys2*-801 *trp1*-Δ1/*trp1*-Δ1 *his3*-Δ200/*his3*-Δ200 *leu2*-Δ1/*leu2*-Δ1

Table 3S.2: List of plasmids used in this study.

Plasmid	Description
pVL6294	2 µ *LEU2* GAL-*tlc1*-A474C, C475T
pVL7292	Chr IX(415,379)::*TRP1*-Tel01L-*HIS3*
pVL7298	Chr XV(1,055,929)::*TRP1*-Tel01L-*HIS3*
pVL5484	2 µ *LEU2 CDC13*-$(FLAG)_7$
pVL1084	*CEN LEU2 CDC13*
pVL1086	*CEN LEU2 CDC13*-$(myc)_{18}$
pVL2820	*CEN LEU2 cdc13*-F539A-$(myc)_{18}$

MATERIALS AND METHODS

Yeast genetic and molecular methods

Standard methods were used for propagation of diploid and haploid strains, sporulation and dissection to generate haploid derivatives, and plating for 5-FOA resistant colonies. The full list of strains and plasmids used in this study are described in Tables 3S.1and 3S.2, respectively. Strains bearing mutations in the t-RPA complex (*cdc13*-F539A or *stn1*-W466E) were constructed by integrating mutations into the genome in place of wild type *CDC13* or *STN1*, respectively, using standard methods as previously described (Paschini et al. 2012). The replication fork collapse assay strain was constructed by introducing the interstitial $G_{1\text{-}3}T$ telomeric tract into Chr IX, downstream of ARS922, as a linearized plasmid containing a 692 bp terminal fragment from the Chr I-L telomere and appropriate nutritional markers, flanked by homology to the target location. Subsequent strain modifications (introduction of the *ADE2* gene on the distal portion of Chr IX and a corresponding deletion of the endogenous *ADE2* locus) allowed loss of the distal segment to be monitored by a visual assay, through the detection of Ade^{-} sectors, which accumulate a distinctive red pigment (due to oxidation of an intermediate, phosphoribosylamino imidazole, that accumulates when the adenine biosynthetic pathway is blocked; Woods 1969). Using this modified strain, the frequency of replication fork collapse was determined by plating early-log-phase cells (O.D. 0.3) at low density (≤150 colonies/plate) on rich media with no adenine supplement. Plates were incubated at 30° until colonies were fully grown (2 to 5 days, depending on genotype), and an additional ~5 days at room

temperature to allow Ade$^-$ sectors to become readily detectable. The integrity of the 390 bp of $G_{1\text{-}3}T$ telomeric DNA tract was also confirmed after each strain construction, by PCR amplification and sequence analysis, prior to assaying replication fork collapse.

Cloning and sequencing of telomeres

Yeast genomic DNA was prepared from 2 ml cultures grown in rich media from single colonies using Wizard® Genomic DNA Purification Kit (Promega), and 150 ng of genomic DNA was treated with terminal transferase in the presence of 1 mM dCTP to introduce a poly$(C)_n$ tract at chromosome ends (Förstemann et al. 2000). Chr IL was amplified using 5'-GCGGTACCAGGGTTAGATTAGGGCTG-3' and 5'-CGGGATCCGGGGGGGGGGGGGGGGG-3', which recognized the sub-telomeric region of Chr IL and the poly$(C)_n$ tract introduced by terminal transferase, respectively. Genomic DNA + primers were denatured at 94°C and cycled 35 times, with annealing (20 sec, 60°C) and extension (90 sec, 72°C) for each cycle, followed by a final extension step (10 min, 72°C). Two methods were used to prepare PCR products for cloning: (1) for telomere length profiles (Figures 3.1, 3.6 and 3S.7), PCR products were precipitated prior to cloning, to ensure no bias with regard to the spectrum of sizes recovered; (2) for analysis of sequence features (Figures 3.2 – 4, 3.7, 3S.1 – 3S.4), where short telomeres were less informative, PCR products were gel-purified. PCR reactions recovered by either method were TA-cloned into the pCR^{TM}2.1 vector, transformed into DH5α *E. coli*, and plated on LB plates (pre-warmed to 36°C) containing 60 μg/ml carbinecillin and X-gal (5-bromo-4-chloro-3-

indolyl-β-D-galactopyranoside). Transformants were incubated for 12 hrs at 36° C in a dedicated incubator and immediately inoculated into 1.5 ml of pre-warmed LB-Carb and grown to saturation at 36° C. All steps involving passage through E. coli were monitored to avoid temperature fluctuations, as our empirical observations suggested that even minor temperature shifts during E. coli propagation increased the frequency of deletions in the telomeric insert. Plasmid DNA was prepared using the QIAprep Spin Miniprep Kit (Qiagen), and the G1-3T insert was sequenced by Eton Bioscience, Inc. using a protocol optimized for difficult-to-sequence templates. Cloned Chr IL telomeres were sequenced using M13 Forward (-40) primer, which exploited the fact that the $G_{1\text{-}3}T$ tract exhibited an extremely strong cloning bias with regard to orientation (≥ 99% of inserts were recovered in one orientation). For clones with exceptionally long inserts, reverse sequencing with M13 Reverse primer was used to increase sequence fidelity. *De novo* telomeres generated following replication fork collapse were sequenced with a primer (5'-TTCCCAGTCACGACGTTGTAAAACG-3') that recognized a unique sequence upstream of the inserted interstitial telomeric tract.

Sequence alignments

Telomere length profiles were constructed from multiple independent PCR reactions from multiple yeast genomic preps, to avoid an outlier PCR reaction from dominating a profile. Duplicate clones were rare (< 1%) and one isolate was removed if recovered from the same PCR reaction. For the telomere length profiles shown in Figures 3.1, 3.7 and 3S.7, clones that lacked the poly$(C)_n$ tract or contained a deletion

in the junction between sub-telomeric and telomeric DNA were eliminated, on the assumption that these deletions were indicative of errors (generated during PCR amplification or propagation through *E. coli*) that compromised the integrity of the $G_{1-3}T$ tract.

Cloned telomere sequences were aligned using MacVector. Gaps in the $G_{1-3}T$ tract were introduced only when the downstream homology was > 25 bp; this high gap penalty ensured that multiple gaps within a single telomere clone, that artificially maximized multiple short stretches of homology, were not permitted. The resulting alignments (Figure 3S.1 and data not shown) were used to identify sequences inherited from the founder Chr I-L telomere vs. sequences synthesized by telomerase, for each telomere, in order to construct the images shown in Figures 3.6 and 3S.7. The founder telomere sequence for each colony was defined as an identical stretch of $G_{1-3}T$ sequence present in three of the longest cloned telomeres (see boxes in Figure 3S.1); this conservative definition may slightly under-estimate the extent of founder sequence. Once founder sequences were identified for each telomere, deletions or snap-backs greater than 2 nucleotides were removed prior to constructing telomere length profiles, based on the assumption that these deletions were generated in yeast (and hence their removal would accurately report on the *in vivo* length of each telomere); even if incorrect, this assumption only underestimates telomere length for each profile by less than 1%. Furthermore, we have observed numerous clonal examples of deletions, duplications or missense mutations that arose in yeast in the $G_{1-3}T$ tracts of Chr I-L or Chr IX-R (in each case, a second round of amplification,

cloning and sequencing was used to confirm that such events pre-existed in the yeast genomic DNA); one example is the 34 bp deletion in the *tlc1*-Δ colony in Figure 3S.2 D.

The fidelity of the single-nucleotide sequence analysis of cloned telomeres was evaluated with several reconstruction experiments. First, sequencing fidelity was assessed by duplicate sequence analysis (via independent sequence runs) of 16 clones with $G_{1\text{-}3}T$ insert sizes ranging in size from 249 to 536 bp, for a total of 5,475 bp. Re-sequencing detected 4 errors due to mis-reads of GGG as GGGG at the end of the read for all 4 errors (Figure 3S.8 A), resulting in a sequencing error rate of 0.07%. Notably, no deletions due to sequence mis-reads were identified. In a second experiment, the error rate during PCR amplification and/or propagation through *E. coli* was evaluated; the interstitial tract (240 bp of sub-telomeric DNA and 390 bp of $G_{1\text{-}3}T$ DNA) from YVL4836 was amplified, TA-cloned and sequenced, employing the same protocol used to amplify native telomeres. A total of 170 sequenced clones from 24 independent amplifications (40,800 and 66,300 bp of sub-telomeric and telomere DNA, respectively) were analyzed, with error frequencies for different categories of mutations summarized in Figure 3S.8 C.

Statistical analysis

Fischer's exact test was used to determine two-sided *p*-values for the RepFC assays, and Kolmorogov Smirnov tests were used to compare telomere length profiles from different yeast strains.

Chromatin immunoprecipitation

Yeast cultures expressing either Cdc13-$FLAG_3$ or untagged Cdc13 were grown to mid-log (O.D. 0.7), incubated with 1% paraformaldehyde at 30° C for 15 min, pelleted and washed 1X in H_2O and 1X in FA buffer (140 mM NaCl, 50 mM HEPES-KOH pH7.5, 1mM EDTA pH8.0, 0.1% w/v Sodium deoxycholate, 1% v/v Triton X-100 plus protease inhibitors). Extracts were prepared by grinding in the presence of liquid N_2, and clarified by 3X centrifugation (10 min at 4°C). The resulting supernatant was sheared by sonication (Branson Sonifire 450 microtip, 4 cycles for 5 sec at 30% output), and clarified by 3X centrifugation (10 min at 4°C). Samples were set aside for input DNA and evaluation of shear size, and the remainder was immunoprecipitated with anti-FLAG M2 affinity gel (Sigma) for 2 hr at 4°C. Anti-FLAG beads were washed 3X in FA buffer, 1X in in LiCl buffer (250 mM LiCl, 10 mM Tris-HCl, pH8, 0.5% NP-50, 0.5% Deoxycholic acid, 1 mM EDTA,) and 1X in TE (10 mM Tris-HCl, 1 mM EDTA), and eluted with 100 µl TE, 1% SDS at 65° C for 1 hr. The resulting eluate was incubated at 65° C with Proteinase K to reverse cross-links, and DNA was purified by QIAquick PCR Purification Kit (QIAGEN). qPCR was performed using Syber Green master mix (ThermoFisher) in a ABI7900 Real Time PCR System using the following primer pairs:

ACT1: 5'-CCAATGAACCCTAAATCAAACAGAG-3' and

5'-ATGGCGTGAGGTAGAGAGAAACC-3'

Chr VI-R: 5'-ATATGGCGTACGCACACGTATG-3' and

5'-AAGGGTAAAAACCAGTGAGGCC-3'

Linear standard curves were performed for each qPCR reaction and 3 technical replicas represented each sample. Threshold analysis was performed with the SDS v2.4 software from Applied Biosystems.

Cdc13-ssDNA binding assays:

A 65 nt ssDNA oligonucleotide containing 24 nt of telomeric DNA (5'-GTACTGGTGAAGTACTGACGTGTGTGGGTGTGTGGGTGTGTGGGGCGTCA GCGTAGAATTCACT-3') flanked by 20 nt of non-telomeric DNA sequence on either end (underlined) was annealed to single-stranded oligonucleotides complementary to the flanking non-telomeric sequences. Recombinant full-length Cdc13 was purified from baculovirus-infected insect cells using an improved protocol (Lewis et al. 2014), under conditions that allowed the protein to form dimers in solution; the affinity-purified protein was subsequently subjected to size exclusion chromatography to ensure that Cdc13 was not aggregated. The resulting Cdc13 protein yielded an apparent binding affinity of 13 pM for its cognate Tel11 telomeric sequence, over an order of magnitude tighter than previous protein preparations (Nugent et al. 1996). DNA binding activity was measured by gel electromobility shift assay, using an optimized protocol that enabled the resolution of monomer- and dimer-bound ligand while also minimizing the amount of protein that was retained in the wells (Lewis et al. 2014). Briefly, 2 pM of radiolabeled DNA ligand was incubated with the indicated concentrations of recombinant Cdc13 protein in the optimized binding buffer (50 mM Tris [pH 7.5], 75 mM KCl, 1 mM DTT, 0.1 mg/mL BSA, 15% glycerol) on ice for 1 hr. Protein-bound DNA was rapidly separated from unbound

DNA on ice-cold 6.7% acrylamide (19:1 acrylamide/bisacrylamide) Tris-borate-EDTA (TBE) gels containing 5% glycerol in a running buffer of 1X TBE + 5% glycerol at 200 V for 20 min. Gels were dried, imaged, and quantitated as described (Lewis et al. 2014).

Assaying Cdc13 binding to sheared chromatin

Yeast cultures expressing Cdc13, Cdc13-$(myc)_{18}$, or Cdc13-F539A-$(myc)_{18}$ were grown to early/mid-log (O.D. 0.3-0.5), pelleted and resuspended in IP/lysis buffer (150 mM NaCl, 50 mM Tris-HCl pH 7.5, 5 mM EDTA, 0.5% NP-40, 1.0% Triton X-100 with 1x Complete protease inhibitors). Resuspended cells were added to 0.5 g zircon beads, disrupted by vortexing for 40 min at 4°C and insoluble debris removed by a pulse spin. Chromatin was sheared by sonication (Branson Sonifire 450 microtip, 6 cycles for 5 sec at 90% output, with 1 min on ice between each cycle) and clarified 3X by centrifugation (10 min at 14,000 at 4°C). Aliquots were set aside for input DNA, western and shear size evaluation, and the remainder was immunoprecipitated with anti-myc 9E10 Ab (Covance) overnight at 4°C. Samples were eluted (10 mM Tris-Cl, pH 8.0, 1mM EDTA, 1% SDS) for 10 minutes at 65°C, spun for 1 min, and supernatant recovered, with a portion set aside for assessment of IP efficiency. Eluates were purified with Qiagen PCR kit, and DNA was quantitated by real time PCR on an ABI 7900HT using SYBR Green PCR master mix (50°C for 2 min, 95°C for 10 min, 40 cycles of 95°C for 10 sec and 60°C for 1 min), using the following primer pairs:

ACT1: (5'-CCAATGAACCCTAAATCAAACAGAG-3' and

5’-ATGGCGTGAGGTAGAGAGAAACC-3’)

Chr XV-R: (5’-CTAACCCTGTCCAACCTGTCTCC-3’ and

5’-AGATGTGGATCGTGGTTCGC-3’)

Linear standard curves were performed for each qPCR reaction, and 3 technical replicates of IP and input samples with both primers were used to control for pipetting errors within each full repeat of the experiment. For anti-myc westerns, samples were resolved on 8% SDS-PAGE gels which were probed with 9E10 anti-myc antibody and subsequently with IRDye 800CW Goat Anti-Mouse IgG (LiCor); membranes were scanned on LiCor Odyssey system and quantified using ImageGauge software.

ACKNOWLEDGEMENTS

We thank Ted Weinert for his brilliant suggestion that led to the development of the RepFC assay, Ted Weinert and Carol Greider for insightful conversations throughout this work and members of the Lundblad lab, both past and present, for many useful suggestions during the course of this study. This work was supported by National Institutes of Health grants T32 GM007240 (to C.M.R.), R01 GM059414 (to D.S.W.), R01 GM106060 and R01 AG011728 (to V.L.) and P30 CA014195 (to the Salk Institute Cancer Center), NSF grants IIS-1254123, IIS-1724421 and IOS-1556388 (to T.O.S), a Graduate Fellowship from the Glenn Center for Aging Research at the Salk Institute (to C.M.R.), a Salk Innovations Grant award (to V.L. and T.O.S) and the Becky and Ralph S. O'Connor Chair (to V.L.).

This chapter is currently being prepared for submission for publication of the material. Paschini, Margherita; Reyes, Cynthia M.; Mandell, Edward K.; Lewis, Karen A.; Glustrom, Leslie W.; Sharpee, Tanya O.; Wuttke, Deborah S.; Lundblad, Victoria. The dissertation author and Margherita Paschini are the primary investigators and co-first authors of this material.

REFERENCES

Aksenova AY, Greenwell PW, Dominska M, Shishkin, A.A.,Kim, J.C.,Petes, T.D., and Mirkin, S.M. (2013). Genome rearrangements caused by interstitial telomeric sequences in yeast. *Proc. Natl. Acad. Sci. USA 110*, 19866–19871.

Anderson, E.M., Halsey, W.A., and Wuttke, D.S. (2003). Site-directed mutagenesis reveals the thermodynamic requirements for single-stranded DNA recognition by the telomere-binding protein Cdc13. *Biochemistry* 42, 3751–3758.

Baird, D.M., Britt-Compton, B., Rowson, J., Amso, N.N., Gregory, L. and Kipling, D. (2006). Telomere instability in the male germline. *Hum. Mol. Genet.* 15, 45-51.

Baumann, P. and Cech, T.R. (2001). Pot1, the putative telomere end-binding protein in fission yeast and humans. *Science* 292, 1171–1175.

Bentsen, I.B., Nielsen, I., Lisby, M., Nielsen, H.B., Gupta, S.S., Mundbjerg, K, Andersen, A.H. and Bjergbaek, L. (2013). MRX protects fork integrity at protein-DNA barriers, and its absence causes checkpoint activation dependent on chromatin context. *Nucleic Acids Res.* 41, 3173-3189.

Bianchi, A., Negrini, S. and Shore, D. (2004). Delivery of yeast telomerase to a DNA break depends on the recruitment functions of Cdc13 and Est1. *Mol. Cell* 16, 139-146.

Bianchi, A., and Shore, D. (2007). Early replication of short telomeres in budding yeast. *Cell* 128, 1051- 1062.

Bianchi, A. and Shore, D. (2009). Telomere length regulation: coupling DNA end processing to feedback regulation of telomerase. *EMBO J.* 28, 2309-2322.

Boeke, J.D., Trueheart, J., Natsoulis, G. and Fink, G.R. (1987). 5-Fluoroorotic acid as a selective agent in yeast molecular genetics. *Methods Enzymol.* 154, 164-175.

Booth, C., Griffith, E., Brady, G., and Lydall, D. (2001). Quantitative amplification of single-stranded DNA (QAOS) demonstrates that cdc13-1 mutants generate ssDNA in a telomere to centromere direction. *Nucleic Acids Res.* 29, 4414–4422.

Carson, M.J. and Hartwell, L. (1985). CDC17: an essential gene that prevents telomere elongation in yeast. *Cell* 42, 249-257.

Casteel, D.E., Zhuang, S., Zeng, Y., Perrino, F.W., Boss, G.R., Goulian, M., and Pilz, R.B. (2009). A DNA polymerase R/primase cofactor with homology to replication protein A-32 regulates DNA replication in mammalian cells. *J. Biol. Chem.* 284, 5807–5818.

Celli, G.B., and de Lange, T. (2005). DNA processing is not required for ATM-mediated telomere damage response after TRF2 deletion. *Nat. Cell Biol.* 7, 712–718.

Chang, M., Arneric, M., and Lingner, J. (2007). Telomerase repeat addition processivity is increased at critically short telomeres in a Tel1-dependent manner in Saccharomyces cerevisiae. *Genes & Development* 21, 2485–2494.

Chen, C. and Kolodner, R.D. (1999). Gross chromosomal rearrangements in Saccharomyces cerevisiae replication and recombination defective mutants. *Nat. Genet.* 23, 81-85.

Chen, L.-Y., Majerska, J. and Lingner, J. (2012). Molecular basis of telomere syndrome caused by CTC1 mutations. *Genes & Development* 27, 2099–2108.

Costanzo, V. (2011). Brca2, Rad51 and Mre11: performing balancing acts on replication forks. *DNA Repair (Amst)* 10, 1060-1065.

Cooper, J.P., Nimmo, E.R., Allshire, R.C., and Cech, T.R. (1997). Regulation of telomere length and function by a Myb-domain protein in fission yeast. *Nature* 385, 744–747.

Cotta-Ramusino, C., Fachinetti, D., Lucca, C., Doksani, Y., Lopes, M., Sogo, J. and Foiani, M. (2005). Exo1 processes stalled replication forks and counteracts fork reversal in checkpoint-defective cells. *Mol. Cell* 17, 153-159.

Crabbe, L., Verdun, R.E., Haggblom, C.I., and Karlseder, J. (2004). Defective telomere lagging strand synthesis in cells lacking WRN helicase activity. *Science* 306, 1951–1953.

Dehé, P.M., Rog, O., Ferreira, M.G., Greenwood, J. and Cooper, J.P. (2012). Taz1 enforces cell-cycle regulation of telomere synthesis. *Mol. Cell* 46, 797-808.

de Lange, T. (2005). Shelterin: the protein complex that shapes and safeguards human telomeres. *Genes & Development* 19, 2100–2110.

Derboven, E., Ekker, H., Kusenda, B., Bulankova, P. and Riha, K. (2014). Role of STN1 and DNA polymerase α in telomere stability and genome-wide replication in Arabidopsis. *PLoS Genet.* 10, e1004682.

Desany, B.A., Alcasabas, A.A., Bachant, J.B. and Elledge, S.J. (1998). Recovery from DNA replication stress is the essential function of the S-phase checkpoint pathway. *Genes & Development* 12, 2956- 2970.

Dionne, I., and Wellinger, R.J. (1998). Processing of telomeric DNA ends requires the passage of a replication fork. *Nucleic Acids Res.* 26, 5365–5371.

Ding, H., Schertzer, M., Wu, X., Gertsenstein, M., Selig, S., Kammori, M., Pourvali, R., Poon, S., Vulto, I., Chavez, E., Tam, P.P., Nagy, A. and Lansdorp, P.M. (2004). Regulation of murine telomere length by Rtel: an essential gene encoding a helicase-like protein. *Cell* 117, 873-886.

Ferreira, M.G., and Cooper, J.P. (2001). The fission yeast Taz1 protein protects chromosomes from Ku-dependent end-to-end fusions. *Mol. Cell.* 7, 55–63.

Ferreira, M.G., and Cooper, J.P. (2004). Two modes of DNA double-strand break repair are reciprocally regulated through the fission yeast cell cycle. *Genes & Development* 18, 2249–2254.

Förstemann, K., Höss, M. and Lingner, J. (2000). Telomerase-dependent repeat divergence at the 3' ends of yeast telomeres. *Nucleic Acids Res.* 28, 2690-2694.

Forstemann, K. and Lingner, J. (2001). Molecular basis for telomere repeat divergence in budding yeast. *Mol. Cell. Biol.* 21, 7277–7286.

Förstemann, K., Zaug, A.J., Cech, T.R. and Lingner, J. (2003). Yeast telomerase is specialized for C/A- rich RNA templates. *Nucleic Acids Res*. 31, 1646-1655.

Fouché, N., Ozgür, S., Roy, D. and Griffith J.D. (2006). Replication fork regression in repetitive DNAs. *Nucleic Acids Res*. 34, 6044-6050.

Frank, A.K., Tran, D.C., Qu, R.W., Stohr, B.A., Segal, D.J. and Xu, L. (2015). The Shelterin TIN2 Subunit Mediates Recruitment of Telomerase to Telomeres. *PLoS Genet.* 11, e1005410.

Gao, H., Cervantes, R.B., Mandell, E.K., Otero, J.H. and Lundblad, V. (2007). RPA-like proteins mediate yeast telomere function. *Nat. Struct. Mol. Biol.* 14, 208–214.

Garvik, B., Carson, M., and Hartwell, L. (1995). Single-stranded DNA arising at telomeres in cdc13 mutants may constitute a specific signal for the RAD9 checkpoint. *Mol. Cell. Biol.* 15, 6128–6138.

Gelinas, A.D., Paschini, M., Reyes, F.E., Héroux, A., Batey, R.T., Lundblad, V., and Wuttke, D.S. (2009). The telomere capping proteins Stn1 and Ten1 are structurally related to RPA32 and RPA14. *Proc. Natl. Acad. Sci. USA* 106, 19298-19303.

Gottschling, D.E. and Cech, T.R. (1984). Chromatin structure of the molecular ends of Oxytricha macronuclear DNA: phased nucleosomes and a telomeric complex. *Cell* 38, 501-510.

Gottschling, D.E. and Zakian, V.A. (1986). Telomere proteins: specific recognition and protection of the natural termini of Oxytricha macronuclear DNA. *Cell* 47, 195-205.

Goulian, M., Heard, C.J., and Grimm, S.L. (1990). Purification and properties of an accessory protein for DNA polymerase R/primase. *J. Biol. Chem.* 265, 13221–13230.

Greider, C.W. and Blackburn, E.H. (1985). Identification of a specific telomere terminal transferase activity in Tetrahymena extracts. *Cell* 43, 405-413.

Greider, C.W. (2016). Regulating telomere length from the inside out: the replication fork model. *Genes & Development* 30, 1483-1491.

Gu, P., Min, J.N., Wang, Y., Huang, C., Peng, T., Chai, W. and Chang S. (2012). CTC1 deletion results in defective telomere replication, leading to catastrophic telomere loss and stem cell exhaustion. *EMBO J.* 31, 2309-2321.

Gutiérrez, P.J. and Wang, T.S. (2003). Genomic instability induced by mutations in *Saccharomyces cerevisiae* POL1. *Genetics* 165, 65-81.

Hector, R.E., Shtofman, R.L., Ray, A., Chen, B.R., Nyun, T., Berkner, K.L., and Runge, K.W. (2007). Tel1p preferentially associates with short telomeres to stimulate their elongation. *Mol. Cell* 27, 851-858.

Hockemeyer, D., Palm, W., Else, T., Daniels, J.P., Takai, K.K., Ye, J.Z., Keegan, C.E., de Lange, T. and Hammer, G.D. (2007). Telomere protection by mammalian Pot1 requires interaction with Tpp1. *Nat. Struct. Mol. Biol.* 14, 754–761.

Horvath, M.P., Schweiker, V.L., Bevilacqua, J.M., Ruggles, J.A. and Schultz, S.C. (1998). Crystal structure of the Oxytricha nova telomere end binding protein complexed with single strand DNA. *Cell* 95, 963–974.

Higgins, N.P., Kato, K. and Strauss, B. (1976). A model for replication repair in mammalian cells. *J. Mol. Biol.* 101, 417–425.

Jiang, J., Chan, H., Cash, D.D., Miracco, E.J., Ogorzalek Loo, R.R., Upton, H.E., Cascio, D., O'Brien Johnson, R., Collins, K., Loo, J.A., Zhou, Z.H. and Feigon, J. (2015). Structure of Tetrahymena telomerase reveals previously unknown subunits, functions, and interactions. *Science* 350, aab4070.

Kaul, Z., Cesare, A.J., Huschtscha, L.I., Neumann, A.A. and Reddel, R.R. (2011). Five dysfunctional telomeres predict onset of senescence in human cells. *EMBO Rep*. 13, 52-59.

Kolinjivadi, A.M., Sannino, V., De Antoni, A., Zadorozhny, K., Kilkenny, M., Técher, H., Baldi, G., Shen, R., Ciccia, A., Pellegrini, L., Krejci, L. and Costanzo, V. (2017). Smarcal1-Mediated Fork Reversal Triggers Mre11-Dependent Degradation of Nascent DNA in the Absence of Brca2 and Stable Rad51 Nucleofilaments. *Mol. Cell* 67, 867-881.

Lambert, S., Watson, A., Sheedy, D.M., Martin, B. and Carr, A.M. (2005). Gross chromosomal rearrangements and elevated recombination at an inducible site-specific replication fork barrier. *Cell* 121, 689-702.

Larrivée, M., LeBel, C. and Wellinger, R.J. (2004). The generation of proper constitutive G-tails on yeast telomeres is dependent on the MRX complex. *Genes & Development* 18, 1391-1396.

Lewis, KA, Pfaff, DA, Earley, JN, Altschuler, S.E. and Wuttke, D.S. (2014). The tenacious recognition of yeast telomere sequence by Cdc13 is fully exerted by a single OB-fold domain. *Nucleic Acids Res.* 42, 475-484.

Lingner, J., Cooper, J.P. and Cech, T.R. (1995). Telomerase and DNA end replication: no longer a lagging strand problem? *Science* 269, 1533-1534.

Lopes, M., Cotta-Ramusino, C., Pellicioli, A., Liberi, G., Plevani, P., Muzi-Falconi, M., Newlon, C.S. and Foiani, M. (2001). The DNA replication checkpoint response stabilizes stalled replication forks. *Nature* 412, 557-561.

Lydall D and Weinert T. (1995). Yeast checkpoint genes in DNA damage processing: implications for repair and arrest. *Science* 270, 1488-1491.

Lustig, AJ (2001). Cdc13 subcomplexes regulate multiple telomere functions. *Nat. Struct. Mol. Biol.* 8, 297-299.

Marcand S, Gilson E and Shore D (1997). A protein-counting mechanism for telomere length regulation in yeast. *Science* 275, 986-990.

Marcand S, Brevet V, Mann C and Gilson, E. (2000). Cell-cycle restriction of telomere elongation. *Curr. Biol.* 10, 487-490.

Maringele L and Lydall D. (2002). EXO1-dependent single-stranded DNA at telomeres activates subsets of DNA damage and spindle checkpoint pathways in budding yeast yku70Δ mutants. *Genes & Development* 16, 1919-1933.

Martina, M., Clerici, M., Baldo, V., Bonetti, D., Lucchini, G. and Longhese, M.P. (2012). A balancebetween Tel1 and Rif2 activities regulates nucleolytic processing and elongation at telomeres. *Mol. Cell. Biol.* 32, 1604-1617.

Martínez, P., Thanasoula, M., Muñoz, P., Liao, C., Tejera, A., McNees, C., Flores, J.M., Fernández- Capetillo, O., Tarsounas M. and Blasco, M.A. (2009). Increased telomere fragility and fusions resulting from TRF1 deficiency lead to degenerative pathologies and increased cancer in mice. *Genes & Development* 23, 2060-2075.

Makovets, S., Herskowitz, I. and Blackburn, E.H. (2004). Anatomy and dynamics of DNA replication fork movement in yeast telomeric regions. *Mol. Cell. Biol.* 24, 4019-4031.

Marcand, S., Brevet, V. and Gilson, E. (1999). Progressive cis-inhibition of telomerase upon telomere elongation. *EMBO J.* 18, 3509-3519.

Margalef, P., Kotsantis, P., Borel, V., Bellelli, R., Panier, S. and Boulton, S.J. (2018). Stabilization of Reversed Replication Forks by Telomerase Drives Telomere Catastrophe. *Cell* 172, 439-453.

McGee, J.S., Phillips, J.A., Chan, A., Sabourin, M., Paeschke, K., and Zakian, V.A. (2010). Reduced Rif2 and lack of Mec1 target short telomeres for elongation rather than double-strand break repair. *Nat. Struct. Mol. Biol.* 17, 1438–1445.

Miller, K.M., Rog, O., and Cooper, J.P. (2006). Semi-conservative DNA replication through telomeres requires Taz1. *Nature* 440, 824–828.

McGuffee, S.R., Smith, D.J. and Whitehouse, I. (2013). Quantitative, genome-wide analysis of eukaryotic replication initiation and termination. *Mol. Cell* 50, 123-135.

Nugent, C., Hughes, T.R., Lue, N.F. and Lundblad, V. (1996). Cdc13p: A single-strand telomeric DNA- binding protein with a dual role in yeast telomere maintenance. *Science* 274, 249-252.

Matmati, S., Vaurs, M., Escandell, J.M., Maestroni, L., Nakamura, T.M., Ferreira, M.G., Géli, V. and Coulon, S. (2018). The fission yeast Stn1-Ten1 complex limits telomerase activity via its SUMO- interacting motif and promotes telomeres replication. *Sci. Adv.* 4, eaar2740.

McClintock, B. (1941). The Stability of Broken Ends of Chromosomes in Zea Mays. *Genetics* 26, 234- 82.

Milton-Fry, R. M., Anderson, E. M., Hughes, T. R., Lundblad, V., and Wuttke, D. S. (2002). Conserved elements for single-stranded telomeric DNA recognition. *Science* 296, 145–147.

Miyoshi, T., Kanoh, J., Saito, M. and Ishikawa, F. (2008). Fission yeast Pot1-Tpp1 protects telomeres and regulates telomere length. *Science* 320, 1341-1344.

Nakaoka, H., Nishiyama, A., Saito, M. and Ishikawa F. (2012). Xenopus laevis Ctc1-Stn1-Ten1 (xCST) protein complex is involved in priming DNA synthesis on single-stranded DNA template in Xenopus egg extract. *J. Biol. Chem.* 287, 619-627.

Nandakumar J, Bell CF, Weidenfeld I, Zaug AJ, Leinwand LA and Cech, T.R. (2012). The TEL patch of telomere protein TPP1 mediates telomerase recruitment and processivity. *Nature* 492, 285–289.

Palm, W., and de Lange, T. (2008). How shelterin protects mammalian telomeres. *Annu. Rev. Genet.* 42, 301–334.

Paschini, M., Mandell, E.K. and Lundblad, V. (2010). Structure prediction-driven genetics in Saccharomyces cerevisiae identifies an interface between the t-RPA proteins Stn1 and Ten1. *Genetics* 185, 11-21.

Paschini, M., Toro, T.B, Lubin, J., Braunstein-Ballew, B., Morris, D.K. and Lundblad, V. (2012). A naturally thermolabile activity compromises genetic analysis of telomere function in Saccharomyces cerevisiae. *Genetics* 191, 79-93.

Petreaca, R.C., Chiu, H.C. and Nugent, C.I. (2007). The role of Stn1p in Saccharomyces cerevisiae telomere capping can be separated from its interaction With Cdc13p. *Genetics* 177, 1459–1474.

Pfeiffer, V. and Lingner, J. (2013). Replication of telomeres and the regulation of telomerase. *Cold Spring Harb. Perspect. Biol.* 5, a010405.

Rog, O. and Cooper, J.P. (2008). Telomeres in drag: Dressing as DNA damage to engage telomerase. *Curr. Opin. Genet. Dev*. 18, 212-220.

Roman, H. (1956). Studies of gene mutation in Saccharomyces. *Cold Spring Harb. Symp. Quant. Biol*. 21, 175-185.

Sabourin, M., Tuzon, C.T., and Zakian, V.A. (2007). Telomerase and Tel1p preferentially associate with short telomeres in *S. cerevisiae. Mol. Cell* 27, 550–561.
Saharia, A., Teasley, D.C., Duxin, J.P., Dao, B., Chiappinelli, K.B. and Stewart, S.A. (2010). FEN1 ensures telomere stability by facilitating replication fork re-initiation. *J Biol Chem.* 285, 27057-27066.

Segurado, M. and Diffley, J.F. (2008). Separate roles for the DNA damage checkpoint protein kinases in stabilizing DNA replication forks. *Genes & Development* 22, 1816-1827.

Sfeir, A., Kosiyatrakul, S.T., Hockemeyer, D., MacRae, S.L., Karlseder, J., Schildkraut, C.L. and de Lange, T. (2009). Mammalian telomeres resemble fragile sites and require TRF1 for efficient replication. *Cell* 138, 90–103.

Sfeir, A., and de Lange, T. (2012). Removal of shelterin reveals the telomere end-protection problem. *Science* 336, 593–597.

Shampay, J., Szostak, J.W. and Blackburn, E.H. (1984). DNA sequences of telomeres maintained in yeast. *Nature* 310, 154-157.

Singer, M.S. and Gottschling, D.E. (1994). TLC1: Template RNA component of Saccharomyces cerevisiae telomerase. *Science* 266, 404-409.

Smogorzewska, A., van Steensel, B., Bianchi, A., Oelmann, S., Schaefer, M.R., Schnapp, G. and de Lange, T. (2000). Control of human telomere length by TRF1 and TRF2. *Mol. Cell. Biol.* 20, 1659-1568.

Smogorzewska, A. and de Lange, T. (2004). Regulation of telomerase by telomeric proteins. *Annu. Rev. Biochem*. 73, 177-208.

Sogo, J.M., Lopes, M. and Foiani, M. (2002). Fork reversal and ssDNA accumulation at stalled replication forks owing to checkpoint defects. *Science* 297, 599-602.

Stewart, J.A., Wang, F., Chaiken, M.F., Kasbek, C., Chastain, P.D., 2nd, Wright, W.E., and Price, C.M. (2012). Human CST promotes telomere duplex replication and general replication restart after fork stalling. *EMBO J.* 31, 3537–3549.

Sun, J., Yu, E.Y., Yang, Y., Confer, L.A., Sun, S.H., Wan, K., Lue, N.F., and Lei, M. (2009). Stn1-Ten1 is an Rpa2-Rpa3-like complex at telomeres. *Genes & Development* 23, 2900–2914.

Takai, H., Smogorzewska, A., and de Lange, T. (2003). DNA damage foci at dysfunctional telomeres. *Curr. Biol.* 13, 1549–1556.

Takikawa, M., Tarumoto, Y. and Ishikawa, F. (2017). Fission yeast Stn1 is crucial for semi-conservative replication at telomeres and subtelomeres. *Nucleic Acids Res.* 45, 1255-1269.

Teixeira, M.T., Arneric, M., Sperisen, P., and Lingner, J. (2004). Telomere length homeostasis is achieved via a switch between telomerase-extendible and -nonextendible states. *Cell* 117, 323–335.

Tucey T.M. and Lundblad, V. (2013). A yeast telomerase complex containing the Est1 recruitment protein is assembled early in the cell cycle. *Biochemistry* 52, 1131-1133.

Vannier, J.B., Sandhu, S., Petalcorin, M.I., Wu, X., Nabi, Z., Ding, H. and Boulton, S.J. (2013). RTEL1 is a replisome-associated helicase that promotes telomere and genome-wide replication. *Science* 342, 239-242.

van Steensel, B. and de Lange, T. (1997). Control of telomere length by the human telomeric protein TRF1. *Nature* 385, 740-743.

van Steensel, B., Smogorzewska, A. and de Lange, T. (1998). TRF2 protects human telomeres from end-to-end fusions. *Cell* 92, 401–413.

Woods, R.A. (1969). Response of ad-2 mutants of Saccharomyces cerevisiae to carbon dioxide. *Mol. Gen. Genet.* 105, 314-316.

Wu, R.A., Upton, H.E., Vogan, J.M. and Collins, K. (2017). Telomerase Mechanism of Telomere Synthesis. *Annu. Rev. Biochem.* 86, 439-460.

Xin, H., Liu, D., Wan, M., Safari, A., Kim, H., Sun, W., O'Connor, M.S., and Songyang, Z. (2007). TPP1 is a homologue of ciliate TEBP-beta and interacts with POT1 to recruit telomerase. *Nature* 445, 559- 562.

Xu, L., Petreaca, R.C., Gasparyan, H.J., Vu, S. and Nugent, C.I. (2009). TEN1 is essential for CDC13- mediated telomere capping. Genetics 183, 793-810.

Zhong, F.L., Batista, L.F., Freund, A., Pech, M.F., Venteicher, A.S. and Artandi, S.E. (2012). TPP1 OB- fold domain controls telomere maintenance by recruiting telomerase to chromosome ends. *Cell* 150, 481-494.

Zubko, M.K., Guillard, S., and Lydall, D. (2004). Exo1 and Rad24 differentially regulate generation of ssDNA at telomeres of Saccharomyces cerevisiae cdc13-1 mutants. *Genetics* 168, 103-115.

CHAPTER FOUR:

A redundant set of pathways for replication fork collapse mediates telomere homeostasis

In Chapter 3, a new model for telomere length regulation was presented that changed how we think about what drives telomere length homeostasis. This model is focused on the contribution of one specific mechanism that has significant effects on telomere length, due to errors that occur during replication through duplex telomeric DNA. Before this, the prevailing model revolved around the assumption that the main contributors to telomere length impose their effects after the complete replication of telomeres. We were able to form this new model, due in part to new and more sensitive assays developed in the lab, which allowed us to study the dynamics of replication through telomeric DNA and the factors that contribute to this process. This current chapter shows evidence that a number of previously identified telomere regulators contribute to efficient telomere replication. Using sensitized strains that have either a subtle or substantial defect in telomere replication, I identified genes that can either exacerbate replication fork collapse at telomeres, or alleviate it. This modification to the replication fork collapse (RepFC) assay makes it a more effective tool to re-examine genes that have historically been implicated in telomere length homeostasis by different mechanisms and study their role in telomere replication.

INTRODUCTION

The ends of linear chromosomes are composed of unique structures that maintain chromosome stability and cellular viability. Therefore, understanding the mechanisms that regulate telomere length homeostasis has significant implications. One characteristic of telomeric DNA poses an obstacle for the replication machinery.

Telomeric DNA is composed of repetitive DNA, which like many other forms of repetitive DNA is difficult to (Makovets et al. 2004; Fouché et al. 2006; Sfeir et al. 2009; Aksenova et al. 2013). Additionally, the G-rich content of telomeric DNA is thought to cause the formation of secondary structures (Williamson et al. 1989; Burge et al. 2006; Maizels et al. 2006), contributing to its complexity. Along with placement in the genome, which prevents replication fork rescue by a converging fork, telomeres are heavily bound by telomere specific proteins. All of these features make telomeres a vulnerable region in the genome, that the cell is tasked with efficiently and fully replicating at every cell division.

The previous chapter introduced a new model for telomere maintenance where homeostasis is governed by a balance between replication fork collapse and the subsequent response by telomerase and its regulatory network. The telomere dedicated RPA (t-RPA) complex was shown to have an essential role in ensuring efficient replication of telomeres, in addition to its known function of recruiting telomerase to telomeres. The t-RPA complex is made up of three essential proteins; Cdc13, Stn1, and Ten1 (Grandin et al. 1997; Grandin et al. 2001). Structure-driven mutations in the DNA binding domain (DBD) of Cdc13, and in the winged helix-loop-helix (wHLH) domain of Stn1 (Appendix A), allowed us to investigate the role of t-RPA in the replication of telomeres. To study effects on telomere replication we used an assay called the RepFC assay (for Replication Fork Collapse) that monitors spontaneous replication fork collapse at an internal $G_{1\text{-}3}T$ telomeric tract. Using this assay I showed, in collaboration with Margherita Paschini, that when t-RPA is defective, in

either *cdc13*^{DBD} or *stn1*$^{-wHLH}$ mutant strains, a dramatic increase in fork collapse frequency is observed. When telomere length of the natural end of Chr 1-L was measured, the increased replication fork collapse frequency in these two t-RPA alleles was accompanied with a telomere length phenotype where both the average telomere length was altered and the populations of ultra short and over elongated telomeres was increased. We called this phenotype the t-DAM phenotype (for deviation away from the mean).

Our new model, and the assays developed to study it, opened new possibilities to probe previously categorized telomere length regulators. This was prompted by the results I obtained analyzing Rif2. I found that the loss of *RIF2*, a central component in the prior "protein counting" model for telomere length regulation (Wotton & Shore 1997), led to a t-DAM phenotype where there was an increase in the population of ultra short and over elongated telomeres, and not solely an over elongated telomere phenotype as predicted by the old model. This chapter focuses on the progress in identifying additional genes that contribute to efficient telomere replication and those that act to destabilize it. By exploiting previously obtained t-RPA alleles, I was able to modify the RepFC assay to increase its sensitivity and successfully identify genes that effect telomere replication.

RESULTS

Assessing replication fork collapse frequencies in strains defective for known telomere length regulators

As a starting point for this study, I took previously identified telomere length regulators and asked if the loss of any of them had an effect on the frequency of replication fork collapse at an internal $G_{1\text{-}3}T$ telomeric tract. If the gene in question were contributing to the stability of telomere replication, I would expect to detect that in the RepFC assay. For each mutant strain, I tested between 2,600-19,000 colonies (detailed in table 4.1). None of the mutations tested were able to effect replication fork collapse frequency to a level notably higher than wild type (Figure 4.1). Each data set is representative of at least two independent experiments. It is important to note that the current experimental design would only be able to assay for changes that cause an increase in replication fork collapse, as a frequency below 0.07% or 1 in 1400 (wild type fork collapse frequency) while conceptually possible, would be logistically unfeasible.

Additionally, I included the known telomere length regulator Yku70/80 in this study. The heterodimer Yku70/80 (Ku70 and Ku80 in humans) is known for its roles at both DSBs and in telomere regulation (Liang et al. 1996; Boulton & Jackson 1996a; Boulton & Jackson 1996b; Boulton & Jackson 1998). Moreover, cells deficient for both telomerase and Ku exhibit greatly accelerated senescence progression (Gravel et al. 1998). There was no increase in replication fork collapse frequency in either *yku70*-Δ or *yku80*-Δ, based on 9615 and 19677 colonies surveyed, respectively. Finally, I tested the effect of loss of two genes (*MMS1* and *MMS22*) that have been shown to stabilize the replisome upon replication stress (Vaisica et al. 2011). Again, neither the

loss of *MMS1* or *MMS2* exhibited a replication fork collapse frequency above wild type (Figure 4.1 B).

A panel of t-RPA alleles that exhibit a gradient of phenotypes

In the Chapter 3, the t-RPA complex was identified as a telomere-associated factor that played an essential role in efficient telomere replication. Structure-driven mutations in two surfaces of the t-RPA complex (*cdc13*-F539A and *stn1*-W466E; Appendix A) had substantial effects on replication fork collapse frequency in the RepFC assay (10-20 fold increase in replication fork collapse compared to wild type). The RepFC assay monitors effects on the replication of an internal telomeric tract; to better understand the effects of the t-RPA complex in telomere homeostasis, both mutants were analyzed for effects on natural telomeres by examining telomere length of one specific telomere (Chr 1-L). The results were an increase in a sub-population of both ultra short telomeres (≤100bp) and the proportion of elongated telomeres, the t-DAM phenotype. Both the frequency of fork collapse in the RepFC assay and the t-DAM phenotype were partially suppressed by a mutation that effects replication fork breakdown (*exo1*-Δ; detailed in Chapter 3) arguing that both phenotypes are driven by replication fork collapse. Additionally, the prominent growth defect that accompanies both t-RPA alleles was also alleviated by the loss of *EXO1*.

The two structure-driven mutations mentioned above were part of a much larger analysis of t-RPA that identified two classes of t-RPA alleles (*cdc13*^{DBD} and *stn1*^{WHLH}) and helped define the essential function of the t-RPA complex (Paschini 2015; Gelinas et al. 2009; Appendix A). For Cdc13, multiple residues that disrupt the

high affinity DNA-binding domain (DBD) were identified, which displayed a gradient in both binding affinity and growth defects (Appendix 5). One of these alleles, *cdc13*-Y556A Y558A (*cdcd13*-YYAA) was analyzed for telomere length at high resolution. Chr 1-L termini were PCR-amplified from multiple *cdcd13*-YYAA single colonies, and 132 independent cloned PCR products were sequenced. The resulting telomere length profile for *cdcd13*-YYAA, when compared to the wild type profile, revealed a clear increase in the category of very short telomeres (≤100bp, 5% in WT vs. 15% in *cdcd13*-YYAA; Figure 4.2 A) and elongated telomeres, a prominent t-DAM phenotype. However, in contrast to another *cdc13*^{DBD} allele (*cdc13*-F539A; Chapter 3), the *cdc13*-YYAA t-DAM phenotype was not accompanied by a detectable increase in frequency of replication fork collapse (Figure 4.2 B).

A similar result was seen with the *stn1*^{WHLH} allele *stn1*-H486A. The amplification of 139 Chr 1-L termini showed an obvious t-DAM phenotype with a 3-fold increase in the number of telomeres ≤100bp, and a substantial increase in elongated telomeres (Figure 4.2 A). Again, this t-DAM phenotype was not accompanied by an increase frequency of replication fork collapse in the RepFC assay (personal communication, M. Paschini). Both *cdc13*-YYAA and *stn1*-H486A have a growth defect that is not as severe as either *cdc13*-F539A (Figure 4.2 C) and *stn1*-W466E, which could be indicative of a defect in telomere replication that is also less severe. This suggests that there is a mild replication fork collapse defect in these less severe t-RPA alleles that are below the detection limit of the RepFC assay.

Using sensitized t-RPA alleles to identify factors that contribute to efficient telomere replication

The above suggested that degree of replication fork collapse might be correlated to the degree of growth defect. With this in mind, I probed for growth defects when *cdc13*-YYAA was combined with loss of *GENE X*. This was done by deleting genes in a diploid strain background that was heterozygous for *cdc13*-YYAA mutation and monitoring growth of haploids after dissection. In the case of *cdc13*-YYAA *rif1*-Δ, *cdc13*-YYAA *tel1*-Δ and *cdc13*-YYAA *rad50*-Δ, the double mutants displayed a growth defect significantly larger than a haploid bearing a single *cdc13*-YYAA mutation (Figure 4.3 A, red box). All three were subsequently assayed using the RepFC assay, and in each case there was a significant increase (p <0.001 for all three, Figure 4.3 B) in replication fork collapse frequency.

In addition to testing the effects of known telomere effectors, I was also interested in studying the roles of genes known for their effects on replication fork dynamics, to see if their roles in the genome were analogous in replication of telomeres. To this end, Mrc1 (mediator of the replication checkpoint) and Tof1 (topoisomerase I interacting-factor) were included in my analysis. Together with Csm3, these proteins act as replication checkpoint-specific mediators in yeast (Bando et al. 2009). They are part of replisome progression complex and have been found to play multiple roles in checkpoint activation after damage, replication pausing, and recovery of DNA synthesis after replication fork stalling (Alcasabas et al. 2001, Foss 2001, Katou et al. 2003). The loss of *MRC1* did not have a detectable effect of

replication fork collapse (Figure 4.4 B) on its own. A total of 16,555 colonies were analyzed for their frequency of fork collapse, and only seven (or 0.042%) lost the distal chromosome after a fork collapse at the internal telomeric tract in the first cell division. Notably, however, a substantial fork collapse frequency could be detected when the *cdc13*-YYAA and *mrc1*-Δ mutations were combined. Using the same strategy as the one detailed above, a heterozygous diploid strain bearing both *cdc13*-YYAA and *mrc1*-Δ was dissected and haploids monitored for growth defects. The growth defect of the *cdc13*-YYAA *mrc1*-Δ was so pronounced that a visible colony did not appear until many days after *cdc13*-YYAA *MRC1* had already formed (Figure 4.4, red box). Strikingly, this exacerbation in growth defect was accompanied by a significant (p <0.001) increase in replication fork collapse frequency. Similarly *cdc13*-YYAA *tof1*-Δ had a severe growth defect and a significant increase in frequency of replication fork collapse frequency (p <0.001, Figure 4.4).

To further our understanding of canonical replication factors at telomeres I also tested effects of the loss of *POL32*. Pol32 is the third subunit of *Saccharomyces cerevisiae* DNA polymerase delta (Gerik 1998). As a single, mutant this strain does not have a growth defect or an increase in replication fork collapse. However, when combined with *cdc13*-YYAA, the double mutant strain displays both a severe growth defect and a significant replication fork collapse frequency (Figure 4.4). Together, these results demonstrate that I was successful in identifying factors that contribute to efficient replication of telomeres by combining them with t-RPA alleles.

Using sensitized t-RPA alleles to identify factors that act to destabilize telomere replication

Up to this point the Rep-FC assay has been used to identify factors that contribute to efficient telomere replication by measuring replication fork collapse in strains where those factors are mutant. It is equally important to identify factors that destabilize telomere replication, by looking for a decrease in replication fork collapse when factors are absent. Using *cdc13*-F539A, a *cdc13*^{DBD} allele with a high frequency of fork collapse, I probed for candidates that could decrease replication fork collapse. Again, I used growth as my initial readout. In the Chapter 3, the deletion of *EXO1* led to a 4-fold decrease in replication fork collapse in *stn1*-W466E background. Here I tested if a similar effect would be reached with *cdc13*-F539A. As expected, *cdc13*-F539A *exo1*-Δ had a significant (p <0.0001) reduction in fork collapse frequency (10 – fold reduction). This decrease again was accompanied by suppression in growth defect (data not shown).

Similar results were observed when these t-RPA-defective alleles were combined with *bmh1*-Δ. Bmh1 (and its paralog Bmh2) are 14-3-3 proteins that regulate Exo1-dependent processing of stalled replication forks (Engels et al. 2011). While the deletion of both *bm1*-Δ and *bmh2*-Δ is lethal, the single mutant does not have a detectable growth defect. When I combined *bmh1*-Δ with *cdc13*-F539A, the substantial growth defect of *cdc13*-F539A was greatly reduced (Figure 4.5 A, middle panel). A similar effect was observed with a less severe *cdc13*^{DBD} allele, *cdc13*-YYAA (Figure 4.5 A, top panel). In this case, the colony size of *cdc13*-YYAA *bmh1*-Δ was

equivalent to colony size of *CDC13 BMH1*. This suggests that the dramatic frequency of fork collapse in *cdc13*-F539A should also be greatly reduced in *cdc13*-F539A *bmh1*-Δ. As expected, the replication fork collapse frequency of *cdc13*-F539A *bmh1*-Δ was reduced significantly when compared to *cdc13*-F539A *BMH1* (Figure 4.5 B). This result was not limited to $cdc13^{DBD}$ alleles, as a similar result using another t-RPA allele ($stn1^{WHLH}$) was achieved when I combined *bmh1*-Δ with *stn1*-W466E. Both the growth defect and the frequency of replication fork collapse were reduced in *stn1*-W466E *bmh1*-Δ, compared to *stn1*-W466E *BMH1*.

DISCUSSION

Our recent discovery that telomere replication drives telomere length homeostasis, prompted us to re-evaluate previously categorized telomere length regulators. Most of the historical telomere length regulators were categorized as such because of their phenotype in low resolution based assays. These assays were unable to detect variant sub-populations of telomeres (the t-DAM phenotype) as well as subtle telomere length changes, and therefore built an incomplete picture of telomere length regulation. Chapter 3 introduced two new high-resolution assays that allowed us to study replication fork dynamics at telomeres (RepFC assay) and how an increase in fork collapse (caused by a defective t-RPA complex) caused telomere length dysregulation. In this chapter, I used t-RPA alleles to sensitize the RepFC assay and subsequently showed that it could successfully be used to identify both factors that

contribute to efficient telomere replication and those that destabilize it, overcoming the previous detection limit.

The starting point to this study was my prior observation that a well-known telomere length regulator and key player in the prevalent "protein counting model" (Marcand et al.1997; Wotton & Shore 1997), Rif2, displayed a t-DAM phenotype. This protein is thought to impose its telomere length regulation by inhibiting the access of telomerase to the end of fully replicated telomeres. Again, this assumption stemmed from its phenotype in telomere restriction fragment analysis done by low resolution Southern blot. When I analyzed individual Chr 1-L termini, a different result was revealed. Both the population of ultra short and over elongated telomeres were present in *rif2*-Δ, a result that cannot be easily be explained by the "protein counting model" but which fits perfectly with our model of telomere replication as the major driver of telomere length regulation. This suggested that other factors, initially identified on the basis of their analysis through relatively low-resolution assays, might similarly be effecting telomere homeostasis by contributing to DNA intermediates (collapsed forks) that occur during telomere replication and not access of telomerase or other activities restricted to fully replicated telomeres.

Consistent with this premise, the data in this study shows that Rif1, Tel1, and Rad50, contribute to a redundant pathway for telomere length regulation. In strains that are defective for telomere replication (by defective t-RPA), the loss of *RIF1*, *TEL1*, or *RAD50* led to a significant increase in replication fork collapse frequency at an internal $G_{1\text{-}3}T$ telomeric tract (Figure 4.3). Rif1, like Rif2, is a key player in the

"protein counting model" (Marcand et al. 1997). Here I show that its role in telomere regulation, like Rif2, is facilitating efficient replication through duplex telomeric DNA. Again, the long telomere phenotype that was observed in numerous telomere restriction analysis experiments (Hardy et al. 1992; Wotton & Shore 1997) was a result of the lack of sensitivity for detecting small populations of telomeres.

TEL1 was initially discovered based on its short telomere phenotype in *tel1*-Δ (Lustig & Petes 1986). *RAD50,* while initially identified as a player in recombination, was shown to play a role in telomere regulation as *rad50*-Δ also displays a short telomere phenotype (Kironmai & Muniyappa 1997). This is somewhat perplexing, since *RIF1*, *TEL1*, and *RAD50* all contribute to efficient telomere replication, but display opposite telomere length phenotypes when absent. One possible explanation for this result is a difference in the structure created after fork collapse at telomeric DNA. If the absence of either *TEL1* or *RAD50* decreases the efficiency of replication through duplex telomeric DNA (resulting in increase replication fork collapse) but leads to the formation of a less than optimal substrate for telomerase, then the increase in fork collapse would result in an increased accumulation of short telomeres that cannot be elongated as efficiently by telomerase. This is a question that can be addressed by sequencing the progeny of a collapsed fork in the first cell division, and looking at the footprint of telomerase addition. Currently another graduate student, Abby Gillispie, is studying the effect of fork remodelers and how they effect substrate generation and subsequent telomerase elongation, and therefore telomere length.

Interestingly, when I looked at genes with known effects on genome-wide replication, the loss of *MRC1*, *TOF1*, or *POL32* did not increase replication fork collapse beyond what I observed for wild type (Figure 4.4) in our RepFC assay. Again, I turned to *cdc13*-YYAA as a sensitized strain for replication defects at telomeres. This allowed me to show that the degree of replication fork collapse at an internal $G_{1\text{-}3}T$ telomeric tract significantly increased when both the telomere specific replication complex (t-RPA) and genome-wide replication efficiency is defective. Moreover this result may be experimentally advantageous down the line. The increase in replication fork collapse reported in this Chapter, was found in combination with a t-RPA allele (*cdc13*-YYAA) with an assumed telomere replication defect of its own. Figure 4.2 shows that *cdc13*-YYAA has a degree of replication fork collapse that is biologically significant (t-DAM phenotype in A) but below the detection limit of the RepFC assay (B). The same could be said for the genes that showed a significant increase in fork collapse when combined with *cdc13*-YYAA (*MRC1*, *TOF1*, and *POL32*). The advantage to using the latter set is that the level of telomerase recruitment is not affected, as it is with the $cdc13^{DBD}$ mutants. This is important when analyzing the telomerase footprint after collapse, and therefore experimentally beneficial.

To study both sides of telomere length regulation through efficient replication of duplex telomeric DNA I also analyzed factors that add to its instability. To focus on genes that exacerbate telomere replication I employed severe t-RPA alleles (*cdc13*-F539A and *stn1*-W466E), which had a replication fork collapse frequency that was 10-

20 fold higher than wild type (Chapter 3). As before, I could use these t-RPA alleles as sensitized strains, this time to check for decreases in fork collapse frequency in our RepFC assay. The loss of *EXO1* in *cdc13*-F539A and *cdc13*-YYAA led to an alleviation in growth defect and replication fork collapse frequency, similar to the results obtained with *stn1*-W466E in Chapter 3. Additionally, by combining *cdc13*^{DBD} alleles or *stn1*-W466E with a deletion of *BMH1* I observed alleviation in the growth defect of t-RPA alleles (Figure 4.5 A; data not shown) that also resulted in a significant decrease in replication fork collapse in *cdc13*-F539A *bmh1*Δ and *stn1*-W466E *bmh1*-Δ (Figure 4.5 B). Bmh1 (and the paralog Bmh2) are 14-3-3 proteins that regulate Exo1-dependent processing of stalled replication forks (Engels, et al. 2011). This result is also in agreement with a number of studies that found that a *BMH1* deletion rescued the temperature sensitivity of a t-RPA defective allele (Addinall et al 2008, Downey et al. 2006).

The long-standing premise that Cdc13 (together with Stn1-Ten1) functions as a "telomere capping" complex (Maringele & Lydall 2002), by preventing end resection, has been driven in part by the observations that the growth of *cdc13* mutant strains is significantly improved by the loss of *EXO1* function. This genetic interaction has been interpreted as an end-specific phenomenon; i.e. exonucleolytic resection of exposed DNA termini by Exo1 contributes to the impaired growth of *cd13* mutant strains. However, Exo1, which is a Rad2-like flap-endonuclease contributes to both endo- and exo-nucleolytic activities (Fiorentinin et al. 1997; Lee & Wilson 1999; Tran et al. 2002). Furthermore, replication fork breakdown can be rescued by loss of *EXO1*

(Segurado & Diffley 2008). So the alternative interpretation of the genetic interaction between *EXO1* and *CDC13* is that in *cdc13* mutant cells, replication fork stalling occurs in duplex telomeric DNA, but these stalled forks can be rescued in an *exo1*-Δ background. Consistent with this alternative interpretation, the substantial increase in the frequency of replication fork collapse displayed by the *cdc13*-F539A and *stn1*-W466E as well as the severe growth defect, was suppressed by in an *exo1*-Δ or *bmh1*-Δ background (Figure 4.5). The above shows that the mutations originally isolated as suppressors of *cdc13*-ts growth also suppress the replication fork collapse defects of t-RPA defective strains.

Together these findings, combined with the findings in Chapter 3, add to mounting data that argue that the efficient replication of telomeres has been long been an undervalued mechanism that regulates telomere length homeostasis. It is likely, that a large number of additional known telomere length regulators that have not yet been studied for their effects on telomere replication with our high resolution assays will display similar effects to the ones detailed in this chapter.

FIGURES

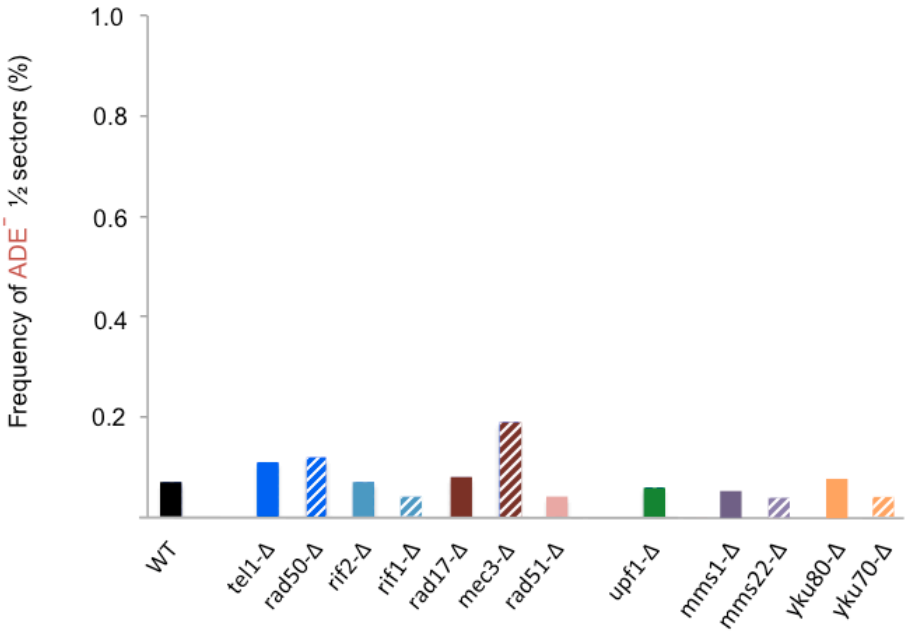

Figure 4.1: Replication fork collapse frequency for strains defective for known telomere length regulators. Percent frequency of replication fork collapse at an interstitial telomeric tract in different genetic backgrounds is summarized.

Table 4.1: Detailed summary for replication fork collapse frequency of multiple known telomere length regulators. Raw data for RepFC experiments detailing the number of colonies surveyed for every genotype and the frequency of replication fork collapse. The data shown in the graph in Figure 4.1 is a product of multiple experiments.

Genotype	½ sector	total	% frequency	*p*-value
WT	16	22468	0.07%	
tel1-Δ	7	6534	0.11%	0.5
rad50-Δ	11	8883	0.12%	0.2
rif2-Δ	3	4294	0.07%	1
rif1-Δ	6	15132	0.04%	0.3
rad17-Δ *(9-1-1)*	4	4961	0.08%	0.8
mec3-Δ *(9-1-1)*	8	4296	0.19%	0.04
rad51-Δ	1	2688	0.04%	0.8
upf1-Δ	9	16034	0.06%	0.7
mms1-Δ	2	4059	0.05%	0.9
mms22-Δ	2	16034	0.01%	0.8
yku70-Δ	8	9615	0.08%	0.9
yku80-Δ	6	19677	0.03%	0.1

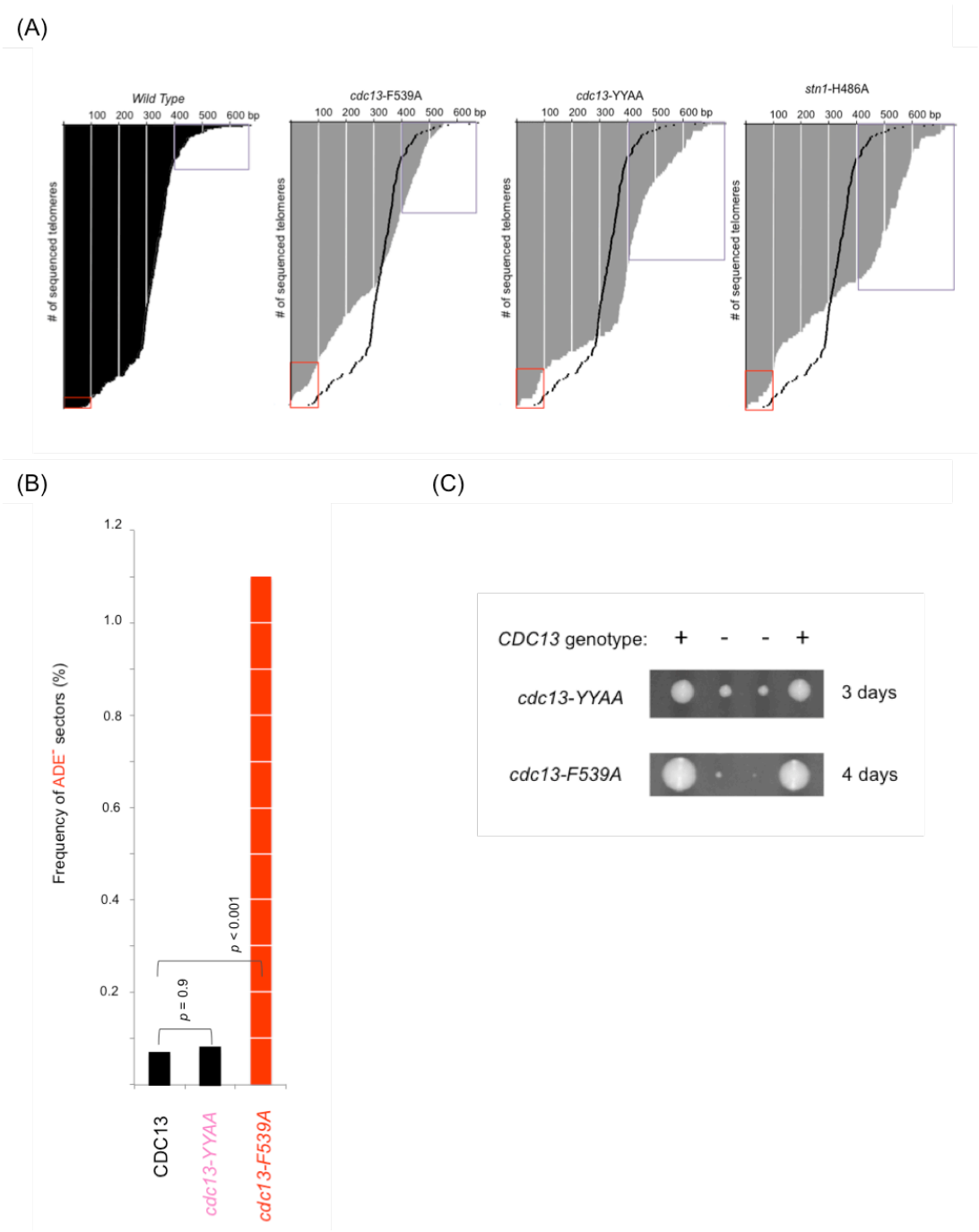

Figure 4.2: A panel of t-RPA alleles that exhibit a gradient of phenotype. (A) Telomere length profiles generated for wild type, *cdc13*^{DBD} (*cdc13*-F539A and *cdc13*-YYAA) and *stn1*^{WHLH} (*stn1*-H486A) alleles. The wild type telomere length signature is superimposed on all t-RPA allele telomere length profiles as a solid black line. The population of very short telomeres (≤100bp) is boxed in red and over elongated telomeres (≥400bp) in purple. (B) RepFC data for two *cdc13*^{DBD} alleles, compared to CDC13. (C) Growth of CDC13, *cdc13*-YYAA and *cdc13*-F539A haploid strains on rich media at 30˚, following dissection of the appropriate heterozygous diploids.

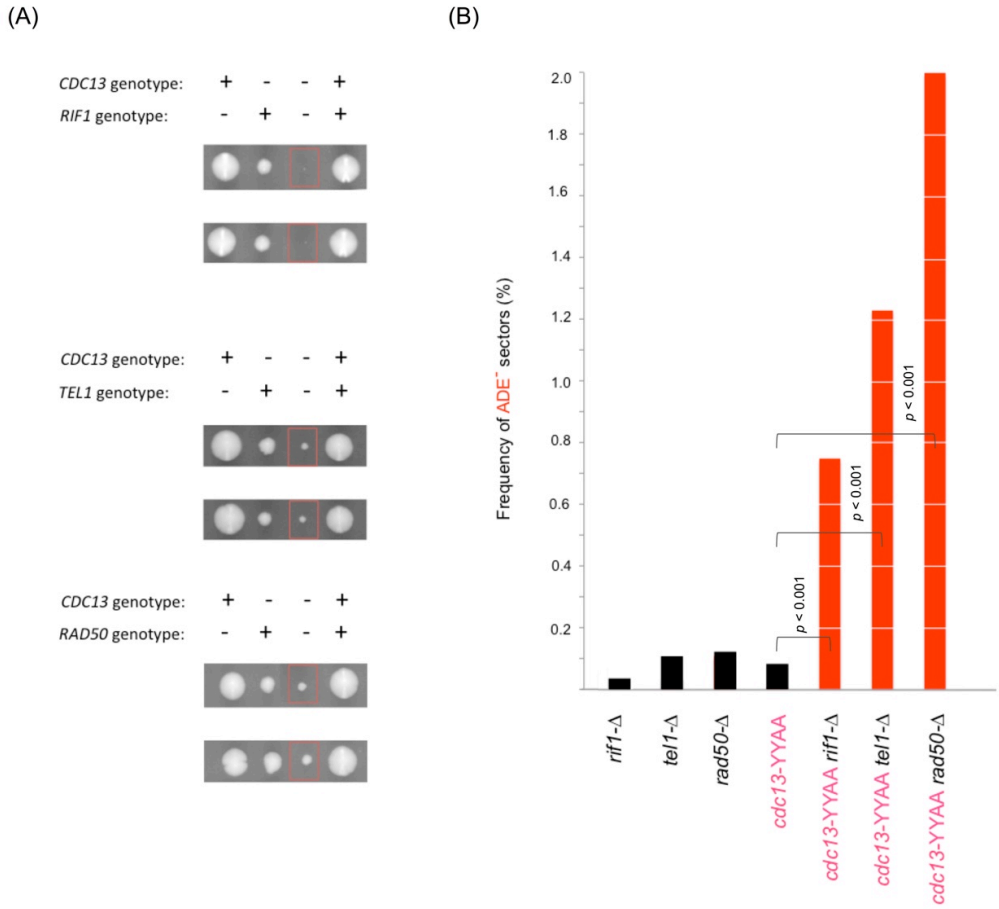

Figure 4.3: Using *cdc13*-YYAA as a sensitized strain for identifying factors that contribute to efficient telomere replication. (A) Growth of relevant haploid strains after dissection of a heterozygous diploid bearing *cdc13*-YYAA and either *rif1*-Δ, *tel1*-Δ, or *rad50*-Δ, grown on rich media at 30˚ for 3 days. Double mutants are boxed in red, and show a growth defect when compared to *cdc13*-YYAA. (B) RepFC data for single mutants that shows a comparable wild type frequency of fork collapse and significant increase in the frequency of fork collapse in combination with *cdc13*-YYAA.

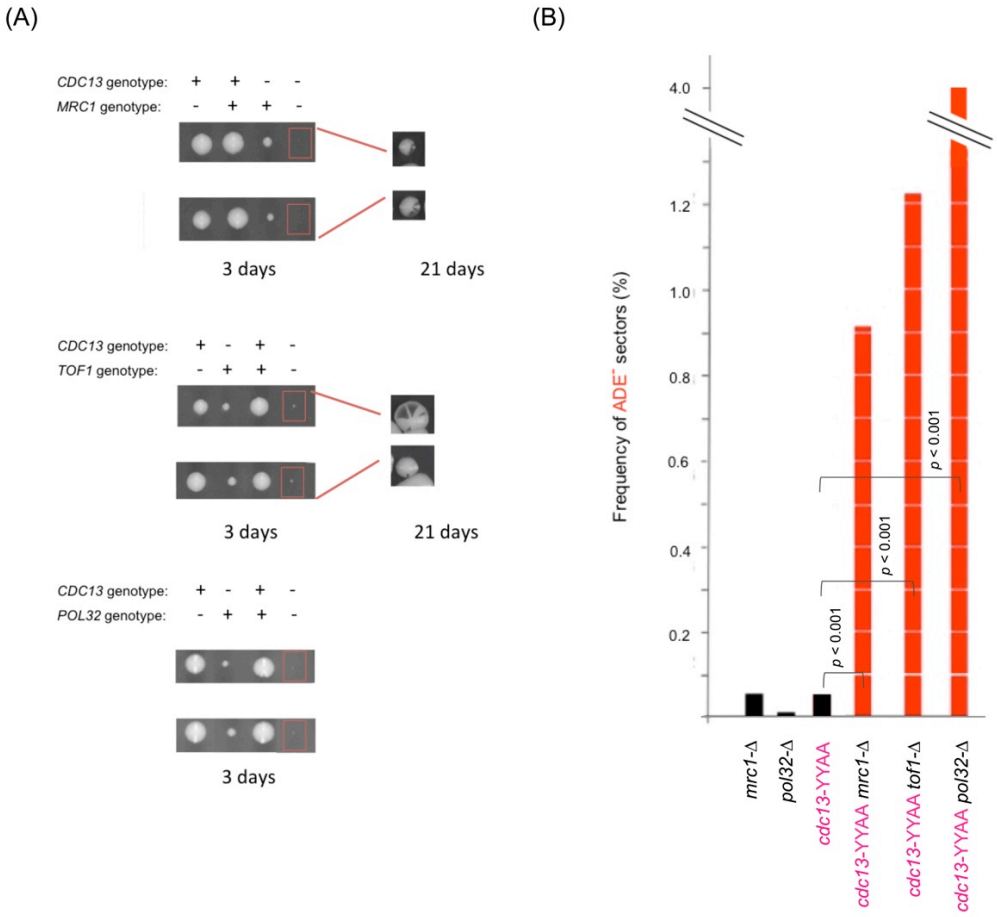

Figure 4.4: Using *cdc13*-YYAA as a sensitized strain to identify additional factors that contribute to efficient telomere replication. (A) Growth of relevant haploid strains after dissection of a heterozygous diploid bearing *cdc13*-YYAA and either *mrc1*-Δ, *tof1*-Δ, or *pol32*-Δ, grown on rich media at 30˚ for 3-21 days. Double mutants are boxed in red, and show a growth defect when compared to *cdc13*-YYAA. (B) RepFC data for single mutants that shows a comparable wild type frequency of fork collapse and significant increase in the frequency of fork collapse in combination with *cdc13*-YYAA.

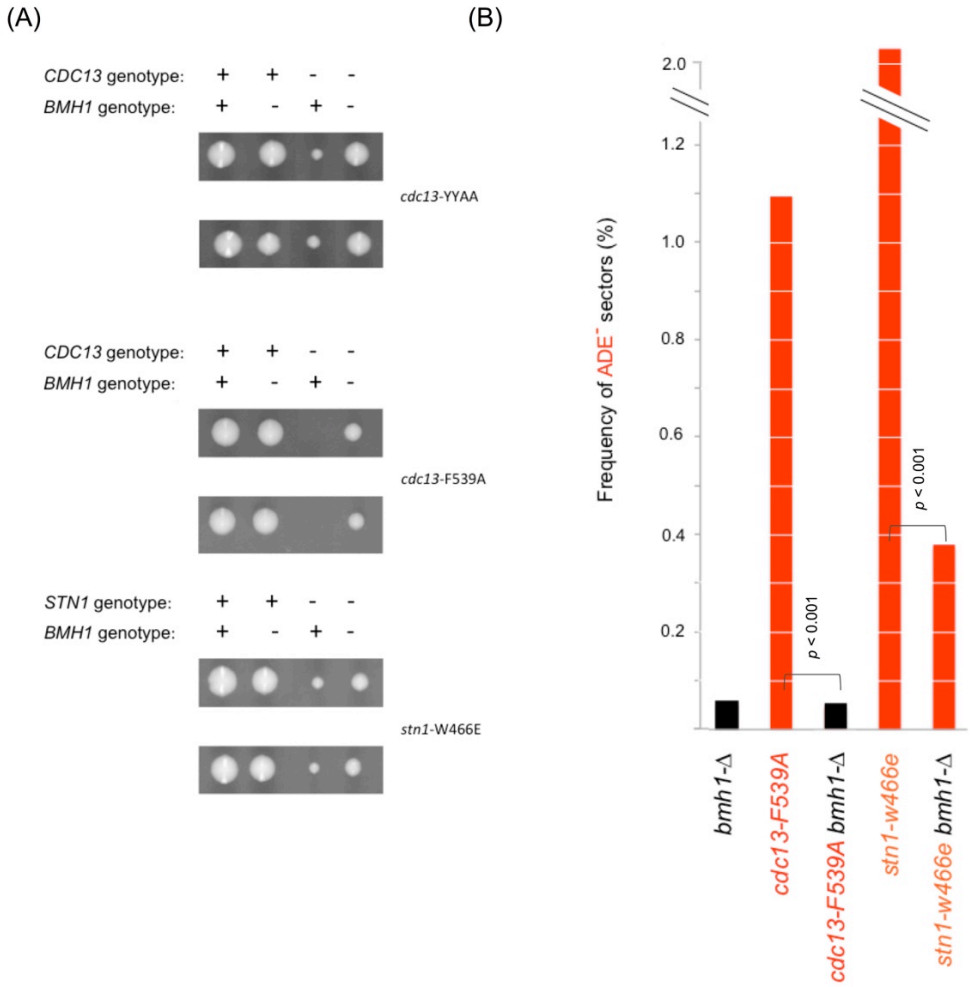

Figure 4.5 Using t-RPA alleles as sensitized strains for identifying factors that contribute to destabilization of telomere replication. (A) Growth of relevant haploid strains after dissection of a heterozygous diploid bearing a t-RPA allele (*cdc13*-YYAA, *cdc13*-F539A, or *stn1*-W466E) and *bmh1*-Δ, grown on rich media at 30˚ for 3 days. Double mutants show an alleviation of growth defect when compared to relevant t-RPA allele. (B) RepFC data shows a comparable wild type frequency of fork collapse for single mutants, and a significant decrease in the frequency of fork collapse in combination with either *cdc13*-F539A or *stn1*-W466E.

Table 4.2: Summary of replication fork collapse frequency for mutant combinations tested in the RepFC assay.

Genotype	½ sector	total	% frequency	*p*-value
WT	16	22468	0.07%	
mrc1-Δ	7	16,555	0.04%	0.3407
pol32-Δ	3	5600	0.05%	0.8674
bmh1-Δ	2	3515	0.06%	0.7642
cdc13-YYAA	1	1226	0.08%	0.8951
cdc13-F539A	31	2836	1.09%	<0.0001
stn1-W466E	112	5891	1.90%	<0.0001
cdc13-YYAA rif1-Δ	131	17402	0.75%	<0.0001
cdc13-YYAA tel1-Δ	86	7012	1.23%	<0.0001
cdc13-YYAA rad50-Δ	94	4727	2%	<0.0001
cdc13-YYAA mrc1-Δ	139	6015	2.30%	<0.0001
cdc13-YYAA tof1-Δ	28	2299	1.22%	<0.0001
cdc13-YYAA pol32-Δ	240	5428	4%	<0.0001
cdc13-F539A bmh1-Δ	6	12223	0.05%	<0.0001
cdc13-F539A exo1-Δ	11	10344	0.11%	<0.0001
stn1-W466E bmh1-Δ	35	9171	0.38%	<0.0001

Table 4.3 Strains used in this study.

YVL	Genotype
4836	*MAT**a** ura3-52 lys2-801 trp-Δ1 his3-Δ200 leu2-Δ1 ade2::LEU2 ADE2 inserted at 425434, ChrIX*
4837	*MAT**a** cdc13-YYAA ura3-52 lys2-801 trp-Δ1 his3-Δ200 leu2-Δ1 ade2::LEU2 ADE2 inserted at 425434, ChrIX*
4839	*MAT**a** cdc13-F539A ura3-52 lys2-801 trp-Δ1 his3-Δ200 leu2-Δ1 ade2::LEU2 ADE2 inserted at 425434, ChrIX*
4844	*MAT**a** stn1-W466E ura3-52 lys2-801 trp-Δ1 his3-Δ200 leu2-Δ1 ade2::LEU2 ADE2 inserted at 425434, ChrIX*
5262	*MAT**a** mrc1-Δ::kanMX6 ura3-52 lys2-801 trp-Δ1 his3-Δ200 leu2-Δ1 ade2::LEU2 ADE2 inserted at 425434, ChrIX*
5274	*MAT**a** tel1-Δ::kanMX6 ura3-52 lys2-801 trp-Δ1 his3-Δ200 leu2-Δ1 ade2::LEU2 ADE2 inserted at 425434, ChrIX*
5265	*MAT**a** rad50-Δ::kanMX6 ura3-52 lys2-801 trp-Δ1 his3-Δ200 leu2-Δ1 ade2::LEU2 ADE2 inserted at 425434, ChrIX*
5267	*MAT**a** rif2-Δ::kanMX6 ura3-52 lys2-801 trp-Δ1 his3-Δ200 leu2-Δ1 ade2::LEU2 ADE2 inserted at 425434, ChrIX*
5266	*MAT**a** rif1-Δ::kanMX6 ura3-52 lys2-801 trp-Δ1 his3-Δ200 leu2-Δ1 ade2::LEU2 ADE2 inserted at 425434, ChrIX*
5268	*MAT**a** rad17-Δ::kanMX6 ura3-52 lys2-801 trp-Δ1 his3-Δ200 leu2-Δ1 ade2::LEU2 ADE2 inserted at 425434, ChrIX*
5263	*MAT**a** mec3-Δ::kanMX6 ura3-52 lys2-801 trp-Δ1 his3-Δ200 leu2-Δ1 ade2::LEU2 ADE2 inserted at 425434, ChrIX*
5264	*MAT**a** rad51-Δ::kanMX6 ura3-52 lys2-801 trp-Δ1 his3-Δ200 leu2-Δ1 ade2::LEU2 ADE2 inserted at 425434, ChrIX*
5273	*MAT**a** upf1-Δ::kanMX6 ura3-52 lys2-801 trp-Δ1 his3-Δ200 leu2-Δ1 ade2::LEU2 ADE2 inserted at 425434, ChrIX*
5271	*MAT**a** mms1-Δ::kanMX6 ura3-52 lys2-801 trp-Δ1 his3-Δ200 leu2-Δ1 ade2::LEU2 ADE2 inserted at 425434, ChrIX*
5272	*MAT**a** mms22-Δ::kanMX6 ura3-52 lys2-801 trp-Δ1 his3-Δ200 leu2-Δ1 ade2::LEU2 ADE2 inserted at 425434, ChrIX*
5269	*MAT**a** yku70-Δ::kanMX6 ura3-52 lys2-801 trp-Δ1 his3-Δ200 leu2-Δ1 ade2::LEU2 ADE2 inserted at 425434, ChrIX*
5270	*MAT**a** yku80-Δ::kanMX6 ura3-52 lys2-801 trp-Δ1 his3-Δ200 leu2-Δ1 ade2::LEU2 ADE2 inserted at 425434, ChrIX*
5346	*MAT**a**/α cdc13-YYAA/CDC13 rif1-Δ::kanMX6/RIF1 ura3-52 lys2-801 trp-Δ1 his3-Δ200 leu2-Δ1 ade2::LEU2 ADE2 inserted at 425434, ChrIX*
5345	*MAT**a**/α cdc13-YYAA/CDC13 tel1-Δ::kanMX6/TEL1 ura3-52 lys2-801 trp-Δ1 his3-Δ200 leu2-Δ1 ade2::LEU2 ADE2 inserted at 425434, ChrIX*
5347	*MAT**a**/α cdc13-YYAA/CDC13 rad50-Δ::kanMX6/RAD50 ura3-52 lys2-801 trp-Δ1 his3-Δ200 leu2-Δ1 ade2::LEU2 ADE2 inserted at 425434, ChrIX*
5289	*MAT**a**/αcdc13-YYAA/CDC13 mrc1-Δ::kanMX6/MRC1 ura3-52 lys2-801 trp-Δ1 his3-Δ200 leu2-Δ1 ade2::LEU2 ADE2 inserted at 425434, ChrIX*
5291	*MAT**a**/α cdc13-YYAA/CDC13 tof1-Δ::kanMX6/TOF1ura3-52 lys2-801 trp-Δ1 his3-Δ200 leu2-Δ1 ade2::LEU2 ADE2 inserted at 425434, ChrIX*
5364	*MAT**a**/α cdc13-YYAA/CDC13 pol32-Δ::kanMX6/POL32 ura3-52 lys2-801 trp-Δ1 his3-Δ200 leu2-Δ1 ade2::LEU2 ADE2 inserted at 425434, ChrIX*
5371	*MAT**a**/α cdc13-F539A/CDC13 bmh1-Δ::kanMX6/BMH1ura3-52 lys2-801 trp-Δ1 his3-Δ200 leu2-Δ1 ade2::LEU2 ADE2 inserted at 425434, ChrIX*
5433	*MAT**a**/α stn1-w466E/STN1 bmh1-Δ::kanMX6/BMH1 ura3-52 lys2-801 trp-Δ1 his3-Δ200 leu2-Δ1 ade2::LEU2 ADE2 inserted at 425434, ChrIX*
additional genotype: **ITT**: TRP + subtelo+tel01L + HIS inserted 3.3Kbp downstream of ARS922	

MATERIALS AND METHODS

Yeast strains

All yeast strains in table 4.3 were derived from the parental YVL 4836, with the exception of YVL4837. Details of this strain's construction are in the previous chapter. Additional gene knockouts are complete deletions of the open reading frames and were made through PCR-generated gene disruption fragments using either kanMX6 or natMX4 cassettes as templates, and using lithium acetate transformation method (Schiestl and Gietz, 1989). Strains were verified by both molecular and genetic methods. PCR amplification of the region encompassing the gene knockout was done on mutant haploids, to verify both size difference between *GENE X* and *gene X*-Δ, and digestion pattern. Known phenotypes of gene knockouts were also verified. All strains used in this study are isogenic to YVL2967, which is derived from S288C and is the parent to all strains currently constructed in the Lundblad lab.

Genetic methods

To obtain our relevant haploids, parental diploids were sporulated in liquid sporulation medium for 3-5 days. For each experimental strain 8-20 tetrads were dissected on full media, and allowed to grow for 3-21 days (depending on growth defect) at 30˚.

RepFC assay

To monitor the frequency of fork collapse at an internal $G_{1\text{-}3}T$ telomeric tract,

relevant strains were grown up overnight at 30˚ in –HIS dropout media (to select for the downstream marker and therefore for cells that have maintained the internal telomeric tract intact). Cells were plated on YPD media at a density of about 100-120 cells per plate to allow for even distribution. Colonies were grown for 3 days at 30˚, and then placed bench top to allow for the accumulation of red pigment in the Ade^{-} colonies. After an additional 5 days, colonies were classified as whole red colony, ½ sector, ¼ sector or slice (less than a ¼).½ sectors are indicative of a replication fork collapse that occurred in the first cell division, sectors smaller than ½ would be indicative of a fork collapse that occurred in subsequent cell divisions. Due to experimental strain construction the Ade^{-} sectors are also His^{-}, and that gives the Ade^{-} sectors a significant growth disadvantage. This growth disadvantage complicates the confident designation of anything smaller than a half sector and so only half sectors are considered in the calculation of frequency of fork collapse in the RepFC assay.The total number of colonies was either a count of every single colony used (as was the case for wild type) or based on the average colony count per plate for half the total plates used. Each frequency is the product of at least two independent experiments for that strain background.

Statistical analysis:

A chi-square analysis with Yate's correction was used to determine two-sided *p*-values for the RepFC assay.

Telomere Length Profiles

Profiles were constructed by cloning and sequencing telomeres (>100 sequences) from 1-8 individual colonies for each genetic backgrounds. The PCR, cloning, and sequencing protocols for telomeres are detailed in the Materials and Methods section of Chapter 3. Sequenced telomeres were aligned by length using the alignment visualization toolkit MacVector.

REFERENCES

Addinall SG, Downey M, Yu M, Zubko M, Dewar J, Leake A, Hallinan J, Shaw O, James K, Wilkinson DJ, Wipat A, Durocher D & Lydall D (2008) Genomewide suppressor and enhancer analysis of cdc13-1 reveals varied cellular processes influencing telomere capping in Saccharomyces cerevisiae. *Genetics* 180, 2251-2266.

Alcasabas AA, Osborn AJ, Bachant J, Hu F, Werler PJ, Bousset K, Furuya K, Diffley JF, Carr AM & Elledge SJ (2001) Mrc1 transduces signals of DNA replication stress to activate Rad53. *Nature Cell Biol.* 3, 958-965.

Anderson EM, Halsey WA & Wuttke DS (2002) Delineation of the high-affinity single-stranded telomeric DNA-binding domain of Saccharomyces cerevisiae Cdc13. *Nucleic Acids Res.* 30, 4305-4313.

Askenova AY, Greenwell P, Dominska M, Shiskin AA, Kim JC, Petes TD & Mirkin SM (2013) Genome rearrangements caused by interstitial telomeric sequences in yeast. *Proc. Natl. Acad. Sci. USA* 110, 1986-19871.

Bando M, Katou U, Komata M, Tanaka H, Itoh T, Sutani T & Shirahige K (2009) Csm3, Tof1, and Mrc1 forms a heterotrimeric mediator complex that associates with DNA replication forks. *J. Biol. Chem* 284, 34355-34365.

Boulton SJ & Jackson SP (1996a) Saccharomyces cerevisiae Ku70 potentiates illegitimate DNA double-strand break repair and serves as a barrier to error-prone DNA repair pathways. *EMBO J* 15, 5093-5103.

Boulton SJ & Jackson SP (1996b) Identification of a Saccharomyces cerevisiae Ku80 homologue: roles in DNA double strand break rejoining and in telomeric maintenance. *Nucleic Acids Res.* 24, 4639-4648.

Boulton SJ & Jackson SP (1998) Components of the Ku-dependent non-homologous end-joining pathway are involved in telomeric length maintenance and telomeric silencing. *EMBO J* 17, 1819-1828.

Burge S, Parkison Gn, Hazel P, Todd AK & Neidle S (2006) Quadruplex DNA: sequence, topology and structure. Nucleic Acids Res. 34, 5402-5415. Downey M, Houlsworth R, Marigele L, Rollie A, Brehme M, Galicia S, Guilliard S, Partington M,

Zubko M, Krogar NJ, Emili A, Greenblatt JF, Harrington L, Lydall D & Durocher D (2006) A genome-wide screen identifies the evolutionary conserved KEOPS complex as a telomere regulator. *Cell* 124, 1155-1168.

Engels K, Giannattasio M, Muzi-Falconi M, Lopes M & Ferrari S (2011) 14-3-3 proteins regulare exonucleases 1-dependent processing of stalled replication forks. PLoS Genetics 7, e1001367. Foss E (2000) Tof1p regulates DNA damage responses during S phase in Saccharomyces cerevisiae. *Genetics* 157, 567-577.

Fouché N, Özgür S, Roy D & Griffith JD (2006) Replication fork regression in repetitive DNAs. *Nucleic Acid Res.* 34, 6044-6050.

Gelinas AD, Paschini M, Reyes FE, Héroux A, Batey RT, Lundblad V & Wuttke DS (2009) Telomere capping proteins are structurally related to RPA with an additional telomere-specific domain. *Proc. Natl. Acad. Sci. USA*. 106, 19298-19303.

Gerik KJ, Li X, Pautx A & Burgers PMJ (1998) Characterization of the two small subunits of Saccharomyces cerevisiae DNA polymerase σ. JCB 31, 19747-19755.

Grandin N, Damon C & Charbonneau M (2001) Ten1 functions in telomere end protection and length regulation in association with Stn1 and Cdc13. *EMBO J.* 20, 1173-1183.

Grandin N, Reed SI & Charbonneau M (1997) Stn1, a new Saccharomyces cerevisiae protein, is implicated in telomere size regulation in association with Cdc13. *Genes & Development* 11, 512-527.

Gravel S, Larrivée M, Labrecque P & Wellinger RJ (1998) Yeast Ky as a regulator of chromosomal DNA end structure. *Science* 280, 741-744.

Fiorentini P, Huang KN, Tishkoff DX, Kolodner RD & Symington LS (1997) Exonuclease I of Saccharomyces cerevisiae functions in mitotic recombination in vivo and in vitro. *Mol. Cell. Biol.* 17, 2764-2773.

Hardy CF, Sussel L & Shore D (1992) A RAP1-interacting protein involved in transcriptional silencing and telomere length regulation. *Genes & Development* 6,801-814.

Katou Y, Kanoh Y, Bando M, Noguchi H, Tanaka H, Ashikari T, Sugimoto K & Shirahige K (2003) S-pahse checkpoint proteins Tof1 and Mrc1 from a stable replication-pausing complex. Nature 424, 1078-1083.

Kironmai MK & Muniyappa K (1997) Alteration of telomeric sequences and senescence caused by mutations in RAD50 of Saccharomyces cerevisiae. *Genes to Cells* 2, 443-455.

Liang F, Romanienko PJ, Weaver DT, Jeggo PA & Jasin M (1996) Chromosomal double-strand break repair in Ku80-deficient cells. *Proc. Natl. Acad. Sci. USA* 93, 8929-8933.

Lee BI & Wilson DM (1999) The RAD2 domain of human exonucleases 1 exhibits 5' to 3' exonucleases and flap structure-specific endonuclease activities. *J. Biol. Chem.* 274, 37763-37769.

Lustig AJ & Petes TD (1986) Identification of yeast mutants with altered telomere structure. *Proc. Natl. Acad. Sci. USA* 83, 1398-1402.

Makovets S, Herskowitz I, Blackburn EH (2004) Anatomy and dynamics of DNA replication fork movement in yeast telomeric regions. *Mol Cell. Biol*. 24, 4019-4031.

Maizels N (2015) G4-associated human disease. *EMBO Rep*. 16, 910-922.

Marcand S, Wotton D, Gilson E & Shore D (1997) Rap1p and telomere length regulation in yeast. *Ciba Found. Symp.* 211, 76-93.

Maringele L & Lydall D (2002) EXO1-dependent single-stranded DNA at telomeres actiates subsets of DNA damage spindle checkpoint in budding yeast yku70-Δ mutants. *Genes & Development* 16, 1919-1933.

Paschini M (2015) A telomere-dedicated RPA complex is essential for the replication of duplex telomeric DNA (Doctoral Dissertation).

Segurado M & Diffley JF (2008) Separate roles for the DNA damage checkpoint protein kinases in stabilizing DNA replication forks. *Gene & Development* 22, 1816-1827.

Sfeir A, Kosiyatrakul ST, Hockemeyer D, MacRae SL, Karlseder J, Schildkraut CL & de Lange T (2009) Mammalian telomeres resemble fragile sites and require TRF1 for efficient replication. *Cell* 138, 90-103.

Tran PT, Erdeniz N, Dudley S & Liskay RM (2002) Characterization of nuclease-dependent functions of Exo1p in Saccharomyces cerevisiae. *DNA Repair* 1, 895-912.

Vaisica JA, Baryshinikova A, Costanzo M, Boone C & Brown G (2010) Mms1 and Mms22 stabilize the replisome during replication stress. *Mol. Biol. Cell.* 22, 2396-2408.

Williamson JR, Raghuraman MK, Cech TR (1989) Monovalent cation-induced structure of telomeric DNA: the G-quartet model. *Cell* 59, 871-880.

Wotton D & Shore D (1997) A novel Rap1p-interacting factor, Rif2p, cooperates wit Rfi1p to regulate telomere length in *Saccharomyces cerevisiae*. *Genes & Development* 11, 748-760.

APPENDIX A:

A single-stranded telomere binding protein employs a dual rheostat for binding affinity and specificity that drives function

Single-stranded DNA, which is involved in numerous aspects of chromosome biology, is managed by a suite of proteins with tailored activities. The majority of these ssDNA- interaction proteins bind ssDNA indiscriminately, exhibiting little apparent sequence preferences. However, there are several notable exceptions, including the *S. cerevisiae* Cdc13 protein, which is vital for yeast telomere maintenance. Cdc13 is one of the tightest known binders of ssDNA and is specific for G-rich telomeric sequences. To investigate how these two different biochemical features, affinity and specificity, contribute to function, we created an unbiased panel of alanine mutations across the Cdc13 DNA-binding interface, including several aromatic amino acids that play critical roles binding activity. A subset of mutant proteins exhibited significant loss in affinity *in vitro* that, as expected, conferred a profound loss of viability *in vivo*. Unexpectedly, a second category of mutant proteins displayed an increase in specificity, manifest as an inability to accommodate changes in ssDNA sequence. Yeast strains with specificity- enhanced mutations displayed a gradient of viability *in vivo* that paralleled the loss in sequence tolerance *in vitro*, arguing that binding specificity can be fine-tuned to ensure optimal function. We propose that DNA binding by Cdc13 employs a highly cooperative interface whereby sequence diversity is accommodated through plastic binding modes. This suggests that sequence specificity is not a binary choice but rather a continuum. Even in proteins that are thought to be "specific" nucleic acid binders, sequence tolerance through the utilization of multiple binding modes may be a broader phenomenon than previously appreciated.

Proteins that bind nucleic acids are frequently categorized as being either specific or non-specific, with interfaces to match that activity. In this study, we have found that a telomere-binding protein exhibits a degree of specificity that is finely tuned for its function, which includes specificity for G-rich sequence with some tolerance for substitution. Mutations of the protein that dramatically impact its affinity for single-stranded telomeric DNA are lethal, as expected; however, mutations that alter specificity also impact biological function. Unexpectedly, we found mutations that make the protein more specific are also deleterious, suggesting that specificity and non-specificity may be achieved through more nuanced mechanisms than currently recognized.

INTRODUCTION

The proper management of ssDNA in the cell is required for numerous aspects of chromosome biology. In all kingdoms of life, ssDNA is formed transiently during the execution of many essential cellular processes including transcription, DNA replication, recombination, and repair. To coordinate these numerous activities, a diverse array of proteins have evolved to bind ssDNA, to facilitate normal events such as DNA replication or to signal the appearance of inappropriate ssDNA and initiate repair (Dickey et al. 2013a).

Several of these ssDNA-binding proteins function in genome-wide maintenance (Dickey et al. 2013a; Fanning et al. 2006). Widely studied examples include the bacterial single-strand binding protein (SSB) and its functional equivalent

in eukaryotes, replication protein A (RPA) (Lohman & Ferrari 1994; Wold 1997; Iftode et al. 1999; Bochkarev & Bochkareva 2004). SSB and RPA are both essential for DNA replication by binding nascent ssDNA that is generated when duplex DNA is unwound, thereby preventing re-annealing and/or formation of secondary structures that would impede progression of the replisome. Both proteins are also central to the cellular response to DNA lesions. Although RPA and SSB exhibit no sequence homology, they each employ an array of OB-folds for contacting ssDNA. Detailed analysis of RPA has revealed that it utilizes these OB- folds to contact ssDNA in distinct modes, engaging differing lengths of ssDNA with different subunits, presumably to orchestrate higher order manipulations (Fanning et al. 2006; Chen et al. 2016). Thus, to interact consistently throughout the genome, RPA also needs to bind ssDNA indiscriminately. Commensurate with this expectation, RPA displays little obvious sequence preference *in vitro*, binding ssDNA tenaciously with single-digit nanomolar affinities (Dickey et al. 2013a; Wold 1997).

In contrast to the genome-wide, and the apparently sequence non-specific role performed by the canonical RPA complex, proteins that interact with ssDNA overhangs at telomeres exhibit sequence specificity tuned to the G-rich telomeric repeats (Lei et al. 2004; Eldridge et al. 2006; Croy & Wuttke 2006). These telomere-dedicated proteins also show exceptional affinities for their ssDNA ligands, ranging from the tight nanomolar binding by human Pot1 to single-digit picomolar binding by the *S. cerevisiae* Cdc13 protein (Lei et al. 2004; Croy & Wuttke 2006; Lewis et al. 2014). Remarkably, the Cdc13 protein performs its telomere-dedicated role as a

subunit of a heterotrimeric complex with a domain architecture that closely parallels that of RPA (Gao et al. 2007). In both complexes, the large subunit is constitutively associated with two smaller proteins, Stn1/Ten1with Cdc13 and Rpa32/Rpa14 with RPA70, and for both complexes, high affinity for ssDNA is conferred by the large subunit (Wold 1997; Gao et al. 2007; Grandin et al. 1997; Grandin et al. 2001; Anderson et al. 2002; Gelinas et al. 2009; Sun et al. 2009). However, ssDNA binding by the telomere dedicated RPA complex (t-RPA) is notably distinct from RPA, suggesting that these structurally similar domains have taken on distinct biochemical roles. Unlike RPA70, which uses 2 OB fold domains for its core recognition of ssDNA, Cdc13 employs a single OB-fold, augmented by an unusually long β2-3 loop (Figure A.1; Mitton-Fry et al. 2002), to contact DNA with exceptionally tight picomolar affinity. Furthermore, Cdc13 binds ssDNA with distinct specificity for G-rich sequence (Lewis et al. 2014; Anderson et al. 2002), which it achieves through recognition of a GxGT motif embedded in a larger oligonucleotide. Nevertheless, although Cdc13 shows clear specificity for G-rich sequences, it also needs to show sequence flexibility to accommodate the heterogeneity of yeast telomeres (Förstemann & Lingner 2001). The sequence specificity and affinity displayed by Cdc13 provides a unique system for investigating how these two biochemical properties contribute to function *in vivo*. To do so, this study examined an extensive panel of mutations across the DNA-binding interface for their effects on both binding affinity and specificity and subsequently determined how perturbations in either property affected Cdc13 function *in vivo*. Not surprisingly, substantial reductions in Cdc13 binding affinity were lethal

in vivo, whereas less severe declines in affinity were better tolerated. Unexpectedly, this approach also identified a category of mutations that had little effect on affinity but dramatic effects on specificity *in vitro*. These specificity mutations reduced the ability of Cdc13 to tolerate variations in telomere sequence and substantially impaired Cdc13 function *in vivo*. Moreover, the magnitude of the viability defect closely correlated with the extent to which specificity was altered. Thus, by conducting a systematic analysis of the Cdc13 DBD interface, we have uncovered a finely tuned rheostat of specificity and affinity that confers optimal biological function *in vivo*.

RESULTS

Systematic mutagenesis of the DNA-binding interface of Cdc13 identifies a 35-fold span in affinity.

To address how the biochemical features of Cdc13 allow it to perform its biological roles, we introduced a set of 8 alanine mutations into the DNA-binding domain (DBD) across the binding interface (Mitton-Fry et al. 2002; Anderson et al. 2003), with an emphasis on the aromatic residues that play key roles in affinity and specificity, and measured the impact of these changes on binding characteristics (Figure A.1 A). The change in binding affinity to the minimal Tel11 substrate (GTGTGGGTGTG) exhibited by these mutant proteins was measured at the physiological salt conditions identified previously using an EMSA binding assay (Figure AS.1)(Lewis et al. 2014). The DBD constructs exhibited a range of binding affinities, from slightly tighter than the very tight wild type value of 2 pM to 70 pM

(Figure A.1 B, Table AS.1). Thus, the impact on binding affinity to the Tel11 substrate exhibited by these mutant proteins spanned almost 35-fold, creating a set of proteins exhibiting a wide range, or rheostat, of binding affinities.

Large defects in binding affinity correlate with large impacts on *in vivo* viability.

This range of binding affinities allowed us to ask whether the unusually tight affinity exhibited by Cdc13 was required, and indeed what level of DNA binding was necessary, for function *in vivo*. To do so, the mutations described above were examined for their effects *in vivo* by integrating each mutation into the genome of a diploid strain of yeast in place of one copy of the wild type *CDC13* gene. This panel of diploid strains was used to generate *cdc13*-DBD$^-$ haploid strains, which revealed a gradient of viability (Figure A.2). Changes in viability were not explained by changes in protein levels (Figure AS.2).

Not unexpectedly, the *cdc13*-Y522A and *cdc13*-K622A mutant strains were capable of only 2 to 5 cell divisions (Figure A.2 A), consistent with the large reduction in binding affinity for the minimal Tel11 substrate associated with these two mutations (Figure A.1 B). For both strains, this severe growth defect was partially suppressed by *exo1*-Δ and *rad9*-Δ mutations (Figure A.2 A); this recapitulates the behavior of previously characterized *cdc13*$^-$ mutations (Weinert et al. 1994; Zubko et al. 2004; Paschini et al. 2012), arguing that defects in Cdc13 DNA binding behaved in a manner comparable to other loss-of-function mutations in *CDC13*. Notably, the growth of the *cdc13*-K622A mutant strain (with a 15-fold reduction in binding affinity) was reproducibly less impaired than the *cdc13*-Y522A strain (with a 34-fold reduction in

in vitro binding), providing a striking correlation between the *in vitro* biochemical properties of these two mutations (with 15- and 34-fold reductions in binding affinities, respectively) and their *in vivo* phenotypes.

Moderate defects in binding affinity only partially correlate with *in vivo* viability.

Surprisingly, the correlation between *in vitro* and *in vivo* behavior did not extend to other mutations introduced into the DBD interface of Cdc13. For example, two mutations, *cdc13*- F539A and *cdc13*-Y626A, with only modest declines in affinity for the Tel11 substrate, nevertheless exhibited pronounced growth defects. Both of these haploid mutant strains gave rise to barely visible colonies (Figure A.2 A and data not shown), which was also accompanied by a high percentage of inviable individual cells for both strains (data not shown), resulting in a long delay in forming visible colonies. Thus, despite only a 3.5-fold effect on *in vitro* binding affinity for each of these two mutations, the *cdc13*-F539A and *cdc13*-Y626A mutant strains exhibited a severe degree of *in vivo* telomere dysfunction.

Mutations that increase Cdc13 binding affinity show growth defects in strains sensitized to telomere dysfunction.

Equally striking was the behavior of strains expressing mutant proteins that slightly increased the affinity for the Tel11 substrate, relative to the affinity of the wild type protein for Tel11 (Figure A.1 B and Table AS.1). In an otherwise wild type yeast background, strains bearing mutations in Y556, I578 or Y561 exhibited a growth phenotype that was indistinguishable from that of a wild type strain (Figure A.2 A and data not shown). However, when *cdc13*-Y561A or *cdc13*-I578A mutations were

introduced into a strain background that is impaired for an additional aspect of telomere homeostasis (a telomerase deficiency), these mutant proteins were incapable of conferring the same level of function as the wild type Cdc13 protein. Immediately following loss of telomerase, the growth of a telomerase-defective strain is initially indistinguishable from a telomerase-proficient strain, although a decline in viability eventually becomes evident with continued propagation (Lendvay et al. 1996). In contrast, a newly generated telomerase-defective strain that also bore either a *cdc13*-Y561A or *cdc13*-I578A mutation exhibited an immediate decline in viability (Figure A.2 B and data not shown). Similarly, these same mutations also exhibited a pronounced synthetic growth defect when combined with a mutation in the Ku heterodimer as the *cdc13*-Y556A *yuk80*-Δ, *cdc13*-I578A *yuk80*-Δ, and *cdc13*-Y561A *yuk80*-Δ double mutant strains were close to inviable (Figure AS.3 A). The synthetic lethalities due to these mutations in the DBD interface were not readily explained by their small increase in affinity for the Tel11 substrate.

Binding specificity is profoundly altered by mutations in the DNA-binding interface.

The above results strongly suggested that affinity was not the only important biochemical feature that was required for Cdc13 function *in vivo*. We therefore asked whether an additional biochemical property, binding specificity for telomeric substrates, was altered by these mutations. We have previously assessed Cdc13 specificity by measuring binding affinities for oligonucleotides with substitutions for the "pool" of the 3 other bases at specific positions within the minimal Tel11

oligonucleotide (Eldridge et al. 2006). This approach revealed a "specificity profile" defined by the relative loss of affinity when the identity of a base in the ligand is altered. The larger the loss in affinity for the pool relative to the cognate ligand, the more specifically the cognate base is recognized. This strategy revealed that bases at positions G1, G3 and T4 within the Tel11 ("GTGTGGGTGTG) substrate are the most specifically recognized by both the Cdc13-DBD and the full length Cdc13 protein (Eldrige et al. 2006). Substitutions at these three positions in the Tel11 sequence led to a significant loss of affinity (up to 87-fold) by the wild-type protein, whereas the change in affinity at G9 upon substitution, a site which is less specifically recognized, was more modest (Table A.1, Figure AS.1).

To determine how specificity is impacted by mutations across the DBD interface, binding to these pools of oligonucleotides was performed with all mutant proteins (Figure A.3 A, Table A.1, Table AS.1). A wide range of effects was observed when the pool of bases was substituted at positions in the Tel 11 oligo, with the reductions in affinity ranging from 4.5-fold to nearly 3,000- fold reductions in affinity.

A standard double-mutant thermodynamic cycle can be used to assess the effects of independently mutating the protein or the nucleic acid substrate, and then combining these two different alterations, to the protein/nucleic acid interface (Carter et al. 1984; Wells 1990; Schreiber & Fersht 1995; Johansson et al. 1998). If these are independent changes, the effects on binding free energy of implementing them simultaneously will simply be additive, with the net observed K_DS being the product of the K_DS for the individual changes. However, if the combination has a non-additive

effect on affinity, it suggests the two alterations are thermodynamically coupled in some way. A net effect that is *less* than simply additive could be due to the fact that the sites are physically proximal, such that the loss represents both sides of a direct amino acid/base contact, and removing either side of the interaction is sufficient to abrogate it. For this reason, strong couplings are most commonly observed for physically proximal residues (Carter et al. 1984; Wells 1990; Schreiber & Fersht 1995). Moreover, it could also suggest that a mechanism of accommodation is in place, whereby the loss of a favorable interaction is compensated for by the gain of a new favorable interaction, as seen previously in our ssDNA/protein complexes (Dickey et al. 2013b; Lloyd et al. 2016). Conversely, a net effect that is *greater* than the sum of the free energy changes of the individual alterations could suggest a loss of cooperativity or a structural change at the interface. This classic analysis allows us to identify those amino acids that perform unexpected roles in determining binding specificity.

Simple thermodynamic additivity explained the binding affinities observed for several double mutant pairs. For example, the weakest binding mutant of Cdc13 DBD, Y522A, which has been previously designated as a hotspot for binding affinity, showed the most substantial decline in binding to the wild type Tel11 ligand (34-fold, to 71 pM). Similarly, substitutions at the most specifically recognized site on the oligonucleotide, T4, resulted in an 87-fold decline in affinity, to 183 pM, for the wild type protein. If these effects were simply additive, the reduction in affinity would be predicted to be 2958-fold, when assessing binding of the mutant protein (Y522A) to

the modified ligand, which is quite similar to the observed value of 2840-fold (Table AS.1). The fact that these sites behave independently is consistent with their ~15 Å separation in the structure (31). Y522, however, is physically proximal to G1. Here, the impact on binding in the doubly substituted Y522A/H1 complex was less than additive, with the observed net affinity down 200-fold relative to wild type where the additive effect would be ~500 fold. This deviation from a simply additive result supports the prediction from the structure that Y522 specifically recognizes G1.

To visually identify protein/nucleic acid pairs whose combined alterations deviate from thermodynamic additivity, we divided the affinities for the binding of the doubly substituted pairs by the binding affinity of each mutant protein for Tel11 (Figure A.3 B, Table AS.1). Thermodynamic additivity would predict that, with this normalization, the mutant proteins would show the same specificity profiles as observed for wild type Cdc13. This scaled specificity profile indeed revealed that, for mutants where the effects were close to additive, such as Y522A, the specificity profile mirrored that of wild type. Exceptions included sites of direct contact where the impact on binding was smaller than expected, as discussed above for the Y522A/H1 pair.

Several mutant Cdc13 proteins unexpectedly exhibited a deviation from additivity where the pairs led to a greater loss of affinity than predicted by additivity. This was particularly evident for Y626A and F539A, and to a lesser extent for Y561A (Figure A.3 B, Table AS.1). A case in point was the interaction of F539A with H1, where the combined reduction in affinity (600 fold) was about 40-fold greater than the

product of the F539 vs. Tel 11 (3.5 fold) and WT vs. H1 (15 fold) differences between WT binding with Tel 11. This was also the case for the interaction between F539A and position H3 in the DNA, where F539A exhibited a 1260 fold loss in binding affinity at this site even though F539A exhibited only 3.5-fold reduction in Tel11 binding. Again, the net impact of the combination of amino acid change and oligonucleotide substitution was highly non-additive. This binding profile for the F539A mutation argues that the Cdc13-F539A protein was *more* specific for the Tel11 sequence, as substitution of the oligonucleotide base led to greater losses in binding than observed for the wild type protein. A key observation is that this enhanced specificity was not due to tighter binding of the mutant proteins to Tel11, rather it arose from a decreased tolerance for the substitutions in the oligonucleotide. Notably, these effects were not simply manifest at the base closest to the site of alanine mutation in the structure (Figure A.1 A), suggesting that long-range effects across the DBD interface dictate binding specificity. F539A illustrates this nicely; although this substitution had a large, non-additive impact on H1 and H3 binding, it is poised between T4 and G5 in the structure of the complex (Mitton-Fry et al. 2004).

Binding specificity in conjunction with affinity more accurately predicts *in vivo* phenotypes.

We noted above that *in vivo* phenotypes roughly correlated with severe losses of binding affinity, but that more moderate changes in binding affinity did not fully explain the phenotypes. The reduced tolerance by F539A and Y626A for deviations from the Tel11 sequence (i.e., increased specificity) provides a biological explanation

for their *in vivo* phenotypes, which were significantly functionally impaired, particularly when contrasted with the similarly affinity impaired Y565A. The severe growth defects associated with the *cdc13*-F539A and *cdc13*-Y626A strains, as well as the more subtle growth defects in the *cdc13*-Y565A, *cdc13*-Y561A or *cdc13*-Y556A yeast strains (with mutations that conferred increased affinity but reduced specificity) demonstrates that binding specificity contributes as much as affinity to Cdc13 function.

DISCUSSION

In this study, we have performed a systematic analysis of the ssDNA-binding surface of Cdc13 by generating a panel of alanine mutations that span the interface, and then probing the impact of these mutations on binding affinity and specificity. This detailed biochemical analysis was combined with an *in vivo* phenotypic read-out that was sensitive enough to detect even minor differences in function, revealing a gradient, or rheostat, of functionality. Strains expressing mutant proteins with a dramatically reduced binding affinity were inviable, demonstrating that DNA binding is an essential function of the yeast t-RPA complex which contains the Cdc13 protein. Surprisingly, this systematic analysis identified a category of mutations that did not confer dramatic changes in ssDNA binding affinity but altered the ssDNA binding specificity of the Cdc13 binding interface, such that the surface was less tolerant to mutations. Unexpectedly, this increase in specificity had a substantial impact on function *in vivo*.

The dramatic *loss* of sequence tolerance, combined with a minimal loss of affinity, upon mutation of the surface of the protein observed here was not anticipated. More typically, the removal of a contacting amino acid might be expected to reduce specificity, that is, increase sequence tolerance, by removing the H-bond donors and acceptors and steric interactions that enforce specific recognition. This is particularly surprising given the extended conformation of the oligonucleotide and the localized nature of the amino acid contacts per base (Figure A.1 A). The long range effects observed, where removal of an amino acid impacts specificity in the recognition of a base 10 Å away, suggest a highly cooperative interface. Furthermore, removal of the aromatics from the interface does not generally make binding more promiscuous, suggesting that these side chains are not driving local specificity and are instead accommodating sequence diversity.

Analysis of the biochemical data in the context of the Cdc13 DBD/Tel11 structure points to three distinct functional parts of the interface (Mitton-Fry et al. 2004). The first region is the segment of the OB-fold barrel that interacts with the 5' end (colored burgundy in Figure A.1 A), identified in previous mutagenesis studies as driving both affinity and specificity of interaction. This region includes Y522 and K622, the residues whose substitution has the most dramatic impact on affinity without significant changes in specificity. The second is the long β2-3 loop (highlighted in blue in Figure A.1 A), encompassing mutations spanning residues Y556A to K568A that interacts with the 3' end of the ligand. Mutations in this loop have more moderate impacts on affinity and specificity, consistent with a "Velcro-like

function," that is, a sticky surface suited to binding any sequence. The final structural region bridges these two, spanning the middle part of the barrel (colored yellow in Figure A.1 A). Here substitution of two key aromatic residues, F539A and Y626A, results in a modest loss in affinity but a significant increase in specificity, characterized by the dramatic loss of tolerance of substitutions at the rather distant sites of G1 and G3. Thus, this middle region appears to control the plasticity of the recognition such that Cdc13's ability to accommodate sequence alterations is impaired upon loss of these aromatic residues. The behavior is reminiscent of another sequence-tolerant telomere end binding protein, Pot1pC of *S. pombe*, where sequence tolerance is implemented through new binding modes that thermodynamically compensate for base-substitutions through alternate stacking interactions and new H-bonding networks (Dickey et al. 2013b). Our data suggest that loss of key aromatic residues in this middle region impairs the ability of the protein to tolerate alternative sequences, perhaps due to their ability to stack on the exposed bases of ssDNA and affect plasticity (Wilson et al. 2014).

In vivo, the phenotypes displayed by strains bearing mutations in the DBD interface showed numerous similarities to previously described mutations in CDC13 that confer viability defects, arguing that this set of *cdc13*-DBD^{-} mutations are impacting the primary Cdc13 function. Severely impaired *cdc13*-DBD^{-} strains displayed a DNA damage response and impaired cell cycle progression (Figure AS.2 and data not shown) comparable to that of previously characterized *cdc13*-defective strains (Lydall & Weinert 1995). This panel of *cdc13*-DBD^{-} mutant strains also

exhibited a profile of genetic interactions (in response to *rad9*-Δ, *rad24*-Δ and *exo1*-Δ mutations; Figure 2 and data not shown) that recapitulated the behavior of *cdc13*-ts strains (Paschini et al. 2012; Lydall & Weinert 1995). However, there was one notable difference. In *cdc13*-ts strains grown at non-permissive temperatures, there is a marked increase in the extent of exposed telomeric G-strand ssDNA (Garvik et al. 1995, Booth et al. 2001). This observation, combined with the enhanced DNA damage response observed in *cdc13*-impaired strains, led to the premise that telomeric ssDNA creates a specific signal that elicits a cell cycle checkpoint (Lydall & Weinert 1995; Garvik et al. 1995). In contrast, none of the *cdc13*-DBD mutant strains – even those that were severely impaired – exhibited any detectable increase in the extent of G-strand ssDNA at chromosome ends (Figure AS.3 B). This suggests that the primary DNA lesion eliciting a checkpoint response in *cdc13*-impaired cells may not in fact be ssDNA, but some other intermediate that arises during DNA replication stress.

The behavior of yeast strains expressing three mutations highlight the *in vivo* importance of rigorously tuning specificity. F539A, Y565A and Y626A all exhibit similar reductions in affinity (2.2 to 3.5 fold, Table A.1) but vary dramatically with regard to specificity (Figure A.3 B). Y565A is modestly more specific than wild type, while F539A and Y626A are significantly more specific. This *in vitro* gradient of specificity generates a comparable *in vivo* gradient, as a strain expressing the mutant *cdc13*-Y565A protein is slightly less functional than wild type, whereas *cdc13*-F539A and *cdc13*-Y626A are severely impaired. This surprising result shows that a gain in specificity can actually be deleterious to function *in vivo*. It also underscores that DNA

binding specificity is not a binary ("specific" or "non-specific") trait, but rather there is a continuum of specificity that is critical to the biological functioning of many DNA-binding protein. Specifically, our results indicate that that ssDNA recognition by Cdc13 relies on a finely tuned balance of both affinity and specificity, to ensure that the t-RPA complex can readily localize to a limited region of the genome and still accommodate the sequence heterogeneity present at yeast telomeres.

The observation that mutations in the DNA-binding interface of Cdc13 render the protein more specific, and less functional, was unexpected. As a systematic evaluation of the binding specificity of mutant proteins is not commonly undertaken, this disruption of multiple biochemical behaviors may be a broader phenomenon than previously appreciated. A case in point is the CST complex, a heterotrimer with a domain organization very similar to that of t-RPA (Casteel et al. 2009; Miyake et al. 2009; Surovtseva et al. 2009). Unlike t-RPA, the human CST complex is not a strictly telomere-dedicated protein; although it displays a preference for G-rich sequences the arrangement of guanosine nucleotides needed for high affinity binding does not correspond to the repeat characteristic of telomeres (Wan et al. 2015; Hom & Wuttke 2017; Chastain et al. 2016; Bhattacharjee et al. 2017). This allows the complex to function as a replication accessory factor genome wide as well as facilitating proper maintenance of G-rich sequence at telomeres (Wan et al. 2015; Hom & Wuttke 2017). We suggest that the results reported here for Cdc13 may extrapolate to other modestly specific ssDNA binding complexes such as CST. Moreover, perhaps ssDNA-binding proteins, such as RPA and SSB, which are thought to be largely non-specific, achieve

non-specific binding through more sophisticated mechanisms than previously appreciated. As the alteration in the specificity of Cdc13 was only discovered through the comprehensive mutagenesis of the protein surface that contacts DNA, it suggests that the systematic mutation and characterization of an entire interaction surface is essential to understanding the full complexity underlying binding.

FIGURES

Table A.1 Apparent binding constants (K_DS) for wild type and mutant Cdc13 DBD proteins to Tel11 variants

	Tel 11 (pM)	± (pM)		H1 (pM)	± (pM)		H3 (pM)	±(pM)		V4 (pM)	± (pM)		H9 (pM)	±(pM)
WT	2.10	0.20		31.6	4.7		85	21		183	43		9.40	0.90
Y556A	0.64	0.14		302	26		311	51		569	180		43.0	4.0
I578A	1.00	0.25		420	18		135	20		278	70		20.0	2.5
Y561A	1.64	0.22		154	26		434	83		381	29		16.0	2.0
Y565A	4.70	0.80		330	55		259	22		368	67		34.0	5.0
Y626A	7.20	0.90		1230	57		2500	610		290	75		181	11
F539A	7.40	0.22		1260	140		2640	450		1300	150		180	10
K622A	31.7	3.5		2390	430		1210	170		4550	1300		208	65
Y522A	71.0	16.0		426	46		769	200		5970	1200		1230	280

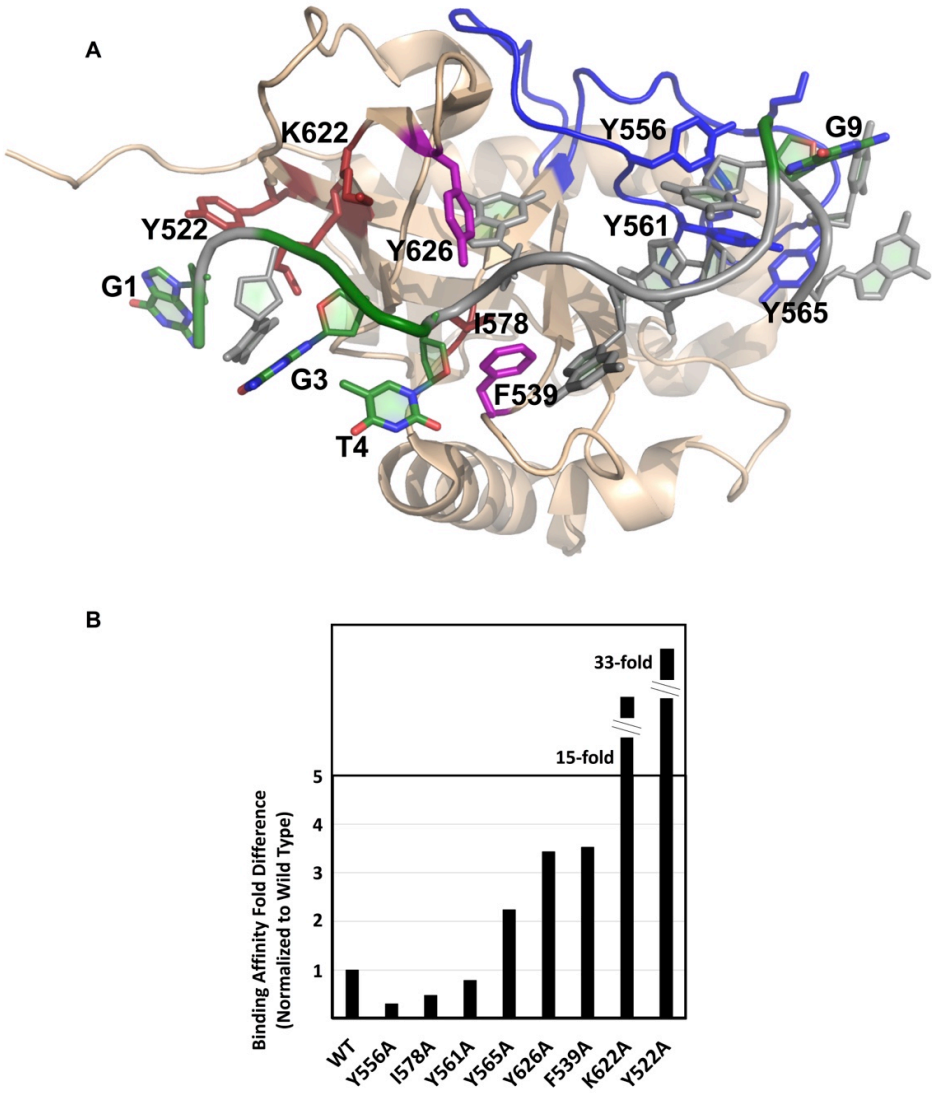

Figure A.1: Mutations across the surface of the Cdc13-DBD exhibit a range of loss of affinity (A) Structure of the Cdc13 DBD/Tel11 complex with sites of interest highlighted. Backbone of the protein in wheat, with amino acids highlighted in red, purple and blue that has been individually substituted with alanine. The β2-3 loop is shown in blue. Tel11 is in gray and green, with green highlighting sites modified for the investigation of specificity. (B) Binding affinities of the wild type and mutant Cdc13 DBD for the Tel11 substrate, with fold loss of binding affinity represented by bar graphs.

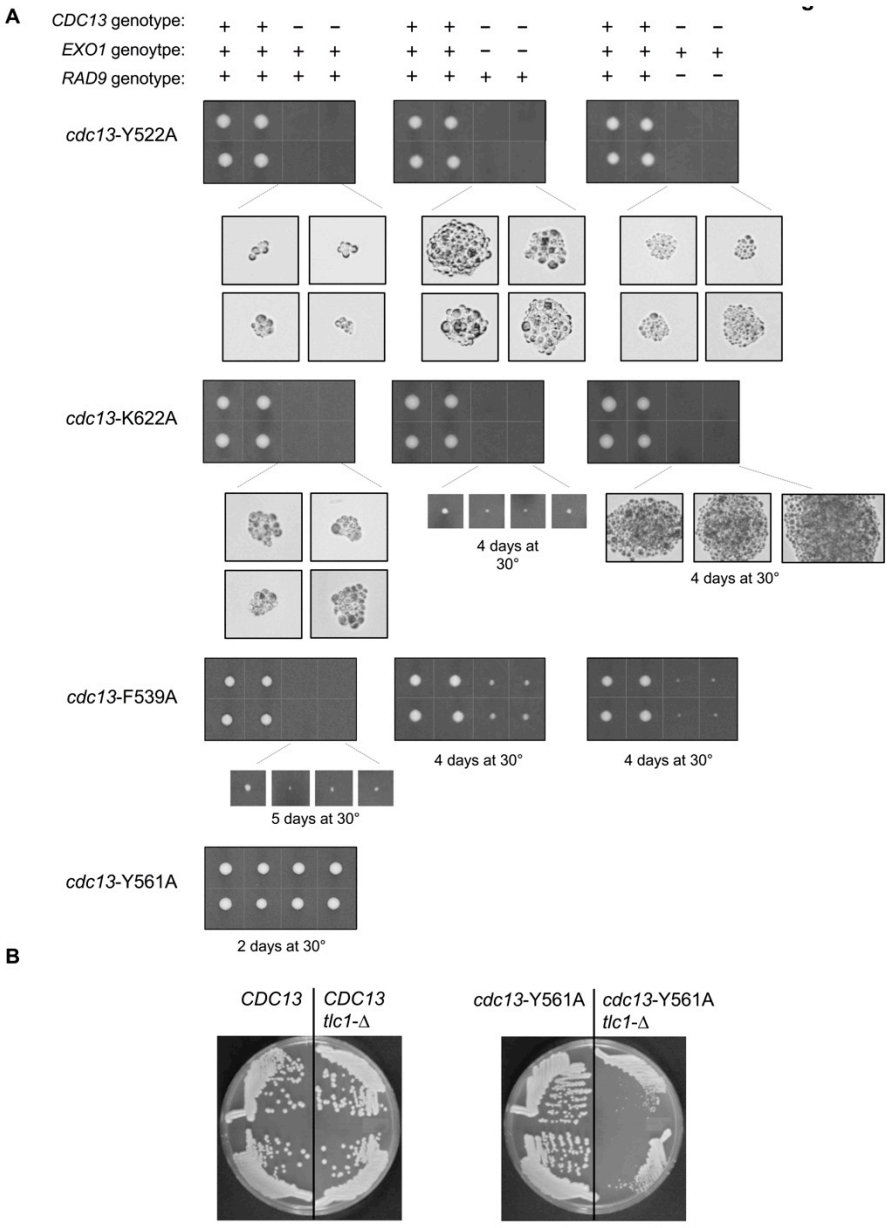

Figure A.2: Mutations in the Cdc13 DBD interface exhibit a gradient of viability *in vivo*. (A) Viability of yeast strains bearing the indicated *cdc13*-DBD⁻ mutations was assessed by monitoring the ability to form visible colonies (or microcolonies), following sporulation and tetrad dissection of *cdc13*-DBD⁻/*CDC13* diploid strains, with or without *exo1*-Δ/*EXO1* or *rad9*-Δ/*RAD9*, to generate haploid strains with the specified genotypes The resulting haploid strains were grown at 30° for 48 hours, unless otherwise indicated. Photographs were taken with a Zeiss Axioskop 50 with a Nikon Digital Sight DS-5M camera, as described previously (Paschini et al. 2012). Multiple isolates were examined for each genotype, and representative examples are shown. (B) Two isolates each of haploid strains with the indicated genotypes were streaked onto rich media and photographed after growth for 48 hrs at 30°C, in order to assess the extent of visible colony formation. Strains that were telomerase-proficient (*TLC1*) or telomerase-deficient (*tlc1*-Δ, with a deletion of the telomerase RNA gene (Singer & Gottschling 1994)) were generated by sporulation and tetrad dissection of isogenic *CDC13*/*CDC13 tlc1*-Δ/*TLC1* and *cdc13*-Y561A/*CDC13 tlc1*-Δ/*TLC1* diploid strains.

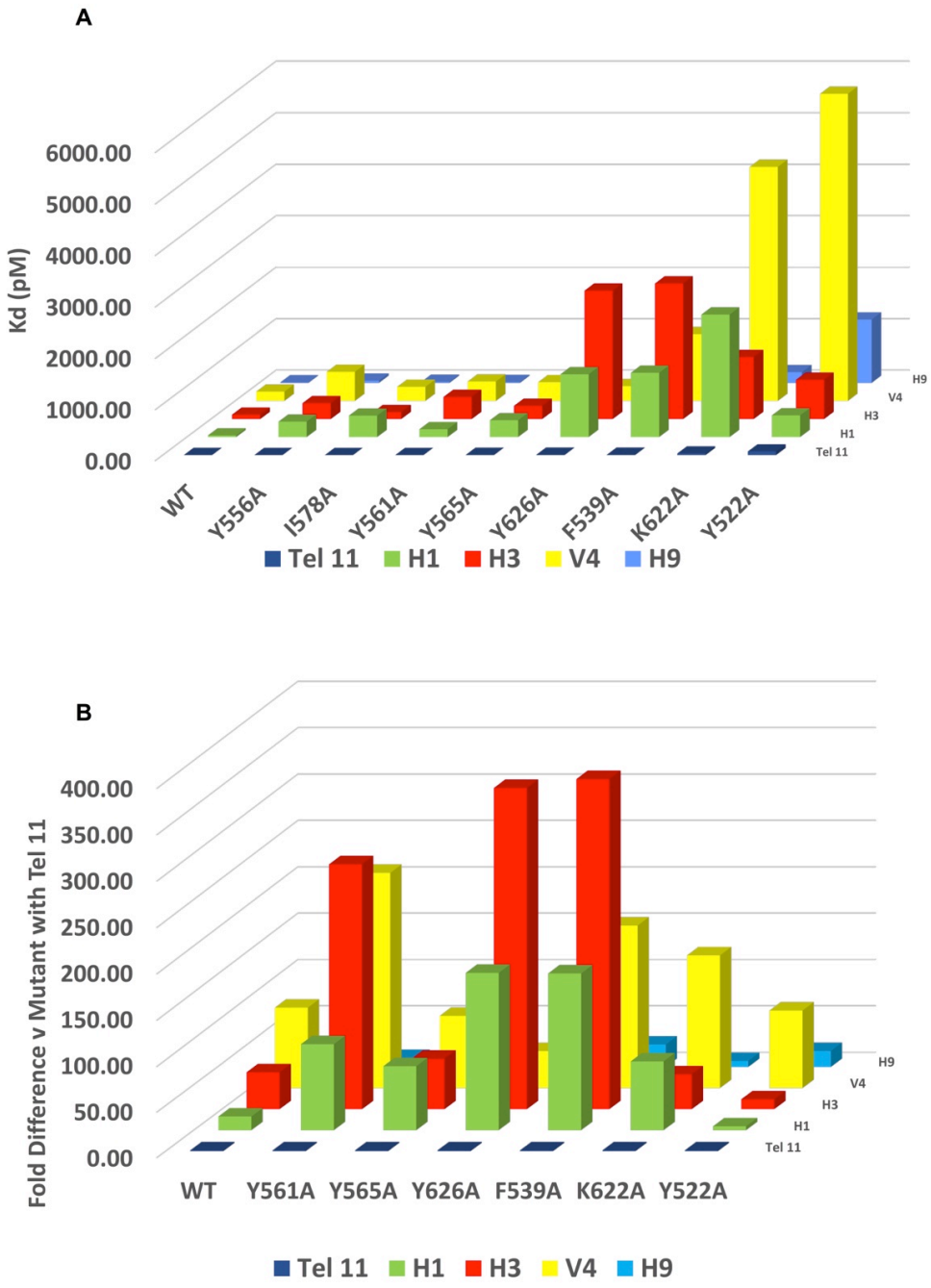

Figure A.3: Creation of a rheostat of binding affinities in Cdc13. (A) Skyscraper plot of K_D for each alanine mutant of Cdc13 DBD mutant protein with various substituted oligonucleotides. H refers to an equimolar pool of A, C and T; V an equimolar pool of G, C and A. (B) Specificity data for select mutant proteins scaled to the loss of affinity observed for that mutant to Tel11. Data used to construct this plot are in Table AS.1.

SUPPLEMENTAL FIGURES

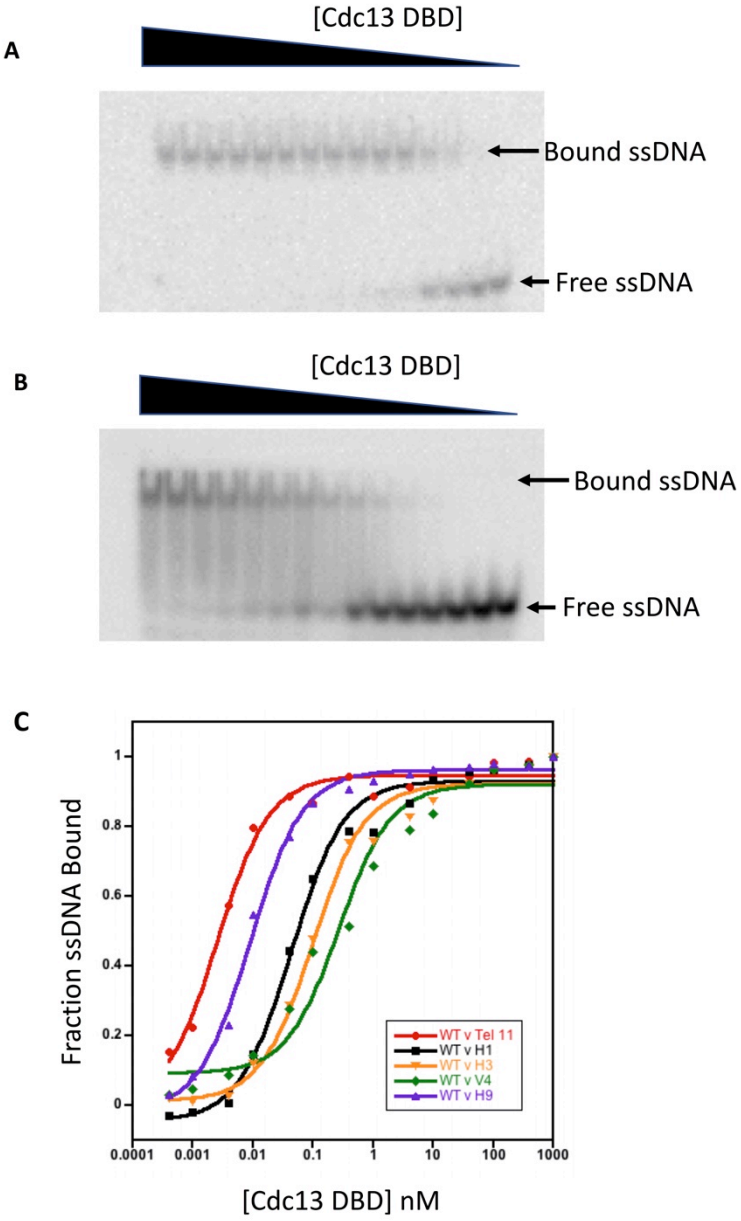

Figure AS1: Representative binding data for Cdc3-DBD/ssDNA interactions. (A) Representative Electrophoretic Mobility Shift Assay (EMSA) gel of WT Cdc13 DBD binding to radiolabled Tel 11. Protein concentrations for the binding experiment span a wide concentration range from 0.0004 nM to 1000 nM as indicated qualitatively by the triangle above the gels. Experiment performed as described in the methods section. (B) Representative EMSA gel of WT Cdc13 DBD binding H3. Protein concentrations for the binding experiment span a wide concentration range from 0.0004 nM to 1000 nM as indicated qualitatively by the triangle above the gels. (C) Representative K_D plot showing fraction bound as a function of concentration of Cdc13 DBD for wild type protein vs. the Tel 11, H1, H3, V4 and H9 oligonucleotides. Data fit to a standard Langmuir isotherm as described in the methods section.

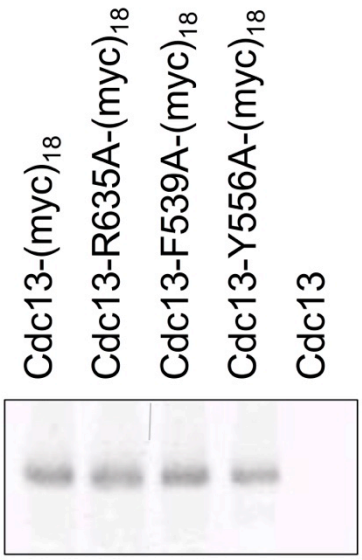

Figure AS.2: **Mutations in DNA binding interface do not affect Cdc13 protein stability.** Anti-myc western of extracts from yeast strains expressing the Cdc13-$(myc)_{18}$ protein or the indicated mutations, resolved by 8% SDS-PAGE, demonstrates that mutations in the DNA binding interface do not alter Cdc13 protein stability *in vivo*.

Figure AS.3: Additional analysis of the *in vivo* effects of mutations in the Cdc13 DBD interface. (A) The *cdc13*-Y561A, *cdc13*-Y556A and *cdc13*-I578A mutations confer synthetic lethality when combined with a *yku80*-Δ mutation, which affects multiple aspects of telomere homeostasis (Gravel et al. 1998), as revealed by plating five-fold serial dilutions of *cdc13*-Δ *yku80*-Δ strains containing a CEN plasmid expressing the indicated *cdc13*-DBD$^-$ mutations (left-hand panel). The right hand panel shows the viability of the same strains, in the presence of an additional CEN plasmid expressing a wild type copy of *YKU80*. The left panel was plated on media that selects for the presence of both plasmids, whereas the right panel was plated on media that selects for those cells that have lost the plasmid expressing *YKU80* but retain the plasmid expressing the indicated *cdc13*-DBD$^-$ mutation. (B) Assessment of the extent of G-strand ssDNA at chromosome ends in a panel of *cdc13*-DBD$^-$ mutant strains. Telomeric G-strand ssDNA was detected by hybridization of XhoI-digested genomic DNA with an oligomeric probe specific for the G-rich strand, using native gel electrophoresis (top), followed by in-gel denaturation and re-hybridization with the same oligomeric probe (bottom), as described previously (Bertuch & Lundblad 2003). Indicated below the native gel is the ratio of native to denatured telomeric restriction fragment signals, normalized to wild type for each genotype; the *yku80*-Δ strain exhibits a substantial increase in the extent of single stranded G-strand DNA, consistent with prior observations (Gravel et al. 1998). This analysis was performed with asynchronous cultures (not shown) as well as with cultures arrested with nocodazole (shown here); the latter condition, in which cells are arrested during a period in the cell cycle when the terminal G-stand overhang is transiently longer (Dionne & Wellinger 1996), rules out the possibility that a failure to observe a change in single-stranded DNA was due to altered progression through the cell cycle in the *cdc13*-DBD$^-$ mutant strains. (C) The *cdc13*-Δ/p CEN LEU2 *cdc13*-F539A strain exhibited a strong DNA damage response, as indicated by an increase in Rad53 phosphorylation (Sanchez et al. 1996), similar to the enhanced Rad53 phosphorylation previously observed in *cdc13*-defective strains (Tsolou & Lydall 2007).

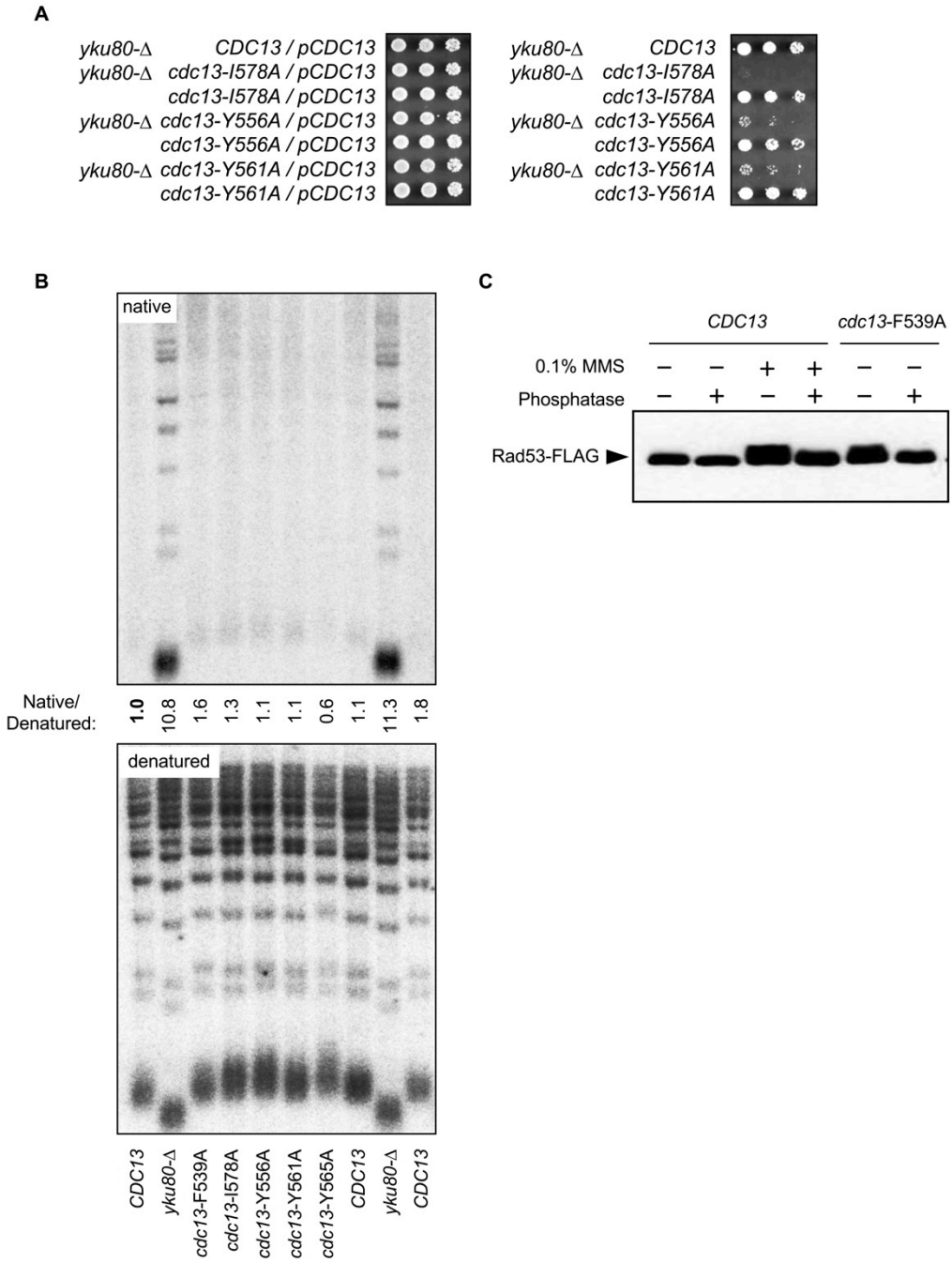
A
yku80-Δ CDC13 / pCDC13
yku80-Δ cdc13-I578A / pCDC13
cdc13-I578A / pCDC13
yku80-Δ cdc13-Y556A / pCDC13
cdc13-Y556A / pCDC13
yku80-Δ cdc13-Y561A / pCDC13
cdc13-Y561A / pCDC13
yku80-Δ CDC13
yku80-Δ cdc13-I578A
cdc13-I578A
yku80-Δ cdc13-Y556A
cdc13-Y556A
yku80-Δ cdc13-Y561A
cdc13-Y561A
B
native
Native/
Denatured:
1.0
10.8
1.6
1.3
1.1
1.1
0.6
1.1
11.3
1.8
denatured
CDC13
yku80-Δ
cdc13-F539A
cdc13-I578A
cdc13-Y556A
cdc13-Y561A
cdc13-Y565A
CDC13
yku80-Δ
CDC13
C
CDC13
cdc13-F539A
0.1% MMS
Phosphatase
Rad53-FLAG

Table AS.1: Absolute and K_D values of Cdc13 DBD wild type and mutants versus Tel11 and 4 variant 11mer oligonucleotides.

	Tel 11 (pM)	± (pM)	Fold Diff v WT w Tel 11		H1 (pM)	± (pM)	Fold Diff v WT w Tel 11	Fold Diff v WT w H1		H3 (pM)	± (pM)	Fold Diff v WT w Tel 11	Fold Diff v WT w H3		V4 (pM)	± (pM)	Fold Diff v WT w Tel 11	Fold Diff v WT w V4		H9 (pM)	± (pM)	Fold Diff v WT w Tel 11	Fold Diff v WT w H9
WT	2.10	0.20	1.00		31.6	4.7	15.0	1		85	21	40.5	1.0		183	43	87.1	1.00		9.4	0.9	4.48	1.00
Y556A	0.640	0.14	0.305		302	26	144	9.56		311	51	148	3.7		569	176	271	3.11		43.0	4.0	20.5	4.57
I578A	1.00	0.25	0.476		420	18	200	13.3		135	20	64.3	1.6		278	70	132	1.52		20.0	2.5	9.52	2.13
Y561A	1.64	0.22	0.780		154	26	73.3	4.87		434	83	207	5.1		381	29	181	2.08		16.0	2.0	7.62	1.70
Y565A	4.70	0.80	2.24		330	55	157	10.4		259	22	123	3.0		368	67	175	2.01		34.0	5.0	16.2	3.62
Y626A	7.20	0.90	3.43		1230	57	586	38.9		2500	610	1190	29.4		290	75	138	1.58		181	11	86.2	19.3
F539A	7.40	0.22	3.52		1260	140	600	39.9		2640	450	1257	31.1		1300	150	619	7.10		180	10	85.7	19.1
K622A	31.7	3.5	15.1		2390	431	1138	75.6		1210	174	576	14.2		4550	1304	2167	24.9		208	65	99.0	22.1
Y522A	71.0	16.0	33.8		426	46	203	13.5		769	205	366	9.0		5970	1240	2843	32.6		1230	280	586	131

Table AS.2: List of yeast strains used.

Strain	Genotype
YVL5535*	*MAT***a** /MATα *cdc13-Y522A*/*CDC13*
YVL5536*	*MAT***a** /MATα *cdc13-Y522A*/*CDC13 exo1-*Δ:: KAN^R/*EXO1*
YVL5537*	*MAT***a** /MATα *cdc13-Y522A*/*CDC13 rad9-*Δ:: KAN^R/*RAD9*
YVL5568*	*MAT***a** /MATα *cdc13-K622A*/*CDC13*
YVL4098*	*MAT***a** /MATα *cdc13-K622A*/*CDC13 exo1-*Δ:: KAN^R/*EXO1*
YVL5570*	*MAT***a** /MATα *cdc13-K622A*/*CDC13 rad9-*Δ:: KAN^R/*RAD9*
YVL5569*	*MAT***a** /MATα *cdc13-Y626A*/*CDC13*
YVL5383*	*MAT***a** /MATα *cdc13-F539A*/*CDC13*
YVL4097*	*MAT***a** /MATα *cdc13-F539A*/*CDC13 exo1-*Δ:: KAN^R/*EXO1*
YVL5385*	*MAT***a** /MATα *cdc13-F539A*/*CDC13 rad9-*Δ:: KAN^R/*RAD9*
YVL5387*	*MAT***a** /MATα *cdc13-Y561A*/*CDC13*
YVL3584*	*MAT***a** /MATα *tlc1-*Δ/*TLC1*
YVL3914*	*MAT***a** /MATα *tlc1-*Δ/*TLC1 cdc13-I578A*/*CDC13*
YVL3915*	*MAT***a** /MATα *tlc1-*Δ/*TLC1 cdc13-Y561A*/*CDC13*
YVL3006*	*MAT*α *cdc13-*Δ::*LYS2* / p CEN *URA3 CDC13*
YVL3086*	*MAT*α *cdc13-*Δ::*LYS2 yku80-*Δ/p CEN *URA3 CDC13*
YVL3197**	*MAT***a** *RAD53*-(FLAG)$_6$ *cdc13-*Δ::KAN^R/p CEN *URA3 CDC13*

* *ura3*-52 *lys2*-801 *trp1*-Δ1 *his3*-Δ200 *leu2*-Δ1

** *leu2*$^-$ *trp1*$^-$ *ura3*-52 *prb1*$^-$ *prc1*$^-$ *pep4*-3

Table AS.3: List of plasmids used.

Plasmid	Description	Vector backbone
pVL7770	*URA3 cdc13*-Y522A	YIplac211
pVL7796	*URA3 cdc13*-Y626A	YIplac211
pVL5886	*URA3 cdc13*-K622A	YIplac211
pVL5887	*URA3 cdc13*-F539A	YIplac211
pVL5885	*URA3 cdc13*-Y561A	YIplac211
pVL5583	*URA3 cdc13*-I578A	YIplac211
pVL438	*CEN URA3 CDC13*	YCplac33
pVL440	*CEN LEU2 CDC13*	YCplac111
pVL2834	*CEN LEU2 cdc13*-F539A	pVL440
pVL2232	*CEN LEU2 cdc13*-Y561A	pVL440
pVL2219	*CEN LEU2 cdc13*-Y556A	pVL440
pVL2233	*CEN LEU2 cdc13*-Y565A	pVL440
pVL2893	*CEN LEU2 cdc13*-I578A	pVL440
pVL1086	*CEN LEU2 CDC13*-$(myc)_{18}$	pVL440
pVL2815	*CEN LEU2 cdc13-R635A*-$(myc)_{18}$	pVL440
pVL2820	*CEN LEU2 cdc13-F539A*-$(myc)_{18}$	pVL440
pVL2824	*CEN LEU2 cdc13-Y556A*-$(myc)_{18}$	pVL440

MATERIALS AND METHODS

Site-Directed Mutagenesis of the Cdc13 DBD

The Cdc13 DBD protein expression constructs (amino acids 497-694) were cloned and expressed with a C-terminal His 6 -tag as described previously (Lewis et al. 2014; Anderson et al. 2002). Additional mutations were introduced using the QuickChange (Agilent Genomics) protocol with appropriate primers using standard procedures. The presence of the desired mutation was verified by DNA sequencing.

Expression and Purification of Wild Type and Mutant DBD Proteins

Protein purification was achieved using a previously reported protocol with minor changes (Lewis et al. 2014; Anderson et al. 2002). The cell pellet from l liter of growth in LB was suspended in 30 ml of lysis buffer (50 mM potassium phosphate, pH 7.0, 100 mM NaCl, 100 mM Na_2SO4, 1 mM Na_2 EDTA, 5 mM BME with one protease tablet (Roche) and sonicated on ice for 2 minutes total (20 seconds on, 20 seconds off). Lysate was cleared by centrifugation for 20 minutes at 30,000 x g at 4°C. Polyethylenimine (PEI, 5%) was added to supernatant to a final concentration of 0.1%, stirred for 2 hours at 4°C and cleared as above. NaCl was added to bring the supernatant to 1M NaCl. 5% PEI was added to the supernatant to a final concentration of 0.2%, stirred for 2 hours at 4°C and spun as above. The supernatant was dialyzed overnight into 50 mM potassium phosphate, pH 7.0, 50 mM NaCl, 5 mM BME. The dialysate was spun as above and filtered through a 0.2 μ filter. Imidazole was added to a final concentration of 10 mM and Na_2SO4 to a concentration of 100 mM before purification through a Ni-affinity column followed by size exclusion (G25, GE)

chromatography. Protein purity was assessed as >98% using SDS-PAGE analysis with Coomassie staining.

Electrophoretic Mobility Shift Assay (EMSA) Experiments

Apparent equilibrium binding constants (K_DS) were determined using EMSAs optimized for measuring tight binding constants as described previously (Lewis et al. 2014; Altschuler et al. 2013) using a binding buffer of 50 mM Tris pH 7.5, 75 mM KCl, 75 mM NaCl, 2 mM DTT, 0.1 mg/ml BSA, and 15% glycerol. Radiolabeled oligonucleotides were heated to 95°C for 20 minutes and then snap cooled at 4°C for 10 minutes before being used in binding reactions. Binding reactions were electrophoresed for 20 minutes at 200V through 9% acrylamide (19:1 acrylamide/bisacrylamide) Tris-Borate-EDTA gels containing 15% glycerol. Gels were imaged on a Typhoon FLA 9500 (GE) and quantified with Image Quant software. Binding data were fit to a standard Langmuir isotherm using Kaleidagraph fitting software as described previously (Altschuler et al. 2013). Each value is the average of at least 3 (and in many cases 4-8) replicates, with the error reported being the standard error of the mean.

In vivo analysis of mutant *cdc13*-DBD$^-$strains

Strains bearing *cdc13*-DBD$^-$ mutations were constructed by introducing the relevant mutation, in place of one of the two copies of the *CDC13* gene in a diploid strain, using a standard integration method as previously described (Paschini et al. 2012). Correct integration was confirmed by molecular methods (PCR and sequence analysis across the coding region of the gene), to rule out rearrangement of the

endogenous locus or unlinked missense mutations. Additional mutations in *EXO1*, *RAD9* and *TLC1* were constructed by one- step gene replacement, in which the wild type gene was replaced by a selectable drug-resistant cassette. Standard growth media and methods were used to propagate yeast strains and generate haploid strains by sporulation of diploid strains and subsequent tetrad dissection. The yeast strains and plasmids used in this study are listed in Tables AS.2 and AS.3, respectively.

Specificity Assays

Binding studies to determine the specificity requirements of the Cdc13 DBD mutant proteins were carried out as described above with oligonucleotides randomized individually with equimolar mixtures of the three non-cognate bases at each position in Tel 11 and labeled and diluted as described previously (Eldridge et al. 2006; Lewis et al. 2014). Only one shifted species was observed in all cases, and the binding data were readily fit to a single K_D value, consistent with prior data suggesting each alternate base is equally perturbing (Eldridge et al. 2006). Per convention, a mixture of A, C, and T is labeled H; a mixture of G, A, and C is labeled V.

Strains used for *in vivo* analysis

The strains used in Figure AS.3 expressed *cdc13*-DBD$^-$ mutations on single copy CEN plasmids in a *cdc13*-Δ haploid strain, which allowed inclusion of the *cdc13*-F539A mutation in these analyses. A mutant strain with the *cdc13*-F539A mutation integrated into the genome was not viable enough for the experimental manipulations required for parts (B) and C). In contrast, a *cdc13*-Δ strain expressing the *cdc13*-F539A mutation from a plasmid exhibited slightly improved growth,

sufficient to grow up cultures for analysis (we have previously suggested that an increase in plasmid copy number, due to a selection pressure for viability, is responsible for this slight enhancement in growth; (Dickey et al. 2013)).

Analysis of Cdc13 protein stability *in vivo*

Extracts were prepared from a protease-deficient yeast strain transformed with plasmids expressing wild type or mutant Cdc13-$(myc)_{18}$ proteins, by glass bead disruption; extracts were cleared by 2 x 14,000 rpm at 4° C, resolved on 8% SDS-PAGE gels and probed with anti-myc 9E10 antibody (1:2500), followed by a secondary incubation with IRDye 800CW Goat Anti-Mouse IgG (LiCor) and imaging with LiCor Odyssey.

Detection of hyper-phosphorylated Rad53

Extracts were prepared from cdc13-Δ/p CEN LEU2 CDC13 or *cdc13*-Δ/p CEN LEU2 *cdc13*-F539A strains expressing Rad53-$(FLAG)_6$ which were grown to mid-log phase, pelleted and resuspended in 100µl breaking buffer (50 mM sodium phosphate pH 7.4, 1 mM EDTA, 5% glycerol) plus complete protease inhibitor (Roche). An equal volume of acid-washed glass beads was added and the mixture was vortexed at 4° C for 5 min. Lysates were clarified by centrifugation at 4° C for 10 min, and treated (or mock-treated) with λ phosphatase (NEB) for 1 hr at 30°. The MMS-treated strain was incubated at 0.1% MMS for 1 hr, immediately prior to extract preparation. Samples were resolved on 6% SDS-PAGE, transferred to nitrocellulose and probed with anti-FLAG antibody (Sigma-Aldrich) at 1:10,000 dilution followed by anti-rabbit IgG HRP conjugate (Promega) at 1:10,000; signal was detected using enhanced

chemiluminescence (ECL).

ACKNOWLEDGEMENTS:

We thank Neil Lloyd for help with the figures, and useful comments by Olke Uhlenbeck. This work was supported by National Institutes of Health grants R01 GM106060 (to V.L.), R01 GM059414 (to D.S.W.), T32 GM007240 (to C.M.R.), and P30 CA014195 (to the Salk Institute Cancer Center) and a Graduate Fellowship from the Glenn Center for Aging Research at the Salk Institute (to C.M.R.).

The material in this Appendix is currently under review at *PNAS*. Glustrom, Leslie W.; Lyon, Kenneth R.; Paschini, Margherita; Reyes, Cynthia M., Toro, Tasha B.; Lundblad, Victoria; Wuttke, Deborah S. The dissertation author was a collaborator and a contributing author of this material.

REFERENCES

Anderson EM, Halsey WA, Wuttke DS (2002) Delineation of the high-affinity single-stranded telomeric DNA-binding domain of *Saccharomyces cerevisiae* Cdc13. *Nucleic Acids Res.* 30, 4305-4313.

Anderson EM, Halsey WA, Wuttke DS (2003) Site-directed mutagenesis reveals the thermodynamic requirements for single-stranded DNA recognition by the telomere-binding protein Cdc13. *Biochemistry* 42, 3751-3758.

Altschuler SE, Lewis KA, Wuttke DS (2013) Practical strategies for the evaluation of high-affinity protein/nucleic acid interactions. *J. Nucleic Acids Investig.* 4,19-28.

Bertuch AA, Lundblad V (2003) The Ku heterodimer performs separable activities at double-strand breaks and chromosome termini. *Mol.Cell. Biol.* 23, 82028215.

Bhattacharjee A, Wang Y, Diao J, Price CM (2017) Dynamic DNA binding, junction recognition and G4 melting activity underlie the telomeric and genome-wide roles of human CST. *Nucleic Acids Res.* 45, 2311-12324.

Bochkarev A, Bochkareva E (2004) From RPA to BRCA2: lessons from single-stranded DNA binding by the OB-fold. *Curr. Opin. Struct. Biol.* 14, 36-42.

Booth C, Griffith E, Brady G, Lydall D (2001) Quantitative amplification of single-stranded DNA (QAOS) demonstrates that *cdc13*-1 mutants generate ssDNA in a telomere to centromere direction. *Nucleic Acids Res.* 29, 4414-4422.

Carter PJ, Winter G, Wilkinson AJ, Fersht AR (1984) The use of double mutants to detect structural changes in the active site of the tyrosyl-tRNA synthetase (Bacillus stearothermophilus). *Cell* 38, 835-840.

Casteel DE, Zhuang S, Zeng Y, Perrino FW, Boss GR, Goulian M & Pilz RB (2009) A DNA polymerase-α primase cofactor with homology to replication protein A-32 regulates DNA replication in mammalian cells. *J. Biol. Chem.* 284, 5807-5818.

Chastain M, Zhou Q, Shiva O, Fadri-Moskwik, Whitmore L, Jia P, Dai X, Huange C, Ye P & Chai W (2016) Human CST facilitates genome-wide *RAD51* recruitment to

GC-rich repetitive sequences in response to replication stress. *Cell Rep.* 16, 1300-1314.

Chen R, Subramanyam S, Elcock AH, Spies M, Wold MS (2016) Dynamic binding of replication protein A is required for DNA repair. *Nucleic Acids Res.* 44, 5758-72.

Croy JE, Wuttke DS (2006) Themes in ssDNA recognition by telomere-end protection proteins. *Trends Biochem. Sci.* 31,516-525.

Dickey TH, Altschuler SE, Wuttke DS (2013a) Single-stranded DNA-binding proteins: multiple domains for multiple functions. *Structure* 21, 1074-1084.

Dickey TH, McKercher MA, Wuttke DS (2013b) Nonspecific recognition is achieved in Pot1pC through the use of multiple binding modes. *Structure* 21, 121-132.

Dionne I, Wellinger RJ (1996) Cell cycle-regulated generation of single-stranded G-rich DNA in the absence of telomerase. *Proc. Natl. Acad. Sci. USA* 93, 13902-13907.

Eldridge AM, Halsey WA, Wuttke DS (2006) Identification of the determinants for the specific recognition of single-strand telomeric DNA by Cdc13. *Biochemistry* 45, 871-879.

Fanning E, Klimovich V, Nager AR (2006) A dynamic model for replication protein A (RPA) function in DNA processing pathways. *Nucleic Acids Res.* 34, 4126-4137.

Förstemann K, Lingner J (2001) Molecular basis for telomere repeat divergence in budding yeast. *Mol. Cell. Biol.* 21, 7277-7286.

Gao H, Cervantes RB, Mandell EK, Otero JH, Lundblad V (2007) RPA-like proteins mediate yeast telomere function. *Nat. Struct. Mol. Biol.* 14, 208-214.

Garvik B, Carson M, Hartwell L (1995) Single-stranded DNA arising at telomeres in cdc13 mutants may constitute a specific signal for the *RAD9* checkpoint. *Mol. Cell. Biol.* 15, 6128-6138.

Gelinas AD, Paschini M, Reyes F, Héroux, Batey RT, Lundblad V & Wuttke DS (2009) Telomere capping proteins are structurally related to RPA with an additional telomere-specific domain. *Proc. Natl. Acad. Sci. USA* 106, 9298-19303.

Grandin N, Reed SI, Charbonneau M (1997) Stn1, a new *Saccharomyces cerevisiae* protein, is implicated in telomere size regulation in association with Cdc13. *Genes & Development* 11, 512-527.

Grandin N, Damon C, Charbonneau M (2001) Ten1 functions in telomere end protection and length regulation in association with Stn1 and Cdc13. *EMBO J* 20, 1173-1183.

Gravel S, Larrivee M, Labrecque P, Wellinger RJ (1998) Yeast Ku as a regulator of chromosomal DNA end structure. *Science* 280, 741-744.

Hom RA, Wuttke DS (2017) Human CST prefers G-rich but not necessarily telomeric sequences. *Biochemistry* 56, 4210-4218.

Iftode C, Daniely Y, Borowiec JA (1999) Replication protein A (RPA): the eukaryotic SSB.*Crit Rev Biochem and Mol Biol* 34,141-180.

Johansson HE, Dertinger D, LeCuyer KA, Behlen LS, Greef CH & Uhlenbeck OC (1998) A thermodynamic analysis of the sequence-specific binding of RNA by bacteriophage MS2 coat protein. *Proc. Natl. Acad. Sci. USA* 95, 9244-9249.

Lei M, Podell ER, Cech TR (2004) Structure of human POT1 bound to telomeric single-stranded DNA provides a model for chromosome end-protection. *Nat. Struct. Mol. Biol.* 11, 1223-1229.

Lendvay TS, Morris DK, Sah J, Balasubramanian B, Lundblad V (1996) Senescence mutants of *Saccharomyces cerevisiae* with a defect in telomere replication identify three additional EST genes. *Genetics* 144, 1399-1412.

Lewis KA, Pfaff DA, Earley JN, Altschuler SE, Wuttke DS (2014) The tenacious recognition of yeast telomere sequence by Cdc13 is fully exerted by a single OB-fold domain. *Nucleic Acids Res.* 42, 475-484.

Lloyd NR, Dickey TH, Hom RA, Wuttke DS (2016) Tying up the ends: plasticity in the recognition of single-stranded DNA at telomeres. *Biochemistry* 55, 5326-5340.

Lohman TM, Ferrari ME (1994) *Escherichia coli* single-stranded DNA-binding protein: multiple DNA-binding modes and cooperativities. *Annu Rev Biochem* 63, 527-570.

Lydall D, Weinert T (1995) Yeast checkpoint genes in DNA damage processing: implications for repair and arrest. *Science* 270, 488-491.

Mitton-Fry RM, Anderson EM, Hughes TR, Lundblad V, Wuttke DS (2002) Conserved structure for single-stranded telomeric DNA recognition. *Science* 296, 145-147.

Mitton-Fry RM, Anderson EM, Theobald DL, Glustrom LW, Wuttke DS (2004) Structural basis for telomeric single-stranded DNA recognition by yeast Cdc13. *J. Mol. Biol.* 338, 241-255.

Miyake Y, Nakamura M, Nebetani A, Shimamura S, Tamura M, Yonehara S, Saito M and Ishikawa F (2009) RPA-like mammalian Ctc1-Stn1-Ten1 complex binds to single-stranded DNA and protects telomeres independently of the Pot1 pathway. *Mol. Cell.* 36, 193-206.

Paschini M, Mandell EK, Lundblad V (2010) Structure prediction-driven genetics in *Saccharomyces cerevisiae* identifies an interface between the t-RPA proteins Stn1 and Ten1. *Genetics* 185,11-21.

Paschini M, Toro TB, Lubin JW, Braunstein-Ballew B, Morris DK & Lundblad V (2012) A naturally thermolabile activity compromises genetic analysis of telomere function in *Saccharomyces cerevisiae*. *Genetics* 191, 79-93.

Sanchez Y, Desany BA, Lones WJ, Liu Q, Wang B & Elledge S. (1996) Regulation of *RAD53* by the ATM-like kinases *MEC1* and *TEL1* in yeast cell cycle checkpoint pathways. *Science* 271, 357-360.

Schreiber G, Fersht AR (1995) Energetics of protein-protein interactions: analysis of the barnase-barstar interface by single mutations and double mutant cycles. *J. Mol. Biol.* 248, 478-486.

Singer MS, Gottschling DE (1994) *TLC1*: template RNA component of *Saccharomyces cerevisiae* telomerase. *Science* 266, 404-409.

Sun J, Yu EY, Yang Y, Confer LA, Sun SH, Wan K, Lue NF & Lei M (2009) Stn1-Ten1 is an Rpa2-Rpa3-like complex at telomeres. *Genes & Development* 23, 2900-2914.

Surovtseva YV, Churikov D, Boltz KA, Song X, Lamb JC, Warrington R, Leehy K, Heacock M, Price CM & Shippen DE (2009) Conserved telomere maintenance component 1 interacts with *STN1* and maintains chromosome ends in higher eukaryotes. *Mol. Cell.* 36, 207-218.

Tsolou A, Lydall D (2007) Mrc1 protects uncapped budding yeast telomeres from exonuclease EXO1. *DNA Repair* 6, 1607-1617.

Wan B, Tant T, Upton H, Shuai J, Zhou Y, Li S, Chen J, Bruzelle JS, Zeng Z, Collins C, Wu J & Lei M (2015) The Tetrahymena telomerase p75-p45-p19 subcomplex is a unique CST complex. *Nat. Struct. Mol. Biol.* 22, 1023-1026.

Weinert TA, Kiser GL, Hartwell LH (1994) Mitotic checkpoint genes in budding yeast and the dependence of mitosis on DNA replication and repair. *Genes & Development* 8, 652-665.

Wells JA (1990) Additivity of mutational effects in proteins. *Biochemistry* 29, 8509-8517.

Wilson KA, Kellie JL, Wetmore SD (2014) DNA-protein π-interactions in nature: abundance, structure, composition and strength of contacts between aromatic amino acids and DNA nucleobases or deoxyribose sugar. *Nucleic Acids Res.* 42, 6726-6741.

Wold MS (1997) Replication protein A: a heterotrimeric, single-stranded DNA-binding protein required for eukaryotic DNA metabolism. *Annu Rev Biochem* 66, 61-92.

Zubko MK, Guillard S, Lydall D (2004) Exo1 and Rad24 differentially regulate generation of ssDNA at telomeres of *Saccharomyces cerevisiae cdc13*-1 mutants. *Genetics* 168, 103-115.

APPENDIX B:

High-resolution assays for telomere length shortening

A lot of what is discussed in this thesis addressed the previous and current obstacles in accurately and robustly examining telomere length. While Chapters 2-4 detail my progress with multiple new assays and how that led to novel findings about telomere homeostasis, Margherita Paschini and I also spent some time on additional assay development. This appendix describes three such assays that were aimed at detecting subtle changes in telomere shortening, and the variable degrees of success I encountered with each.

As discussed earlier, the senescence phenotype can be highly variable. The goal of the epistasis experiments detailed in Chapter 2 was to identify pathways that effect telomere shortening by monitoring replicative senescence. But the effects observed in replicative senescence could be due to either a change in the rate of telomere shortening, or to a change in the response to this shortening. To address this, both Margherita and I pursued the development of assays that would be of high enough resolution to detect even small differences in telomere shortening in more direct approaches. All three approaches described here used a telomerase defective strain of yeast lacking the telomerase RNA component (*TLC1*), so that telomere shortening would not be counterbalance by telomerase activity. The goal was to have an assay that would allow us to definitively state that the rate of telomere shortening in *geneX*-Δ *tlc1*-Δ is different than the rate of telomere shortening in *GENE X tlc1*-Δ.

Polyacrylamide gel electrophoresis (PAGE) resolution of individual telomeres

My initial attempt at a molecular assay to directly monitor telomere length involved the analysis of PCR-amplified telomere products on high resolution on PAGE gels. Previously, I was able to detect a small range of telomeres on an ethidium bromide stained gel following PCR amplification of a specific telomere (1L or 6R). By modifying the protocol with radioactive end labeling of PCR products and resolution by PAGE, I thought I could attain a much more sensitive assay for telomere length analysis. The rational is pretty straightforward. On an ethidium bromide gel, the detection limit stems from the inability of smaller PCR products to bind sufficient ethidium bromide molecules to elicit a strong signal. This is also true for smaller populations of products. What you see is the strongest signal for longer and more abundant products (the average telomere length), giving you what is essentially a size-biased assay. There is a similar issue with Southern blots, and why we are so quick to point out the huge limitation of such assays. By replacing ethidium bromide staining with radioactive end labeling, you get an experimental condition in which each molecule is labeled with a radioactive molecule, regardless of length. This would mean that a short telomere would generate the same signal intensity as a medium-long telomere, thereby eliminating size bias. Through this I could increase the detection of a wider range of telomeres.

Unfortunately, I was never able to get this protocol to work efficiently and so shifted focus to other effective assays.

Measuring telomere shortening in the absence of telomerase at single-nucleotide resolution

In parallel, Margherita was optimizing a PCR based assay for telomere length. This assay was initially designed by the Lingner lab (Forstemann et al. 2000) and was described in detail in chapter 3. Briefly, sequence analysis of multiple cloned telomeres, following PCR amplification of an individual telomere (1L or 6R) can be used to collect single nucleotide resolution data on telomere length in different genetic backgrounds. Although this assay resulted in higher resolution, it also had high variance. This assay was used extensively on telomerase positive strains, and gave abundant information on telomere length and composition, but using it in a telomerase-defective background proved to be less effective. Telomeres exhibit a high degree of variability, as was discussed throughout this thesis, and this variability is magnified in the absence of telomerase. The increase in variability would require an increase in the number of samples needed to statistically measure differences between *geneX*-Δ *tlc1*-Δ is and *GENE X tlc1*-Δ. This assay besides being labor-intensive is also expensive, and therefore it has not been possible to collect high enough quality data to observe the subtle shifts in the rate of telomere shortening.

Measuring telomere loss in the presence of a sub-terminal telomeric tract in telomerase null cells

Margherita developed a third assay to monitor telomere loss in a telomerase defective background. This assay employs a simple genetic read-out for telomere

shortening that can be applied to multiple genetic backgrounds in a way that is cost effective and experimentally robust. A strain was constructed by introducing an internal telomeric tract consisting of 302 bps of subtelomeric region and 390 bps of telomeric DNA ($G_{1\text{-}3}T$) directly adjacent to the natural telomere of chromosome VI-R. The interstitial telomeric tract has nutritional markers (*TRP1* and *URA3*) upstream and downstream, respectively, to the $G_{1\text{-}3}T$ tract. The inclusion of these nutritional markers allows us to easily monitor events occurring at that chromosome end (figure B.1 A). In the absence of telomerase, the natural telomere shortens, and once it is completely lost, the loss of *URA3* follows (figure B.1 B). This loss of the natural telomere VI-R is tolerated by the cell due to the presence of the ectopic telomeric tract. The cell remains viable and the consequences of telomere shortening are readily detectible by monitoring URA^- colonies. Unlike the molecular assays mentioned at the beginning of this appendix, this approach provides a simple, inexpensive, alternative to observing telomere shortening rates across multiple genetic backgrounds. Its experimental simplicity also allows for the use of large number of colonies, presumably overcoming the variance problem of replicative senescence.

RESULTS

I began using this assay in hopes of testing the epistatic relationships detailed in Chapter 2, in a more direct assay for telomere sequence loss. The first goal was to take genes involved in each arm of my epistasis map (figure B.3 A) and integrate them into the experimental strain background. I chose to begin with *Tel1*, *Rif2*, *Rad51*,

Rad17, and *Upf1*. Each one of these genes had a significant effect (either an exacerbation or attenuation) on replicative senescence and the objective was to correlate that effect directly with telomere loss.

Initially, I underestimated the need for large numbers in this assay and was not able to generate enough isolates for each genetic background. Each experiment begins with the dissection of *tlc1*-Δ/TLC1 *geneX*-Δ/GENE X diploid strain. I was only able to generate a large enough dataset for *tlc1*-Δ. The analysis of 11 isolates, and over 3,000 colonies showed a large disparity in the frequency of telomere loss amongst isolates of the identical genotype (figure B.2). From the limited number of experiments I ran on a wide range of genetic backgrounds, I observed a wide range of telomere frequency loss (figure B.3). Due to very limited number of these experiments, I am unable to ask if the frequency of loss in any of my mutants were significantly different than what I saw in *tlc1*-Δ.

DISCUSSION

This assay defines another attempt at studying telomere length homeostasis, by directly asking what is the frequency of telomere loss and what factors contribute to this frequency. Unfortunately, I was never able to fully exploit the strengths of this assay. I was however, able to add to an overwhelming amount of evidence that shows that the field is underestimating the degree of variability in telomere length in the absence of telomerase. This assay has the potential to answer longstanding questions in telomere biology. Through minor modifications you can introduce fluorescent

markers in place of the nutritional markers it currently contains. This could lead to experimental conditions where you could measure the frequency of telomere loss in thousands of cells instead of hundreds, in different genetic backgrounds, all monitored by fluorescent microscopy. This would increase the data set, and decrease the labor intensity.

FIGURES

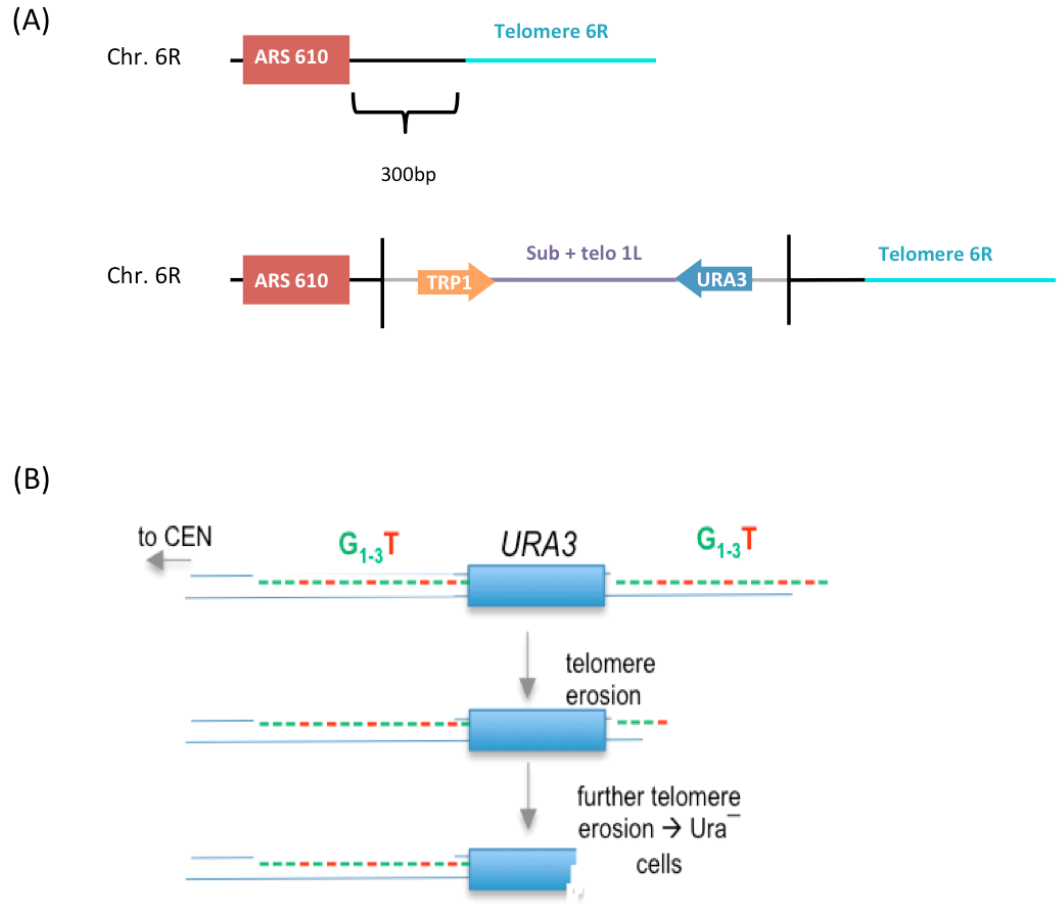

Figure B.1: A molecular assay for telomere loss. A.) Schematic of the interstitial telomeric tract placed adjacent to natural telomere VI-R. The telomeric tract is flanked by both TRP1 and URA3 nutritional markers, and was placed upstream of ARS 610. B.) Cartoon of the effects of telomere erosion on this experimental strain, leading to Ura¯ viable cells.

Ura⁻	total
8	402
2	260
0	267
13	295
2	304
1	247
0	164
1	581
5	503
17	271
7	474

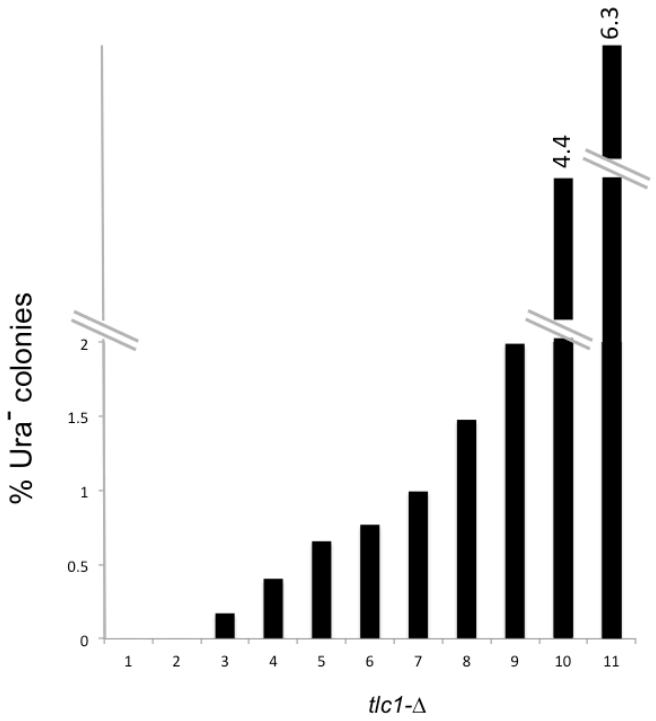

Figure B.2: Loss of *URA3* in telomerase null populations is highly variable. Left: Tally of Ura⁻ colonies compared to total colonies analyzed. Right: Percentage of Ura⁻ colonies fro 11 isolates of *tlc1*-Δ populations.

(A)

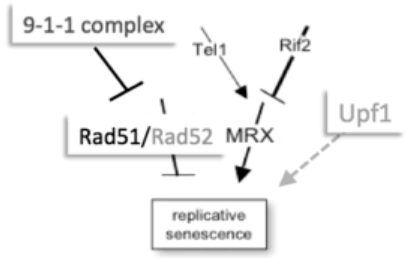

(B)

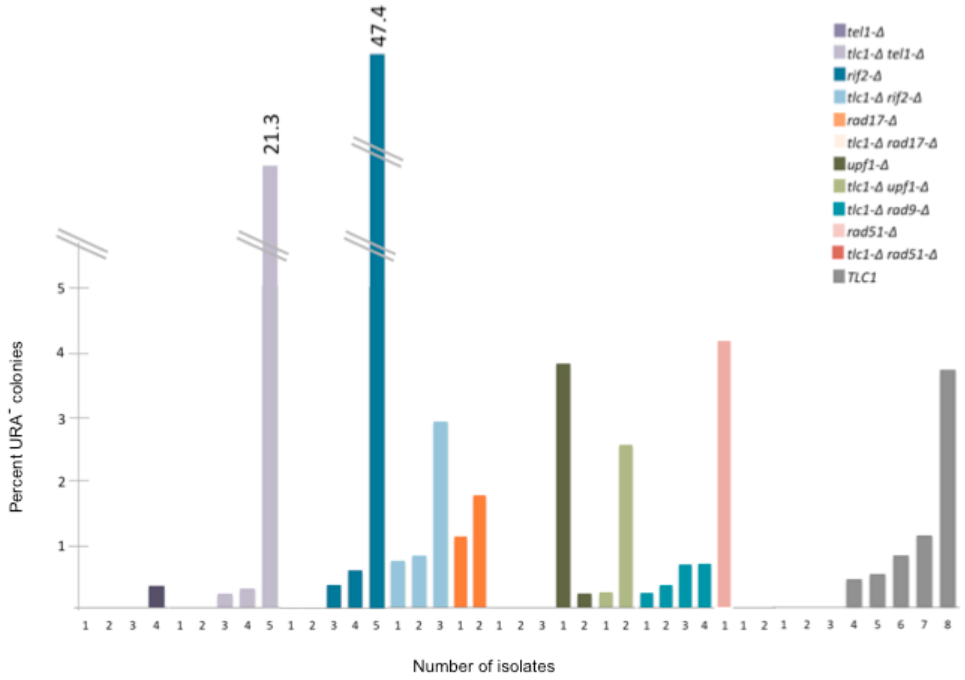

Figure B.3: *URA3* loss is variable across multiple genetic backgrounds. Percent of Ura$^-$ colonies in a population was monitored in a wide range of genetic backgrounds. Strains that were both proficient and defective for telomerase were included in this experiment.

Table B.1: *URA3* loss is variable across multiple genetic backgrounds. Tally of URA loss colonies from the different genetic backgrounds represented in previous histogram in figure A3. The total number of colonies monitored for *URA3* loss is detailed. *URA3* loss was monitored in both proficient and defective for telomerase backgrounds.

tlc1-Δ/TLC1 rad9-Δ/RAD9		***tlc1-Δ/TLC1 tel1-Δ/TEL1***		***tlc1-Δ/TLC1 rif2-Δ/RIF2***		***tlc1-Δ/TLC1 rad17-Δ/RAD17***		***tlc1-Δ/TLC1 rad51-Δ/RAD51***		***tlc1-Δ/TLC1 upf1-Δ/UPF1***	
tlc1-Δ rad9-Δ		***tlc1-Δ tel1-Δ***		***tlc1-Δ rif2-Δ***		***tlc1-Δ rad17-Δ***		***tlc1-Δ rad51-Δ***		***tlc1-Δ upf1-Δ***	
URA⁻	*total*	*URA⁻*	*total*	*URA⁻*	*total*	*URA⁻*	*total*	*URA⁻*	*total*	*URA⁻*	*total*
1	440	84	394	2	278	0	395	8	199	1	425
2	298	0	304	8	280	0	251	***tlc1-Δ***		11	436
1	287	1	333	2	251	0	167	1	247	***TLC1***	
2	293	0	372	***tlc1-Δ***		***rad17-Δ***		0	164	4	335
TLC1		1	452	*0*	267	7	403	***rad51-Δ***		46	331
1	192	***tel1-Δ***		13	295	4	363	0	187	***upf1-Δ***	
6	536	1	192	***rif2-Δ***		***tlc1-Δ***		0	196	7	185
		0	200	109	230	2	304			1	459
		0	530	*0*	319	***TLC1***					
		0	220	1	282	1	272				
		tlc1-Δ		3	510	2	247				
		8	402	0	232	0	347				
		2	260								
		TLC1									
		2	456								
		0	367								
		0	408								
		0	302								

Table B.2: Strain construction details.

Parental strain A	Parental Strain B	Genotype
YVL 3996	YVL4769	MATa/α **tlc1-Δ::HIS3/TLC1 rad9-Δ::kanMX6/RAD9**
YVL 3015	YVL4769	MATa/α **tlc1-::HIS3/TLC1 tel1-Δ::kanMX6/TEL1**
YVL3568	YVL4770	MATa/α **tlc1-Δ::HIS3/TLC1 rif2-Δ::kanMX6/RIF2**
YVL3997	YVL4769	MATa/α **tlc1-Δ::HIS3/TLC1 rad17-Δ::kanMX6/RAD17**
YVL3882	YVL4769	MATa/α **tlc1-Δ::HIS3/TLC1 rad51-Δ::kanMX6/RAD51**
YVL5573	YVL4769	MATa/α **tlc1-Δ::HIS3/TLC1 upf1-Δ::kanMX6/UPF1**
additional genotype: ura3-52 lys2-801 trp-Δ1 his3-Δ200 leu2-Δ1 ITT: TRP + subtelo+tel01L +URA inserted 100bp downstream of ARS610 (telomere 6R)		

MATERIAL AND METHODS

Experimental isolates

Each experiment is done immediately after loss of telomerase. Diploids strains were grown overnight and then sporulated in liquid medium for 3-4 days at room temperature. Strains were dissected and allowed to grow on full media plates for 2 days before they were genotyped for *tlc1*-Δ (His3^{+}), gene of interest (kanMX6 or natMX4), and presence of the telomeric construct (Ura^{+}). For isolates that tested positive, the whole colony was placed into 2mls of sterile water. From that suspension, multiple dilutions were plated on to full media plates (YPAD). Cells were allowed to grow for 3 days at 30˚. Plates that had no more than approximately 100 colonies per plate were included in the experiment. Plates with signicantly more colonies were eliminated because they are suboptimal for replica plating. Plates were replica plated onto $^{-}$*URA* plates and allowed to grow for 2 days. By comparing colony pattern on the YPAD plate vs. the colony pattern on the $^{-}$*URA* plate, the number of colonies that lost *URA* was tallied. That number was compared to the total number of colonies in the experiment and the frequency of loss of $^{-}$*URA* was calculated.

Yeast strains

All yeast strains in Table B.2 were derived through mating with the original experimental sub-terminal telomeric tract strain YVL4769 or its isogenic partner YVL4770 (Mat::a). Heterozygous diploids containing desired mutations (*tlc1*-Δ*/TLC1 geneX*-Δ*/GENEX*) were dissected, and Mat::α isolates with desired genotype were identified (*tlc1*-Δ *geneX*-Δ Mat::α), and then mated with YVL4769 or YVL4770 to

create the diploids used in the experiment. All strains used in this study are isogenic to YVL2967, which is derived from S288C and is the parent to all strains currently constructed in the Lundblad lab.

APPENDIX C:

Regulatory contributions to telomere homeostasis by the N-terminal domain of Cdc13

As discussed earlier, the t-RPA complex (made up of Cdc13, Stn1, and Ten1) plays a critical role in telomere length regulation. In Chapters 3, we showed that its essential role is in preventing replication stress (collapsed replication forks) at duplex telomeric DNA. For Cdc13, the mutations studied were in its DNA binding domain, but this multi-domain protein effects telomere length in a variety of ways and not all domains have an associated function (Figure C.1). In order to fully understand the regulatory contributions that Cdc13 makes to telomere homeostasis, Johnathan Lubin, a graduate student, conducted a structure-guided mutagenesis of all solvent-accessible residues on the surface of the N- and C-terminal domains of Cdc13. On the N-terminal domain, he identified multiple adjacent clusters of residues that were highly conserved (figure C.2), and required for both positive and negative telomere length control. These clusters are distinct from the cluster of residues that the Skordalakes and Lei laboratories have previously proposed mediate dimerization. On the basis of this, I took the mutations and integrated them into the *Saccharomyces cerevisiae* genome. In this way I could better analyze these surfaces of Cdc13 by asking whether they act in the telomerase pathway (through epistasis analysis with telomerase null mutations) and whether they contribute to a proposed role for Cdc13 in replication of duplex telomeric DNA. I determined that the phenotypes caused by a subset of Cdc13 N-terminal domain mutations (*cdc13*^{NTerm}) were dependent on telomerase, as the *tlc1*-Δ *cdc13*^{NTerm} senescence phenotype was indistinguishable from that of *tlc1*-Δ isolates. This result indicates the identification of a new telomerase regulatory domain on the

N-terminal domain of Cdc13. This appendix summarizes the work that led to that conclusion.

RESULTS

Initial analysis of integrated mutations

The starting point to this study was to verify the phenotypes found through the structure-guided mutagenesis of Cdc13, carried out through plasmid shuffle (ectopic expression of *cdc13*^{NTerm} in *cdc13*-Δ background). To do this, I integrated the desired mutations into the *S. saccharomyces* genome using basic molecular techniques (pop-in/pop-out) and assayed telomere length via TRF (telomere restriction fragment) southern blot. For all but one mutation tested, the telomere length phenotypes matched those observed with carrier plasmid (Figure C.3). For *cdc13*-D150R L91A, the slightly long telomere phenotype observed previously appeared closer to wild type telomere length when the mutation was integrated into the genome. Telomere length phenotypes are summarized in Table C.1.

The *cdc13*^{NTerm} strains were also checked for viability and temperature sensitivity. None of the *cdc13*^{NTerm} mutations had a growth defect (Figure C.5) and only *cdc13*-L91A showed temperature sensitivity (Figure C.4), a phenotype previously reported by the Lei lab (at 37˚). Therefore, while this residue is not important for normal cell growth, upon increased stress is not dispensable.

Mutations of the N-terminal domain of Cdc13 effects replicative senescence

To better understand the roles of the multiple residues on the N-terminal domain of Cdc13, I tested their combined effects on replicative senescence. As previously discussed, subtle effects on telomere length can be examined through a semi-quantitative assay for senescence (Chapter 2). To do this I integrated mutations in the N-terminal domain of Cdc13 into a strain background that lacked the telomerase RNA subunit (*tlc1*-Δ) and compared growth characteristics of both *tlc1*-Δ and *tlc1*-Δ *cdc13*^{NTerm}. Of the Cdc13 residues studied, *cdc13*-D150R and *cdc13*-F142A conferred a long telomere phenotype (figure C.3, Table C.1). In two experiments, that included the comparison of 36 *tlc1*-Δ *cdc13*-D150R and 54 *tlc1*-Δ, there was no significant effect on senescence. Isolates were monitored from 75 generations (figure C.5). An experiment comparing 33 *tlc1*-Δ *cdc13*-F142A and *31 tlc1*-Δ isolates, resulted in a subtle transient effect on senescence, that was just short of being statistically significant (p =0.06, figure C.5). These results argue that the effects of *cdc13*-D150R *(*and presumably *cdc13*-F142A*)* are dependent on telomerase, and thus in the absence of a functional telomerase there is no significant effect on senescence.

Next, I tested a set of N-terminal mutations that conferred a short telomere phenotype, *cdc13*-L91A and *cdc13*-K129E K147E (KEKE). In an experiment comparing 16 *tlc1*-Δ *cdc13*-L91A and 20 *tlc1*-Δ, the effect on senescence was instant. At 25 generations the relative senescence was significantly higher than in *tlc-1*-Δ isolates (p =0.00002). The same was seen for *tlc1*-Δ *cdc13*-KEKE (p = 0.0001; Figure C.7). In both situations, the effect on senescence was restricted to 25 generations, and

was not statistically different from *tlc1*-Δ by 50 generations. The phenotype of either *cdc13*- KEKE or *cdc13*-L91A (short telomeres) is reversed to a wild type-long telomere phenotype when combined with *cdc13*-D150R (Figure C.3, Table C.1). To see what effect this combination conferred in the absence of telomerase, I first compared 24 *tlc1*-Δ *cdc13*-D150R L91A to 32 *tlc1*-Δ isolate. The result was an accelerated senescence, statistically significant at both 25 and 50 generations (p =0.000002 and p =0.0000006, respectively). The pattern shifted from a significant effect on early senescence in *tlc1*-Δ *cdc13*-L91A (Figure C.7 A) to a sustained accelerated senescence in *tlc1*-Δ *cdc13*-D150R L91A at both 25 and 50 generations (Figure C.8 A). By 75 generations, most isolates were dead or had shifted to the survivor pathway.

When I compared growth characteristics in *tlc1*-Δ *cdc13*-D150R KEKE and *tlc1*-Δ isolates, accelerated senescence was detectable by 50 generations (p =0.0006). Here, the pattern of senescence is shifted from early (25 generations) in *tlc1*Δ *cdc13*-KEKE (figure C.7 B), to only significant at 50 generations in *tlc1*Δ *cdc13*-D150R KEKE (Figure C.8 B). To better understand this shift in onset of accelerated senescence, I compared the growth scores for each mutation at 25 generations (Figure C.9). All the isolates that were derived from a *cdc13*-D150R/CDC13 background or D150R in combination with another $cdc13^{N\text{-}TERM}$ mutation, showed better health scores at 25 generations than those with an un-mutated D150 residue. It is important to note that this phenomenon was also observed *tlc1*-Δ single mutants that were derived from a heterozygous diploid bearing *cdc13*-D150R/CDC13. One possible explanation

for this type of effect could be that the D150R mutation is conferring an elongated telomere phenotype even in the heterozygous diploid. Therefore, strains start off with longer telomeres, senesce slower and display higher growth scores at 25 generations than those that started off with shorter telomeres. To test this, I grew up the heterozygous diploids and subjected them to TRF analysis by southern blot. None of the strains showed a detectable difference in telomere length (Figure C.10).

It is difficult to interpret small changes in senescence when comparing effects observed in separate experiments. To better understand the effects of these two sets of *cdc13*$^{N\text{-}Term}$ mutations (long vs. short telomere) it might be beneficial to run this experiment with a diploid *tlc1*-Δ/TLC1 strain that carries both *cdc13*-KEKE and *cdc13*-D150R KEKE. This way the growth characteristics of both could be compared in the same experiment. Even so, it is clear that in terms of effect on replicative senescence, the phenotype of either *cdc13*- KEKE or *cdc13*-L91A (accelerated senescence) is not reversed by introducing *cdc13*-D150R.

DISCUSSION

The analysis of 4 specific sites on the N-terminal domain of Cdc13 can be separated into two categories, those that produce short telomeres and those that produce long telomeres. Two of these residues, F142 and L91 (that elicit opposite effects on telomere length) have been implicated in effecting Cdc13 dimerization (Lei lab and Skordalakes lab) and thereby effecting DNA binding (specifically F142A). The analyses described in this appendix does not address binding or protein

dimerization, but rather telomere length effects and the consequences of those effects in the absence of telomerase.

Residues D150 and K129 K147 are novel sites with no assigned function. The results of my experiments (in combination with those carried out by Johnathan Lubin) indicate that they define two separate regulatory sites. D150 is involved in keeping telomeres from getting too long (mutation leads to long telomeres) possibly through an interaction with telomerase (*tlc1*-Δ D150R = *tlc1*-Δ, figure C.6 A*)*. K129 K147 is responsible for the opposite, ensuring telomeres do not get too short (mutation leads to short telomeres). The telomere length data suggests that the function at K129 K147 is dependent on the function at D150, as a mutation at both sites is indistinguishable from a mutation at just D150. This could be indicative of a temporal relationship between the two sites, where an event must first occur at D150 for the function of K129 K147 to elicit a response. This is somewhat perplexing because of the pattern of accelerated senescence (compared to *tlc1*-Δ) observed in both *tlc1*-Δ *cdc13*- KEKE and *tlc1*Δ *cdc13*-D150R KEKE isolates. If these residues defined sites of action dependent on telomerase, then in the absence of telomerase you would not expect to see a significant effect like the one shown in figures C.7 and C.8. For the *cdc13*^{NTERM} mutations that displayed a short telomere phenotype (L91A and KEKE) the combination with *tlc1*-Δ, led to a significantly accelerated senescence. And that unlike the result in the presence of telomerase, where the combination with the D150R mutation increases telomere length, in the absence of telomerase the accelerated senescence phenotype was not alleviated, although slightly shifted. Again, more

experiments would be needed to verify this, possibly by re-designing the experimental strain so that you could compare the double mutant to the triple mutant in the same experiment.

The preliminary data summarized in this appendix suggest many interesting relationships, but further work is needed to confirm these results. It would also be interesting to link the changes in telomere length to a specific mechanism. One possibility would to study the effects of these mutations on replication fork collapse at telomeric DNA. As previously discussed, this mechanism contributes significantly to telomere length homeostasis and thus it is quite possible that it is playing a role in the phenotypes observed here.

FIGURES

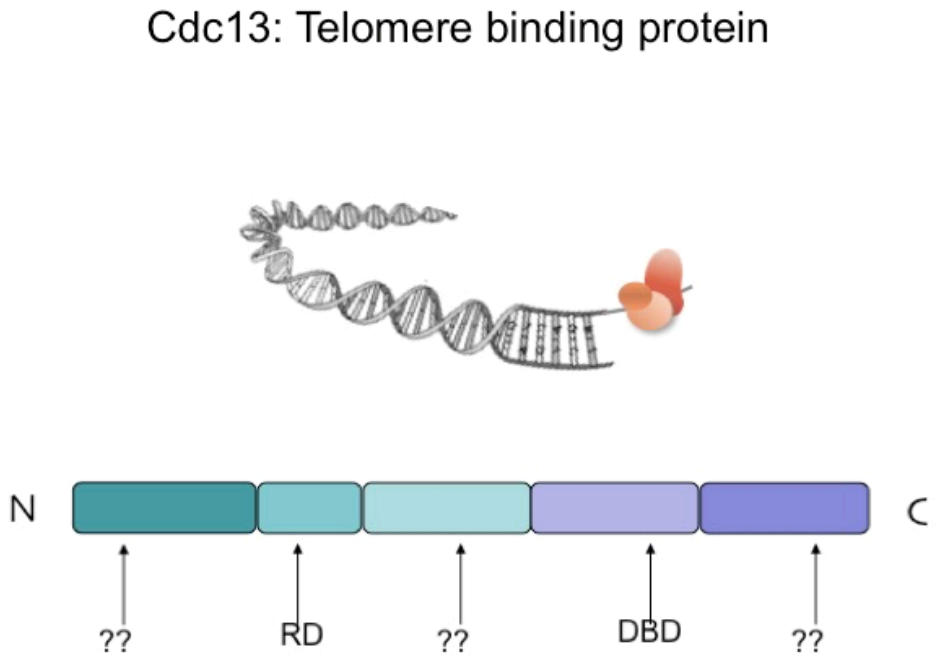

Figure C.1: A schematic of CDC13: telomere binding protein. The telomere specific binding protein CDC13, is made up of multiple domains. One is a designated recruitment domain (RD) and another is the DNA binding domain (DBD). Multiple domains have no designated function, including the N-terminal domain.

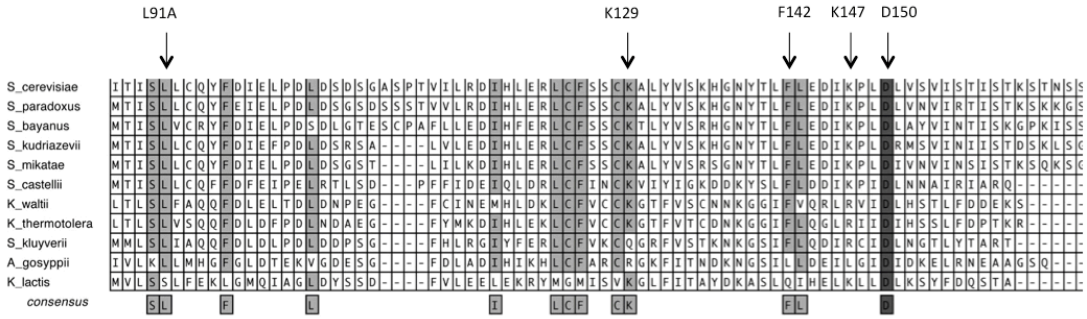

Figure C.2: Cdc13 amino acid sequence alignment for 11 fungal species. Arrows point to residues of interest. Grey highlight is given to residues with greater than 80% conservation across species. Dark grey is used for 100% conserved residues.

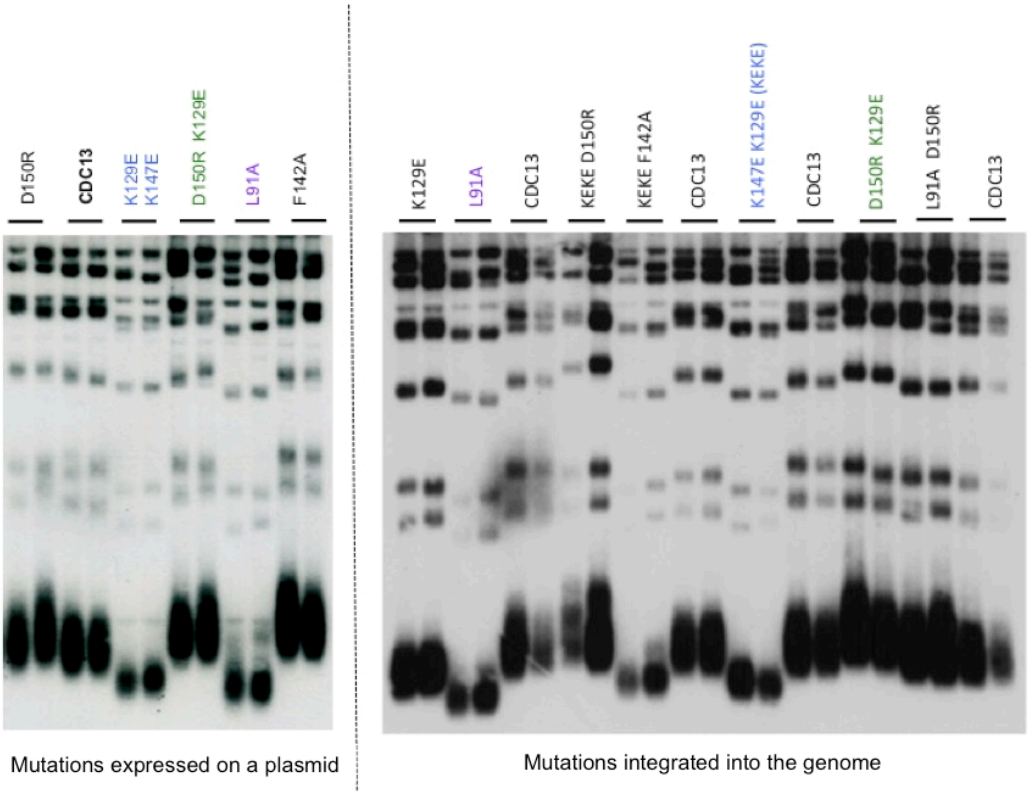

Figure C.3: Telomere length of *cdc13*$^{N\ term}$ mutants from ectopic plasmid expression (left) or integrated into the genome (right). The indicated strains were grown, and gDNA collected and subjected to restriction digest and analyzed by southern blot with a telomere specific probe.

Table C.1: Telomere length phenotypes for *cdc13*^{NTERM}. Telomere length phenotypes shown in figure C.1 are listed here for simplicity.

Residue mutation	on a plasmid	integrated into the genome
D150R	slightly long	slightly long (data not shown)
F142A	slightly long	slightly long (data not shown)
L91A	short	short
K129E	slightly short (data not shown)	slightly short
K129E K147E (KEKE)	short	short
D150R KEKE	slightly long (data not shown)	slightly long (data not shown)
D150R K129E	slightly long	slightly long
D150R L91A	slightly long (data not shown)	Wt length
KEKE F142A	short (data not shown)	short

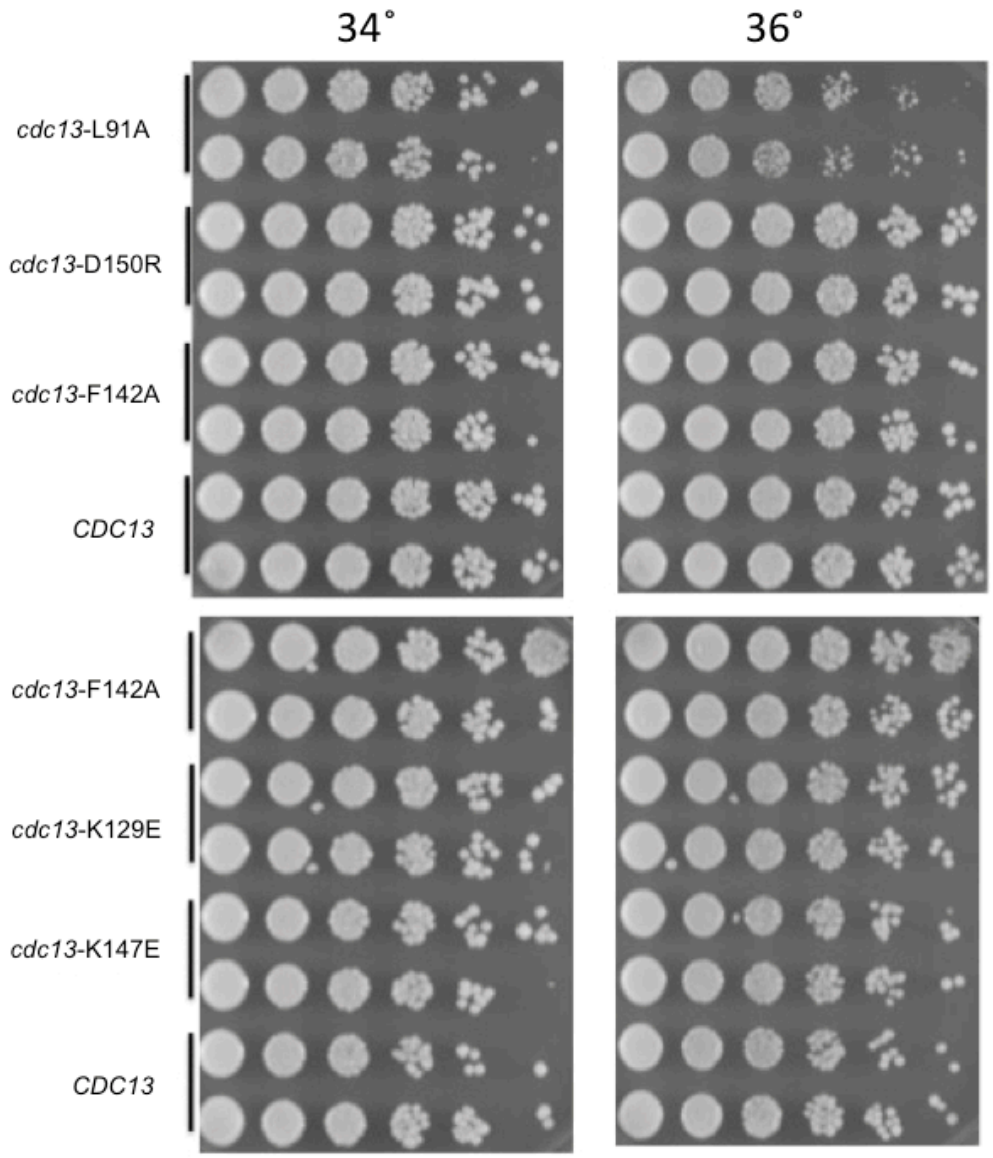

Figure C.4: Growth of *cdc13*^{NTERM} mutations at increased temperatures. Multiple *cdc13*^{Nterm} mutants were grown in liquid culture O/N and dilutions plated on to rich media and allowed to grow at increased temperatures for 3 consecutive days. Only cdc13-L91A showed an effect.

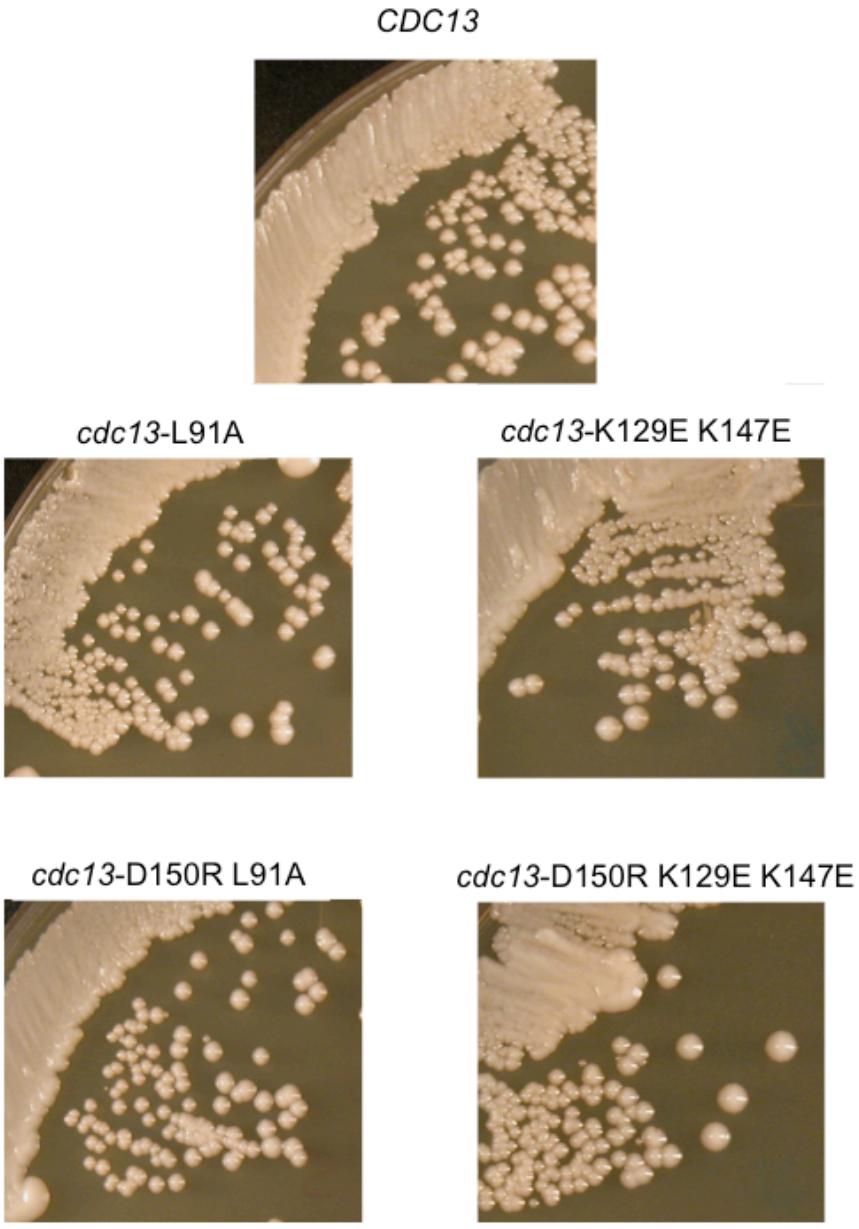

Figure C.5: No visible growth defects at 30˚ for any *cdc13*^{NTERM}. Strains carrying specified mutations were streaked for single colonies on to rich media and allowed to grow for 3 days at 30˚. There was no significant difference between *cdc13*^{Nterm} and *CDC13*.

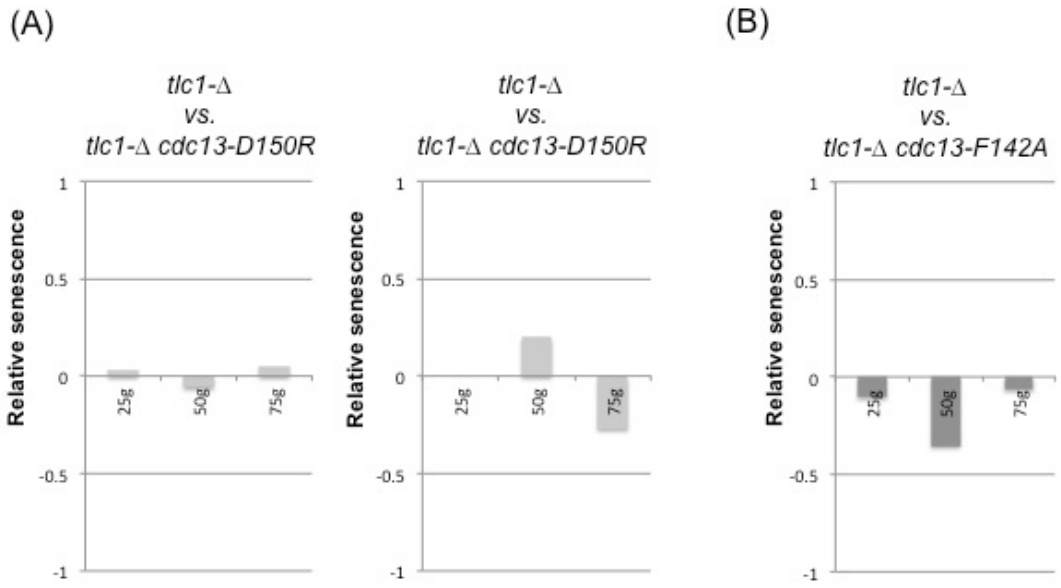

Figure C.6: *cdc13*^{NTerm} mutations with long telomere phenotype have no significant impact on senescence. Average phenotypic score for *cdc13*^{NTerm} were normalized to average phenotypic score of *tlc1*-Δ. Negative values are given to those that accelerate senescence and positive values to those that alleviate senescence.

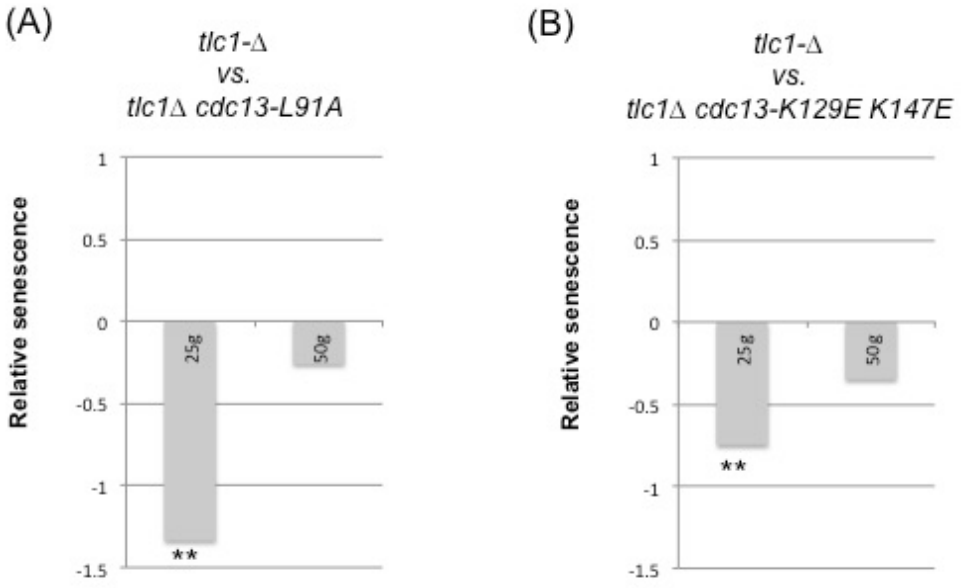

Figure C.7: cdc13^{NTerm} mutations with short telomere phenotype show immediate effects on senescence. Average phenotypic score for cdc13^{NTerm} were normalized to average phenotypic score of *tlc1*-Δ. Negative values are given to those that accelerate senescence and positive values to those that alleviate senescence.

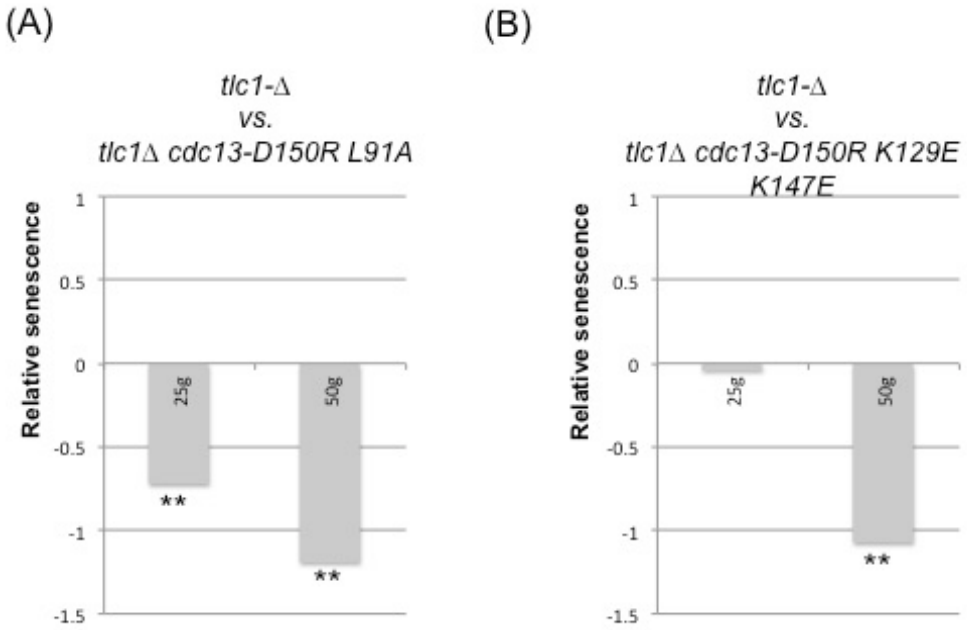

Figure C.8: Combining short telomere mutants with *cdc13*-D150R does not reverse the accelerated senescence. Average phenotypic score for $cdc13^{NTerm}$ were normalized to average phenotypic score of *tlc1*-Δ. Negative values are given to those that accelerate senescence and positive values to those that alleviate senescence.

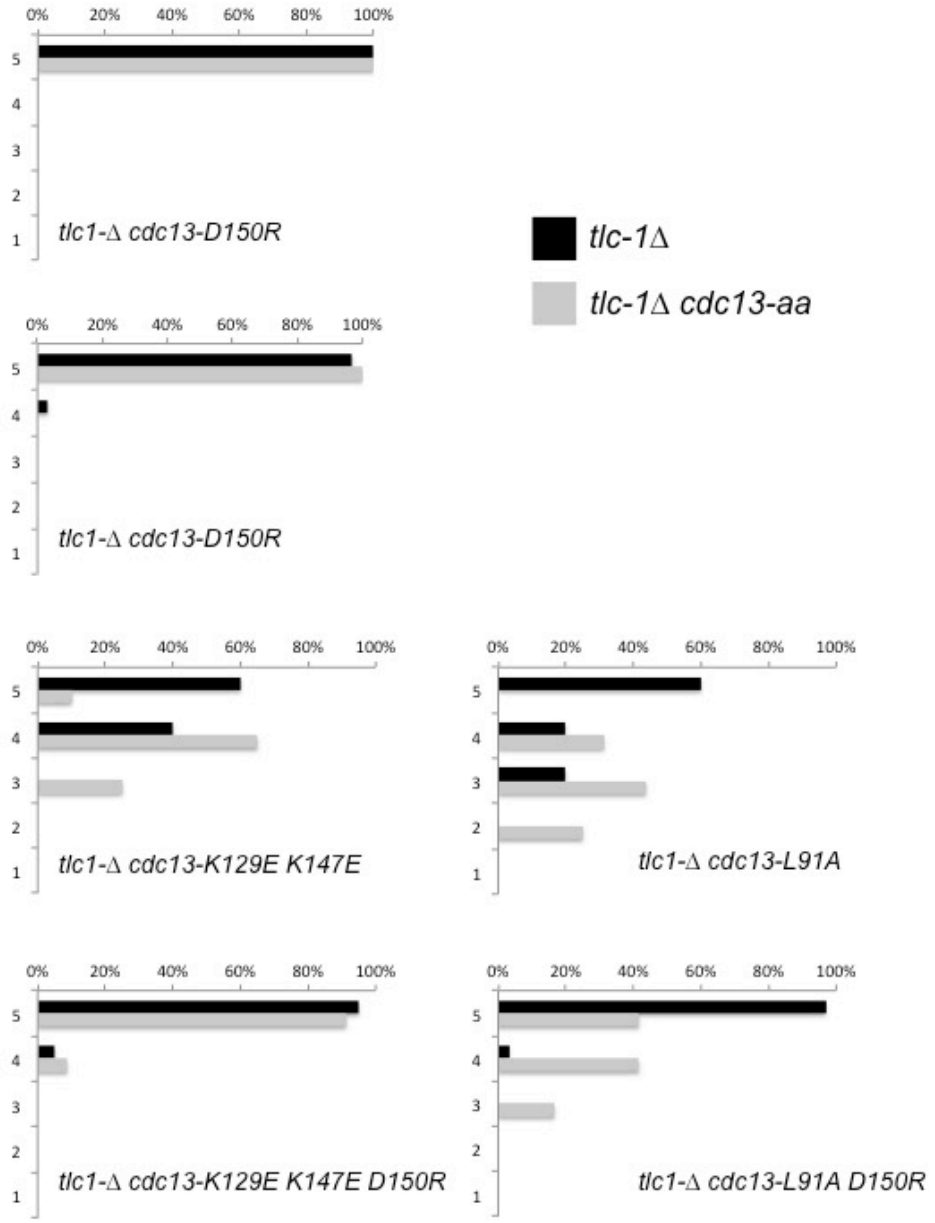

Figure C.9: Isolates derived from parent diploids bearing a single *cdc13*-D150R mutation are healthier upon loss of telomerase when compared to other *cdc13*^{NTerm} mutants. Isolates were given score from 1-5 (5 = healthiest). Scores given at 25 generations; first generation monitored after loss of telomerase (*tlc1*-Δ). Compare *tlc1*-Δ single mutant scores (black) to double mutants (grey).

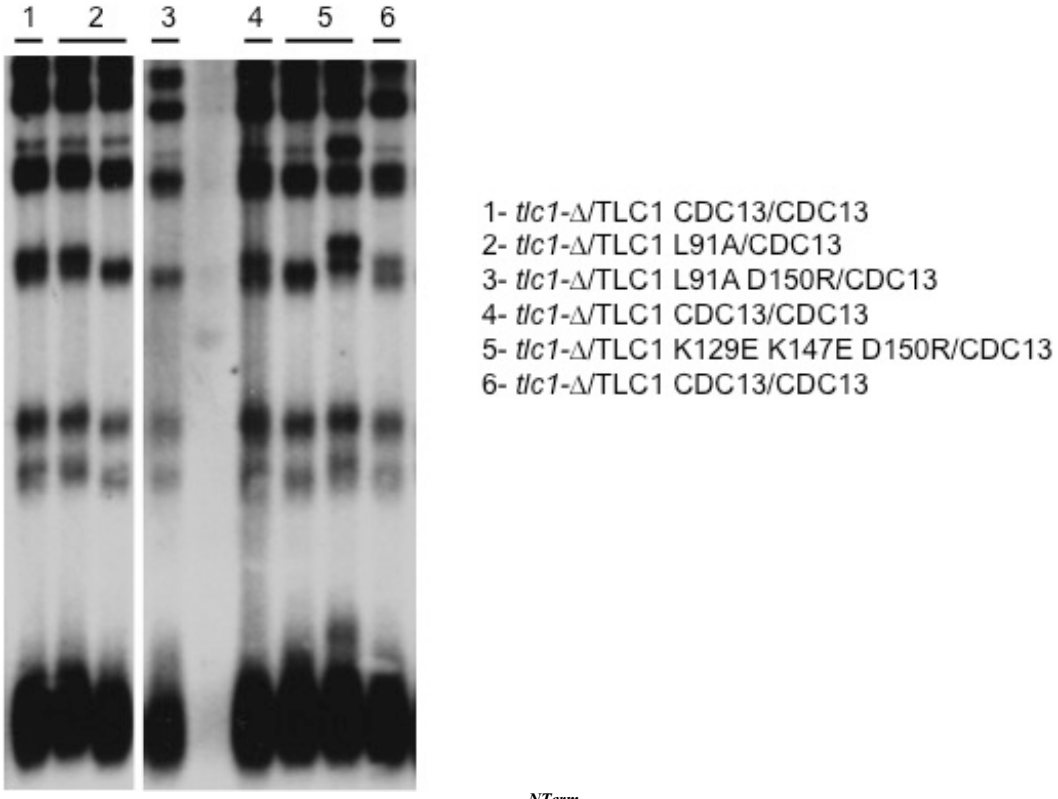

Figure C.10: Telomere length of diploid *cdc13*^{NTerm} /CDC13 *tlc1*-Δ/TLC1 are indistinguishable from CDC13/CDC13 *tlc1*-Δ/TLC1. The indicated strains were grown, and gDNA collected and subjected to restriction digest and analyzed by southern blot with a telomere specific probe.

Table C.2: List of yeast strains used.

YVL	Genenotype
3584	*MAT**a**/α tlc1-Δ::HIS3/TLC1*
5638	*MAT**a**/α tlc1-Δ::HIS3/TLC1 cdc13-L91A/CDC13*
5639	*MAT**a**/α tlc1-Δ::HIS3/TLC1 cdc13-D150R/CDC13*
5640	*MAT**a**/α tlc1-Δ::HIS3/TLC1 cdc13-F142A/CDC13*
5641	*MAT**a**/α tlc1-Δ::HIS3/TLC1 cdc13-K129E K147E/CDC13*
5642	*MAT**a**/α tlc1-Δ::HIS3/TLC1 cdc13-L91A D150R/CDC13*
5643	*MAT**a**/α tlc1-Δ::HIS3/TLC1 cdc13-K129E K147E D150R/CDC13*
additional genotypes: ura3-52/ura3-52 lys2-801/lys2-801 trp-Δ1/trp1-Δ1 his3-Δ200/his3-Δ200 leu2-Δ1/leu2-Δ1	